METAL OXIDE-FACILITATED OXIDATION OF ANTIBACTERIAL AGENTS

A Dissertation
Presented to
The Academic Faculty

by

Huichun Zhang

In Partial Fulfillment
Of the Requirements for the Degree
Doctor of Philosophy in the
School of Civil and Environmental Engineering

Georgia Institute of Technology

July, 2004

Copyright © Huichun Zhang 2004

METAL OXIDE-FACILITATED OXIDATION OF ANTIBACTERIAL AGENTS

Approved by:

Prof. Ching-Hua Huang, Advisor

Prof. James Mulholland

Prof. Spyros G. Pavlostathis

Prof. Paul Wine

Prof. Sotira Yiacoumi

Date Approved: May 26, 2004

ACKNOWLEDGMENTS

I would like to express my sincere appreciation and gratitude to my advisor Dr. Ching-Hua Huang for her invaluable guidance, patience and continuous support throughout my studies.

I would like to thank Dr. James Mulholland, Dr. Spyros G. Pavlostathis, Dr. Paul Wine, and Dr. Sotira Yiacoumi for serving as my committee members. Comments and suggestions of my committee members were indeed very helpful in improving this thesis. Dr. Spyros G. Pavlostathis and Dr. Sotira Yiacoumi are especially acknowledged for their help in my job search.

I sincerely appreciate Dr. Zhu for his guidance and assistance throughout my four years of research in the Daniel Lab and in the ES&T building. Also many thanks go to Dr. Guofeng Li for assistance in FTIR analyses, to Mark Poggi and Dr. Lawrence Bottomley for assistance in SEM analyses, to Dr. Alan T. Stone for helpful discussions related to Chapter I, and to Dr. E. Michael Perdue and Jason Ritchie for assistance in freeze-drying the synthesized Mn and Fe oxides. Additionally, I would like to acknowledge the financial support from National Science Foundation for this work.

Throughout the preparation of this thesis and throughout my studies, I have received help, advice, and moral support from all of my friends. I am very thankful to my very good friends Lingjun and Di for being with me all this time. Without them, the time I spent in Atlanta would not be this much fun. I also appreciate the kindness and

continuous support of my past and present lab members, Jay, Mike, Kristen, Amisha, Wan-Ru, Kin, Seung-Jin, Piti, and Sung Hyunk who have been helpful in the lab.

I would like to thank my parents Chaohui Zhang and Gainan Wang, my brother Lei Zhang. Their love and support have always been very important to me. Special thank you goes to my son Alan who has brought me the greatest happiness I've ever had and gives me the motivation to move on.

Most importantly, I would like to thank my husband, Pinhong Han, whose love, encouragement, understanding and support have made it possible all that I have achieved.

TABLE OF CONTENTS

LIST OF TABLES

LIST OF FIGURES

LIST OF SYMBOLS OR ABBREVIATIONS

ACN – Acetonitrile

Ald-FeOOH – Aldrich goethite

APCI – Atmospheric pressure chemical ionization

BET - Brunauer, Emmett and Teller

C_s – the adsorbed amount in mmol/g

C_w – the dissolved amount in mmol/L

C_{max} – Maximum adsorption capacity

CHES – 2-(cyclohexylamino)ethanesulfonic acid

Cipro – Ciprofloxacin

CDX – Carbadox

Desoxy-CDX – Desoxy-carbadox

Enro – Enrofloxacin

α-Fe_2O_3 – Hematite

FeO^- – Negatively charged Fe oxide surface

$>FeOH_2^+$ – Positively charged Fe oxide surface

$[>FeOH_2^+]$*$[HQ/HQ^{\pm}]$ – Product of $[>FeOH_2^+]$ and $[HQ/HQ^{\pm}]$

α-FeOOH – Goethite

FLU – Flumequine

FQ – Fluoroquinolone

FTIR - Fourier transform infrared spectrometer

GC/MS – Gas chromatograph/mass spectrometer

HCl – Hydrogen chloride

HNO_3 – Nitric acid

HPLC – High-performance liquid chromatograph

HQ^+ – FQ cation

HQ^- – FQ anion

HQ – Neutral form

$HQ^{\pm}$ – Zwitterions

ICP – Inductively coupled plasma spectrometer

IR – Infrared Spectrometer

K_d – Distribution coefficient

K_L – Langmuir distribution coefficient

k_{obs} - Initial reaction rate constant

K_{ow} – Octanol-water partition coefficient

LC/MS – Liquid chromatograph/mass spectrometer

Lome – Lomefloxacin

$MeCl_2$ – Methylene chloride

δ-MnO_2 – Manganese dioxide

MnOOH – Manganite

MOPS – 4-morpholinepropanesulfonic acid

MTO – Methyltrioxorhenium

NaCl – Sodium chloride

NaOH – Sodium hydroxide

Nor – Norfloxacin

ODX – Olaquindox

Oflox – Ofloxacin

PA – Pipemidic acid

PD – 4-Phenylpiperidine

pH_{zpc} – pH at the zero point of charge

PM – N-Phenylmorpholine

PP – 1-Phenylpiperazine

QDX – Quindoxin

QN – Quinoline

QNO – Quinoline-*N*-oxide

QX – Quinoxaline

QXO – Quinoxaline-*N*-oxide

r_{init} – Initial reaction rate

SEM – Scanning Electron Microscopy

SOM – Soil organic matter

SPE – Solid phase extraction

Syn-FeOOH – Synthesized goethite

UV/Vis – Ultraviolet/visible

SUMMARY

The issue that proliferation of antibiotic-resistant pathogens may be linked to antibacterial microcontaminants in the aquatic environment has necessitated a better understanding of the environmental fate of these compounds. Metal oxide-facilitated transformation is likely an important degradation pathway of antibacterial agents at soil-water interfaces. Phenolic disinfectants (triclosan and chlorophene), fluoroquinolones (FQs), and aromatic *N*-oxides are of particular concern due to their widespread usage, potential toxicity and frequent detection in the environment. Results of the present study show that the above antibacterial agents are highly susceptible to Mn and Fe oxide-facilitated oxidation.

The interfacial reactions exhibit complex reaction kinetics, which are affected by solution pH, the presence of co-solutes, surface properties of metal oxides, and structural characteristics of antibacterial agents. For Mn oxides, a relatively fast initial reaction period is generally followed by a gradually slowed reaction, likely due to the limited number of active surface sites. For Fe oxides, three apparent stages of oxidation were observed: (i) stage 1 proceeds with a fast degradation, (ii) stage 2 involves a slowed reaction which is believed to result from the delayed release of Fe^{2+} ions generated during reduction of goethite, and (iii) stage 3 involves a fast reaction rate similar to that in stage 1. Adsorption of the antibacterial agents to Mn and Fe oxide surfaces generally proceeds faster than oxidation reactions of these compounds by Mn and Fe oxides, especially in the case of Fe oxides.

Reaction intermediates and end products are identified by GC/MS and/or LC/MS. FTIR spectroscopy is employed in one case for structural confirmation. Structurally-related model compounds are examined to facilitate reaction site and mechanism elucidation. On the basis of experimental results and literature, reaction schemes are proposed. In general, the antibacterial agent examined in the experiments is adsorbed to the oxide surface, forming a precursor complex. Electrons are transferred within the precursor complex from the antibacterial agent to the metal oxide, followed by releasing of the antibacterial agent radical intermediates which undergo further reactions to generate oxidation products through various pathways. The precursor complex formation and electron transfer are likely rate-limiting.

For triclosan, phenoxy radicals are critical intermediates to form subsequent oxidation products through three separate pathways (i.e., radical coupling, further oxidation of the phenoxy radical, and breakdown of an ether bond within the phenoxy radical). The first two pathways are also operative in the oxidation of chlorophene by Mn oxides. For FQs, oxidation generates radical intermediates that are most likely centered on the inner N in the piperazine ring. The radical intermediates then undergo three major pathways (i.e., radical coupling, *N*-dealkylation, and hydroxylation) to yield a variety of products. Other minor pathways are also possible in forming the final products in FQ oxidation. For aromatic *N*-oxides, an *N*-oxide radical intermediate is generated upon oxidation by MnO_2, followed by the loss of oxygen from the *N*-oxide moiety and the formation of a hydroxyl group at the C-atom adjacent to the *N*-oxide moiety.

Overall, a fundamental understanding of the reaction mechanisms between three classes of antibacterial agents and metal oxides has been obtained. This study has

yielded important insight for predicting the abiotic transformation of these categories of antibacterial agents and other structurally-related contaminants at the soil-water interface in the natural environment.

CHAPTER I

INTRODUCTION

1.1 Research Issues and Objectives

During the last three decades, the research on the impact of chemical pollution has focused primarily on the conventional "priority" pollutants, especially those acutely toxic/carcinogenic pesticides and industrial intermediates that display persistence in the environment. Bioactive chemicals such as antibacterial agents have received little attention as potential environmental pollutants. Due to their large quantities of use, antibacterial chemicals are continuously introduced to the aquatic environment via treated and untreated sewage and sludge, and agricultural waste and runoffs. Among antibacterial agents, triclosan and chlorophene (often referred to as antiseptics), fluoroquinolones, and aromatic *N*-oxides merit special attention.

Triclosan (5-chloro-2- (2,4-dichlorophenoxy)phenol, Figure 1.1) has been widely used as an active disinfectant and preservative since 1960s. Fluoroquinolones (FQs, Figure 1.1) are probably among the most important classes of synthetic antibacterial agents used in human and veterinary medicines (Golet et al. 2001). Quinoxaline-*N,N'*-dioxides (Figure 1.1), as an important group of aromatic *N*-oxide compounds, are generally added to pig feeds as growth promoters and to prevent diseases in farm animals (Massy and McKillop 1996, Hutchinson et al. 2002). The frequent usage of these antibacterial agents has led to their ubiquitous presence in the environment. The potential toxicities of these antibacterial microcontaminants in the environment necessitate further investigation on their transformation in order to properly evaluate their risks. Triclosan

and chlorophene are likely to partition significantly to sediments due to their relatively high hydrophobicity (log K_{ow} of 4.86 and 3.99, respectively, ChemProp 2002). Although fluoroquinolones have relatively low log K_{ow} values (e.g., 0.28 and 1.03 for ciprofloxacin and norfloxacin, respectively), strong adsorption of these compounds to soils and sediments has been reported (Tolls 2001). Information on the environmental behavior of aromatic *N*-oxides is quite limited. Moderate sorption of one aromatic *N*-oxide, olaquindox, to different types of soils has been documented (Rabolle and Spliid 2000). The favorable interactions of antibacterial agents with soils and sediment point to the potentially significant role of minerals in the environmental fate of these compounds. Currently, little information is available on the transformation and fate of antibacterial agents at the mineral-water interfaces and a systematic investigation is highly needed.

Metal oxides (e.g., Mn, Fe, Al and Si oxides) commonly found in soils and sediments are known to facilitate abiotic reactions of organic pollutants via hydrolysis, oxidation or reduction. They can play an important role in retarding organic pollutants in subsoils and aquifers that are classified as porous media with low organic carbon contents (reviewed in Karthikeyan et al. 1999). Iron (III) and manganese (III/IV) oxides are among the most important naturally-occurring catalysts that are effective in organic pollutant transformation with reduction potentials of 0.67 V, 1.50 V, and 1.23 V for FeOOH, MnOOH and MnO_2, respectively (Stone 1987). Manganese and iron oxides have been shown to be effective oxidants for a wide range of organic pollutants including phenols (e.g. Stone 1987, Ukrainczyk and McBride 1993a), anilines (Laha and Luthy 1990, Klausen et al. 1997), aliphatic amines (McArdell et al., 1998), and triazines (Wang

et al., 1999). Aluminum oxides have also been shown to catalyze oxidation of phenolic compounds in the presence of oxygen (Karthikeyan et al. 1999).

The ultimate goal of this study is to obtain a mechanistic understanding of the oxidation of antibacterial agents with metal oxides and to develop an information basis that can facilitate predicting the transformation of related organic pollutants in the environment. The specific research tasks are:

1) Determination of reaction rates and kinetics.
2) Assessment of reaction mechanisms by identification of reaction intermediates and products and by examination of structurally-related compounds.
3) Evaluation of the influence of environmental factors (e.g. pH and the presence of co-solutes such as metal ions and natural organic matter) on reaction kinetics and product distribution.
4) Quantification of adsorption extent and assessment of adsorption sites between antibacterial agents and metal oxides.
5) Assessment of the influence of metal oxide properties on reaction rates and product distribution by comparing different metal oxides including birnessite (δ-MnO_2), manganite (MnOOH), and goethite (α-FeOOH).
6) Characterization of the metal oxides examined in this study to better correlate oxide reactivity with surface structures and properties.
7) Development of novel and robust analytical techniques to monitor the reactions. The range of techniques includes HPLC methods for antibacterial agents and LC/MS, GC/MS and IR spectroscopic methods for reaction intermediates and end-products.

Phenolic Compounds

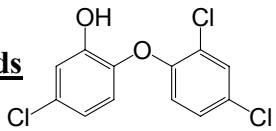

Triclosan

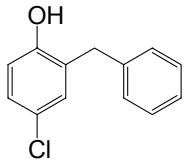

Chlorophene

Fluoroquinolones (FQs)

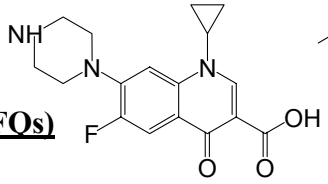

Ciprofloxacin

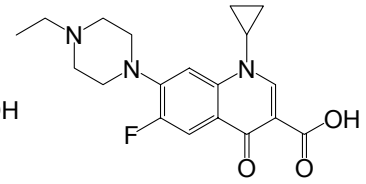

Enrofloxacin

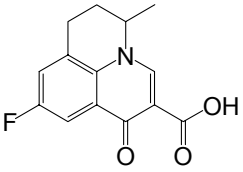

Flumequine

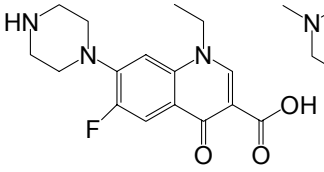

Norfloxacin

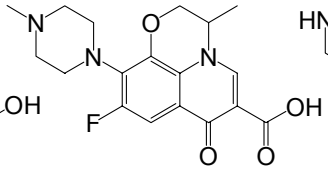

Ofloxacin

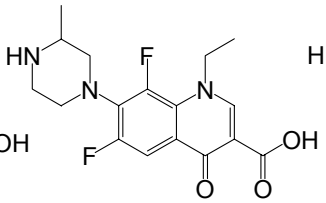

Lomefloxacin

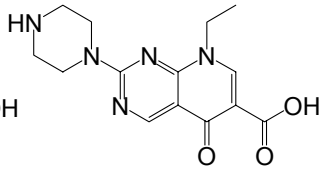

Pipemidic Acid

Quinoxaline-*N*,*N*'-dioxides and Related Compounds

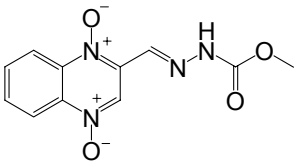

Carbadox

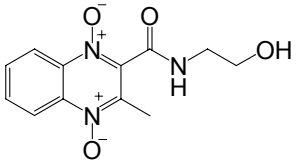

Olaquindox

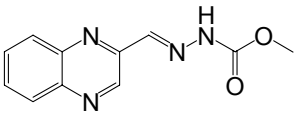

Desoxy-carbadox

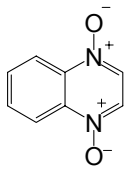

Quindoxin

Figure 1.1. Triclosan, chlorophene, fluoroquinolones, and quinoxaline *N*,*N*'-dioxides examined in this study.

1.2 Background

1.2.1 Literature Review on Triclosan, Chlorophene, Fluoroquinolone and Aromatic *N*-oxide Antibacterial Agents

1.2.1.1 Triclosan and Chlorophene

Triclosan (5-chloro-2-(2,4-dichlorophenoxy)phenol) and chlorophene (4-chloro-2-(phenylmethyl)phenol) are commonly used broad-spectrum antibacterial agents (Figure 1.1). Triclosan, commercially known as Irgasan DP 300 or Irgacare MP, is widely used in many personal care (e.g., toothpaste, soaps, deodorants, shampoos, and cosmetics) and consumer (e.g., plastic kitchenware and footware) products with typical concentrations in the range of 0.1 – 0.3 % by weight. Triclosan is also incorporated in polymers and fiber products (e.g., mattress pads, food cutting boards, shoes, and sportswear) to give these materials antibacterial properties (Cox 1987, DeSalva et al. 1989, Bhargava et al. 1996, Daughton and Ternes 1999, Sabaliunas et al. 2003). Chlorophene, commercially known as Nipacide BCP, is commonly used at 3 – 10 % by weight (diluted with water by about 1:40 – 1:120 ratios in the final use) in hospitals and households for general cleaning and disinfecting. Chlorophene also finds its application in industrial and farming environments as an active agent in disinfectant formulations. The chlorophene product can be used either alone or in combination with other phenolic biocides (Payne 1998).

As a consumer product ingredient, the majority of triclosan and chlorophene receives treatment in local wastewater treatment plants (WWTPs). During wastewater treatment, primary sedimentation could remove 44 – 92 % of triclosan (Lindstrom et al. 2002), while advanced trickling filter and activated sludge wastewater treatment could remove triclosan by more than 95 % (Sabaliunas et al. 2003). Chlorophene, at

concentrations of 0.1 mg/L and 50 mg/L, was found to degrade by 80 % in activated sludge sewage systems within 8 hours and 7 days, respectively (Payne 1998). Despite these high levels of treatment efficiency, in a recent USGS study surveying the occurrence of emerging organic pollutants in surface streams, triclosan was one of the most frequently detected compounds with a median concentration of 0.14 μg/L (Kolpin et al. 2002). Others also reported detectable triclosan in urban wastewater treatment plants (at influent concentrations of 0.6 – 1.3 μg/L and effluent concentrations of 110 – 650 ng/L) (Paxéus 1996, Lindstrom et al. 2002, McAvoy et al. 2002), surface waters (at up to 74 ng/L in Switzerland and at 0.05 – 0.15 μg/L in Japan) (Okumura and Nishikawa 1996, Lindstrom et al. 2002), sediments (at detection limits of 1.7 – 4.6 ng/g) (Okumura and Nishikawa 1996), fish (at detection limits of 0.89 – 2.5 ng/g) (Okumura and Nishikawa 1996) and human milk (at less than 300 μg per kg lipid weight) (Adolfsson-Erici et al. 2000). Occurrence of chlorophene in aquatic environments is, on the contrary, much less documented thus far. The recent study by Thomas et al. (2002) reported detection of chlorophene in sediments collected from estuaries in the United Kingdom

Several concerns have been raised about triclosan and chlorophene. As a biocide, triclosan blocks lipid biosynthesis by specifically inhibiting the enzyme enoyl acyl carrier protein reductase and may induce bacterial resistance development (McMurry et al. 1998, Levy et al. 1999). The compound is acutely toxic to aquatic organisms such as fish (EC_{50}, rainbow trout = 350 μg/L) (Adolfsson-Erici et al. 2000). Orvos et al. (2002) recently examined the toxicity of triclosan on various aquatic organisms and determined that certain algae species are the most susceptible organisms. Furthermore, triclosan may form chlorodioxins during heating and incineration (Kanetoshi et al. 1987, Kanetoshi et

al. 1988) and under the influence of sunlight (Kanetoshi et al. 1988, Latch et al. 2003). Chlorophene is an aryl halide biocide with insufficient evidence to be considered potential human carcinogen and has a low order of toxicity (oral LD_{50} for rates = 4.1 g/kg bodyweight) (Payne 1998). However, there was some evidence of carcinogenic activity of chlorophene in male B6C3F1 mice based on 2-year gavage studies (National Toxicology Program 1994). Chlorophene also appeared to be nephrotoxic for male and female F344/N rats and B6C3F1 mice (National Toxicology Program 1994). In addition, chlorophene is irritating to both skin and eyes (Parent 2000). Mutagenic activity of triclosan and chlorophene was both confirmed on Mutatox TM bioassays (Thomas et al. 2002).

To properly assess the risks of triclosan and chlorophene, a better understanding of their environmental fate is imperative. Sorption to activated sludge and aerobic biodegradation have been suggested as the dominant mechanisms for high removal of triclosan and chlorophene (Payne 1998, Federle et al. 2002, McAvoy et al. 2002). Direct photolysis was recently proved to be an elimination pathway for dissolved triclosan in sunlit lake water. The direct photolysis is much more important at pH values where triclosan is present in its phenolic form (reported pK_a at 7.9-8.1) (Lindstrom et al. 2002, Tixier et al. 2002). Triclosan and chlorophene are both relatively hydrophobic, with estimated log K_{ow} (octanol-water partition coefficient) of 4.86 and 3.99, respectively (ChemProp 2002). Because of their hydrophobic nature, triclosan and chlorophene are likely to partition to soils and sediments once entering the aquatic environment. Their reactions with metal oxides in soils and sediments may significantly impact their

environmental fate, particularly when conditions are not suitable for biological or photochemical transformation.

1.2.1.2 Fluoroquinolones

Fluoroquinolones (FQs) are among the most important classes of synthetic antibacterial agents used in human and veterinary medicines (Figure 1.1, Golet et al. 2001). They are active against many pathogenic bacterial species (both gram-negative and gram-positive) as gyrase inhibitors, which selectively inhibit bacterial DNA synthesis (Scheer 1987). Among FQs, flumequine and pipemidic acid belong to the first-generation quinolones (Kuhlmann et al. 1998). Ciprofloxacin is used to treat infections of the urinary, respiratory, and gastrointestinal tracts (Schacht 1998) and has been the most frequently prescribed clinical fluoroquinolone. Lomefloxacin is suitable for oral and parenteral administration and has been approved in several countries to treat various infections caused particularly by gram-negative bacilli (Naber 2002). Norfloxacin and ofloxacin are also common human antibacterial agents. Norfloxain is more widely prescribed in Europe than in the United States (RxList 2000). Ofloxacin has been mostly replaced by its (-)-*S*-enantiomer (levofloxacin) since 1998 and levofloxacin is rather frequently prescribed in the US currently (RxList 2000). Enrofloxacin is a veterinary chemotherapeutic agent widely used for the treatment of infections in pets and livestock. A significant portion of the administered FQ antibacterial agents is expected to be excreted intact and introduced into the nature through wastewater (Hartmann et al. 1998).

Because of the extensive usage of FQs, the presence and accumulation of FQ antibacterial agents in aquatic environments have been widely reported in the literature,

among which 249 to 405 ng/L of ciprofloxacin and 45 to 120 ng/L of norfloxacin have been detected in domestic wastewater in Switzerland (Golet et al. 2001, Golet et al. 2002). Higher concentrations of some FQs (0.6 – 2 μg/L) were also recently detected in wastewaters in the United States (Renew and Huang 2004). Median concentrations of 0.02 μg/L and 0.12 μg/L were reported for ciprofloxacin and norfloxacin, respectively, for samples from 139 surface streams across the United States (Kolpin et al. 2002). Additionally, a range of 0.7 to 124.5 μg/L of ciproflaoxacin was found in Swiss hospital wastewater (Hartmann et al. 1999).

These consistent, low-levels of antibiotic contaminations may pose threats to the ecosystem and human health by inducing increase and spread of bacteria drug-resistance (Volmer et al. 1997). For example, an emergence of resistance to ciprofloxacin has been seen in various infection models (Craig and Dalhoff 1998). Antibiotic-resistant bacteria have also been isolated from different environments, including rivers, streams, drinking water, wastewater treatment plant effluents, etc. (Al-Ghazali et al. 1988, Jazrawi et al. 1988, Radtke and Gist 1989). Furthermore, FQs, especially ciprofloxacin, have been linked to genotoxicity of wastewater effluent in German and Swiss Hospital Wastewaters for causing primary DNA damage in bacteria, assessed by a bacterial SOS repair assay (umuC-test) (Hartmann et al. 1998, Hartmann et al. 1999).

As antibacterial agents, FQs were shown not to undergo microbial degradation to any significant extent (e.g. Al-Almad et al. 1999, Kümmerer et al. 2000, Marengo et al. 2001). However, other studies have shown that FQ antibacterial agents can be degraded by certain fungi species (e.g. Parshikov et al. 1999, Wetzstein et al. 1999). Photodegradation has been demonstrated to be very important in the fate of FQs in the

environment (e.g. Phillips et al. 1990, Burhenne et al. 1999, Fasani et al. 1999, Fasani et al. 2001, Mella et al. 2001). Depending on the reaction conditions such as pH buffer, co-solutes, etc., more than 10 photodegradation products from various pathways, including dealkylation, defluorination and hydroxylation have been identified (Fasani et al. 1999, Fasani et al. 2001, Mella et al. 2001). Sorption towards soils, sediments, or dissolved organic matter is believed to be another important environmental sink for FQs (Nowara et al. 1997, Lützhøft et al. 2000a, Tolls 2001). For example, Nowara et al. found that 95.2% to 99.7% of enrofloxacin could adsorb to five different soils from Brazil, France, Germany, the Philippines, and Sweden (Nowara et al. 1997), and sorption coefficients vary little among the FQs. The strong adsorption of FQs may result in less free antibacterial agents and thus reduce both their photodegradation and biodegradation (Lützhøft et al. 2000b).

1.2.1.3 Aromatic *N*-oxides

Quinoline-*N*-oxides and quinoxaline-*N,N'*-dioxides represent a structural class of aromatic *N*-oxides that are common in many pharmaceuticals, agrochemicals and industrial chemicals (Albini and Pietra 1991, Katritzky and Lagowski 1971). Aromatic *N*-oxide structures have also been observed in metabolites of many drugs and xenobiotics, as well as in intermediates of synthetic chemical processes (Gorrod and Beckett 1978). For example, quinoline *N*-oxide was documented to be a microbiological oxidation product of quinoline (Sutherland et al. 1994). To our particular interest, quinoxaline-*N*,*N*'-dioxides (Figure 1.1) have been developed as potent antibacterial agents for use as growth promoters to prevent swine dysentery and bacterial enteritis in

farm animals (Hutchinson et al. 2002, FAO/WHO 1990, JECFA 1991). Quindoxin (Figure 1.1), whose antibiotic activity was first reported in 1943 (McIlwain 1943), is probably the historical prototype for this class of medicinal agents. In addition to damaging cellular DNA (Suter et al. 1978), quindoxin has been reported to be carcinogenic in rats and mutagenic in bacteria and yeast (Tucker 1975, Voogd et al. 1980, Nunoshiba and Nishioka 1989). Carbadox (methyl-3-(2-quinoxalinylmethylene) carbazate-N,N'-dioxide) (Figure 1.1), commercially known as Mecadox® and Fortigo® (Pfizer) and approved for use since 1970s, is a widely used *N*-oxide antibacterial agent (FAO/WHO 1990, JECFA 1991). Olaquindox (2-methyl-3-[N-(2-hydroxyethyl)carbamoyl]quinoxaline N,N'-dioxide) (Figure 1.1) is another common *N*-oxide antibacterial agent, used solely as a growth promoter in order to increase the rate of pig growth and improve feed efficiency (FAO/WHO 1990, JECFA 1991). The amounts of olaquindox used in Denmark for growth promoting purposes were reported to increase drastically from 16 tones in 1995 to 28 tones in 1998 (Rabolle and Spliid 2000).

Because carbadox and desoxycarbadox (Figure 1.1), one of its metabolites, are suspected carcinogens and mutagens (FAO/WHO 1990, JECFA 1991), carbadox has been banned in animal feedings in Europe (Commission Regulation No. 2788/98 1998). In the U. S., a withdrawal period (i.e., administration of the drug is stopped some time before slaughter) of 10 weeks is required by the U. S. Food and Drug Administration (FDA) before slaughtering pigs (up to 75 lb) fed by carbadox-treated feeds. Zero tolerance for residues of carbadox in the uncooked, edible tissues of swine is specified by the U. S. Code of Federal Regulations (MacIntosh and Neville 1984). In a recent study on the ability of growth-promoting antibacterial agents to induce Shiga toxin (Stx)-

converting bacteriophages from Stx-producing Escherichia coli (STEC), quinoxaline-*N,N'*-dioxide-type antibacterial agents such as carbadox and olaquindox enhanced the release of Stx-converting phage particles from STEC cells and therefore may contribute to the spread of STEC and development of new STEC pathotypes, according to Kohler and co-workers (Kohler et al. 2000). In addition to quindoxin and carbadox, olaquindox was also found to be mutagenic to bacteria and yeast at very low concentrations (Voogd et al. 1980).

Residue of olaquindox was detected in both egg white (0.002 – 0.02 mg/kg) and egg yolk (up to 0.008 mg/kg) based on different exposure methods (Cornelis and Petz 2000). Rapid decomposition of carbadox to desoxy-carbadox (in vitro metabolism) in kidney and liver samples was reported. Therefore it is quite possilbe that the metabolite desoxy-carbadox will be present more often in the environmental samples than the parent carbadox (Binnendijk et al. 1991). This fast metabolism could be one of the reasons that no detectable carbadox was found in the recent study by USGS, in which analyses of carbadox were conducted based on 104 steam samples from various locations in the U. S. (method detection limit = 0.1 μg/L) (Kolpin et al. 2002).

A comprehensive literature search revealed extremely limited information regarding abiotic or biotic transformation of aromatic *N*-oxides under environmental conditions. In particular the potential transformation of aromatic *N*-oxides with metal oxides in soils is essentially non-existent. So far photolytic activity of carbadox and desoxycarbadox has been observed in the process of sample preparation (i.e., fresh tissue samples being spiked with these compounds followed by extraction and cleanup within duration of about 2 hours) (MacIntosh and Neville 1984). In this study, a minimal

incandescent light in the hood reached the samples and caused degradation especially of desoxy-carbadox, as indicated by their poorer recoveries (at 50 ± 8.8 % and 54 ± 10.8 % with light while 53 ± 13.6 % and 61 ± 7.2 % in near darkness for carbadox and desoxy-carbadox, respectively) (MacIntosh and Neville 1984). Other groups, on the other hand, have extensively examined the photochemical reactions of quinoxaline *N*-oxides and *N*,*N*'-dioxides in various media (Kurasawa et al. 1995). Mild sorption of olaquindox to various soil types with distribution coefficients K_d = 0.7 – 1.7 ml/g has been reported (Rabolle and Spliid 2000, Tolls 2001), quite consistent with the estimated low log K_{ow} value (- 2.3) of this compound (Loke et al. 2002). It was suggested that the highly conjugated structural moieties of olaquindox might favor in forming charge-transfer complexes with soil constituents (Haderleln and Schwarzenbach 1993) and in turn enhance sorption of olaquindox to soils. Furthermore, in experiments simulating conditions of surface water, olaquindox (50-5000 μg/L) was biodegraded both aerobically and anaerobically, though the biodegradation was slower in the anaerobic conditions (Ingerslev et al. 2001). Olaquindox was even mineralized in soil-manure slurries with 50 g of soil per liter (Ingerslev and Halling-Sorensen 2001).

1.2.2 Metal Oxide-Facilitated Oxidation: General Aspects

1.2.2.1 Introduction

While layer silicates are the dominant clay minerals (< 2 μm in diameter) in many soils, for soils that have been subjected to intense or prolonged weathering (e.g., soils in glaciated or arid regions) or for subsoils and aquifers that are classified as porous media with low organic carbon contents, their mineral fraction is typically composed of Fe and

Al oxides and hydroxides (McBride 1994). Mn oxides and hydroxides, though existing at a much lower abundance (Fe : Mn ~ 38 – 81 : 1, Chukhrov and Gorshkov 1981), generally occur simultaneously with Fe and Al oxides and hydroxides. These soils and subsoils usually have very low cation-exchange capacities but large surface areas. The surface charges, though limited, are very sensitive to the pH of the surrounding solution. Additionally, the surfaces have considerable capacity to chemisorb metal ions as well as inorganic and organic anions (McBride 1994).

Iron (III) and manganese (III/IV) oxides have been considered as potential oxidizing agents in the natural systems in degrading organic compounds due to their high reduction potentials (Table 1.1). Several groups of organic compounds, such as hydroquinone, substituted phenols, pyrogallol, anilines, aliphatic amines, and triazines have been found to be reactive in the presence of Fe oxides (e.g., McBride 1987, Kung and McBride 1988, Pizzigallo et al. 1995, Pizzigallo et al. 1998) and Mn oxides (e.g., Stone 1987, Laha and Luthy 1990, Ukrainczyk and McBride 1993a, Klausen et al. 1997, McArdell et al. 1998, Wang et al. 1999, Wang and Huang 2000). The oxidation of phenolic acids by Palouse soil that was predominant in the wheat-growing region in the Pacific Northwest was also attributed to the oxidation activity of Fe and Mn oxides in the soil (Lehmann et al. 1987).

Due to the importance of Fe and Mn oxides in the potential attenuation and transformation of organic pollutants in natural environments, it is interesting to know their occurrence and properties in soils. Chukhrov and Gorshkov (1981) identified a variety of Fe and Mn oxides in soil samples from all over the world. They concluded that the common Fe oxides were goethite, ferroxyhyte, lepidocrocite, hematite and

Table 1.1 Standard-State Reduction Potentials of Half-Reactions involving Fe and Mn oxides and soils.

Reductive Half Reaction	**E_H^0(volts)**
$FeCO_3(s) + 2e^- = Fe(s) + CO_3^{2-}$	-0.76[a]
$Fe^{3+} + e^- = Fe^{2+}$	0.77[a]
$MnO_2(s) + HCO_3^- + 3H^+ + 2e^- = MnCO_3(s) + 2H_2O$	0.94[a]
$(\alpha)FeOOH(s) + HCO_3^- + 2H^+ + e^- = FeCO_3(s) + 2H_2O$	0.78[a]
$(\alpha)FeOOH(s) + 3H^+ + e^- = Fe^{2+} + 2H_2O$	0.80[a]
$(am)Fe(OH)_3(s) + 3H^+ + e^- = Fe^{2+} + 3H_2O$	0.96[a]
$MnO_2(s) + 4H^+ + 2e^- = Mn^{2+} + 2H_2O$	1.29[a]
$Mn^{III}OOH(s) + 3\ H^+ + e^- = Mn^{2+}\ (aq) + 2\ H_2O$	1.45[b]
$Mn^{3+} + e^- = Mn^{2+}$	1.51[b]
Oxidized soils	+0.4 to +0.7 V[c]
Seasonally saturated soils (oxidized)	+0.4 to +0.7 V[c]
Seasonally saturated soils (highly reduced)	-0.25 to -0.3 V[c]

[a] from Pankow 1991; [b] from McBride 1994; [c] from Sparks 1995.

ferrihydrite while the common Mn oxides were vernadite, birnessite, cryptomelane, todorokite and hausmannite. McKenzie (1980) published two review papers about Mn oxides in soils. The formation chemistry and some surface properties of Fe oxides in soils have been reported by Huang and Wang (1997). These previous works summarize an improved understanding of the formation and occurrence of Fe and Mn oxides in soils, providing a foundation to assist the understanding of the redox reactions of Fe and Mn oxides in the natural environment.

1.2.2.2 Manganese Oxides

Manganese oxide minerals have a black color. They generally occur as coatings and cements on other soil and sediment particles, as deposits in cracks and veins, and mixed with Fe oxides and other soil components in nodules. Mn oxide minerals are considered as important constituents in various soils for two reasons: (i) Mn is an essential element for both plants and animals, and (ii) heavy metal ions have a strong affinity toward Mn oxides and hydroxides which may affect the availability of nutrient and toxic trace metals to plants (McKenzie 1989). The following commonly existing soil manganese oxides have been reported: vernadite, birnessite, todorokite, cryptomelane, and hausmannite (Chukhrov and Gorshkov 1981). Taylor (1968) observed that birnessite and lithiophorite were the most common Mn minerals found in a wide range of Australian soils. In addition, soil Mn existed either as birnessite or lithiophorite in five out of seven soils taken separately from Bermuda, Europe, and the Middle East countries. The highest concentrations of birnessite were generally found near the surface of alkaline soils while lithiophorite was found in sub-surface horizons of the more acid soils.

Mn oxides occur as small crystals in soils, with reported crystallites of 0.02 μm and 0.1 μm for birnessite and lithiophorite, respectively (Dixon et al. 1990). With a high surface area to bond with other particles, most Mn oxides in soils may become substrates for crystal growth. Mn oxide nodules are frequently layered in composition. Since Mn is mobilized early in the weathering of newly exposed sediments, Mn precipitates are likely to include trace elements (e.g. Zn, Ni, Co, Ba) through specific adsorption from the soil solution (Dixon et al. 1990).

Mn (IV) is the primary oxidation state of Mn in the oxides (Dixon et al. 1990). Because of the charge imbalance caused by substitution of lower oxidation states of Mn such as Mn(III) and Mn(II), the overall oxidation state of Mn in most natural manganese oxide minerals is < 4. Manganese oxides can act as strong oxidizing agents even in the absence of oxygen, as indicated by their high reduction potentials (Table 1.1). Shindo & Huang (1982) prepared non-crystalline or poorly crystalline oxides of manganese (birnessite, δ-MnO_2). Their data revealed that Mn(IV) oxides are very effective oxidants compared with Fe, Al and Si oxides in the abiotic browning of hydroquinone. This finding indicates that Mn(IV) oxides may have an important role in the formation of humic substances in the environment.

1.2.2.3 Iron Oxides

Iron oxides are widely present in various soils, and are the most abundant metallic oxides in most soils (Taylor 1990). Six different crystalline Fe oxides have been identified in soils: ferroxyhyte (δ-FeOOH), ferrihydrite ($5Fe_2O_3 \bullet 9H_2O$), goethite (α-FeOOH), hematite (α-Fe_2O_3), lepidocrocite (γ-FeOOH) and maghemite (γ-Fe_2O_3)

(Schwertmann et al. 1974, Chukhrov and Gorshkov 1981). Goethite and hematite are the most thermodynamically stable forms under aerobic conditions (Schwertmann and Cornell 2000). Goethite with yellow to brown colors and hematite with red colors are the two common forms of Fe oxides in many soils (Schwertmann and Cornell 2000). When kaolinite is the major clay minerals in the highly weathered soils of tropical and subtropical regions, goethite and hematite generally occur simultaneously (Schwertmann et al. 1974).

Properties of iron oxides such as the crystal morphology and size of iron-oxide crystals are affected by substitution of foreign ions, especially of Al (Huang and Wang 1997). The charge characteristics and sorption behavior of iron oxides are also affected by the presence of foreign ions. The submicroscopic iron-oxide particles generally have high specific surface area and thus act as very efficient sinks for many cations (e.g., Al, Cd, Co, Cu, Mn, Ni, Pb, Ti, V and Zn) and anions (e.g., molybdate, phosphate, silicate and selenite). Specific sorption of Cd, Co, Cu, Mn, Ni and Zn on goethite and hematite may be partly responsible for the association of these elements with iron oxides.

The common association of Mn and Fe in rocks of all kinds of soils reflects their chemical similarity (Krishnamurti and Huang 1988). The standard electrode potentials (E^0) of the redox pairs Fe^{2+}-MnO_2 and Fe^{2+}-Mn_3O_4 indicate that oxidation of Fe^{2+} by Mn oxides is thermodynamically feasible. Additionally, Mn^{4+} and Mn^{3+} in the Mn oxides could be reduced to Mn^{2+} during the formation of Fe oxides. Similar but weaker oxidation ability of iron oxides compared with manganese oxides have been extensively reported (Pizzigallo et al. 1995, Pizzigallo et al. 1998).

1.2.2.4 Adsorption at Metal Oxide Surfaces

The adsorptive sites on all types of metal oxides to aqueous constituents are described as a valence-unsatisfied OH^- or a water ligand coordinated to a surface-bound metal ion (usually Fe^{3+}, Al^{3+}, or $Mn^{3+,4+}$). The chemical behavior of these surface bonding groups has been speculated based on the electron-withdrawing power of the metal cation(s) coordinated to the surface O (Figure 1.2, McBride 1994). For example, the terminal OH^- (an O bonded to one Al^{3+} and one H^+) is more likely to accept an additional proton in acid solution than the bridging OH^- (an O bonded to two Al^{3+} and one H^+) to form a positively charged Al-OH^{2+} site, since an additional Al^{3+} in the latter pulls away more electrons from the OH^- resulting in a less electron-rich O atom which in turn has less tendency to accept a proton. For the same reason, the terminal OH^- should also be less acidic than the bridging OH^- and more difficult to dissociate to the Al-O^- form. Moreover, a separate study confirmed that the terminal and bridging OH groups could interchange leading to substantial oxygen exchange between the dissociated water products (hydroxyls) and the oxygen anions in the surface (Henderson et al. 1998). The surface chemistry of methanol on metal oxides is very similar to that of water, with both molecules dissociatively adsorbed by breaking the O-H bond resulting in terminal species (-OH for H_2O and -OCH_3 for methanol) and bridging OH groups from proton transfer to a bridging O^{2-} site. The bridging and terminal oxygen exchange could even attribute to adsorption and transformation of methanol and potentially other complex organic alcohols at metal oxide surfaces, according to Henderson (2003).

Similar conclusion regarding to adsorption of phenolic compounds by metal oxides was also made by other studies. For example, adsorption of hydroquinone on Fe

oxide surface was investigated (Kung and McBride 1988). A shift was observed when comparing the FTIR spectra of hydroquinone before and after adsorption to hematite surface, which suggested that the molecule likely chemisorbed on the Fe oxide through one of the OH groups. Although not directly interacting with the oxide surfaces, the second *para*-OH group attached to the benzene ring increased the adsorption of hydroquinone compared to that of phenol, presumably for one of the following reasons: (1) it increased the electron-donating effect of the molecule and thus resulted in stronger metal-phenol monodentate complex formation; or (2) the adsorption of molecule to the surface could be assisted by H-bonding of the second OH group to surface OH groups of the oxide. Furthermore, the IR spectra of 2,4,6-trichlorophenol (TCP) sorbed on the surface of Mn oxides suggested that TCP was deprotonated in the adsorption process, and the adsorbed TCP either lost part of its aromatic character or formed an oxidation intermediate on the surface (Ukrainczyk and McBride 1993b).

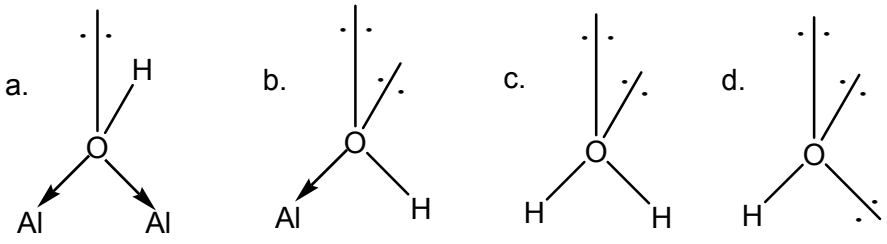

Figure 1.2. Schematic diagram of the oxygen atom in the bonding environment of (a) a bridging hydroxyl of an oxide, (b) a terminal hydroxyl of an oxide, (c) a water molecule, and (d) a free hydroxyl (OH^-) ion (adapted from McBride 1994). Note: the lines pointing to two dots simply indicate one lone pair of electrons in the O atom.

1.2.3 Metal Oxide-Facilitated Oxidation: Phenols and Anilines

1.2.3.1 Reaction Mechanism

Based on the experimental results for oxidation of substituted phenols by manganese(III) oxides, Stone (1987) proposed the following reaction mechanism for the reactions:

Precursor complex formation:

$$>Mn^{III} + ArOH \underset{k_{-1}}{\overset{k_1}{\rightleftharpoons}} (>Mn^{III}, ArOH) \quad (1)$$

Electron transfer:

$$(>Mn^{III}, ArOH) \underset{k_{-2}}{\overset{k_2}{\rightleftharpoons}} (>Mn^{II}, ArO\cdot) + H^+ \quad (2)$$

Release of phenoxy radical:

$$(>Mn^{II}, ArO\cdot) \underset{k_{-3}}{\overset{k_3}{\rightleftharpoons}} >Mn^{II} + ArO\cdot \quad (3)$$

Release of reduced Mn(II):

$$>Mn^{II} \underset{k_{-4}}{\overset{k_4}{\rightleftharpoons}} Mn^{2+} + (>Mn^{III}) \quad (4)$$

Coupling and further oxidation:

$$ArO\cdot + ArO\cdot \longrightarrow \text{quinones, dimers, and polymeric oxidation products} \quad (5)$$

A generic mass balance equation for oxide surface sites is:

$$S_T = [>Mn^{III}] + [Mn^{III}, ArOH] + [Mn^{II}, ArO\bullet] + [>Mn^{II}] \quad (6)$$

Their experimental data suggested that precursor complex formation and electron transfer were the rate-limiting steps (reactions 3-5 are fast) and that back electron transfer was negligible ($k_2 >> k_{-2}$), therefore

$$S_T \cong [>Mn^{III}] + [Mn^{III}, ArOH] \quad (7)$$

The rate of Mn oxide dissolution (i.e., generation of Mn^{2+} ions) could be expressed as follows:

$$v = d[Mn^{2+}]/dt = k_2[Mn^{III}, ArOH] \quad (8)$$

Assuming steady-state surface coverage for substituted phenols:

$$v = \frac{d[Mn^{2+}]}{dt} = \frac{k_1 k_2 S_T[ArOH]}{k_1[ArOH] + k_{-1} + k_2} \quad (9)$$

The relationship between substituted phenol concentration [ArOH] and dissolution rate v resembles a Langmuir adsorption isotherm. This mechanism explains reaction kinetics very well: reaction rates initially increase linearly with the increase in substituted phenol concentration, and eventually level out as the surface becomes saturated with phenols (the maximum rate is $v_m = k_2 S_T$) and electron transfer becomes the only rate-limiting step (when $k_1[ArOH] >> k_{-1} + k_2$).

A similar reaction mechanism has been proposed for oxidation of hydroquinone by iron oxides (McBride 1987). At Fe-oxide surfaces, a Fe(III)–hydroquinone complex forms followed by electron transfer and release of the oxidized molecules into solution:

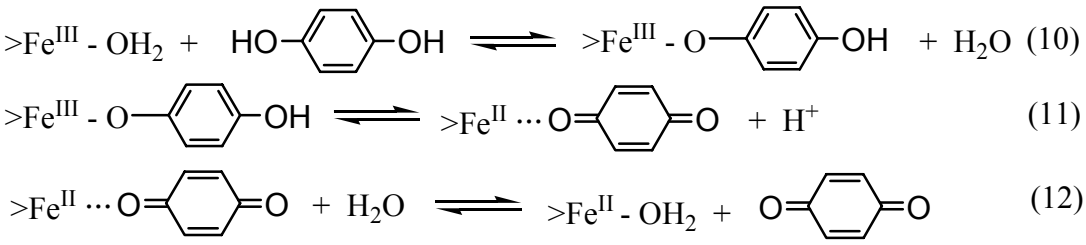

Despite the similar reaction schemes for iron and manganese oxides, one difference exists according to McBride (1987) in terms of the fate of the reduced metal ions. The surface Fe^{2+} can be quickly oxidized by O_2 back to Fe^{3+}, thus the iron oxide was acting as a catalyst for the oxidation of phenolic compounds by O_2 and little Fe^{2+} appeared in aqueous solution. In the case of Mn oxides, Mn^{2+} oxidation by O_2 is very slow except at very high pH, and significant quantities of Mn^{2+} were released into

solution and persisted throughout the oxidation experiments. Thus the Mn oxide was the primary oxidizing agent.

Precursor complex formation and radical mechanism were also believed to be involved in oxidation of aromatic amines by manganese dioxide as shown in Scheme 1.1 (e.g. Laha and Luthy 1990, Pizzigallo et al. 1998).

Scheme 1.1 (adapted from Laha and Luthy 1990):

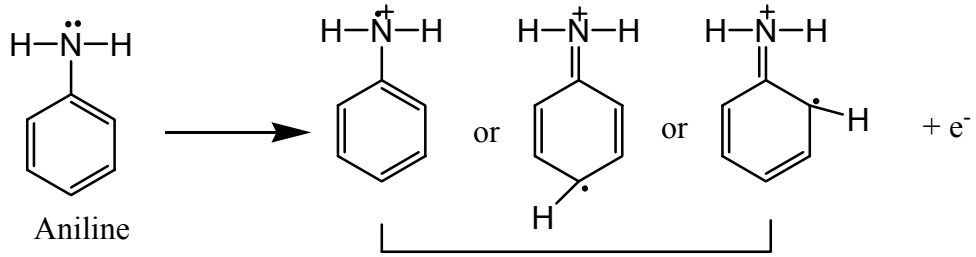

1.2.3.2 Reaction Products

Ukrainczyk and McBride (1993a) reported the oxidation products of chlorophenols with manganese oxides: the *para*-chlorinated phenols such as 4-chlorophenol, 2,4-dichlorphenol, 2,4,6-trichlorophenol, and 4-chloro-2-methylphenol yielded the corresponding *p*-benzoquinones as the detectable water-soluble oxidation products (Scheme 1.2); dimeric products were mainly adsorbed on the oxide surface as they were present only in the extracts obtained by washing the oxide with methylene chloride (Scheme 1.3). 2-Chlorophenol and 2,6-dichlorophenol didn't have any chlorine in the *para*-position and were found more difficult to oxidize, yielding diphenoquinones as the only detectable water-soluble products (Scheme 1.3). In addition, 2,4,6-trichlorophenol was found to be the only one to convert almost stoichiometrically to 2,6-

dichlorobenzoquinone (> 95% yield), with only minor dimeric and 2,6-dichlorohydroquinone products (Ukrainczyk and McBride 1993b). Similar reaction products of hydroquinone oxidation with Fe(III) oxides have also been demonstrated (McBride 1987).

Scheme 1.2. Water-soluble products of *para*-chlorinated phenols (adapted from Ukrainczyk and McBride 1993a):

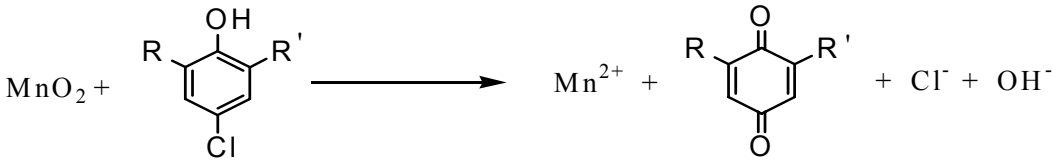

1a, 2a: R = R' = H
1b, 2b: R = Cl, R' = H
1c, 2c: R = R' = Cl
1d, 2d: R = CH_3, R' = H

Scheme 1.3. Dimeric products identified as oxidation products of 2,4-dichlorophenol (3-6), 2,4,6-trichlorophenol (7), 2-chlorophenol (8a, b), 2,6-dichlorophenol (5,9) and phenol (10). The C-O coupled dimeric products may be coupled at different positions (adapted from Ukrainczyk and McBride 1993a).

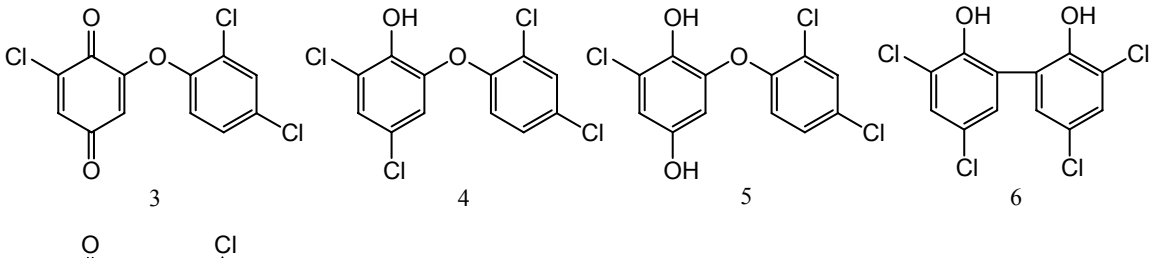

3 4 5 6

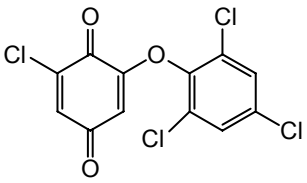

7

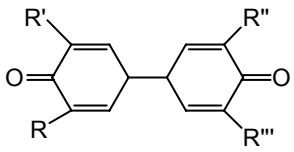

8a: R'=R"=Cl, R=R'"=H; 8b: R'=R'"=Cl, R=R"=H;
9: R=R'=R"=R'"=Cl; 10: R=R'=R"=R'"=H.

The dominant oxidation products of aniline and *p*-toluidine by manganese dioxide at pH 5 were azo-benzene and 4,4'-dimethylazobenzene respectively (Laha and Luthy 1990), forming after the generation of amine radicals (Scheme 1.4).

Scheme 1.4. (adapted from Laha and Luthy 1990):

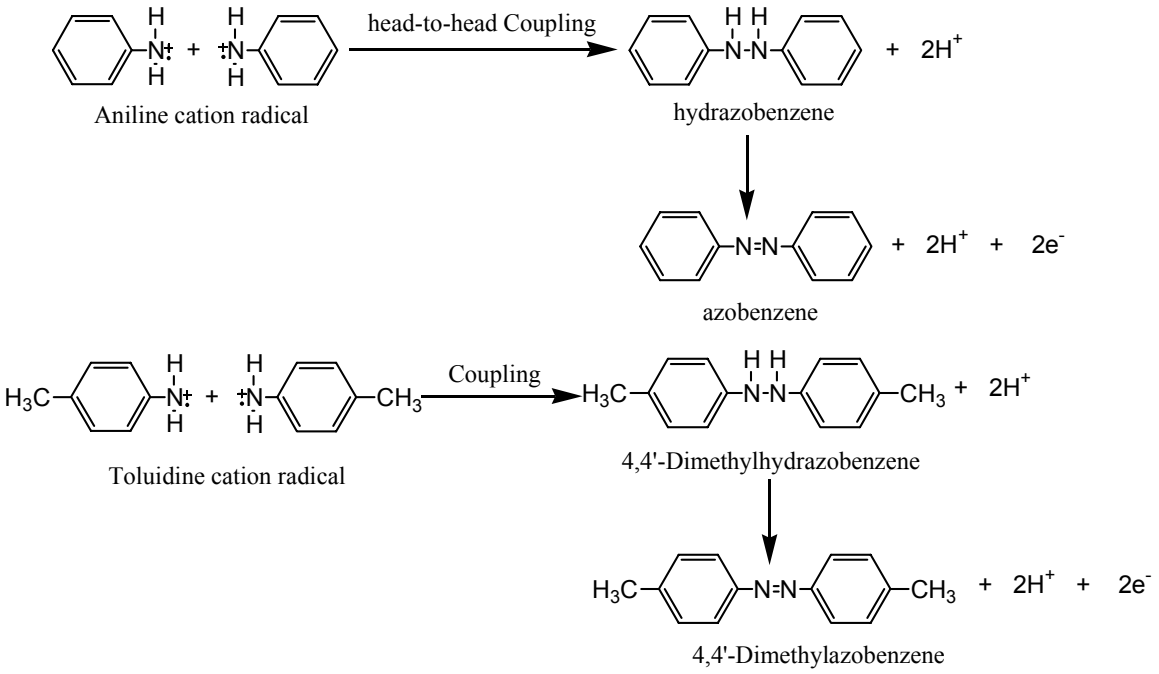

1.2.3.3 Effects of Various Factors on Reaction Kinetics

In the reactions between metal oxides and phenolic compounds, ring substituents affect the reactivity of reductants through steric, resonance, and field effects (Stone 1987, Klausen et al. 1997). Generally reaction rates decrease with decreasing half-wave potentials E^0 of substituted phenols and increasing Hammett constants of ring substituents. For example, carboxy, aceto, nitro, chloro, and other σ electron-withdrawing substituents (with high E^0 and positive Hammett constants) decrease the basicity (lower the pK_a) and thus the reactivity of phenol. Alkyl, alkoxy, and other σ electron-donating substituents (with low E^0 and negative Hammett constants) increase the

basicity and hence the reactivity of phenol. Steric effects could be neglected for simple *meta*- and *para*-substituted phenols, but have to be taken into account for bulkier molecules. Similar dependence of oxidation kinetics of aromatic amines on half-wave potentials and Hammett constants were also observed by Laha and Luthy (1990). In addition to the above factors, 2,4,6-trichlorophenol (TCP) was found to be surprisingly more reactive than phenol toward oxidation by Mn oxides despite the presence of three chloro- substituents that are electronegative and *ortho*- and *para*- deactivating. The possible reasons for the higher reactivity of TCP than phenol are: (a) a lower reduction potential of TCP than that of phenol; (b) the lower pK_a of TCP favors its depronation and thus adsorption at the Mn oxide-water interface; and (c) the stronger bond dipoles associated with the chlorines may promote the overall reaction rate (Ukrainczyk and McBride 1993b).

Significant differences exist in the chemical composition, surface area, mineralogy, and morphology of oxide particles which lead to drastically different reactivity of different oxides. Pyrolusite MnO_2, birnessite, and Fe (III) oxides (hydrated FeOOH) were studied as oxidants for oxidation of chlorophenols and chloroanilines (Pizzigallo et al. 1995, Pizzigallo et al. 1998). The effects observed are consistent with the general mechanism for a surface reaction involving precursor complex formation followed by a radical generation. Furthermore, it was found that birnessite was much more reactive than the other oxides with the reaction rates of chlorophenols and chloroanilines in the order birnessite >> pyrolusite > Fe (III) oxides. The oxidation power of birnessite toward chlorophenols and chloroanilines is in general comparable with that of oxidoreductive enzymes, which are considered to be important in

decontamination of natural environments. The higher reactivity of birnessite mainly comes from its amorphous structure and hence high surface area ranging from 262 to 277 $m^2\ g^{-1}$. The higher reactivity of birnessite is also related to its lower pH_{pzc} of 2.3 (pH_{pzc} for pyrolusite and Fe(III) oxides are 6.4 and 7.0, respectively), resulting in much higher adsorption and hence precursor complex formation within the studied pH range. Ukrainczyk and McBride (1992) also studied oxidation of phenol in acidic aqueous suspensions by three different types of Mn oxides: buserite in Na saturated form ($Na_4Mn_{14}O_{27}\bullet 9H_2O$), manganite (γ-MnOOH), and feitknechtite (β-MnOOH). The reactivity of the oxides were related initially to standard reduction potentials and to their stability and probably the ability to readsorb Mn(II) after the initial stage, following the order of feitknechtite > manganite > buserite during the initial stage and of buserite > manganite > feitknechtite after the initial stage, respectively.

In addition to aromatic ring structures and oxide properties, environmental factors such as pH, Mn(II) and other ion concentration and humic acid (HA) concentration also play an important role in affecting reaction rates (Stone 1987, Klausen et al. 1997). The reaction rates were strongly pH-dependent and increased with decreasing pH. This pH dependence has been attributed to: (1) protonation reactions that promote the formation of precursor complexes, and/or (2) increases in the protonation level of surface precursor complexes that increase rates of electron transfer (Stone 1987). Mn(II) ion, Ca(II) ion, humic acid (HA) and other organic solutes inhibited the oxidation of chlorinated phenols by Mn(IV) oxides for the following reasons (Klausen et al. 1997, Park et al. 1999): (1) adsorbed Ca(II) ions could block reactive Mn(IV) surface sites and thus inhibited the oxidation, and (2) Mn(II) ions, HA and other organic solutes could block surface sites as

well as reductively dissolve MnO_2 and thus form adsorbed Mn(II) that could result in slower reaction rates.

1.2.3.4 Reaction of Soil Samples containing Fe and Mn Oxides

A wide range of redox potentials (-0.4 V to +0.7 V) have been reported for whole soils (Table 1.1) (Sparks 1995). Although there is no direct comparison of these data with redox potentials for pure oxides (because it is not clear how the redox potentials of whole soils were measured), pure Mn and Fe oxides generally have higher oxidizing power with higher redox potentials (reduction potentials of 0.67 V, 1.50 V, and 1.23 V for FeOOH, MnOOH and MnO_2, respectively (Stone 1987)). Also in whole soils, the average reactivity of metals may be much lower than that of pure metal oxides because several amorphous forms of metals with a range of reactivies coexist in soils. Rather than dimerization or polymerization, the formed radicals may prefer to react with soil organic matter (SOM) functional groups which are not present in a pure mineral system. Additionally, there are less reactive sites available in whole soils for radicals to be close enough to polymerize. For all of the above reasons, caution needs to be exercised when extrapolating the results from pure oxides to the natural soil system.

In the oxidation studies of various substituted phenols, an actual soil sample - Palouse soil - was shown to be able to oxidize phenolic acids because of the presence of iron and manganese oxides (Lehmann et al. 1987). Palouse soil - fine-silty, mixed, mesic Pachic Ultic Haploxeroll - is a predominant agricultural soil in the wheat-growing region of the Pacific Northwest. Six phenolic acids reacted at different rates, depending on their structures, with oxidized forms of Fe and Mn in the Palouse soil. The conclusion was

drawn based on the following three observations: (1) reactivity of Palouse soil and of Palouse soil pretreated with LiOBr to remove organic matter were similar, showing the reaction being predominantly chemical not biological; (2) both Fe(II) and Mn(II) were detected as reaction products in the reaction solution; and (3) no reaction was observed if the Palouse soil was pretreated with a sodium dithionite-citrate solution to remove Fe and Mn oxides.

Upon amendment of birnessite with five natural sorbents having SOM of varied diagenetic properties, both "sorption" and "hysteresis" in adsorption and desorption isotherms of hydroxylated aromatic compounds were significantly increased. The authors attributed this to the enhanced coupling ability of hydroxylated aromatic compounds in the presence of an appropriate coupling catalyst, in this case, Mn oxide (Selig et al. 2003). Soil-catalyzed polymerization of phenolics in polluted water was also attributed to inorganic soil components such as Fe and Mn oxides (Colarieti et al. 2002).

For aromatic amines, in addition to their reversible sorption to soil surfaces by cation exchange and hydrophobic partitioning (Zachara et al. 1984, Zachara et al. 1986, Lee et al. 1997, Fabrega et al. 1998, Li et al. 2001), irreversible sorption and transformation in soils could occur through covalent binding to carbonyl moieties in organic matter and oxidative reactions leading to the generation of amine radicals which would further react to form various oxidation products (Li et al. 2000, Weber et al. 2001, Colon et al. 2002). The hypothesis that naturally-occurring soil manganese(III/IV) oxides/hydroxides play an important role in aromatic amine oxidation in whole soils was tested and it was concluded that oxidation by soil Mn did contribute partly to

immobilizing amines within organic matter and to the formation of large aromatic amine polymers (Li et al. 2003).

The catalytic role of Mn-minerals in whole soils to cause the formation of amine radicals was further proved (Li et al. 2000). The subsequent reaction of formed amine radicals with either other amine radicals to form polymers or with SOM through covalent bonding depended on the intrinsic properties of amines, with oxidative radical coupling observed only for amines with $E_{1/2} < 0.54$ V (e.g., *p*-methoxyaniline).

1.2.4 Oxidation Reactions Facilitated by Other Metal Oxides

Al oxides and even silica to a lesser extent, although not containing transition metals capable of acting as electron acceptors in redox reactions, could potentially promote the oxidation and polymerization of polyphenols in aqueous environments (reviewed in McBride et al. 1988). Complexation and catalyzed oxidative polymerization of catechol by Al^{3+} in acidic solution was reported; and it was believed that the surface of Al oxides in water might catalyze the oxidation of phenolic compounds by O_2 in a similar fashion (McBride et al. 1988). In addition, interaction of 1-naphthol with aluminum hydroxide ($Al(OH)_3$) was investigated (Karthikeyan et al. 1999). Instead of directly mediating oxidative polymerization of 1-naphthol, $Al(OH)_3$ serves as a surface sink for 1-naphthol oxidation products (i.e., naphthoquinones, generated from naphthol oxidation by reactive superoxide radicals in water). By removing the reaction products from solution, the $Al(OH)_3$ surface thus provides a driving force for further oxidation of 1-naphthanol.

1.3 Research Tasks and Methodology

Experiments were designed and conducted to achieve the research objective to understand the reaction kinetics and reaction mechanism of metal oxide (especially Mn and Fe oxides) facilitated oxidation of antibacterial agents including phenolic compounds (triclosan and chlorophene), fluoroquinolones, and aromatic *N*-oxides. Two principal methodologies were employed to achieve this goal: (i) structurally-related model compounds were selected with systematic variation in their structural components that were critical in identifying the reactive site(s), and (ii) reaction intermediates and end-products were identified by GC/MS, LC/MS, and/or IR spectroscopic techniques. In the case of no transformation but only adsorption of antibacterial agents toward metal oxides, adsorption isotherms were developed and speciation analysis was conducted.

Two representative metal oxides, δ-MnO_2 (birnessite) and α-FeOOH (goethite), were synthesized and characterized in order to evaluate the effects of surfaces on reaction kinetics and mechanisms. The reactivity of other metal oxides such as manganite (MnOOH) was also compared.

Solution pH is an important variable that affects speciation and reduction potential of reactants; thus the influence of pH on adsorption and reaction kinetics was investigated extensively. The effect of other environmental factors (e.g. the presence of co-solutes such as metal ions and natural organic matter) on reaction kinetics and product distribution was also evaluated in order to extrapolate the experimental results to more realistic natural environments. Analytical methods and experimental protocols for the studies of each group of antibacterial agents are discussed in detail in each chapter.

CHAPTER 2

OXIDATIVE TRANSFORMATION OF TRICLOSAN AND CHLOROPHENE BY MANGANESE OXIDES

2.1 Introduction

Triclosan (5-chloro-2-(2,4-dichlorophenoxy)phenol) and chlorophene (4-chloro-2-(phenylmethyl)phenol) are commonly used broad-spectrum antibacterial agents (Figure 2.1). Triclosan is widely used in many personal care (e.g., toothpaste, soaps, deodorants, shampoos, and cosmetics) and consumer (e.g., plastic kitchenware and footware) products while chlorophene is commonly used in hospitals and households for general cleaning and disinfecting. In a recent USGS study surveying the occurrence of emerging organic pollutants in surface streams, triclosan was one of the most frequently detected compounds with a median concentration of 0.14 μg/L (Kolpin et al. 2002). Others also reported detection of triclosan and its methyl derivative (a potential biotransformation product) in urban wastewater (Paxéus 1996, Lindstrom et al. 2002, McAvoy et al. 2002), surface water (Okumura and Nishikawa 1996, Lindstrom et al. 2002) and sediments (Okumura and Nishikawa 1996) and in fish (Okumura and Nishikawa 1996).

Several concerns have been raised about triclosan. As a biocide, triclosan blocks lipid biosynthesis by specifically inhibiting the enzyme enoyl acyl carrier protein reductase and may induce bacterial resistance development (McMurry et al. 1998, Levy et al. 1999,). Orvos et al. (2002) recently examined the toxicity of triclosan on various aquatic organisms and determined that certain algae species are the most susceptible organisms. Furthermore, triclosan may form chlorodioxins during heating and

incineration (Kanetoshi et al. 1987, Kanetoshi et al. 1988) and under the influence of sunlight (Kanetoshi et al. 1988, Latch et al. 2003).

Figure 2.1. Structures of triclosan and chlorophene.

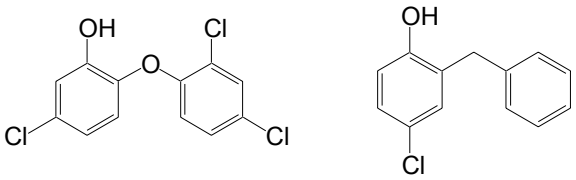

Triclosan Chlorophene

To properly assess the risks of triclosan and chlorophene, a better understanding of their environmental fate is imperative. Sorption to activated sludge and aerobic biodegradation have been suggested as the dominant mechanisms for high removal of triclosan (Federle et al. 2002, McAvoy et al. 2002). Direct photolysis was recently suggested as an elimination pathway for dissolved triclosan in sunlit lake water. The direct photolysis is much more important at pHs where triclosan is present in its phenolic form (reported pK_a at 7.9-8.1) (Lindstrom et al. 2002, Tixier et al. 2002). Triclosan and chlorophene are both relatively hydrophobic, with estimated log K_{ow} (octanol-water partition coefficient) of 4.86 and 3.99, respectively (ChemProp 2002). Because of their hydrophobic nature, triclosan and chlorophene are likely to partition to soils and sediments once entering the aquatic environment. Their reactions with metal oxides in soils and sediments may significantly impact their environmental fate, particularly when conditions are not suitable for biological or photochemical transformation.

Oxides of Mn, Fe and Al commonly found in soils and sediments have been shown in many previous studies to facilitate abiotic reactions of organic pollutants via hydrolysis, oxidation or reduction. As part of the dissertation assessing the potential reactions of triclosan and chlorophene with metal oxides, this chapter reports the transformation with manganese dioxide (MnO_2, similar to the naturally abundant birnessite) and manganite (MnOOH). Manganese (hydr)oxides in soils and sediments are probably one of the most important natural oxidants and play a critical role in affecting the transformation of organic pollutants including phenol, aniline, aliphatic amine and triazine compounds (Stone 1987, Laha and Luthy 1990, Ukrainczyk and McBride 1993a, Klausen et al. 1997, McArdell et al. 1998, Wang et al. 1999). Earlier work has shown

that manganese (hydr)oxides oxidize and promote polymerization of phenolic compounds (Stone and Morgan 1984, McBride 1987, Stone 1987, Ukrainczyk and McBride 1993a, Naidja et al. 1998). As will be shown later, both triclosan and chlorophene are highly susceptible to such transformation reactions.

In this study, experiments were conducted to determine the reaction kinetics and product formation. The influence of environmental conditions (e.g., pH) and the presence of co-solutes (e.g., metal ions and organic matter) on the reaction kinetics were also assessed. Based on the kinetic results and product identification, reaction schemes were proposed. Comparison of triclosan and chlorophene with structurally related substituted phenols was also conducted to assess relative compound reactivities.

2.2 Materials and Methods

2.2.1 Chemicals and Oxide Preparation

Reagent grade water (18.3 MΩ-cm resistivity) was prepared by a Barnstead Nanopure water system. Triclosan, chlorophene, phenol, 3-chlorophenol, 2,4-dichlorophenol, 2-methyl-4-chlorophenol, and 2-(3-chlorophenyl)-[1,4]benzoquinone were purchased from Aldrich (St. Louis, MO) at greater than 98% purity and used without further purification. Other employed chemical reagents including acetic acid, acetonitrile, L-ascorbic acid, 2-(cyclohexylamino)ethanesulfonic acid (CHES), HCl, HNO_3, methylene chloride, methanol, $MnCl_2$, 4-morpholinepropanesulfonic acid (MOPS), NaCl, $NaMnO_4$, and NaOH were obtained from Fisher Scientific (Fairlawn, NJ) or Aldrich (St. Louis, MO) at greater than 98% purity (for solids) or of HPLC and

GC/MS grade (for solvents), unless otherwise specified, and used without further purification.

Manganese dioxide (δ-MnO_2) was synthesized according to the method by Murray (1974). Briefly, 160 mL 0.1 M $NaMnO_4$ and 320 mL 0.1 M NaOH were added to 3.28 L N_2-sparged reagent water, followed by a drop-wise addition of 240 mL 0.1 M $MnCl_2$ (throughout a period of 3 hours) while keeping the solution constantly stirred. The solution was continuously stirred for another half hour after adding $MnCl_2$. The formed MnO_2 particles were allowed to settle and the supernatant was decanted and replaced with reagent water several times until the supernatant reached a conductivity of less than 2 $\mu S\text{-}cm^{-1}$. Finally, the volume of the oxide suspensions was adjusted to 2 L to yield final concentration of 0.02 M. The suspensions were stored at 4 °C and were diluted to appropriate concentrations in the experiments (typically 0.01 mM). A portion of the MnO_2 suspension was freeze-dried and the oxide surface area was determined to be approximately 255 m^2/g by the BET method of N_2 adsorption (Micromeritics). Powder X-ray diffraction analysis indicated that the synthesized MnO_2 is largely amorphous, consistent with the large surface area determined.

Manganite (MnOOH) synthesized according to the method by McArdell et al. (1998) was provided by Dr. A. T. Stone at the Johns Hopkins University. The synthesized MnOOH revealed an average manganese oxidation state of +3.0, morphology of fine needles, and *d*-spacings that are consistent with the mineral manganite (McArdell et al. 1998).

2.2.2 Reactor Setup

All glassware was soaked in 5 N HNO_3 and rinsed with reagent water thoroughly prior to use. Experiments were conducted in 25 mL screw-cap amber glass bottles with Teflon septa. The reaction bottles were continuously stirred on a magnetic stir plate in a 22 °C water basin. Reaction solutions were maintained at constant pH with 10 mM buffer: acetic acid/sodium acetate for pH 4-5, 4-morpholinepropanesulfonic acid (MOPS) and its sodium salt for pH 6-8, and 2-(cyclohexylamino)ethanesulfonic acid (CHES) and its sodium salt for pH 9-10. NaCl was added to all solutions to yield a concentration of 0.01 M. Stocks of triclosan, chlorophene, and related phenols were prepared in methanol at 1-2 mM, stored at 4 °C and used within a month of preparation. After 0.5 to 1 hour of stirring of suspensions containing manganese oxide, buffer, and constant ionic medium, reactions were initiated by adding a small amount of the organic reactant stock. As the reactions took place, changes of pH were no less than 0.05 log of units. Aliquots (1 mL each) were periodically collected for analysis. In the study involving various co-solutes, metal ions or the Suwannee River organic matter were allowed to equilibrate with suspensions containing Mn oxide, buffer and ionic medium for about 3 hours before the initiation of the reaction.

To monitor the reaction time course, three approaches were used to quench the reaction: (i) reaction aliquots were centrifuged (at 12000 rev/min for 20 min) using a Eppendorf 5415C Centrifuge and the supernatants were transferred to separate 2-mL cramp-top autosampler vials for later analysis, (ii) immediately after sampling, the reaction aliquots were added with excess amounts of 0.1 M L-ascorbic acid (10 fold of the initial MnO_2 loading) to convert the remaining Mn oxide to Mn^{II} ions. The reaction aliquots were then transferred to separate vials for later analysis, and (iii) immediately

after sampling, NaOH was added to the reaction aliquots to increase the pH to above 10 (preliminary studies indicated negligible degradation of triclosan by Mn oxides at pHs above 9). The amount of NaOH needed to increase the pH of the reaction suspension to above 10 under different initial pH's is listed in Table 2.1. The pH >10 aliquots were then centrifuged and the supernatants were transferred to separate vials for later analysis.

Preliminary studies were conducted to assess whether the presence of O_2 affected the degradation of triclosan with manganese oxides. Two sets of experiments under N_2-purging anoxic condition and non-N_2-purging air condition were compared, while keeping all other reaction conditions identical. Results showed that within the reaction time period (hours to several days), N_2 purging did not affect reaction rates and thus subsequent experiments were conducted without extra efforts to exclude O_2.

Table 2.1. The amount of 1 M NaOH needed to adjust the pH of the reaction suspension (20 mL) to > 10.0.

pH of the reaction suspension	1M NaOH needed (μL)
4.0	194
5.0	70
6.0	192
7.0	123
8.0	40

2.2.3 Analysis of Organic Reactants and Mn^{II} Ions

Decreases in the concentrations of triclosan, chlorophene and related compounds were monitored using a reverse-phase HPLC with a Zorbax XDB-C18 column (4.6 × 250 mm, 5 μm) and a diode-array UV detector at wavelength 220 nm (1100, Agilent Technology). The injection volumes were 100 μL. The mobile phase consisted of 65% acetonitrile and 35% 2 mM acetic acid solution at a flow rate of 1 mL/min. Compound concentrations were determined by running four levels of calibration standards.

Generation of Mn^{II} ions from reductive dissolution of manganese oxides was monitored using an inductively-coupled plasma (ICP) spectrometer (Thermo Jarrell Ash Trace Analyzer). At predetermined time intervals, samples of 5 mL were taken by 10-mL plastic syringes and passed through Millipore Durapore membrane filters (0.22 μm × 13 mm GVPP). The filtrate was then acidified to contain 1% HNO_3 and the emission of Mn^{2+} was measured at 257.61 nm using yttrium as the internal standard. The concentration of Mn^{2+} was determined by running Mn^{2+} calibration curves. Controls with only manganese oxide and pH buffers but without triclosan revealed that dissolution of manganese oxides did not occur in the absence of triclosan.

2.2.4 Analysis of Organic Products

For product identification, 80-120 mL of reaction suspensions containing the test organic reactant (0.01 mM) and MnO_2 (0.1 mM) were prepared at pH 5 (0.01 M pH acetic acid buffer and 0.01 M NaCl). Reactions were stopped after 1-4 days by adding ascorbic acid or centrifugation. Analyses indicated that the water-soluble products accounted only for a small fraction of the total products. Products adsorbed on the

manganese oxide were difficult to extract and were most adequately detected after dissolving manganese oxide by ascorbic acid. Despite that, similar products were observed by both quenching methods.

For GC/MS analysis, organics from the acid-quenched reaction solutions, the centrifugation supernatants, and manganese oxides were extracted in separatory funnels by shaking with 20 mL methylene chloride ($MeCl_2$) vigorously for 10 minutes. The $MeCl_2$ extract was then concentrated down to 1 mL under a gentle stream of N_2 gas. Controls with only organic reactants, NaCl and pH buffers but without manganese oxides were extracted in a similar fashion and yielded > 90 % extraction efficiency for triclosan, chlorophene, 2,4-dichlorophenol, and 2-(3-chlorophenyl)-[1,4]benzoquinone. Compounds were analyzed by a Hewlett-Packard GC/MS (6890/5973) with a HP-5MS 5% phenyl methyl siloxane capillary column (30m × 250μm × 0.25μm). The GC conditions were as follows: 1 μL splitless injection at 250 °C and the oven temperature from 70 to 280 °C at 10 °C/min followed by a 6-min hold at 280 °C with helium as the carrier gas at 1.2 mL/min. Electron impact ionization at 70 eV with mass scan range 35-550 m/z was conducted. The temperatures of the ion source and the transfer line were 250 °C. Parent compound standards prepared in $MeCl_2$ were analyzed to yield calibration curves. Peaks were identified by matching their chromatographic retention times and mass spectra with those of standards and the library.

For LC/MS analysis, ENVI-18 SPE (solid phase extraction) tubes (3 mL, Supelco) were used to extract organics from the acid-quenched reaction solutions and the filtrates of reaction solutions after passing through 0.5 μm glass-fiber filters. 5 mL acetonitrile was applied to elute organics from the cartridge and was subsequently blown

down to 1 mL under N_2 gas. For manganese oxides left on the filter, 10 mL acetonitrile was used to rinse the oxides and filter, followed by blowing down to 1 mL. Extraction of the control samples yielded extraction efficiency at 26%, 31% and 79% for triclosan, chlorophene, and 2-(3-chlorophenyl)benzo-[1,4]quinone, respectively. Compounds were analyzed by an Agilent LC/MS (1100/1100MSD) system with a Zorbax SB-C18 column (2.1 × 150 mm, 5μm). The injection volumes were 20 μL. The eluent consisted of two mobile phases at 0.20 mL/min: (A) 0.02 % acetic acid in 90/10 water/acetonitrile (v/v) and (B) acetonitrile. The gradient was as follows: B started at 10% for the first min, increased to 60% by 10 min, increased to 80% by 25 min, and increased to 100% by 25.01 min. Then the column was flushed by 100% B for 10 min followed by a 15-min post time which allowed reequilibration of the column. Electrospray negative ionization at fragmentor voltage 80-120 V with mass scan range 50-1000 m/z was conducted. The drying gas was operated at 10 mL/min at 325 °C. The nebulizer pressure was 30 psig and the capillary was set at 4000 V. Parent compound standards prepared in acetonitrile were analyzed to yield calibration curves. Peaks were identified by matching their chromatographic retention times with those of standards and by individual MS fragments. Raw LC/MS chromatograms and mass spectra are available in Appendix I for triclosan and its oxidation products and Appendix II for chlorophene and its oxidation products.

2.3 Results and Discussion

2.3.1 Kinetics of Triclosan and Chlorophene Oxidation by MnO_2

In the absence of manganese oxide, loss of triclosan or chlorophene was not detected after a week. In the presence of manganese oxide, oxidative degradation

occurred readily. A typical time course of triclosan oxidation by MnO_2 is shown in Figure 2.2, where the initial concentrations of triclosan and MnO_2 were 10 μM and 100 μM, respectively. Although the experiments were performed with a 10-fold excess of MnO_2, the loss of triclosan slowed down as the reaction progressed and deviated from the pseudo-first-order kinetics (Figure 2.2b). Such complex reaction kinetics were also observed in previous studies (Stone and Morgan 1984, Stone 1987, Laha and Luthy 1990, Ukrainczyk and McBride 1992, Klausen et al. 1997,) and were attributed to changing properties of manganese oxide as the redox reaction occurred. Thus, the initial reaction rates in mM-h^{-1} (*i.e.*, the slopes over the first few time increments in Figure 2.2a) and the initial rate constants k_{init} in h^{-1} (*i.e.*, the slopes within the time period where pseudo-first-order kinetics can be approximated in Figure 2.2b) were determined to evaluate the reaction kinetics. 95% confidence limits for the reaction rates and rate constants were also determined from the results of replicates.

The three approaches (centrifugation, ascorbic acid addition, and base addition) used to quench the reactions yielded similar k_{init} values for triclosan (1.76-1.90 h^{-1} at pH 5, Figure 2.3), indicating that all three methods are appropriate for determining the reaction kinetics. Compared to centrifugation, addition of ascorbic acid or sodium hydroxide quenched the reaction and also released the adsorbed triclosan from the oxide as shown by the higher triclosan concentrations detected by these two approaches (Figure 2.3). Comparison between centrifugation and ascorbic acid addition indicated that approximately 55% of triclosan was adsorbed to MnO_2 at pH 5. These results show that appreciable amounts of triclosan adsorb onto manganese oxide followed by the transformation reaction.

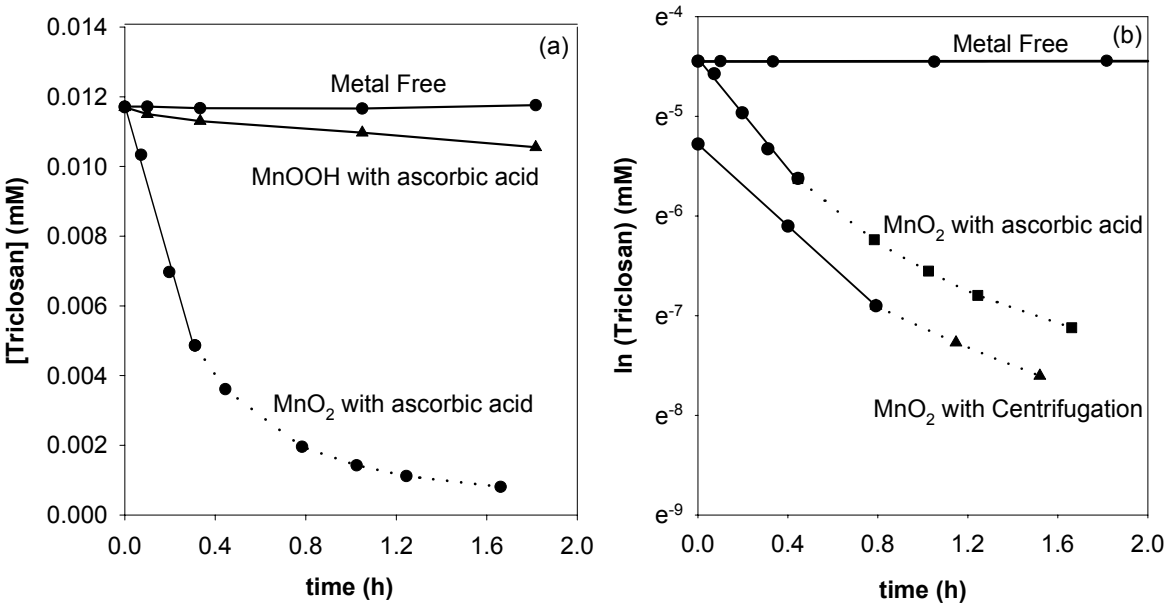

Figure 2.2. A time course of triclosan oxidation by MnO_2 and MnOOH: (a) triclosan concentration vs. time; (b) Logarithm of triclosan concentration vs. time. Reactions contained 100 μM MnO_2 or 1 mM MnOOH and 10 μM triclosan initially with pH 5 acetate buffer at 22 °C.

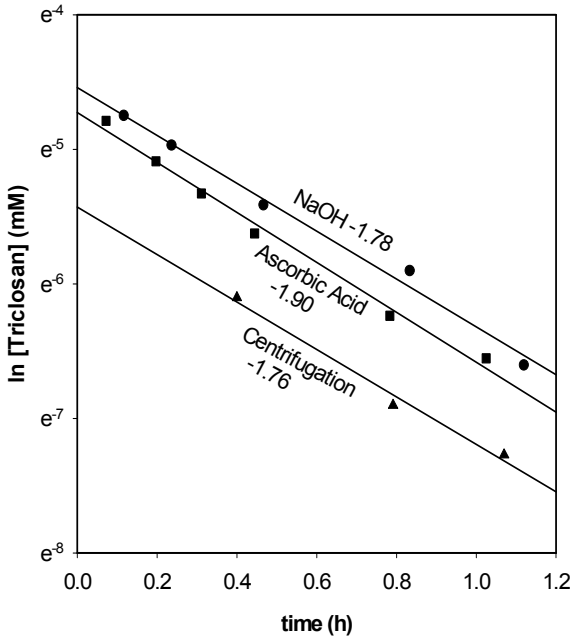

Figure 2.3. Logarithm of triclosan concentration vs. time determined by three different quenching methods: centrifugation, ascorbic acid addition and NaOH addition. The slope of linear regression is shown for each method. Reactions contained 100 μM MnO_2 and 10 μM triclosan initially with pH 5 acetate buffer at 22 °C.

Parallel to monitoring the triclosan loss, the production of Mn^{2+} ions from manganese oxide was also analyzed. Similar to previous studies (Stone and Ulrich 1989, Klausen et al. 1997), tests performed in this study also found strong adsorption of Mn^{2+} to manganese dioxide, *i.e.*, greater than 90% of the added Mn^{2+} adsorbed to 100 μM MnO_2 at pH 5 to 7. As a result, the measured Mn^{2+} concentration was lower than the triclosan loss throughout the reaction. Despite that, the k_{init} values for Mn^{2+} production (1.45 h^{-1}, after adsorption correction) and triclosan loss (1.74 ± 0.08 h^{-1}) were quite comparable. These results indicate that MnO_2 oxidizes triclosan leading to its reductive dissolution and that MnO_2 and triclosan are consumed at similar rates in the initial stage of the reaction.

The reaction kinetics were further investigated for the reaction orders with respect to the triclosan and manganese oxide concentrations and the influence of pH. Experiments were conducted by varying the initial triclosan concentration from 5 to 20 μM at each of three different MnO_2 loadings (20, 48 and 100 μM) (pH 5). The log of the initial reaction rate plotted versus the log of triclosan concentration yielded lines with slopes close to 1 (Figure 2.4). Experiments were conducted with the initial MnO_2 concentration from 20 to 100 μM and the triclosan concentration at 10 μM at pH 5. Plotting the log of the initial reaction rate versus the log of oxide concentration also yielded a line with a slope close to 1. These results indicate that the reaction is first-order with respect to triclosan and manganese oxide within the investigated conditions.

As shown in Figure 2.5a, pH markedly affected the reaction rate of triclosan oxidation by MnO_2. At both MnO_2 loadings, the log k_{init} decreased linearly as the pH was increased by the slope of -0.44 to -0.47, indicating that the reaction order is around 0.46 ±

0.03 with respect to H^+. Adsorption of triclosan to MnO_2 at different pHs was approximated by comparing the results from centrifugation and ascorbic acid addition as described earlier. Adsorption of triclosan to MnO_2 also decreased with increasing pH (Figure 2.5b). Over 55% of triclosan was adsorbed at pH 5 while only about 10% was adsorbed at pH 8.

Oxidation of chlorophene by MnO_2 showed very similar kinetics as triclosan. Under the conditions of 10 μM chlorophene and 100 μM MnO_2 at pH 5, the k_{init} for chlorophene was 2.67 ± 0.37 h^{-1}, comparable to that of triclosan. The log k_{init} of chlorophene decreased linearly by the slope of -0.50 as the pH was increased (Figure 2.6), indicating that the reaction order with respect to H^+ is 0.50. Because of their similar kinetic trends and product formation as discussed later, triclosan and chlorophene are likely oxidized by MnO_2 via similar mechanisms. Although the reaction orders were not determined experimentally, it is reasonable to assume that chlorophene oxidation is also first-order with respect to both chlorophene and MnO_2.

Based upon the kinetic results, the initial rate of triclosan or chlorophene oxidation by MnO_2 can be described by the following kinetic expression:

$$\text{Initial rate} = -\frac{d[\text{Antibacterial}]}{dt} = k_{init}[\text{Antibacterial}] = k_{\exp}[\text{Antibacterial}][MnO_2][H^+]^{0.46-0.50} \quad (1)$$

From the values of k_{init} at various initial MnO_2 loadings and pHs, the third-order rate constant k_{exp} (applicable within the employed experimental conditions) was computed to be 1.82 (± 0.37) × 10^6 $M_{MnO_2}^{-1} \cdot M_{H^+}^{-0.46} \cdot h^{-1}$ (the number of replicates n = 20) for triclosan and 3.50 (± 0.78) × 10^6 $M_{MnO_2}^{-1} \cdot M_{H^+}^{-0.50} \cdot h^{-1}$ (n = 9) for chlorophene.

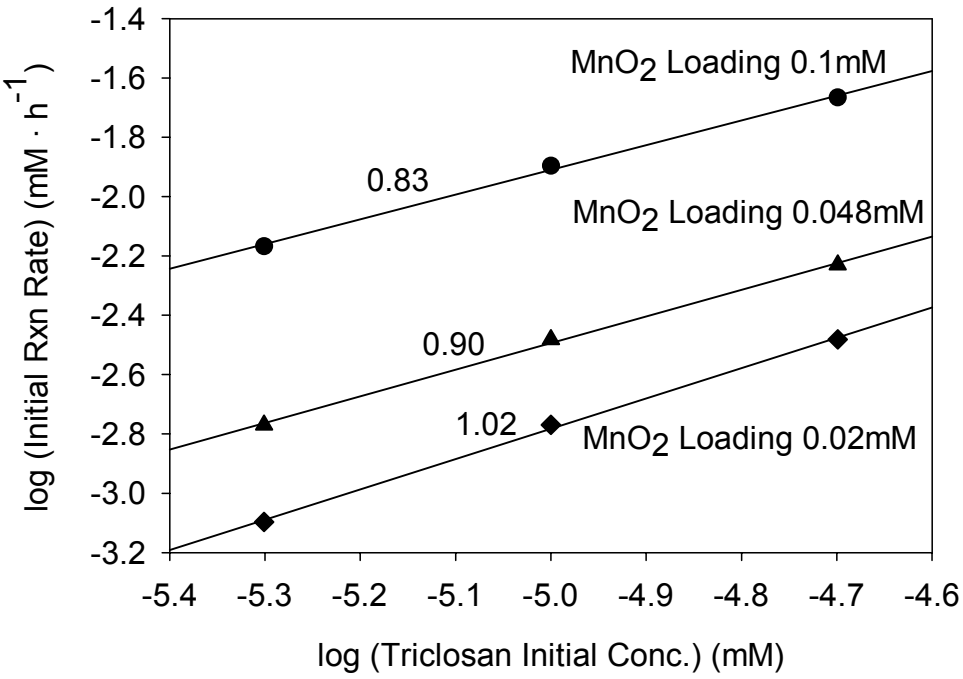

Figure 2.4. Oxidation of triclosan by MnO_2: the reaction order with respect to triclosan. Reaction contained 0.01 M pH 5 acetate buffer and 0.01 M NaCl and 22 °C.

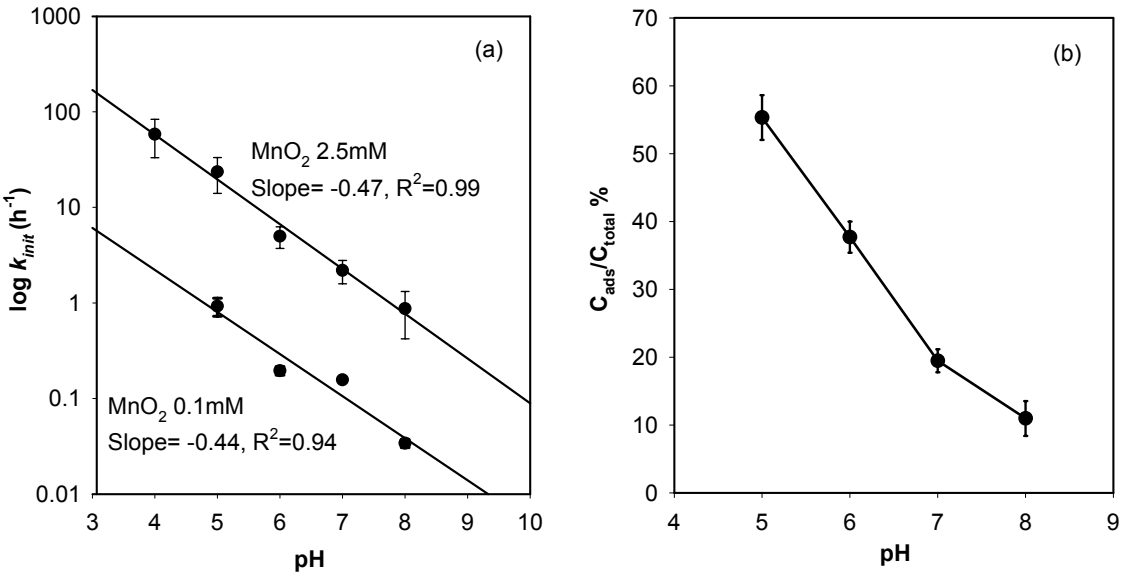

Figure 2.5. (a) Effect of pH on triclosan oxidation at two different initial MnO_2 loadings; (b) Effect of pH on the adsorption of triclosan to 100 μM MnO_2. Reactions contained 10 μM triclosan initially at 22 °C.

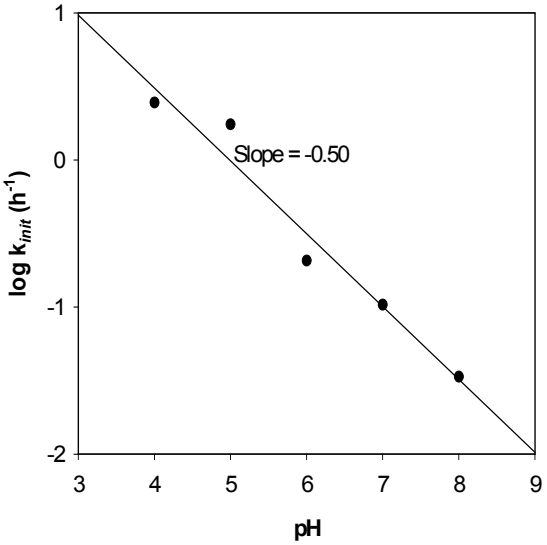

Figure 2.6. Effect of pH on chlorophene oxidation by MnO_2. Reaction contained 10 μM chlorophene and 100 μM MnO_2 initially with 0.01 M pH buffer at 22 °C.

2.3.2 Surface Reactions

Overall, the kinetic trends of triclosan and chlorophene oxidation by MnO_2 are in good agreement with previous studies on the oxidation of hydroquinone, substituted phenols and substituted anilines by manganese oxides (Stone 1987, Stone and Morgan 1984, Laha and Luthy 1990, Klausen et al. 1997,). A surface reaction kinetic model was proposed by Stone (1987) for the oxidation of organics at manganese oxide surfaces and is likely suitable to describe the reactions of triclosan and chlorophene. For the redox reaction to occur, formation of a precursor complex between the organic reductant and the oxide bound Mn^{IV} is necessary. Electron transfer occurs at the closely associated precursor complex followed by release of the organic oxidation products and Mn^{2+} from the oxide. The precursor complex formation and electron transfer are likely to be rate-limiting.

Properties of organic reductants and manganese oxide affect the precursor complex formation and electron transfer reactions. The precursor complex formation is also affected by the concentrations of organic reductant and manganese oxide. At a fixed amount of triclosan, the initial reaction rate increased linearly as expected with increasing amount of MnO_2 because the number of active surface sites and consequently formation of precursor complex were increased. Similarly the results also showed that at a fixed amount of MnO_2, the initial reaction rate increased linearly with increasing triclosan concentration, indicating that the triclosan concentrations employed in this study were below the point of saturating the oxide surface because once the surface sites are saturated with organic, addition of more organic reductant will not increase the formation of precursor complex and the reaction rate. The actual number of active surface sites on

the MnO_2 is not known. The slowing reaction rate even with an excess amount of MnO_2 suggests that the number of active sites which determine the initial reaction rate of triclosan is relatively small. Furthermore, the transformation products of triclosan and MnO_2 may block or react with the oxide surface and thus as more products are formed, the greater the effect in inhibiting the reaction (see more discussion in the following section).

A constant reaction order with respect to H^+ was observed in the oxidation of triclosan and chlorophene. This is in contrast to the results found in the oxidation of substituted phenols where the order with respect to H^+ decreases from 1.3 to 0.45 between pH 7 and pH 4.4 (Stone 1987). Compared to the study by Stone (1987), this study employed a considerably lower organic reductant to manganese oxide ratio (0.1 vs. 1.6-2.8) and utilized a slightly different manganese oxide preparation procedure. These factors may contribute to the different pH dependence observed.

The strong pH dependence of the reaction rate can be attributed to the effect of pH on the adsorption of triclosan to the oxide surface (*i.e.,* precursor complex formation) and on the electron transfer reaction. Deprotonation of triclosan (pK_a = 7.9 to 8.1, Lindstrom et al. 2002, Tixier et al. 2002) becomes significant when solution pH is near or higher than 8. The result that adsorption of triclosan decreased as pH was increased from 5 to 8 (Figure 2.5b) indicates that deprotonated triclosan does not adsorb to MnO_2 as strongly as the protonated form. Using the reported pH_{zpc} (zero point of charge) of 2.4 for δ-MnO_2 (Murray 1974), most oxide surface is negatively charged under the experimental conditions and the negative charge decreases as pH decreases. The observed adsorption trend suggests that lowering the solution pH creates a greater

number of surface species that favor interaction with triclosan. For electron transfer, protons are required for reduction of MnO_2 to release Mn^{2+} ions (*i.e.,* ½ $MnO_{2(s)}$ + 2 H^+ + $e^- \rightarrow$ ½ $Mn^{2+}_{(aq)}$ + H_2O). When pH is decreased from 8 to 4, the reduction potential of MnO_2 (E°(pH)) increases from 0.76 V to 0.99 V (Stumm and Morgan 1996). In addition to the increased reduction potential for the oxidant at lower pH, protonation of the precursor complex may also facilitate the electron transfer reaction. The constant reaction order with respect to H^+ observed in this study suggests that the reaction mechanism did not change as a function of pH within the investigated conditions (Klausen et al. 1997).

2.3.3 Effect of Oxide Properties and Co-Solutes on the Reaction Rate

Selected experiments were conducted on the reaction of triclosan with MnOOH (manganite). In general, triclosan oxidation by MnOOH was slower than by MnO_2 even when a higher loading of MnOOH was employed (Figure 2.2a). When equal amounts of oxides were employed (250 μM oxide and 10 μM triclosan at pH 5), the k_{init} of triclosan oxidation were 23.60 h^{-1} and 7.16×10^{-2} h^{-1} for MnO_2 and MnOOH, respectively. The synthesized MnO_2 is predominately amorphous while MnOOH is more crystalline. The faster reaction rate by MnO_2 is likely due to its large surface area (~255 m^2/g) and highly amorphous nature, rendering the active surface sites more accessible to the incoming organics. The abundance and reactivities of the surface sites may also differ between the two oxides.

As shown in Table 2.2, addition of metal ions and the Suwannee River organic matter considerably decreased the reaction rate of triclosan oxidation by MnO_2. The

inhibitory effect increased as the co-solute concentration was increased, although not in a linear fashion. The presence of low concentrations (at 5% MnO_2 concentration) of Mn^{2+}, Zn^{2+} and Ca^{2+} ions decreased the reaction rate by 41%, 22% and 14%, respectively. Addition of 5 mg/L of the organic matter decreased the reaction rate by 14%. In a river water matrix that was filtered (0.5 μm glass fiber filters) and buffered at pH 5, the reaction rate was slower by 83% than that in reagent water.

As mentioned earlier the number of active surface sites is likely limited, thus small amounts of co-solutes compared to the total added MnO_2 can still cause a significant inhibitory effect by blocking some of the active surface sites. The inhibitory effect of Mn^{2+} is considerably greater than $Zn^{2+}$and Ca^{2+}. Compared to Zn^{2+} and Ca^{2+}, Mn^{2+} adsorbs more strongly to MnO_2 (Morgan and Stumm 1964). Furthermore, the adsorbed Mn^{2+} may oxidize or precipitate at the manganese oxide surfaces and thus block the surface sites (Wersin et al. 1989, Fendorf et al. 1992, Junta and Hochella 1994). Since Mn^{2+} is a reaction product, it likely contributes to the slowing rate observed as the reaction progresses (*i.e.,* an auto-inhibiting effect). The Suwannee River organic matter probably inhibits the reaction by adsorbing and reacting with MnO_2 since humic material is known to adsorb and reductively dissolve manganese oxides (Tipping and Heaton 1983, Sunda and Kieber 1994). The slower rate of triclosan oxidation in the river water is likely caused by a combination of inhibitory effects from dissolved metal ions, natural organic matter and other inorganic anions such as phosphate (Stone and Morgan 1984).

Table 2.2. The initial rate constant k_{init} (h^{-1}) of triclosan oxidation by MnO_2 in various aqueous matrices. Reaction mixtures contained 10 μM triclosan and 100 μM MnO_2 initially with pH 5 acetate buffer at 22 °C. $MnCl_2$, $CaCl_2$, $ZnCl_2$ or the Suwanee River organic matter was added to the reactions.

Matrix	k_{init}			Matrix	k_{init}
Reagent water	1.74 ± 0.08			River water	0.30
M^{2+}(%)[a]	$k_{init}(Mn^{2+})$	$k_{init}(Ca^{2+})$	$k_{init}(Zn^{2+})$	NOM (mg/l)	k_{init}(NOM)
0.1	1.66	-	1.60	5	1.50
0.5	1.65	-	1.59	10	1.12
1	1.60	1.66	1.55	15	0.68
5	1.03	1.50	1.36		
10	0.50	1.51	1.12		
20	-	1.39	-		

a. % of the initial MnO_2 concentration

2.3.4 Oxidation Products of Triclosan

Using solvent extraction and GC/MS analysis, one major and two minor products were detected (Figure 2.7a). The minor product at 5.67 min was 2,4-dichlorophenol. The products at 16.89 min and 17.67 min showed highly similar spectra and a difference of 2 in the m/z ratios of their molecular and the second largest fragment ions (Figure 2.7c and 2.7d), indicating that these two compounds are quinone and hydroquinone of a base structure (Letzel et al. 1999). The spectra indicate that the products are *p*-quinone and *p*-hydroquinone of triclosan, *i.e.,* 2-chloro-5-(2,4-dichlorophenoxy)-[1,4]benzoquinone (A) and 2-chloro-5-(2,4-dichlorophenoxy)benzene-1,4-diol (B). The assignment of the fragment ions from A is shown in Figure 2.7c. Formation of the m/z 185 fragment supports *para*- rather than *ortho*-position for the quinone. In addition, a trace amount of 2,7-dichloro-dibenzo[1,4]dioxin impurity was found in the triclosan control samples (without MnO_2). This amount did not increase after reaction with MnO_2 and other dioxin compounds were not detected.

Because 2,4-dichlorphenol was detected as a product and could also be oxidized by MnO_2, an important question was invoked as to whether the observed products are resulted directly from triclosan or from 2,4-dichlorphenol as an intermediate. Experiments were thus conducted to investigate the oxidation of 2,4-dichlorophenol by MnO_2 and analysis showed a major dimeric product of 2-chloro-6-(2,4-dichlorophenoxy)-[1,4]benzoquinone (C) (Figure 2.8a and 2.8b). The product C was identified previously by Ukrainczyk and McBride and was likely formed by oxidation and coupling of two 2,4-dichlorophenol molecules (Ukrainczyk and McBride 1993a). Product A and C showed nearly identical spectra (Figure 2.7c and 2.8b). When mixed

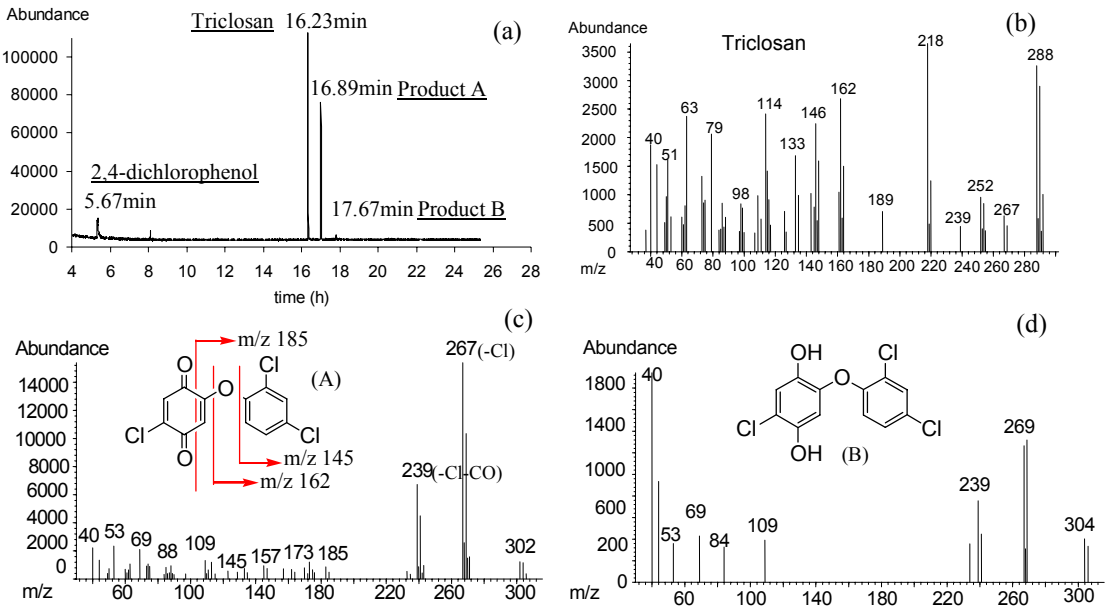

Figure 2.7. Oxidation of triclosan analyzed by GC/MS. (a) The chromatogram of triclosan reaction extract; (b)-(d) The mass spectra of triclosan, product A and product B. The fragmentation of product A is depicted in (c).

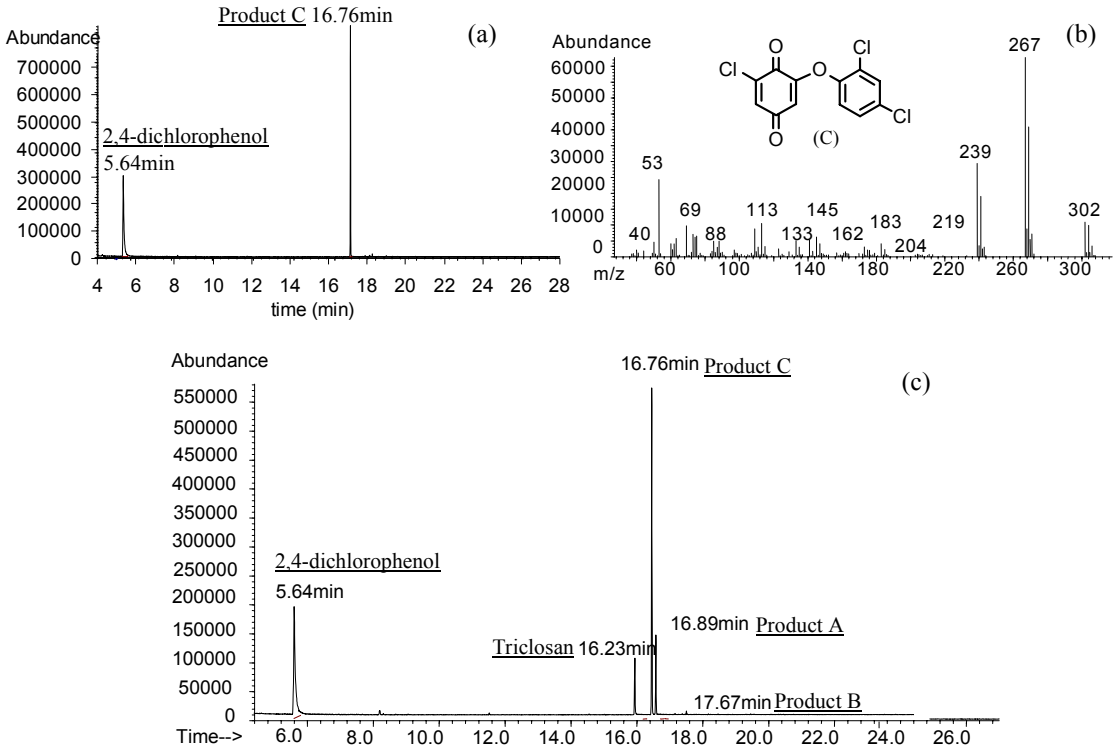

Figure 2.8. Oxidation products of 2,4-dichlorophenol analyzed by GC/MS. (a) The chromatogram of 2,4-dichlorophenol reaction extract; (b) The mass spectrum of product C; (c) The chromatogram of the mixture of triclosan and 2,4-dichlorophenol reaction extracts.

together, A and C yielded two distinct peaks on the GC/MS (Figure 2.8c). These results strongly suggest that A and C are isomers, resembling each other except for the position of chlorine substituent on the quinone ring. These observations confirm that the (hydro)quinone products of triclosan are produced from oxidation of the phenol moiety of triclosan by MnO_2, rather than from oxidation of 2,4-dichlorophenol intermediate. Detection of 2,4-dichlorophenol as a product suggests bond breaking of triclosan during the redox reaction. Such bond breaking, however, accounts for only a small percentage of the overall reaction since 2,4-dichlorophenol was detected at a small amount (<1% of triclosan loss) and its oxidation products were not detected in triclosan oxidation (Figure 2.7a).

Authentic standards of products A and B are not available. Instead, a structurally related quinone, 2-(3-chlorophenyl)-[1,4]benzoquinone, was used as a surrogate standard to quantify A. The quantity of A was estimated to be less than 5% of the triclosan loss. The quantity of product B, although not estimated, is likely to be even smaller based upon the considerably smaller MS response (Figure 2.7a). These results indicate that (hydro)quinone production is not the primary pathway of triclosan oxidation by MnO_2. Products from other reaction pathways are likely present but are unable to be detected by the GC/MS method.

Further investigation of the oxidation products was conducted by LC/MS after solid-phase extraction. As shown in Table 2.3, several more products were detected in addition to 2,4-dichloropenol and product B. The molecular weights of several products indicate that they are dimeric products of triclosan. The molecular weight of 574

Table 2.3. Oxidation products of triclosan analyzed by LC/MS. Each compound's chromatographic retention time, $[M-H]^-$ molecular ion and mass spectrum are listed.

#	RT (min)	$M-H^-$	Compound	m/z
1	12.53	328	-	**328**(330, 332), 171(35%)
2	14.52	468	-	468(60%, 470, 472, 474), **241**
3	15.69	161	2,4-di	357(10%, 359, 361), **161**(163, 165), 143(50%)
4	15.75	377	-	377(95%, 379, 381), **349** (351, 353)
5	16.63	303	product B	**303**(305, 307), 267(100%, 269, 271)
6	19.93	332	-	**332**(334, 336, 338), 293(66%)
7	21.43	287	triclosan	571(5%), **287**(289, 291, 293), 253(15%, 255, 257)
8	26.93	571	dimeric product	**571**(573, 575, 577), 339(72%), 321(15%), 636(6%)
9	27.77	573	dimeric product	**573**(575, 577, 579, 581), 339(25%), 541(10%), 161(5%, 163)
10	30.47	573	dimeric product	573(10%, 575, 577, 579, 581), **227**, 161(5%, 163)
11	31.42	573	dimeric product	**573**(28%, 575, 577, 579), 539(10%), 339(15%)

Note: Each bolded data corresponds to the base peak in each mass spectrum; 2,4-di represents 2,4-dichlorophenol.

corresponds to the adduct of two triclosan molecules after loosing two hydrogen atoms and the molecular weight of 572 corresponds to the quinone of a triclosan dimeric product. Detection of dimeric products of triclosan indicate that beside oxidizing triclosan to hydroquinone and quinone counterparts, manganese oxide also promotes dimerization and potentially polymerization of triclosan likely via radical reactions.

2.3.5 Oxidation Products of Chlorophene

Oxidation products of chlorophene were also studied by both GC/MS and LC/MS. Similar to the results of triclosan, the GC/MS analysis indicated that the products are *p*-quinone and *p*-hydroquinone of chlorophene (*i.e.,* 2-benzyl-[1,4]benzoquinone (D) and 2-benzyl-benzene-1,4-diol (E), Figure 2.9). Similarly, formation of the m/z 115 fragment supports *para*-position for the quinone (Figure 2.9c). Using the surrogate quinone standard, the quantity of product D was estimated to be 3-4% of the chlorophene loss, similar to the percentage of product A to triclosan loss. The LC/MS analysis showed the presence of a variety of products in addition to product E (Table 2.4). The molecular weights of most of the products correspond to dimeric products of chlorophene, indicating that MnO_2 promotes chlorophene dimerization and potentially polymerization. Unlike the detection of 2,4-dichlorophenol in triclosan oxidation, no breakdown products of chlorophene were observed. Compared to the ether linkage of triclosan, the alkyl linkage between the two benzene rings of chlorophene is resistant to substitution and thus are difficult to break under the experimental conditions.

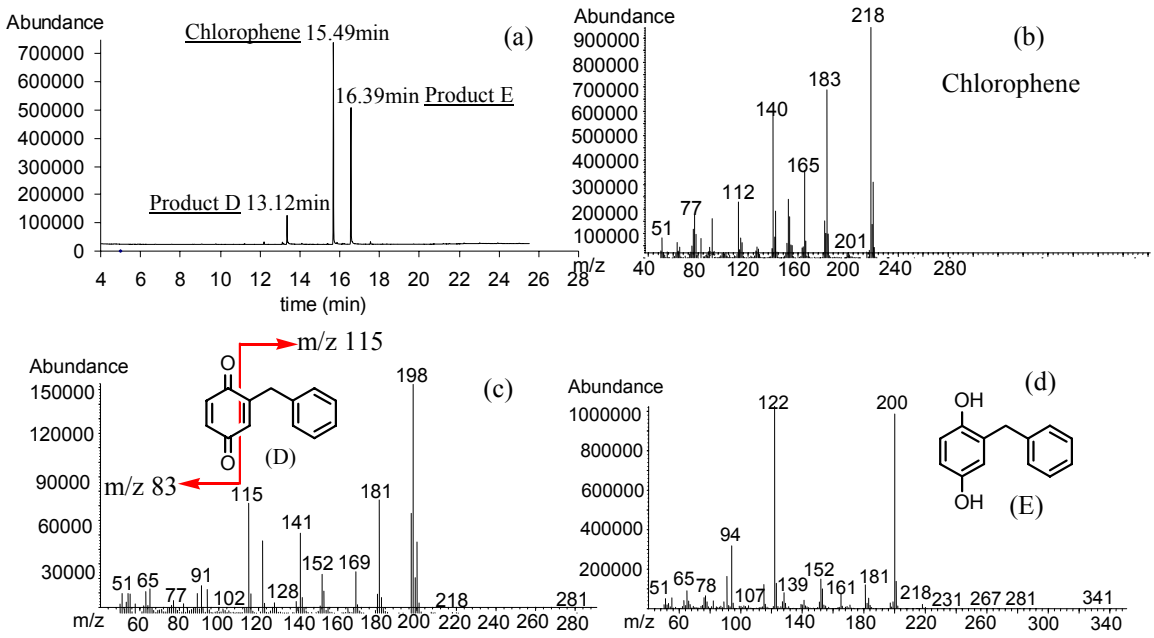

Figure 2.9. Oxidation products of chlorophene analyzed by GC/MS. (a) The chromatogram of chlorophene reaction extract; (b)-(d) The mass spectra of chlorophene, product D and product E.

Table 2.4. Oxidation products of chlorophene analyzed by LC/MS.

#	RT (min)	$M\text{-}H^-$	Compound	m/z
1	14.54	199	product E	**199**(198, 200), 108(12%)
2	17.30	397	dimeric product	397(60%, 398), 297(15%), **233**(235), 197(8%), 141(10%)
3	18.99	395	dimeric product	**395**(397, 399), 304(65%), 217(15%, 219), 265(10%)
4	19.61	217	chlorophene	**217**(219)
5	21.66	415	dimeric product	**415**(417), 325(35%), 233(8%)
6	22.91	415	dimeric product	415(15%, 417), **379**(380)
7	23.97	415	dimeric product	**415**(417), 262(70%, 264)
8	26.52	413	dimeric product	**413**(415), 325(45%)
9	27.35	415	dimeric product	**415**(417), 451(8%), 325(8%)
10	27.73	415	dimeric product	415(60%, 417), **399**(401), 321(10%), 325(10%)
11	28.87	413	dimeric product	449(30%, 451, 453), **413**(415), 339(45%)
12	30.20	597	-	**597**(599, 601), 339(10%)
13	32.95	433	dimeric product	631(30%, 633), **433**(435, 437), 232(15%, 234)

Note: Each bolded data corresponds to the base peak in each mass spectrum.

2.3.6 Reaction Schemes

Based on the observed surface reaction kinetics, product identification and literature on the oxidation of phenolic compounds by oxygen and metal complexes (Shukla et al. 1996, Alfassi 1999, Chauhan et al. 1999, Wiater et al. 2000), the reaction scheme for triclosan oxidation by manganese oxide is proposed in Figure 2.10. Initially triclosan is bound to the surface Mn^{IV} to form a precursor complex. The phenol moiety of triclosan is then oxidized by Mn^{IV} to lose an electron, forming a phenoxy radical. Accordingly the Mn^{IV} is reduced to Mn^{III} and further to Mn^{II} likely through reaction with another triclosan or radical. The phenoxy radical is stabilized by electron resonance within the phenol ring. Further reactions of the phenoxy radicals may occur via three different pathways.

Pathway I is coupling of two phenoxy radicals to yield dimeric products. The coupling reactions most likely occur via C-C or C-O coupling at the *ortho* or *para* positions (Alfassi 1999, Wiater et al. 2000). At least three coupling products (m/z 573) were detected in the product identification and their probable structures are shown in Figure 2.10. Further polymerization is possible; however polymeric products were not detected likely because of low concentrations. Pathway II involves one-electron oxidation of the phenoxy radical by manganese oxide to form hydroquinone B. Further two-electron oxidation of hydroquinone B yields the quinone A. Formation of hydroquinone and quinone accounts for less than 5% of triclosan oxidation. This is consistent with the additional electron transfer reactions required to yield these products. The coupling products may also be subjected to further oxidation to form hydroquinone and quinone products. For instance, oxidation of a dibenzohydroquinone product (m/z

573) to dibenzoquinone (m/z 571) is shown in Figure 2.10. Pathway III involves cleavage of the ether bond of phenoxy radical, possibly via *o*-dealkylation (Urano et al. 1996, Brooks et al. 1999), to yield 2,4-dichlorophenol and other products. Overall, the experimental results suggest that triclosan oxidation by manganese oxide occurs predominantly via pathway I and to a lesser degree pathway II. Pathway III is the least important in the overall reaction.

The reaction scheme of chlorophene oxidation by MnO_2 is believed to be similar to Figure 2.10 because the kinetics and product formation are very similar to those of triclosan. Pathway III, however, can be excluded since breaking of the benzyl linkage of chlorophene does not occur. The reaction pathway II leads to product D and E. The reaction pathway I leads to coupling products of chlorophene. Compared to triclosan, chlorophene exhibits higher complexity in coupling product formation. This is likely due to the fact that the *p*-Cl substituent of chlorophene is susceptible to substitution by hydroxide and consequently increases the variety of product formation. Some plausible structures for the dimeric products of chlorophene are shown in Figure 2.11. The detection of an m/z 597 product for chlorophene suggested that polymerization likely occurred.

Overall, the results show that triclosan and chlorophene oxidation by manganese oxide occurs at their phenol moieties via mechanisms similar to those of substituted phenol oxidation. Dimerization and potentially polymerization occur readily despite the presence of somewhat large substituents (*i.e.*, dichlorophenoxy and benzyl substituents) on the phenol rings of triclosan and chlorophene.

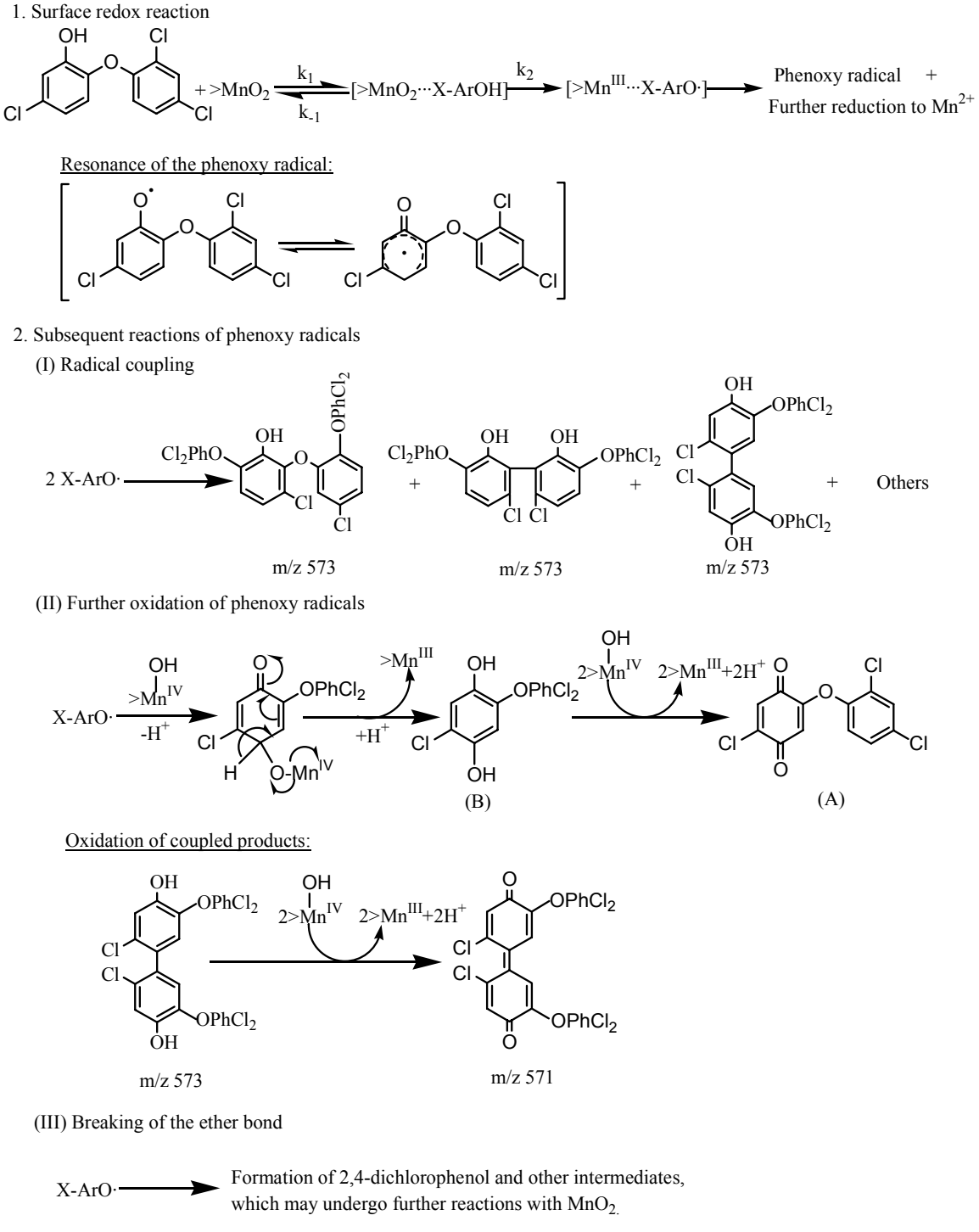

Figure 2.10. Proposed reaction scheme for oxidation of triclosan by MnO_2.

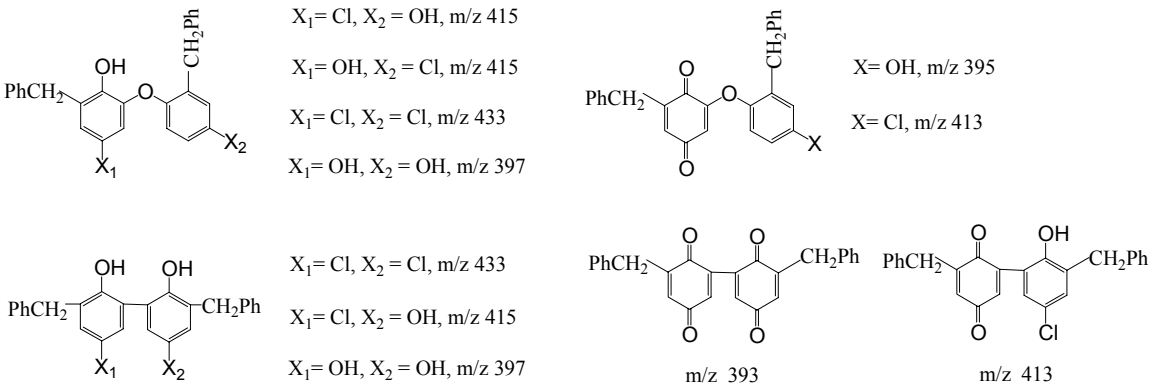

Figure 2.11. Plausible structures for the dimeric products of chlorophene oxidation by MnO_2.

2.3.7 Comparison of Triclosan, Chlorophene and Simple Substituted Phenols

To evaluate the reactivities of triclosan and chlorophene, oxidation of 2-methyl-4-chlorophenol, 2,4-dichlorophenol, 3-chlorophenol, and phenol by MnO_2 was investigated for comparison (Table 2.5). These simple substituted phenols are structurally related to the phenol moieties of triclosan and chlorophene. The results show that triclosan and chlorophene have comparable or higher reactivities than the related substituted phenols (*i.e.*, triclosan ≈ chlorophene ≈ 2-methyl-4-chlorophenol > 2,4-dichlorophenol > phenol > 3-chlorophenol).

Substituents on the aromatic ring affect phenol reactivity by electronic (resonance and inductive) and steric effects (Morrison and Boyd 1987). Generally electron-donating substituents increase the bacisity of phenol and thus the susceptibility toward oxidation while electron-withdrawing substituents exert the opposite effect. The position (*ortho*, *meta*, or *para*) of substituents is also critical in affecting the magnitude of electronic and steric effects. Earlier work by Stone (1987) has shown that the initial oxidation rates of substituted phenols by manganese oxide correlate well with the compounds' pK_a values and half-wave potentials ($E_{1/2}$), particularly when the substituent effect is primarily electronic (The reaction rate increases with increasing pK_a or decreasing $E_{1/2}$). The $E_{1/2}$ is not available for several compounds considered in Table 2.5 including triclosan and chlorophene. A simple trend cannot be established between the k_{init} and pK_a values, suggesting that the initial oxidation rates of triclosan and chlorophene are probably influenced by a combination of factors. The likely influencing factors include the electronic and steric effects of substituents and compound hydrophobicity.

Table 2.5. The initial oxidation rate constant k_{init} (h^{-1}), pK_a and log K_{ow} for triclosan, chlorophene, and related phenols. Reactions contained 10 μM organic reactant and 100 μM MnO_2 initially with pH 5 acetate buffer at 22 °C.

Compound	k_{init}(h^{-1})	k'/k[a]	pK_a[b]	log K_{ow}
Triclosan	1.74 ± 0.08	2.37	7.99	4.86[c]
Chlorophene	2.67 ± 0.37	3.63	9.96	3.99[c]
2-Methyl-4-chloroophenol	1.75 ± 0.58	2.38	9.76	2.63[d]
2,4-Dichlorophenol	1.09 ± 0.30	1.49	7.69	3.06[d]
Phenol	0.73 ± 0.22	1.00	10	1.46[d]
3-Chlorophenol	0.20 ± 0.09	0.27	9.18	2.50[d]

a. k'/k represents the initial rate constant ratio relative to phenol; b. Estimated by the SPARC program; c. Estimated by the ChemProp program; d. Hansch et al. 1995.

In terms of electronic influence, triclosan's *o*-dichlorophenoxy group provides strong resonance and weak electron-withdrawing effects, thus overall an activating effect. Triclosan's *m*-Cl substituent exerts electron-withdrawing effect. The *o*-benzyl group of chlorophene is electron-donating and the *p*-Cl substituent is weakly electron-withdrawing (the *p*-Cl's electron-withdrawing effect is offset somewhat by its weak resonance effect). Comparable electronic effects from chlorine substituents are also present in the related substituted phenols. For instance compared to chlorophene, 2-methyl-4-chlorophenol is expected to experience similar electronic effect because of the similar electronic influence from the *o*-methyl and *p*-Cl substituents.

Besides electronic effects, steric hindrance likely occurs for triclosan, chlorophene, 2-methyl-4-chlorophenol and 2,4-dichorophenol because of *o*-substitution of the phenol ring and the steric hindrance is probably greater for triclosan and chlorophene due to their larger *o*-substituents. Furthermore, the higher hydrophobicity of triclosan and chlorophene may contribute to higher adsorption to manganese oxide than the related substituted phenols since previous work has shown that adsorption of chlorophenols to manganese oxide increases as the compound's K_{ow} increases (Ulrich and Stone 1989). The higher adsorption to manganese oxide may lead to more surface precursor complex formation and thus the faster reaction rate. Taking chlorophene and 2-methyl-4-chlorophenol for comparison, chlorophene likely experiences greater steric hindrance but also greater adsorption to manganese oxide than 2-methyl-4-chlorophenol. Therefore, a combination of the aforementioned factors and others likely results in the high reactivities of triclosan and chlorophene to oxidation by manganese oxide, however more studies are needed to further understand the influencing factors.

2.4 Conclusions

The antibacterial agents triclosan (5-chloro-2-(2,4-dichlorophenoxy)phenol) and chlorophene (4-chloro-2-(phenylmethyl)phenol) showed similar susceptibility to rapid oxidation by manganese oxides (δ-MnO_2 and MnOOH) yielding Mn^{II} ions. Both the initial reaction rate and adsorption of triclosan to oxide surfaces increased as pH decreased, likely due to the higher reduction potential of Mn oxides and the generation of a greater number of surface species that favored interaction with triclosan under lower pH values. The reactions were first-order with respect to the antibacterial agent and MnO_2. The apparent reaction orders to H^+ were determined to be 0.46 ± 0.03 and 0.50 ± 0.03 for triclosan and chlorophene, respectively. Dissolved metal ions (Mn^{II}, Zn^{II} and Ca^{II}) and natural organic matter decreased the reaction rate by competitively adsorbing and/or reacting with MnO_2. The much slower rate of triclosan oxidation in the river water was likely caused by a combination of inhibitory effects from dissolved metal ions, natural organic matter and other inorganic anions such as phosphate.

Product identification by GC/MS and LC/MS supported the reaction mechanism that after formation of a surface precursor complex between the antibacterial agent and the surface-bound Mn^{IV}, triclosan and chlorophene were oxidized to phenoxy radicals at their phenol moieties followed by radical coupling and further oxidation to form the end products. Surface bound $>Mn^{IV}$ was reduced to Mn^{III} ion which was further reduced yielding Mn^{2+}. For triclosan, three pathways were proposed for the formation of end products. Pathway I, as the most important pathway, is coupling of two phenoxy radicals to yield dimeric products. Pathway II accounts for less than 5% of triclosan oxidation and involves one-electron oxidation of the phenoxy radical by manganese oxide to form

hydroquinone. Further two-electron oxidation of hydroquinone yields the quinone analog of triclosan. Pathway III is the least important one and involves cleavage of the ether bond of phenoxy radical, possibly via *o*-dealkylation, to yield trace amount of 2,4-dichlorophenol and other products. Similar pathways were also present for chlorophene except that pathway III can be excluded since breaking of the benzyl linkage of chlorophene does not occur. Additionally, chlorophene exhibited higher complexity in coupling product formation, likely due to the fact that the *p*-Cl substituent of chlorophene is susceptible to substitution by hydroxide and consequently increases the variety of product formation.

Compared to several structurally related substituted phenols (*i.e.*, 2-methyl-4-chlorophenol, 2,4-dichlorophenol, 3-chlorophenol, and phenol), triclosan and chlorophene exhibited comparable or higher reactivities toward oxidation by manganese oxides. The higher reactivities were likely affected by a combination of factors including electronic and steric effects of substituents and compound hydrophobicity. For electronic effects, electron-donating substituents increased the susceptibility of phenols toward oxidation while electron-withdrawing substituents exerted the opposite effect. The steric hindrance was probably greater for triclosan and chlorophene due to their larger *o*-substituents. Furthermore, the higher hydrophobicity of triclosan and chlorophene may contribute to higher adsorption to manganese oxide than the related substituted phenols, which in turn may lead to more surface precursor complex formation and thus the faster reaction rate.

Once released into the environment, partitioning of triclosan and chlorophene to soils and sediments is expected due to their relatively hydrophobic nature. Results of this

study indicate that manganese oxides in soils will facilitate transformation of these antibacterial agents.

2.5 Environmental Significance

This investigation demonstrates high susceptibility of triclosan and chlorophene toward oxidation by manganese oxides and significantly fast reaction rates at pHs below 7. Mild acidic conditions are common in many soils (e.g., Vasudevan et al. 2002, Vulkan et al. 2002). Assuming a condition of pH 6 and 10 μM manganese dioxide (Munger et al. 1983, Vasudevan et al. 2002), the half-lives of triclosan and chlorophene are calculated to be less than 21 hours. However, other constituents such as natural organic matter and dissolved metal ions in natural water and soils likely will slow down the reaction rate by competitively interacting with oxide surfaces. Nevertheless, oxidative transformation by manganese oxides is likely an important attenuation process for triclosan and chlorophene in the soil-water environment. Formation of heavier and more hydrophobic products via dimerization and polymerization will decrease the mobility of these antibacterial agents and potentially decrease the biological effects when the larger products become less available for aquatic organisms.

CHAPTER 3

OXIDATIVE TRANSFORMATION OF FLUOROQUINOLONE ANTIBACTERIAL AGENTS BY MANGANESE DIOXIDE

3.1 Introduction

Fluoroquinolones (FQs) are among the most important classes of synthetic antibacterial agents that are widely used in human and veterinary medicines (Golet et al. 2001 and 2002). Because of their extensive usage, the ubiquity of FQ antibacterial agents in aquatic environments has been reported in many recent studies. Golet et al. (2001 and 2002) reported detection of two FQ antibacterial agents, ciprofloxacin and norfloxacin, in domestic wastewater and surface water that received wastewater discharge in Switzerland. The concentrations of the FQs were around 40 – 570 ng/L in wastewater and from non-detectable to 120 ng/L in surface water (Golet et al. 2002). Detection of FQ antibacterial agents in various wastewaters at 80 ng/L to 2 μg/L (Renew 2003, Renew and Huang 2004) and surface water with mean concentrations from non-detectable to 0.12 μg/L (Kolpin et al. 2002) has also been reported in the United States. The highest concentrations of FQs were found in the hospital wastewater, with 0.7 to 124.5 μg/L of ciproflaoxacin (Hartmann et al. 1999). These ubiquitous antibiotic contaminants in the aquatic environment, albeit at low concentrations, may pose threats to the ecosystem and human health by inducing increase and spread of bacteria drug-resistance (Volmer et al. 1997). FQ antibacterial agents, in particular, have been shown to be the primary cause of genotoxicity in wastewater effluent in inducing primary DNA damage in bacteria (Hartmann et al. 1998, Hartmann et al. 1999).

In order to properly assess the risks of FQ antibacterial agents, a better understanding of their environmental fate is imperative. As antibiotic compounds, FQs have been shown to be relatively resistant to microbial biodegradation (e.g. Al-Almad et al. 1999, Kümmerer et al. 2000, Marengo et al. 2001). On the other hand, studies have reported extensive degradation of the FQs ciprofloxacin and enrofloxacin by hydroxyl radical-mediated enzyme systems characteristic of brown-rot fungi (*sp. Gloeophyllum striatum*) (e.g. Parshikov et al. 1999, Wetzstein et al. 1999). In addition, significant photolytic degradation of FQs by direct UV photolysis or radical-mediated photolysis has been reported (e.g. Phillips et al. 1990, Burhenne et al. 1999, Fasani et al. 1999, Mella et al. 2001, Fasani et al. 2001). Depending on the reaction conditions such as pH buffer, co-solutes, etc., more than ten photodegradation products generated via various pathways including dealkylation, defluorination and hydroxylation were identified (Fasani et al. 1999, Fasani et al. 2001, Mella et al. 2001). Sorption to soils, sediments, or dissolved organic matter was indicated to be another important environmental sink for FQs (Nowara et al. 1997, Lützhøft et al. 2000a, Tolls 2001). For example, Nowara et al. found that greater than 95% of enrofloxacin could adsorb to five different soils from Brazil, France, Germany, the Philippines, and Sweden (Nowara et al. 1997), and that the sorption coefficients K_d vary little among the FQ compounds. The strong adsorption of FQs to soils and sediments may result in a less fewer amount of freely available antibacterial agents and thus reduce their photodegradation and biodegradation (Lützhøft et al. 2000b).

Mn oxides, commonly found in soils and sediments, are among the most important naturally-occurring catalysts in facilitating organic pollutant transformation. δ-

MnO_2, with a reduction potential of 1.23 V, has been shown to be an effective oxidant for a wide range of pollutants including substituted phenols (e.g. Stone 1987, Zhang and Huang 2003) and anilines (e.g. Laha and Luthy 1990, Pizzigallo et al. 1998). The recent work by Li et al demonstrated that soil Mn (III/IV) oxides play the most significant role, in addition to other soil components such as organic matter and iron oxides, in the irreversible oxidation and transformation of aromatic amines (Li et al. 2003). Based on the strong affinity of FQs for soils and sediments (Nowara et al. 1997, Tolls 2001), there is a great possibility for FQs to react with mineral components associated with soils and sediments. As will be discussed later, this study demonstrates that the FQ antibacterial agents are highly susceptible to Mn oxide-facilitated oxidation.

In this study, experiments were conducted to determine the reaction kinetics and product formation in Mn oxide-facilitated oxidation of ciprofloxacin (cipro), enrofloxacin (enro), norfloxacin (nor), ofloxacin (oflox), lomefloxacin (lome), and pipemidic acid (PA) (structures are shown in Table 3.1). Parallel studies on the structurally-related aniline and alicyclic amines including 1-phenylpiperazine (PP), N-phenylmorpholine (PM), and 4-phenylpiperidine (PD) (structures are shown in Table 3.2) were also conducted to facilitate assessing compound reactivities and elucidating reaction mechanisms. On the basis of the kinetic results and product identification, reaction schemes were proposed.

Table 3.1. Pseudo-first order rate constants of fluoroquinolone oxidation by MnO_2[a] (expressed with 95% confidence levels).

Compound	Structure	MW	pK_{a1}[b]	pK_{a2}[b]	pK_{a3}[b]	$k_{obs}(h^{-1})$	Adsorption %[c]
Ciprofloxacin [85721-33-1] (cipro)	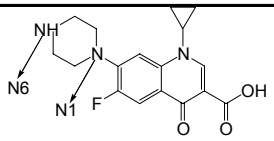	331.3459	5.46	7.67	-0.84	0.81 ± 0.10	76 ± 6
Enrofloxacin [93106-60-6] (enro)	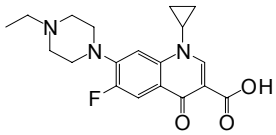	359.3995	5.46	7.03	-0.84	1.11 ± 0.44	62[d]
Norfloxacin [70458-96-7] (nor)	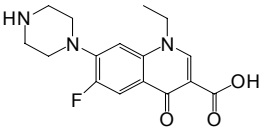	319.3349	5.46	7.67	-0.84	1.40 ± 0.36	69[d]
Ofloxacin [83380-47-6] (oflox)	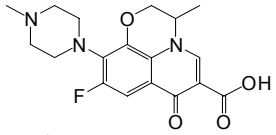	361.3721	5.41	7.08	0.79	0.91 ± 0.26	68[d]
Lomefloxacin [98079-51-7] (lome)	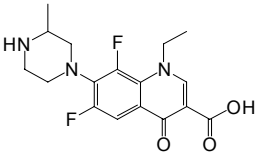	351.3522	5.38	7.85	-1.48	0.54 ± 0.04	44[d]
Pipemidic Acid [51940-44-4] (PA)	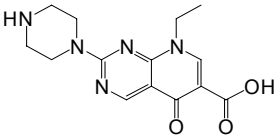	303.32	5.20	6.38	-5.28	0.12 ± 0.04	39 ± 10
Flumequine [42835-25-6] (FLU)	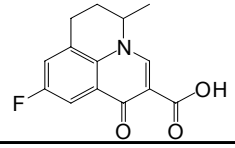	261.2521	5.45	-	-	0	10[d]

[a] Reaction conditions: $[FQ]_0$ = 1.5 μM, $[MnO_2]_0$ = 100 μM, 0.01 M pH 6 MOPS buffer, 0.01 M NaCl, 22°C. [b] Estimated based on SPARC. [c] Adsorption % = C_{ads}/C_{total} %. [d] Only one replicate was conducted.

Table 3.2. Pseudo-first order rate constants of model compound oxidation by MnO_2[a].

Compound	Structure	MW	pK_{a1}[b]	pK_{a2}[b]	$k_{obs}(h^{-1})$	Adsorption %[c]
1-phenylpiperazine [92-54-6] (PP)	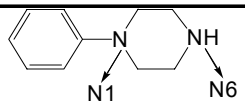	162.23	4.49	8.63	6.70 ± 0.10	53
Aniline [62-53-3]	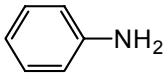	93.13	4.6[d]	-	2.29 ± 1.11	75
N-phenylmorpholine [92-53-5] (PM)	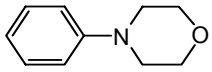	163.21	3.32	-	0.24 ± 0.07	56
4-phenylpiperadine [771-99-3] (PD)	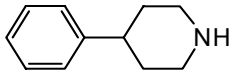	161.25	10.44	-	0.002[c]	19
N-ethylformanilide [5461-49-4]	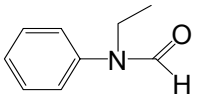	-	-	-	0	7

[a] Reaction conditions: $[Organics]_0$ = 10 μM, $[MnO_2]_0$ = 100 μM, 0.01M pH 5 acetic acid buffer, 0.01 M NaCl, 22°C. [b] Estimated based on SPARC. [c] Adsorption % = C_{ads}/C_{total} %; and only one replicate was conducted. [d] Perrin 1972.

3.2 Methodology

3.2.1 Chemicals and Oxide Preparation

Reagent grade water (18.3 MΩ-cm resistivity) was prepared by a Barnstead Nanopure water system. Cipro, enro, nor, oflox, and flumequine (FLU) were purchased from ICN. Lome, PA, and N-ethylformanilide were purchased from Sigma (St. Louis, MO). The purity of the above compounds was not specified. Aniline, PP and PM were obtained from Aldrich (St. Louis, MO) at greater than 98% of purity. PD was purchased from Acros (Fairlawn, NJ) at 98% of purity. Other employed chemical reagents including acetic acid, acetonitrile (ACN), L-ascorbic acid, 2-(cyclohexylamino)ethanesulfonic acid (CHES), HCl, HNO_3, H_3PO_4, methylene chloride, methanol (MeOH), 4-morpholinepropanesulfonic acid (MOPS), NaCl, NaOH, and NaH_2PO_4 were obtained from Fisher Scientific (Fairlawn, NJ) or Aldrich (St. Louis, MO) at greater than 98% purity (for solids) or of HPLC and GC/MS grade (for solvents), unless otherwise specified. All chemicals were used directly without further purification. Synthesis of Mn dioxide (δ-MnO_2, similar to the naturally occurring birnessite) was based on the method by Murray (1974) and has been described in detail in Chapter 2. FQ stocks were prepared in methanol/H_2O (10/90, v/v), while the structurally-related model compound stocks were prepared in Nanopure water at 100-120 mg/L. All stocks were stored at 4 °C and used within a month of preparation.

3.2.2 Reactor Setup

Details regarding the experimental setup for the oxidation of FQs by Mn oxide are similar to those in the study for triclosan and chlorophene, as described in Chapter 2.

Briefly, all experiments were conducted in 25 ml screw-cap amber glass bottles with Teflon septa. The reaction bottles were placed on a magnetic stir plate in a 22^{o}C water basin and were continuously stirred. Reaction solutions were maintained at constant pH with 10 mM of appropriate buffer. Reactions were initiated by adding an appropriate amount of organic stock solution to solutions containing manganese oxide, buffer, and constant ionic medium. Aliquots were periodically collected and reactions were quenched immediately either by centrifugation (at 12000 rev/min for 20 min) or by ascorbic acid (0.1 M) addition. 100 μL of 1 M H_3PO_4 was added to each quenched sample (1 mL) for the purpose of maintaining the stability of FQs to obtain the best analytical results for the parent compounds. Separate experiments had confirmed that the addition of H_3PO_4 after quenching did not alter the nature of the oxidation reaction of FQs.

Preliminary studies using the procedures described above showed that within the reaction time period from hours to several days, N_2 purging (versus exposure to ambient air) did not affect the reaction rate or product distribution. Thus subsequent experiments were conducted without extra efforts to exclude O_2. Control experiments with Mn^{2+} and FQs in air condition but without MnO_2 were also run to assess the potential catalytic ability of Mn^{2+}/O_2 that was observed in other studies (e.g., Nowack and Stone 2002). No discernable degradation of FQs was observed after 5 days under such conditions.

3.2.3 Analysis of Fluoroquinolones, Model Compounds and Mn^{II} Ions

Decrease in the concentration of FQs and structurally related model compounds was monitored by a reverse-phase high performance liquid chromatography (HPLC)

system with a Zorbax RX-C18 column (4.6 × 250 mm, 5 μm), a fluorescence detector and a diode-array UV/Vis detector (1100, Agilent Technology). The excitation and emission wavelengths of the fluorescence detector were: 210 nm and 360 nm, respectively, for PP, PD, PM, and N-ethylformanilide; 235 nm and 365 nm for FLU; 278 nm and 450 nm for cipro, enro, nor, lome, and PA; 298 nm and 490 nm for oflox. Aniline was detected at 210 nm by the UV detector. The mobile phase consisted of a solution containing 20 mM H_3PO_4 and 20 mM NaH_2PO_4 (eluent A, pH ~ 2.4) and acetonitrile (eluent B) at a flow rate of 1 mL/min. The mobile phase began with 0.5 minute isocratic 2% B (98% A), increased to 10% B in 0.5 minutes, increased to 80% B till 10 minutes, then the column was flushed thoroughly under these conditions for 4 minutes followed by a 5-min post time which allowed re-equilibration of the column.

Generation of Mn^{II} ions from the reductive dissolution of Mn dioxide was monitored using an inductively coupled plasma (ICP) spectrometer (Thermo Jarrell Ash Trace Analyzer). Preparation of the samples was described in Chapter 2. Controls with only Mn oxide and pH buffers revealed that the dissolution of Mn dioxide did not occur in the absence of FQs.

3.2.4 Analysis of Organic Products

Organic reaction products were analyzed by LC/MS, GC/MS and infrared (IR) spectroscopic techniques. For LC/MS analysis, 20 mL of reaction suspensions containing 0.2 mM of FQs and 2 mM of MnO_2 were prepared at pH 5. Reactions were quenched after 1-4 days by centrifugation (at 12000 rev/min for 20 min), and reaction products in supernatant were monitored by a HPLC system with a Zorbax SB-C18

column (2.4 × 150 mm, 5 μm) and a mass spectrometer (1100/1100MSD, Agilent Technology). The mobile phase consisted of 0.02% acetic acid in 90/10 water/acetonitrile (v/v, eluent A) and pure acetonitrile (eluent B) at a flow rate of 0.20 mL/min. The gradient was as follows: B started at 10% for the first minute, increased to 60% by 10 minutes, increased to 80% by 25 minutes. Then the column was flushed by 100% B for 10 minutes followed by a 15-min post time which allowed re-equilibration of the column. The MS analysis was conducted by electrospray positive ionization at fragmentation voltage 80-120 V with mass scan range 50-1000 m/z. The drying gas was operated at 10 mL/min at 325 °C. The nebulizer pressure was 30 psig and the capillary was set at 4000 V. Raw LC/MS chromatogam and mass spectra for cipro and its oxidation products are available in Appendix III.

For GC/MS analysis, 80 mL of reaction suspensions containing 0.2 mM of the model compounds and 2 mM of MnO_2 were prepared at pH 5. The reaction mixture was centrifuged (at 12000 rev/min for 20 min) and the pH of the supernatant was adjusted to ~ 10 by adding NaOH (1 M). The supernatants and MnO_2 solids were extracted respectively by vigorously shaking with 10-15 mL of methylene chloride ($MeCl_2$), which was then concentrated down to 1 mL under a gentle stream of N_2 gas. Controls with only organic reactants were extracted in a similar fashion and yielded extraction efficiencies of 25%, 37%, and 29% and for aniline, PP, and PM, respectively. An Agilent GC/MS (6890/5973) with a HP-5MS 5% phenyl methyl siloxane capillary column (30m × 250μm × 0.25μm) was used to analyze the products. The GC conditions were as follows: splitless injection at 250 °C and the oven temperature from 70 to 280 °C at 10 °C/min followed by a 6-min hold at 280 °C with helium as the carrier gas at 1.2 mL/min. The

MS analysis was conducted by electron ionization at 70 eV with mass scan range 35-550 m/z. The temperatures of the ion source and the transfer line were 250 °C.

For IR analysis, 800 mL of reaction suspensions containing 1 mM of PP and 2 mM of MnO_2 were prepared at pH 5. After 1 day, the reaction mixture was extracted by vigorously shaking with 100 mL of $MeCl_2$, which was then dried under a gentle stream of N_2 gas. Controls with only PP and pH buffers but without Mn oxides were extracted and dried in a similar fashion. The yielded solids were redissolved in 300 μL of MeOH and a droplet of each of the concentrated liquid samples was put on a ZnSe disk (which is IR transparent), and then another ZnSe disk was put on top to make a thin film of the liquid. The spectra were taken with the IR microscope in the transmission mode by a Biorad FTS 6000 Fourier transform infrared spectrometer (FTIR), which was operated under the normal purged air environment and covered the spectral range of 400 – 8,000 cm^{-1}.

3.3 Results

3.3.1 Kinetics of FQ Oxidation by MnO_2

In the absence of Mn oxide, the FQs were stable under the experimental conditions and no measurable loss of the compounds could be detected after a week. In contrast, significant degradation occurred in the presence of Mn oxide for all of the compounds except FLU (Table 3.1). A typical time course of cipro oxidation by MnO_2 is shown in Figure 3.1. Similar kinetic behavior was also observed for other FQs. The reaction kinetics deviated from the pseudo-first-order kinetics even over the first few time increments, thus for the sake of comparison the reaction kinetics were evaluated based upon the initial reaction rates in $\mu M\text{-}h^{-1}$ (i.e., the slopes over the first few time increments

in plotting C (μM) versus time (h)) and the initial reaction rate constants k_{obs} in h^{-1} (i.e., the initial reaction rate divided by the initial FQ concentration). All the kinetic data were calculated based on at least three replicates of experiments and were expressed with their 95% confidence levels (Table 3.1).

Monitoring the production of Mn^{2+} ions from the reductive dissolution of MnO_2 yielded similar kinetic results as those of cipro (Figure 3.2). Despite the strong adsorption of Mn^{2+} to MnO_2 (greater than 90% of the added Mn^{2+} adsorbed to 0.1 mM MnO_2 at pH 5 to 7), the initial rate constants for the increase of Mn^{2+} (0.22 h^{-1}) and the decrease of cipro (0.14 h^{-1}) were comparable. These results provided evidence that Mn oxide was reductively dissolved by the FQs yielding Mn^{2+} and both reactants were consumed at similar initial rates.

As shown in Figure 3.3a, pH exerted a marked influence on the reaction rate of cipro oxidation by Mn oxide. Figure 3.3a indicates that the log of the initial rate constant (log k_{obs}) decreases linearly as the pH increases. Least-square fitting of the Figure 3.3a data gives the average reaction order of 0.49 for H^+. Adsorption of cipro to Mn oxide surfaces was evaluated by comparing experimental results from two different quenching methods (i.e., centrifugation versus ascorbic acid addition) as described in Chapter 2. By adding ascorbic acid, Mn oxide was readily reductively dissolved and the adsorbed yet unreacted cipro could be released from the oxide surface and measured (control experiments have verified the stability of cipro in the presence of ascorbic acid). In contrast, only the non-adsorbed cipro could be detected in the centrifugation supernatant. This comparison showed that approximately 45% of cipro was adsorbed to MnO_2 at pH 5. It is also evident from Figure 3.3b that adsorption of

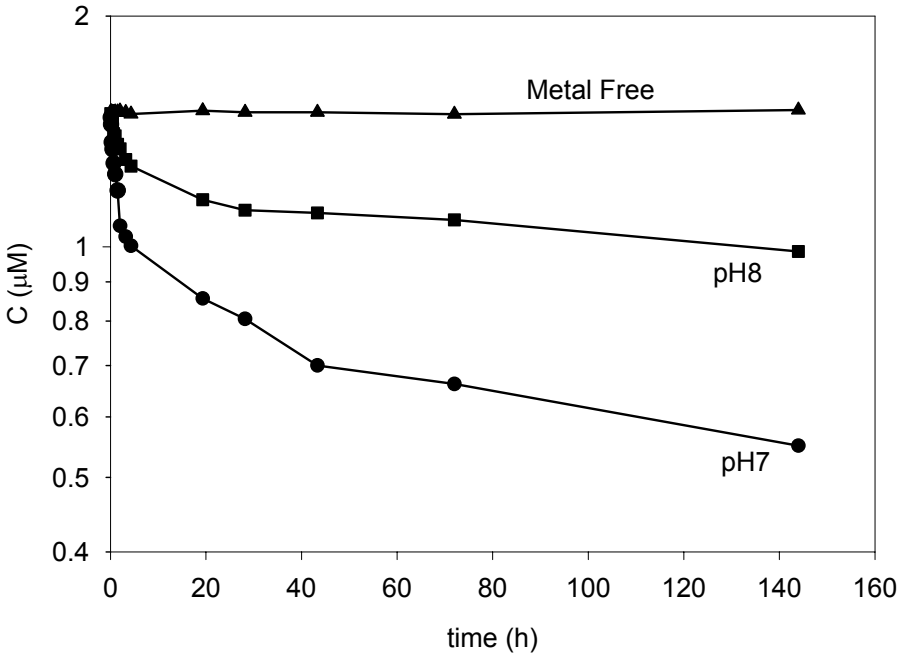

Figure 3.1. Time course of cipro oxidation by MnO_2. Reactions contained 100 μM MnO_2 and 1.5 μM cipro initially at 22 °C.

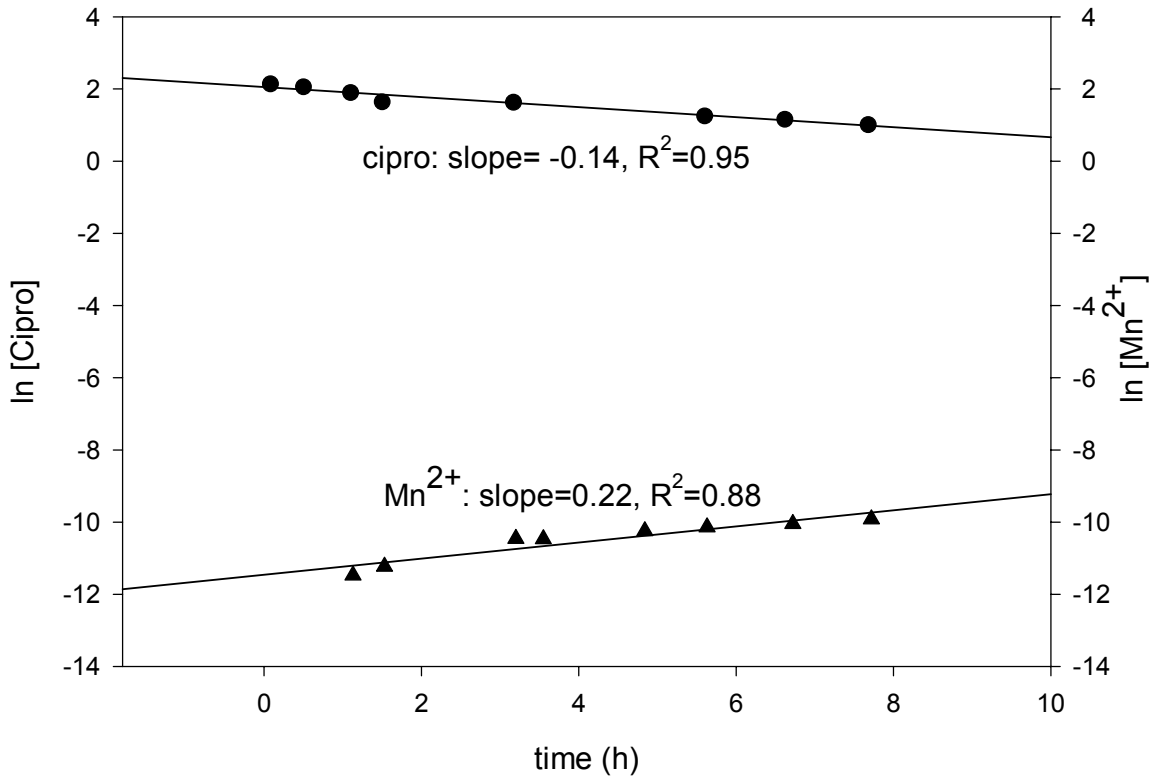

Figure 3.2. Kinetic comparison between cipro and Mn^{2+}. Reactions contained 10 □M cipro & 100 □M MnO_2 with pH 5 acetic acid buffer initially at 22 °C.

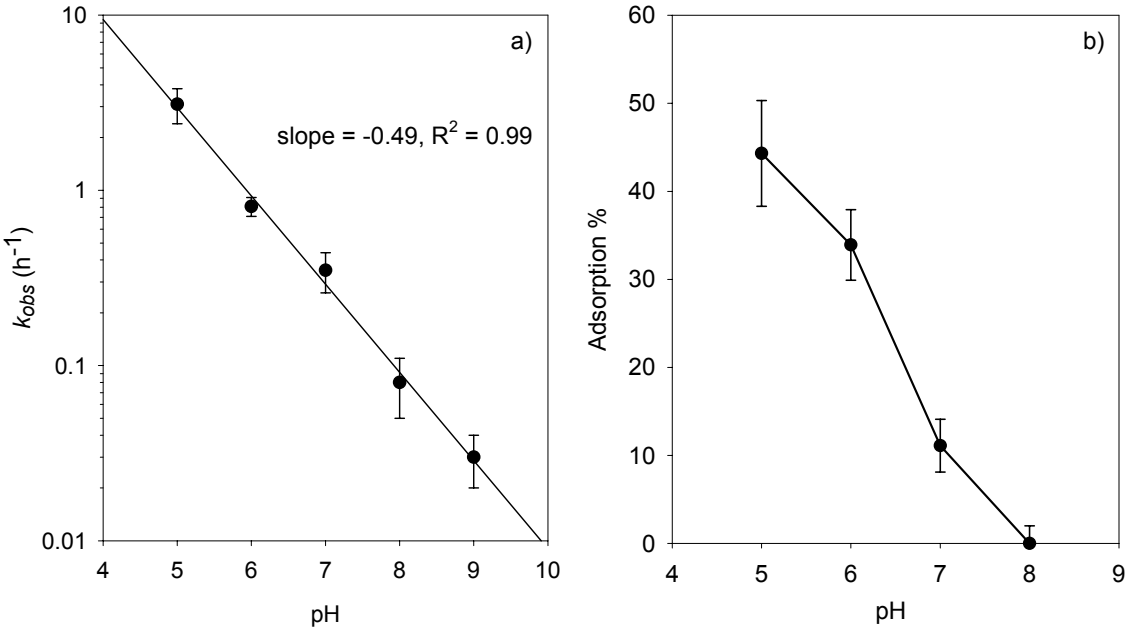

Figure 3.3. (a) Effect of pH on cipro oxidation by MnO_2. Reactions contained 1.5 μM cipro & 100 μM MnO_2 initially at 22 °C; (b) Effect of pH on the adsorption of cipro to MnO_2. Reactions contained 1.5 μM cipro & 20 μM MnO_2 initially at 22 °C.

cipro to Mn oxide decreased as pH was increased. For example, only about 11% of cipro was adsorbed at pH 7 while about 45% of cipro was adsorbed at pH 5.

A series of experiments with varying cipro loadings (0.75 – 10 μM) but a fixed MnO_2 loading (100 μM) or with varying Mn oxide loadings (7.5 – 100 μM) but a fixed cipro loading (1.5 μM) were conducted to assess the initial reaction orders with respect to cipro and Mn oxide. When cipro loading was below 3 μM, plotting the log of the initial reaction rate versus the log of cipro loading yielded a regression line with the slope close to 1. However, when cipro loading was above 3 μM, the curve gradually leveled off (Figure 3.4), resembling the Langmuir behavior which ascertained surface saturation effect in the presence of large amounts of adsorbate. Even though the MnO_2 concentration was at more than 10-fold excess to the cipro concentration, the experimental results indicate that the number of reactive sites on MnO_2 surfaces is limited and can be saturated by a relatively small amount of cipro molecules. This significant surface site limitation or heterogeneity is consistent with other previous work (e.g. Zhang and Huang 2003). For MnO_2, a slope close to 1 was obtained by plotting log of the initial reaction rate versus the log of MnO_2 loading throughout the range of MnO_2 loadings that were investigated (Figure 3.4). Overall the results demonstrated that the reaction orders with respect to both cipro and Mn oxide could be 1 within certain concentration ranges (i.e., pseudo-first-order kinetics for both reactants). Later studies with other FQs were conducted within this concentration range where pseudo-first-order kinetics could be applied.

The experiments showed rapid degradation of all FQs except FLU by MnO_2 within 3 hours at pH 6 (Table 3.1). No discernable degradation of FLU by MnO_2 could

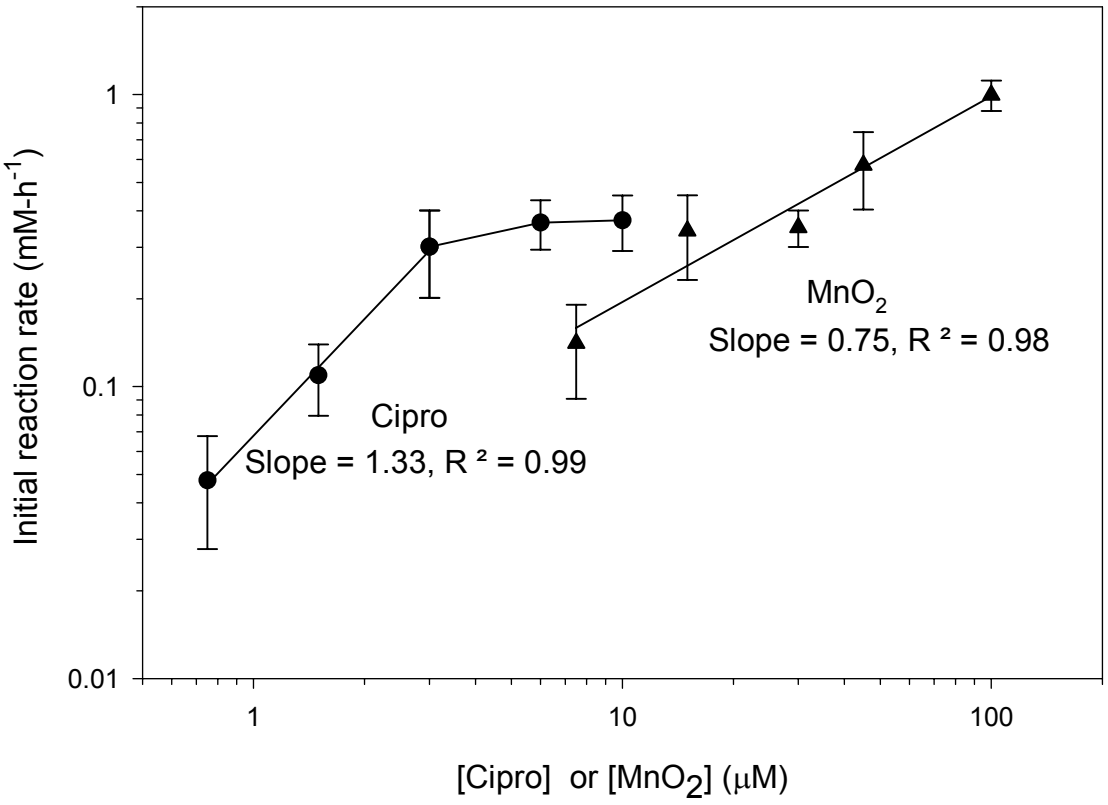

Figure 3.4. Loading effect of cipro and MnO_2 on the initial reaction rate.

be observed after 2 weeks. FLU also exhibited lower adsorption than the other FQs to MnO_2, at ~10% adsorption for FLU versus 76 ± 6% for cipro at pH 6. Excluding FLU, the adsorption of cipro, enro, nor and oflox did not vary significantly, while the adsorption of lome and PA was lower (Table 3.1). Because FLU differs from the rest of FQs most notably by the lack of a piperazine moiety, its inactivity to MnO_2 strongly indicates that the piperazine moiety of FQs plays a critical role in the surface reactions with MnO_2. A comparison of k_{obs} values for the FQs also showed that cipro, enro, nor, and oflox reacted with MnO_2 at very similar rates while lome and PA reacted much more slowly (Table 3.1).

3.3.2 Kinetics of Model Compound Oxidation by MnO_2

The conclusion that the piperazine ring is the likely reactive moiety in FQs prompted more experiments with a range of aniline and alicyclic amines that are structurally related to piperazine and FQs for their reactions with MnO_2. The experiments were conducted at pH 6 with initially 10 μM of amine and 100 μM of MnO_2 at pH 5 and 22 °C (Table 3.2). Experiments were also conducted with PP under reaction conditions identical to those used in the FQ studies (i.e., $[PP]_0$ = 1.5 μM, $[MnO_2]_0$ = 100 μM, pH 6 and 22 °C); and PP yielded an average 3-fold faster reaction rate (k_{obs} = 3.08 ± 0.32 h^{-1}) than FQs (k_{obs} = 0.12 ~ 1.40 h^{-1}, Table 3.1). Among the model amines, the initial reaction rates followed the trend of PP > aniline > PM > PD (Table 3.2). Compared to PP, aniline reacted with MnO_2 about 3-fold slower, PM reacted with MnO_2 about 28-fold slower, and PD reacted with MnO_2 more than 3300-fold slower. In terms of adsorption to MnO_2, it is interesting to find that the lowest adsorption percentage was

observed with PD among the alicyclic amines (Table 3.2), suggesting that the inner N (i.e., N1) may be more active than the outer N (i.e., N6) in association with the Mn oxide surfaces. N-ethylformanilide (Table 3.2) did not react with MnO_2 and was included in the study as an analog of reaction product as will be discussed in a later section.

3.3.3 Oxidation Products of FQs

LC/MS analysis of cipro reaction mixtures indicated the presence of primarily six products with molecular ions of m/z 334, 306, 364, 362, 334 and 263, respectively (Table 3.3). The molecular ion of cipro is m/z 332. These molecular ions were identified based on the difference of 22 in m/z ratios between the sodiated ($[M + Na]^+$) and the molecular ($[M + H]^+$) ions. All products exhibited fragmentation patterns similar to that of cipro, suggesting that they share a common base structure that is the heterocyclic aromatic cluster attached to the piperazine ring (see Table 3.1 for FQ structures). For example, the $[M + H - H_2O]^+$ ion is almost always the base peak among the products - a fragmentation pattern corresponding to the loss of H_2O from the carboxylic acid group in the heterocyclic base structure. Additionally, loss of CO_2, CO, HF, the three-membered ring (∇) attached to the aromatic ring N, and C_2H_5N of the piperazine ring accounts for the various minor fragments (Table 3.3).

The MS results observed in this study are quite comparable with previous studies on FQ photolytic degradation products (e.g., Burhenne et al. 1997). The M-26 (m/z 306) product corresponds to partial dealkylation of the piperazine ring while the $M–NH_2$ (m/z 263) product derives from full dealkylation of the piperazine ring (Figure 3.5). These

Table 3.3. LS-ESI-MS fragments of cipro (M) and its corresponding oxidation products.

		M		M+2		M-26		M+30		M+2		M-NH_2		M+32	
RT (min)		12.78		9.93		13.49		18.75		21.89		23.69		14.76	
		m/z	int.[a]	m/z	int.	m/z	int.	m/z	int.	m/z	int.	m/z	int.	m/z	int.
$[MH]^{+\bullet}$	0	332	100	334	65	306	30	362	45	334	50	263	55	364	80
$[M+Na]^{+\bullet}$	+22	354	6	356	10	328	10	384	15	-	-	285	8	386	8
$[MH-H_2O]^{+\bullet}$	-18	314	98	316	100	288	100	344	100	316	100	245	100	346	100
$[MH-H_2O-HF]^{+\bullet}$	-38	-	-	-	-	268	5	-	-	-	-	-	-	-	-
$[MH-CO_2]^{+\bullet}$	-44	288	60	-	-	-	-	-	-	-	-	-	-	-	-
$[MH-H_2O-CO]^{+\bullet}$	-46	-	-	-	-	-	-	316	10	288	8	217	5	-	-
$[MH-H_2O-\nabla]^{+\bullet}$	-58	274	6	-	-	-	-	-	-	-	-	-	-	306	10
$[MH-H_2O-C_2H_5N]^{+\bullet}$	-61	-	-	273	60	245	12	-	-	-	-	-	-	-	-
$[MH-H_2O-CO_2]^{+\bullet}$	-62	-	-	-	-	-	-	300	8	-	-	-	-	-	-
$[MH-HF-CO_2]^{+\bullet}$	-64	-	-	-	-	-	-	-	-	270	15	-	-	-	-
$[MH-H_2O-2CO]^{+\bullet}$	-74	-	-	-	-	-	-	288	10	-	-	-	-	-	-
$[MH-2H_2O-\nabla]^{+\bullet}$	-76	-	-	-	-	-	-	-	-	-	-	-	-	288	6
$[MH-H_2O-HF-C_2H_5N]^{+\bullet}$	-81	-	-	-	-	-	-	-	-	-	-	-	-	-	-
$[MH-CO_2-C_2H_5N]^{+\bullet}$	-87	245	25	-	-	-	-	-	-	-	-	-	-	-	-
$[MH-H_2O-CO-C_2H_5N]^{+\bullet}$	-89	-	-	-	-	217	5	273	13	-	-	-	-	-	-
$[MH-H_2O-\nabla-C_2H_5N]^{+\bullet}$	-101	231	20	-	-	-	-	-	-	-	-	-	-	-	-
$[MH-HF-\nabla-C_2H_5N]^{+\bullet}$	-103	-	-	231	25	203	6	259	8	-	-	-	-	-	-
$[MH-H_2O-2CO-C_2H_5N]^{+\bullet}$	-117	-	-	-	-	-	-	-	-	217	10	-	-	-	-
$[MH-H_2O-CO-\nabla-C_2H_5N]^{+\bullet}$	-129	203	3	-	-	-	-	-	-	-	-	-	-	-	-
$[MH-H_2O-CO-CO_2-C_2H_5N]^{+\bullet}$	-133	-	-	-	-	-	-	-	-	-	-	-	-	231	10
$[MH-H_2O-3CO-C_2H_5N]^{+\bullet}$	-145	-	-	-	-	-	-	217	6	-	-	-	-	-	-
$[MH-2H_2O-HF-C_2H_5N-\nabla]^{+\bullet}$	-147	-	-	-	-	-	-	-	-	-	-	-	-	217	8
$[MH-H_2O-2CO-CO_2-C_2H_5N]^{+\bullet}$	-161	-	-	-	-	-	-	-	-	-	-	-	-	203	10

[a] int. = MS intensity (%)

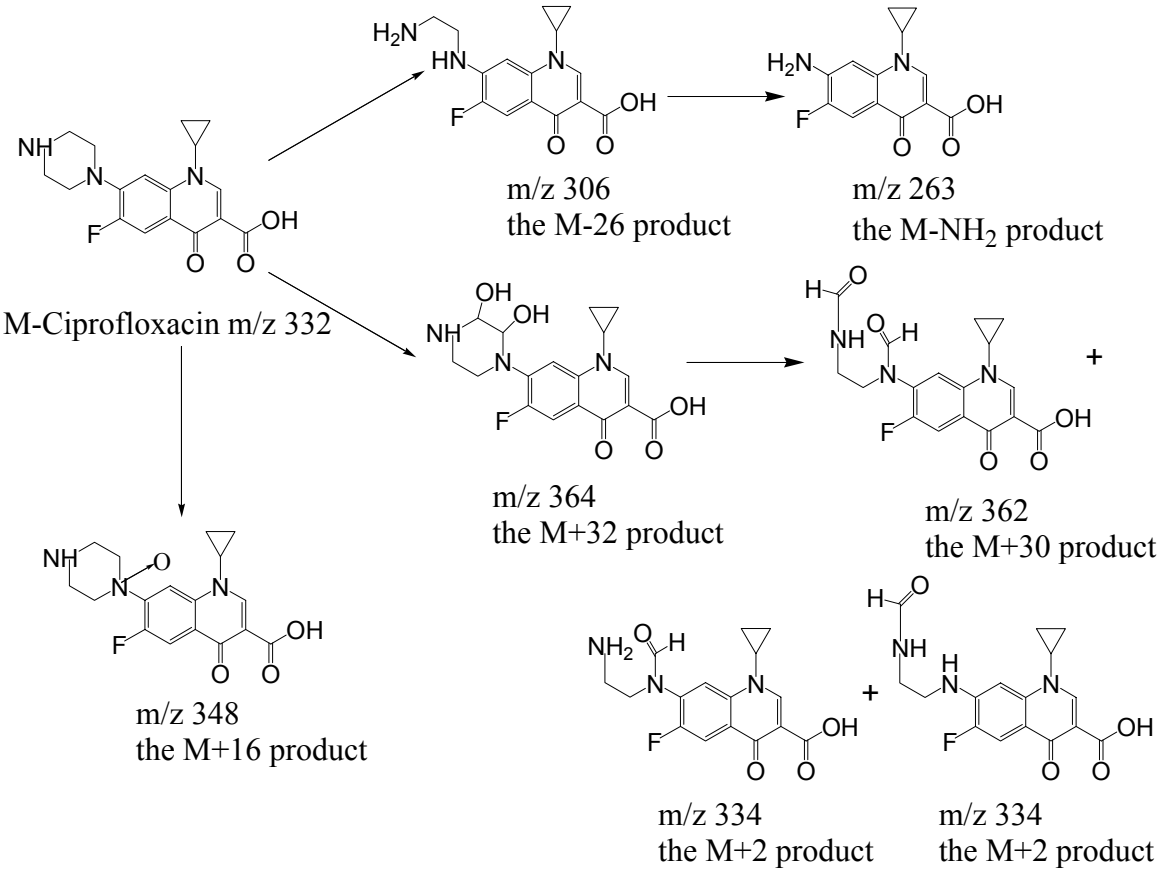

Figure 3.5. Oxidation products of cipro.

two products have been identified in the photodegradation of cipro (e.g., Burhenne et al. 1997). For the other four oxidation products, because there is only one CO and H_2O loss recorded in cipro LC/MS fragments, the additional losses of m/z 28 or 18 observed with these products suggest that additional >C=O or –OH groups are present. For example, there may be 2 >C=O groups in the M+30 product (m/z 362) based on the observation of the m/z 288 daughter ion (i.e., after loss of 2 × 28) and the m/z 217 daughter ion (i.e., after loss of 3 × 28). One additional >C=O group is also plausible in the M+2b product (m/z 334) based on the m/z 217 daughter ion (i.e., after loss of 2 × 28) (Table 3.3). The presence of >C=O group has already been observed in the oxidation products of piperazine-containing compounds (Fasani et al. 1999, Feng et al. 2001). The M+32 product (m/z 364) may contain more than one –OH group in account of the loss of 2 × 18 in its m/z 288 and 217 daughter ions (Table 3.3).

To aid identifying the source of the additional >C=O or –OH groups in cipro reaction products, the following alternative methods were utilized (while keeping other reaction conditions unchanged): (1) purging solutions with N_2 gas initially and excluding the involvement of O_2 throughout the reaction, (2) preparing cipro stock solution in acetonitrile instead of methanol, and (3) using HCl to adjust the pH of the reaction mixture instead of using acetic acid buffer. Reactions were monitored up to 30 days and the same oxidation products were detected throughout the reaction time (4.5h, 2d, 11d, and 30d, data not shown) for all of the above experiments. These results indicate that the >C=O and –OH groups in the cipro oxidation products did not come from atmospheric oxygen, organic solvent or acetic acid buffer solution.

Table 3.4. ESI-MS fragments of enrofloxacin (M) and its oxidation products.

		M		M+2		M-26		Cipro		M+30		M-NH_2		M+2		M+16	
RT (min)		17.289		13.081		14.168		14.814		21.626		23.452		29.161		15.308	
		m/z	int.[a]	m/z	int.	m/z	int.	m/z	int.	m/z	int.	m/z	int.	m/z	int.	m/z	int.
$[MH]^{+\bullet}$	0	360	100	362	60	334	68	332	100	390	98	263	40	362	60	376	30
$[M+Na]^{+\bullet}$	+22	382	10	-	-	356	8	354	10	412	6	285	10	-	-	398	10
$[MH-H_2O]^{+\bullet}$	-18	342	55	344	55	316	100	314	70	372	100	245	100	344	55	358	100
$[MH-H_2O-HF]^{+\bullet}$	-38	-	-	-	-	296	10	-	-	-	-	-	-	-	-	-	-
$[MH-CO_2]^{+\bullet}$	-44	316	80	-	-	-	-	288	62	346	45	-	-	-	-	332	10
$[MH-CO-NH_3]^{+\bullet}$	-45	-	-	317	55	-	-	-	-	-	-	-	-	317	55	-	-
$[MH-H_2O-\nabla]^{+\bullet}$	-58	302	5	-	-	-	-	-	-	-	-	-	-	-	-	-	-
$[MH-H_2O-CO]^{+\bullet}$	-46	-	-	-	-	-	-	-	-	-	-	217	8	-	-	-	-
$[MH-HF-\nabla]^{+\bullet}$	-60	-	-	-	-	-	-	-	-	-	-	-	-	-	-	316	35
$[MH-H_2O-CO_2]^{+\bullet}$	-62	-	-	-	-	-	-	-	-	328	88	-	-	-	-	314	58
$[MH-HF-CO_2]^{+\bullet}$	-64	-	-	298	45	-	-	268	20	-	-	-	-	298	45	-	-
$[MH-C_4H_7N]^{+\bullet}$	-69	-	-	-	-	-	-	263	5	-	-	-	-	-	-	-	-
$[MH-CO-C_2H_5N]^{+\bullet}$	-71	-	-	-	-	263	10	-	-	-	-	-	-	-	-	-	-
$[MH-CO_2-C_2H_5N]^{+\bullet}$	-87	-	-	-	-	-	-	245	55	-	-	-	-	-	-	-	-
$[MH-HF-CO-\nabla]^{+\bullet}$	-88	-	-	-	-	-	-	-	-	-	-	-	-	-	-	288	10
$[MH-H_2O-CO-C_2H_5N]^{+\bullet}$	-89	-	-	273	100	245	12	-	-	301	43	-	-	273	100	-	-
$[MH-CO-CO_2-C_2H_5N]^{+\bullet}$	-115	245	18	-	-	219	8	-	-	-	-	-	-	-	-	-	-
$[MH-H_2O-2CO-C_2H_5N]^{+\bullet}$	-117	-	-	245	28	-	-	-	-	-	-	-	-	245	28	-	-
$[MH-HF-2CO-C_2H_5N]^{+\bullet}$	-119	-	-	-	-	-	-	-	-	-	-	-	-	-	-	257	20
$[MH-H_2O-CO-\nabla-C_2H_5N]^{+\bullet}$	-129	231	8	-	-	-	-	-	-	-	-	-	-	-	-	-	-
$[MH-HF-CO-\nabla-C_2H_5N]^{+\bullet}$	-131	-	-	231	5	-	-	-	-	-	-	-	-	-	-	245	6
$[MH-H_2O-3CO-C_2H_5N]^{+\bullet}$	-145	-	-	217	8	-	-	-	-	-	-	-	-	217	8	-	-

[a] int. = MS intensity (%)

Table 3.5. ESI-MS fragments of norfloxacin (M) and its oxidation products.

		M		M+2		M-26		M+32		M+30		M+2		$M-NH_2$		?	
RT (min)		14.508		8.826		12.54		13.87		18.043		21.046		21.797		16.666	
		m/z	int.[a]	m/z	int.	m/z	int.	m/z	int.	m/z	int.	m/z	int.	m/z	int.	m/z	int.
$[MH]^{+\bullet}$	0	320	100	322	50	294	40	352	40	350	28	322	60	251	20	348	70
$[M+Na]^{+\bullet}$	+22	342	5	-	-	306	15	-	-	372	10	344	15	273	6	370	10
$[MH-H_2O]^{+\bullet}$	-18	302	53	304	100	276	100	334	100	332	100	304	100	233	100	330	15
$[MH-H_2O-HF]^{+\bullet}$	-38	-	-	284	28	256	40	-	-	-	-	-	-	-	-	-	-
$[MH-C_2H_5N]^{+\bullet}$	-43	-	-	-	-	251	5	-	-	-	-	279	43	-	-	-	-
$[MH-CO_2]^{+\bullet}$	-44	276	75	-	-	-	-	-	-	-	-	-	-	-	-	-	-
$[MH-H_2O-CO]^{+\bullet}$	-46	-	-	-	-	-	-	-	-	304	6	-	-	205	15	302	6
$[MH-H_2O-C_2H_5N]^{+\bullet}$	-61	-	-	261	80	233	30	-	-	-	-	261	86	-	-	-	-
$[MH-HF-C_2H_5N]^{+\bullet}$	-63	-	-	-	-	231	5	-	-	-	-	-	-	-	-	-	-
$[MH-CO-C_2H_5N]^{+\bullet}$	-71	-	-	-	-	-	-	-	-	-	-	251	30	-	-	-	-
$[MH-HF-CO-C_2H_5]^{+\bullet}$	-76	-	-	-	-	-	-	276	15	-	-	-	-	-	-	-	-
$[MH-CO_2-C_2H_5N]^{+\bullet}$	-87	233	20	-	-	-	-	-	-	-	-	-	-	-	-	-	-
$[MH-H_2O-CO-C_2H_5N]^{+\bullet}$	-89	-	-	233	20	-	-	-	-	-	-	233	15	-	-	-	-
$[MH-CO-CO_2-C_2H_5N]^{+\bullet}$	-115	205	8	-	-	-	-	-	-	-	-	-	-	-	-	-	-
$[MH-HF-2CO-C_2H_5N]^{+\bullet}$	-119	-	-	-	-	-	-	-	-	231	6	-	-	-	-	-	-
$[MH-HF-3CO-C_2H_5N]^{+\bullet}$	-147	-	-	-	-	-	-	205	10	-	-	-	-	-	-	-	-

[a] int. = MS intensity (%)

Table 3.6. ESI-MS fragments of ofloxacin (M) and its oxidation products.

		M		M+16		M-26		M+30		M-NH_2		M+2		M+2		?		?	
RT (min)		14.163		11.108		13.464		20.831		22.994		24.419		25.116		7.627		17.529	
		m/z	int.[a]	m/z	int.	m/z	int.	m/z	int.	m/z	int.	m/z	int.	m/z	int.	m/z	int.	m/z	int.
$[MH]^{+\bullet}$	0	362	95	378	13	336	86	392	45	279	28	364	100	364	100	314	100	298	25
$[M+Na]^{+\bullet}$	+22	384	5	-	-	358	15	414	5	301	6	386	12	386	20	336	10	320	8
$[MH-H_2O]^{+\bullet}$	-18	344	18	360	100	318	10	374	100	261	100	346	85	346	20	296	70	280	65
$[MH-H_2O-HF]^{+\bullet}$	-38	-	-	-	-	298	40	-	-	-	-	-	-	-	-	-	-	-	-
$[MH-CO_2]^{+\bullet}$	-44	318	100	-	-	-	-	-	-	-	-	-	-	-	-	-	-	-	-
$[MH-H_2O-CO]^{+\bullet}$	-46	-	-	-	-	-	-	346	5	-	-	318	10	-	-	268	8	-	-
$[MH-C_3H_7N]^{+\bullet}$	-57	-	-	-	-	279	43	-	-	-	-	-	-	-	-	-	-	-	-
$[MH-H_2O-C_3H_4]^{+\bullet}$	-58	-	-	-	-	-	-	-	-	-	-	-	-	-	-	-	-	240	45
$[MH-H_2O-CO_2]^{+\bullet}$	-62	-	-	316	55	-	-	-	-	-	-	-	-	-	-	-	-	-	-
$[MH-HF-CO_2]^{+\bullet}$	-64	-	-	-	-	-	-	-	-	-	-	-	-	-	-	250	23	-	-
$[MH-H_2O-C_3H_7N]^{+\bullet}$	-75	-	-	-	-	261	100	-	-	-	-	-	-	-	-	-	-	-	-
$[MH-CO_2-C_3H_4]^{+\bullet}$	-84	-	-	-	-	-	-	-	-	-	-	280	15	-	-	-	-	-	-
$[MH-CO_2-C_3H_7N]^{+\bullet}$	-101	261	40	-	-	235	15	-	-	-	-	263	10	263	8	-	-	-	-
$[MH-H_2O-CO_2-C_3H_4]^{+\bullet}$	-102	-	-	-	-	-	-	-	-	-	-	262	20	-	-	-	-	-	-
$[MH-H_2O-CO-C_3H_7N]^{+\bullet}$	-103	-	-	-	-	-	-	289	8	-	-	-	-	-	-	-	-	-	-
$[MH-CO-CO_2-C_3H_4-C_3H_7N]^{+\bullet}$	-169	-	-	-	-	-	-	223	7	-	-	-	-	-	-	-	-	-	-

[a] int. = MS intensity (%)

Table 3.7. ESI-MS fragments of lomefloxacin (M) and its oxidation products.

		M		M+32		M+2		M+16		M+16		M+30		$M-NH_2$	
RT (min)		16.411		11.493		10.369		12.892		14.252		20.322		25.032	
		m/z	int.[a]	m/z	int.	m/z	int.	m/z	int.	m/z	int.	m/z	int.	m/z	int.
$[MH]^{+\bullet}$	0	352	100	384	10	354	100	368	10	368	6	382	98	269	88
$[M+Na]^{+\bullet}$	+22	-	-	-	-	-	-	-	-	-	-	404	30	291	15
$[MH-H_2O]^{+\bullet}$	-18	334	27	366	25	336	50	350	45	350	100	364	100	251	100
$[MH-CO]^{+\bullet}$	-28	-	-	-	-	-	-	-	-	-	-	-	-	241	40
$[MH-2H_2O]^{+\bullet}$	-36	-	-	348	40	-	-	-	-	-	-	-	-	-	-
$[MH-CO_2]^{+\bullet}$	-44	308	55	-	-	-	-	-	-	-	-	-	-	-	-
$[MH-H_2O-CO]^{+\bullet}$	-46	-	-	-	-	-	-	-	-	-	-	336	6	223	40
$[MH-H_2O-CO_2]^{+\bullet}$	-62	-	-	-	-	-	-	306	100	306	60	-	-	-	-
$[MH-2H_2O-2HF]^{+\bullet}$	-76	-	-	308	30	-	-	-	-	-	-	-	-	-	-
$[MH-CO_2-C_2H_5N]^{+\bullet}$	-87	265	40	-	-	-	-	-	-	-	-	-	-	-	-
$[MH-HF-CO-C_2H_5N]^{+\bullet}$	-91	-	-	-	-	-	-	-	-	-	-	291	10	-	-
$[MH-HF-CO-CO_2]^{+\bullet}$	-92	-	-	-	-	-	-	276	30	-	-	-	-	-	-
$[MH-CO_2-C_3H_7N]^{+\bullet}$	-101	251	11	-	-	-	-	-	-	-	-	-	-	-	-
$[MH-H_2O-CO_2-C_2H_5N]^{+\bullet}$	-105	-	-	-	-	-	-	263	45	-	-	-	-	-	-
$[MH-CO-CO_2-C_2H_5N]^{+\bullet}$	-115	237	10	-	-	-	-	-	-	-	-	-	-	-	-
$[MH-HF-2CO-C_2H_5N]^{+\bullet}$	-119	-	-	265	100	-	-	-	-	-	-	263	6	-	-

[a] int. = MS intensity (%)

Table 3.8. ESI-MS fragments of pipemidic acid (M) and its oxidation products.

		M		M+16		M+2		$M-NH_2$		M+2		M+30	
RT (min)		12.284		7.123		9.236		16.257		17.477		18.988	
		m/z	int.[a]	m/z	int.	m/z	int.	m/z	int.	m/z	int.	m/z	int.
$[MH]^{+\bullet}$	0	304	100	320	98	306	20	235	92	306	75	334	60
$[M+Na]^{+\bullet}$	+22	326	5	342	15	328	14	-	-	328	10	356	70
$[MH-H_2O]^{+\bullet}$	-18	286	53	302	100	288	25	217	100	288	100	316	70
$[MH-CO]^{+\bullet}$	-28	-	-	-	-	278	70	207	70	-	-	306	55
$[MH-C_2H_5N]^{+\bullet}$	-43	-	-	-	-	-	-	-	-	263	10	-	-
$[MH-CO_2]^{+\bullet}$	-44	260	20	-	-	-	-	-	-	-	-	-	-
$[MH-CO-NH_3]^{+\bullet}$	-45	-	-	275	15	-	-	-	-	-	-	-	-
$[MH-H_2O-CO]^{+\bullet}$	-46	-	-	-	-	260	65	189	76	-	-	288	100
$[MH-H_2O-C_2H_5N]^{+\bullet}$	-61	243	10	-	-	-	-	-	-	245	5	-	-
$[MH-H_2O-CO_2]^{+\bullet}$	-62	-	-	258	98	244	80	-	-	-	-	-	-
$[MH-2H_2O-CO]^{+\bullet}$	-64	-	-	-	-	-	-	-	-	242	10	-	-
$[MH-CO_2-C_2H_5N]^{+\bullet}$	-87	217	72	-	-	-	-	-	-	-	-	-	-
$[MH-H_2O-CO-C_2H_5N]^{+\bullet}$	-89	-	-	-	-	217	100	-	-	-	-	-	-
$[MH-2H_2O-2CO]^{+\bullet}$	-92	-	-	-	-	-	-	-	-	-	-	242	20
$[MH-H_2O-2CO-C_2H_5N]^{+\bullet}$	-117	-	-	-	-	189	12	-	-	189	6	-	-

[a] int. = MS intensity (%)

Oxidation products of enro (m/z 360), nor (m/z 320), oflox (m/z 362), lome (m/z 352) and PA (m/z 304) were also analyzed by LC/MS (data are shown in Tables 3.4-3.8). The same types of products were identified for all of these FQs (i.e., M-26, M+32, M+30, M-NH_2 and two M+2 products), suggesting that all of the FQs react with MnO_2 via a similar mechanism. Additionally, a trace amount (based on the small MS response) of M+16 product was also found in the oxidation of enro, oflox, lome and PA. The M+16 product was not detected for cipro and nor; however, it might exist at a concentration below the detection limit. Based on the literature that has characterized oxidation products of tertiary amines (Seto and Guengerich 1993, Smith and March 2001), the M+16 product is likely an *N*-oxide analog of FQ (the structure is proposed in Figure 3.5). Furthermore, there were several minor products that were not common for all FQs, including m/z 332 for enro, m/z 348 for nor, and m/z 314 and 298 for oflox. The m/z 332 could be cipro as an oxidation intermediate of enro (Burhenne et al. 1997). The other three peaks could not be identified from the spectral information. These results give clear evidence of a complicated reaction mechanism for FQ oxidation by MnO_2 with many possible reaction products, some of them even undetectable by LC/MS.

Analyzing the oxidation products of FQs (at pH 5) over several hours showed that the MS peak area of the M-26 product increased sharply at the very beginning and then slowly decreased until below the detection limit. The product evolution pattern was quite similar among all of the FQs and the example of cipro is shown in Figure 3.6. This kinetic behavior of the M-26 product indicates that it is an intermediate. The M+16 and M+32 products are also believed to be intermediates due to the similar kinetic trend as that of the M-26 product, although these two products had much lower MS responses and

faster disappearing rates (data not shown). The product evolution studies showed that the abundance of the other four products (M+2a, M+2b, M+30, and M-NH_2) increased and then nearly plateaued over time (Figure 3.6), suggesting them to be the end products. On the other hand, extended time studies up to several days revealed a small decrease in the abundance for the M–NH_2 product.

The distribution among the oxidation end products was evaluated at two reaction times: 3.5 h and 54 h (Table 3.9a and 3.9b). Because authentic standards for each product are not available and difficult to synthesize, the quantitative comparison was based on the MS areas assuming that all products exhibited similar MS responses. This is a reasonable assumption because all of the oxidation products share a common base structure as discussed earlier. At both reaction times, the percentages of the two M+2 products for all FQs were always the lowest (< 6%, except for PA). Likewise, the percentages of the M–NH_2 products were comparable for all FQs (5 – 15 %, except for PA). However, the percentages of the M+30 products were considerably different among the FQs. The percentages of the M+30 product were less than 10% for cipro, enro and nor, whereas more than 18% for oflox and lome. Due to the much slower reaction rate of PA, the percentages of its reaction products were lower than respective those of the other FQs. Despite that, a much greater proportion of the M+30 product than that of the M–NH_2 product was determined at both reaction times (over 10-fold, Table 3.9), making PA behave similarly as oflox and lome.

As indicated in Table 3.9, the product distribution study based on LC/MS analysis could not achieve an overall mass balance. At 3.5 h, all detectable compounds including the parent compound accounted for 34 – 79 % of the initial FQ. At 54 h, only 15 – 42 %

of the initial FQ could be accounted for. The presence of some undetectable products is evident from these results.

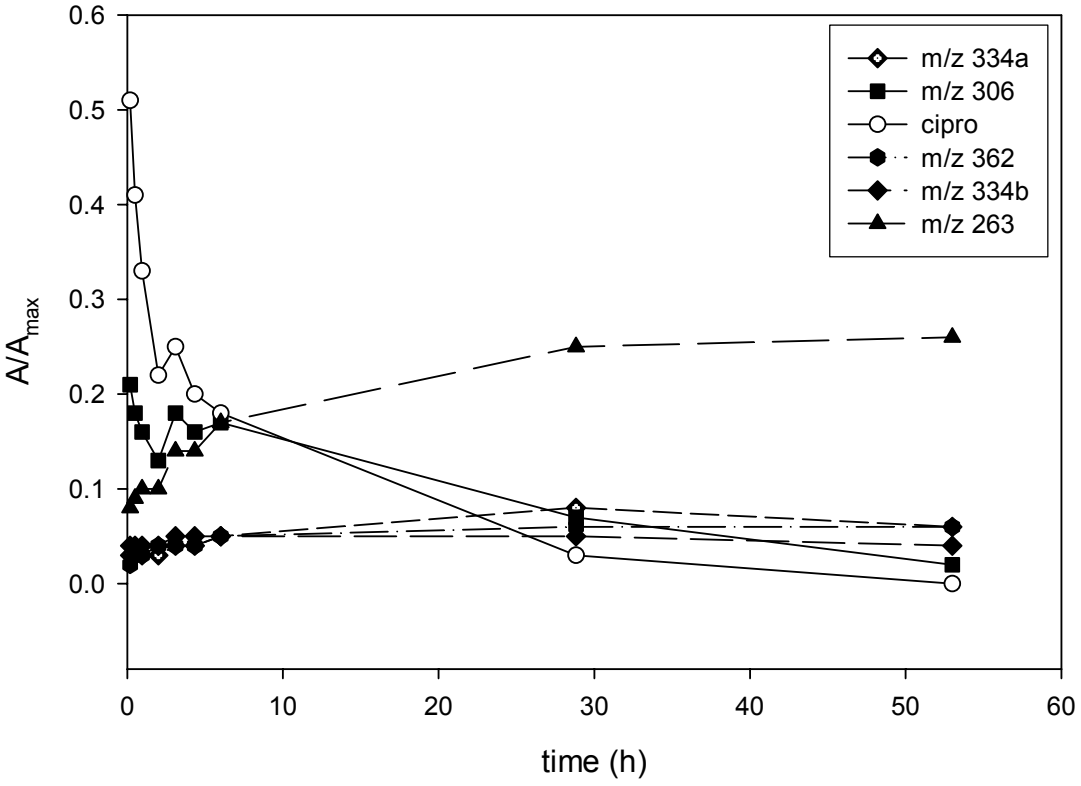

Figure 3.6. Product time evolution study of cipro oxidation by MnO_2. Note: A = MS area of each compound in the reaction mixture at a certain reaction time; A_{max} = MS area of cipro control at a certain reaction time.

Table 3.9. FQs product distribution (%) in reaction with MnO_2[a].

(a). Reaction time 3.5 hours:

	MH^+	M	M+30	M+2[b]	$M-NH_2$	Total [c]
Ciprofloxacin	332	17	6	1	10	34
Enrofloxacin	360	19	10	4	10	42
Norfloxacin	320	22	5	2	10	38
Ofloxacin	362	21	23	<1	5	50
Lomefloxacin	352	45	18	1	15	79
Pipemidic Acid[d]	304	21	8	10	0.3	39

(b). Reaction time 54 hours:

	MH^+	M	M+30	M+2[b]	$M-NH_2$	Total [c]
Ciprofloxacin	332	0	7	3	9	19
Enrofloxacin	360	0	5	6	9	15
Norfloxacin	320	0	8	2	12	21
Ofloxacin	362	0	27	<1	8	36
Lomefloxacin	352	3	24	2	13	42
Pipemidic Acid[e]	304	17	9	14	1	41

[a] Each percentage is the ratio of the corresponding mass spectrum area to the MS area of the control; reaction conditions: $[FQ]_0$ = 0.2 mM, $[MnO_2]_0$ = 2 mM, 0.01 M pH 5 acetic acid buffer, 22°C. [b] The percentage of two peaks with the same mass. [c] The sum of all detectable areas. [d] Reaction time 20 hours. [e] Reaction time 44 hours.

3.3.4 Oxidation Products of the Model Compounds

LC/MS analysis of the PP (m/z 163) reaction mixture exhibited the existence of M-26, M+2, and M+30 products (Table 3.10). Its M–NH_2 product (i.e., aniline) was not detected. This is not surprising since aniline itself reacted relatively fast with MnO_2 (Table 3.2). Additionally, a dimeric product of the M+30 product (m/z 383) appeared in the chromatogram, confirming the occurrence of the dimerization reaction. For PM (m/z 164) reaction mixture, two dimeric products of PM (m/z 327) and one dimeric product of PM reaction intermediate (m/z 355) were detected as major peaks, further supporting the likelihood of dimerization via the inner N (i.e., N1) connecting to the benzene ring (Table 3.11).

GC/MS analysis provided additional fragmentation information for the reaction products of PP (Figure 3.7). The minor peak at 14.22 min corresponds to the M+2 product whereas the major peak at 15.58 min corresponds to the M+30 product. Formation of the m/z 164 and 118 fragments supports the presence of two carbonyl groups in the M+30 product (Figure 3.7d). Likewise, formation of the m/z 119 fragment supports the position for the carbonyl group at the outer N (i.e., N6) for the M+2 product (Figure 3.7c). The fact that the M+2 product with a carbonyl group at the inner N atom (i.e. N1) was not detected does not necessarily exclude its presence in the reaction mixture. One possible reason for its non-detection is the low extraction efficiency, as suggested by that of the parent compound (~ 33% for PP). This low extraction efficiency could also be the reason for the lesser number of products being detected by GC/MS than by LC/MS.

N-ethylformanilide (Table 3.2) was studied as a surrogate standard for the M+2 products. Much less adsorption of N-ethylformanilide to MnO_2 was observed compared to that of the other model compounds. N-ethylformanilide was also found to be stable in the presence of MnO_2 for up to 6 days, verifying the stability of the M+2 products. Both GC/MS and LC/MS chromatograms of N-ethylformanilide exhibited base peaks corresponding to the loss of the carbonyl group, consistent with the spectra for the M+2 and M+30 products (Table 3.12).

PP reaction mixture was further analyzed by a FTIR spectrometer. In contrast to the control solution of PP, the reaction mixture showed one strong peak at 1730 cm^{-1} (Figure 3.8). This peak is characteristic of carbonyl absorbance, providing a strong evidence for the presence of >C=O group in the oxidation products of PP.

Table 3.10. ESI-MS fragments of 1-phenylpiperazine (M) and its oxidation products.

		M		M+2		M-26		M+30		2(M+30)	
RT (min)		7.268		4.076		5.242		12.418		18.408	
		m/z	int.[a]	m/z	int.	m/z	int.	m/z	int.	m/z	int.
$[MH]^{+\bullet}$	0	163	100	165	23	137	15	193	25	383	68
$[2M+Na]^{+\bullet}$	-	-	-	353	30	-	-	-	-	-	-
$[M+Na]^{+\bullet}$	+22	-	-	-	-	-	-	215	50	405	100
$[MH-NH_3]^{+\bullet}$	-17	-	-	148	100	120	100	-	-	-	-
$[MH-H_2O]^{+\bullet}$	-18	-	-	-	-	-	-	175	20	-	-
$[MH-CO]^{+\bullet}$	-28	-	-	-	-	-	-	165	60	355	35
$[MH-C_2H_5N]^{+\bullet}$	-43	120	10	-	-	-	-	-	-	-	-
$[MH-CO-NH_3]^{+\bullet}$	-45	-	-	120	12	-	-	148	100	-	-
$[MH-C_3H_7N]^{+\bullet}$	-58	105	8	-	-	-	-	-	-	-	-
$[MH-2CO]^{+\bullet}$	-56	-	-	-	-	-	-	137	5	-	-
$[MH-2CO-NH_3]^{+\bullet}$	-73	-	-	-	-	-	-	120	10	-	-
$[MH-2CO-CH_3-NH_3]^{+\bullet}$	-88	-	-	-	-	-	-	105	10	-	-
$[MH-HF-CO_2]^{+\bullet}$	-(M+30)+Na	-	-	-	-	-	-	-	-	215	15

[a] int. = MS intensity (%)

Table 3.11. ESI-MS fragments of 1-phenylmorpholine (M) and its oxidation products.

		M		Dimeric product_1		Dimeric product_2		Dimeric product_3		M+2		M+30	
RT (min)		29.142		3.881		5.228		6.626		12.166		25.402	
		m/z	int.[a]	m/z	int.	m/z	int.	m/z	int.	m/z	int.	m/z	int.
$[MH]^{+\bullet}$	0	164	45	327	100	327	10	355	100	166	15	194	3
$[M+Na]^{+\bullet}$	+22	-	-	-	-	-	-	-	-	188	100	216	100
$[MH-H_2O]^{+\bullet}$	-18	146	20	-	-	-	-	-	-	-	-	-	-
$[MH-C_2H_4O]^{+\bullet}$	-44	120	100	283	10	283	100	311	7	-	-	-	-
$[MH-H_2O-CO]^{+\bullet}$	-46	-	-	-	-	-	-	-	-	-	-	148	46
$[MH-C_3H_7O]^{+\bullet}$	-59	105	10	-	-	-	-	-	-	-	-	-	-
$[MH-C_3H_8O]^{+\bullet}$	-60	-	-	267	7	-	-	-	-	-	-	-	-
$[MH-C_2H_4O-H_2O]^{+\bullet}$	-62	-	-	-	-	265	6	-	-	-	-	-	-
$[MH-C_2H_4O-CO]^{+\bullet}$	-72	-	-	-	-	255	25	-	-	-	-	-	-
$[MH-C_4H_9O]^{+\bullet}$	-73	91	9	254	6	-	-	-	-	-	-	-	-
$[MH-C_2H_4O-H_2O-CO]^{+\bullet}$	-88	-	-	-	-	237	35	-	-	-	-	-	-
$[MH-2H_2O-2CO]^{+\bullet}$	-92	-	-	-	-	-	-	263	8	-	-	-	-
$[MH-C_2H_4O-C_4H_9O]^{+\bullet}$	-118	-	-	-	-	209	30	-	-	-	-	-	-
$[MH-2C_3H_8O]^{+\bullet}$	-119	-	-	208	7	-	-	-	-	-	-	-	-

[a] int. = MS intensity (%)

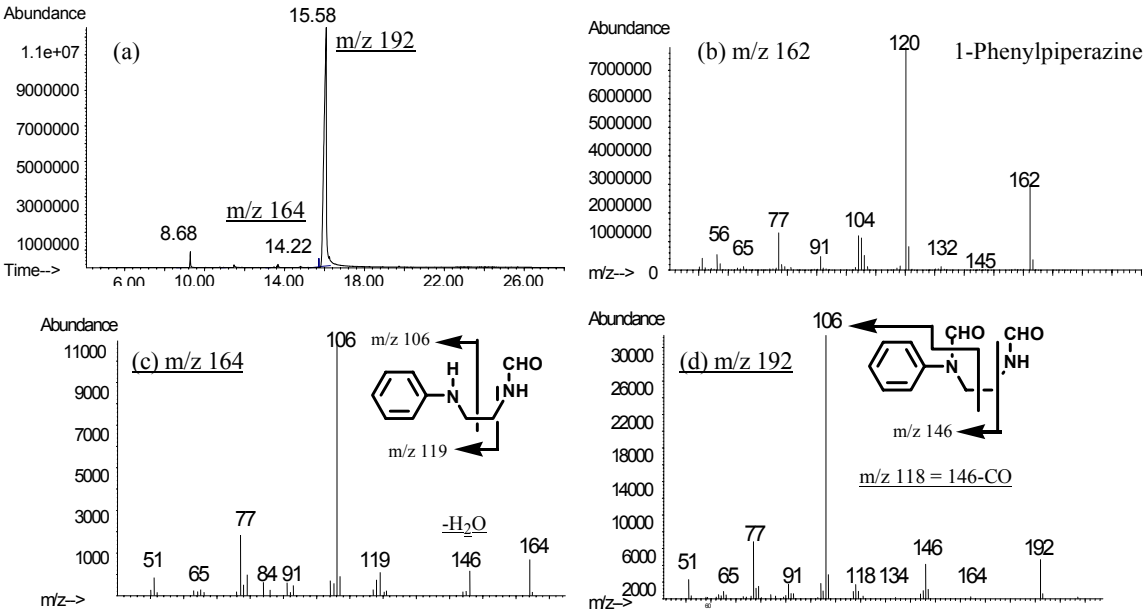

Figure 3.7. Oxidation of 1-phenylpiperazine analyzed by GC/MS. (a) The chromatogram of 1-phenylpiperazine reaction extract; (b)-(d) The mass spectra of 1-phenylpiperazine, product m/z 164 and m/z 192. The fragmentations of two products are depicted in (c) & (d).

Table 3.12. ESI-MS fragments of N-ethylformanilide.

		M	
RT (min)		26.369	
		m/z	int.[a]
$[MH]^{+\bullet}$	0	150	65
$[MH-H_2O]^{+\bullet}$	-18	132	22
$[MH-CO]^{+\bullet}$	-28	122	100
$[MH-CH_4-HCO]^{+\bullet}$	-45	105	68
$[MH-C_2H_4-CO]^{+\bullet}$	-56	94	92
$[MH-C_2H_5N-HCO]^{+\bullet}$	-73	77	8

[a] int. = MS intensity (%)

a) PP reaction mixture:

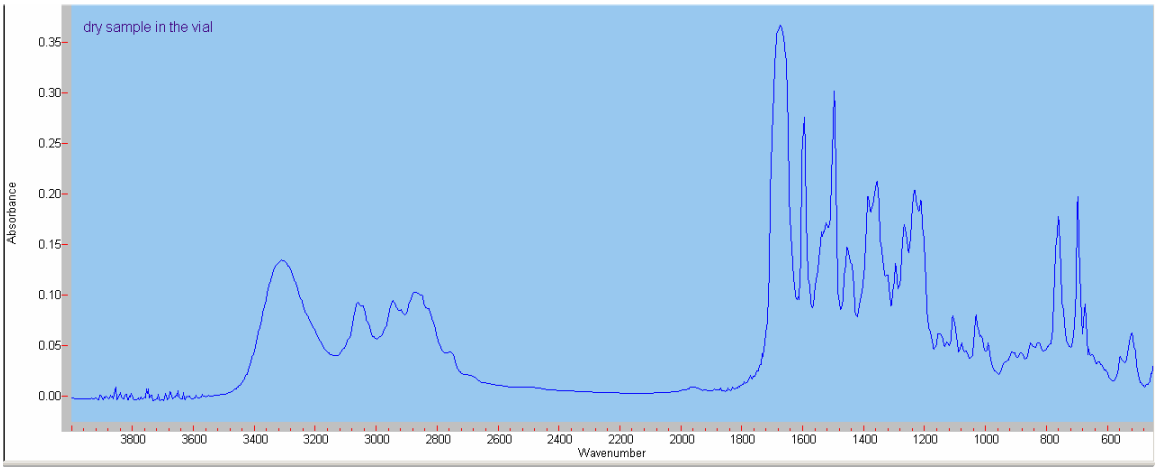

b) PP control

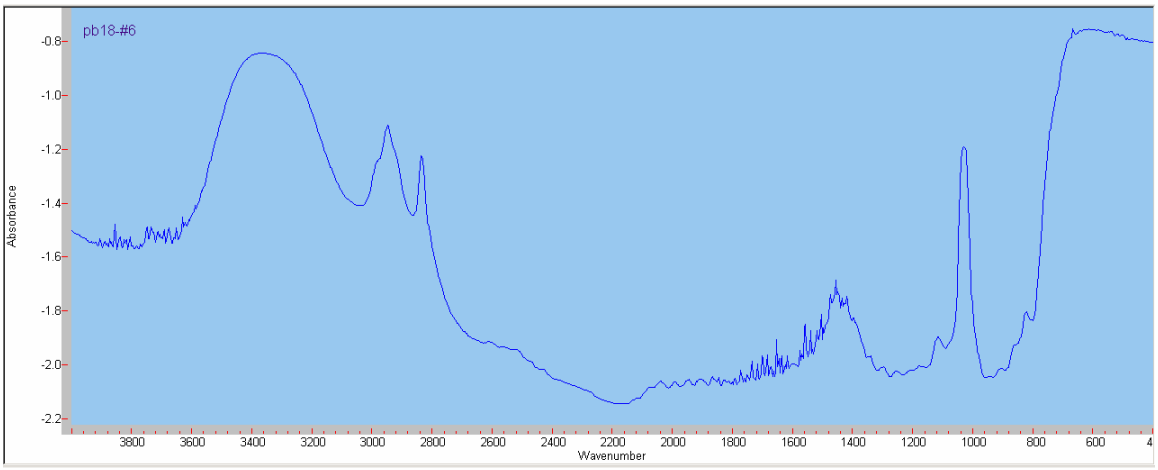

Figure 3.8. FTIR spectra of the extracts for PP reaction mixture and PP control.

3.4 Discussion

3.4.1 Chemical Reactivities and Reactive Sites

The inertness of FLU in contrast to the high reactivities of the other FQs (Table 3.1) strongly suggests that the piperazine ring is the reactive site to oxidation by Mn oxide. Comparison of reactivities among the FQs and model compounds also supports the above conclusion and further points to the inner N (i.e., N1) of the piperazine ring to be the rate-limiting reactive site. For example, cipro and nor differ only in the substituent (i.e., cyclic propanyl versus ethyl) to the N atom of the aromatic heterocyclic ring. The fact that cipro and nor have similar reactivities suggests that the reaction center is unlikely associated with the heterocyclic ring N. Enro differs from cipro only in its additional ethyl substituent at the outer N (i.e., N6) in the piperazine ring; however the reaction rate constants of these two compounds are comparable (Table 3.1). In a previous study on the oxidation of aliphatic amines by aqueous $(batho)_2Cu^{II}$, Wang and Sayre (1992) observed that the reactivities of amines followed the trend of primary < secondary < tertiary owing to the increased bacisity of amine nitrogen atoms, and that tertiary amines reacted at an average 4-fold faster rate than secondary amines. If the rate-limiting steps were associated with the N6 atom, enro (a tertiary amine) would react faster than cipro (a secondary amine) – a scenario that was clearly not observed in the experiments. Additionally the fact that lome and PA showed nearly 2-fold and 10-fold slower reaction rate, respectively than cipro is also consistent with the decreased bacisity of their N1 atoms. The bacisity of the N1 atom was estimated using the SPARC computer program (SPARC) as shown by the pK_{a3} value in Table 3.1: -0.84 for cipro > -1.48 for lome > -5.28 for PA. In other words, the electron-withdrawing substituents present in the

aromatic rings of lome and PA (i.e., the 5-fluorine substituent in lome and the two ring N's in PA) reduce the bacisity of N1 via resonance and electronic effects, and hence slow the reaction rate of lome and PA with MnO_2. The lower adsorption of lome and PA to Mn oxide compared with all the other FQs (Table 3-1) could also be linked to the above mentioned electron-withdrawing effect.

In the model compounds, PM and PD closely resemble PP except that N6 is replaced by an oxygen in PM, and N1 is replaced by a carbon in PD (Table 3.2). The much faster rate of PM (k_{obs} = 0.24 ± 0.07 h^{-1}) than that of PD (k_{obs} = 0.20E-2 h^{-1}) further supports the N1 atom to be the most reactive site. This nearly 2 orders of magnitude difference in the reaction rates can be attributed to several factors including (i) higher reactivity of tertiary amine (in PM) than secondary amine (in PD), (ii) resonance stabilization of N1 by the neighboring benzene ring in PM (see more discussion in the reaction scheme part), and (iii) lower adsorption of PD (19%) than that of PM (56%) to MnO_2.

The experiments also showed a 28-fold faster rate for PP (k_{obs} = 6.70 ± 0.10 h^{-1}) than PM, although both compounds adsorbed to MnO_2 to a similar extent (53 % for PP and 56 % for PM, Table 3.2). These results reflect the reactivity of N6 (in addition to N1) to oxidation in PP versus the inertness of oxygen atom in PM. However, based on the slow reaction rate of PD, the reactivity of N6 alone cannot explain this 28-fold increase in the reaction rate. Interactions could exist between the N1 and N6 atoms during the oxidation reaction and affect the overall reaction rate. As suggested in the work by Wang and Sayre (Wang and Sayre 1992), the oxygen atom present in PM may exert an electron-withdrawing effect on the N1 atom and reduce its reactivity. A similar

phenomenon may also explain the reactivity of oflox. Oflox contains an electron-withdrawing 5-oxygen substituent (on the aromatic ring) that deactivates its N1, as well as a methyl group that activates its N6 (i.e., resulting in a tertiary amine) (Table 3.1). These two effects may cancel out through the N1 and N6 interactions, rendering the reactivity of oflox similar to those of cipro, enro, and nor.

The fact that PP reacts faster than FQs may be explained by steric and electronic effects, in analogy to the oxidation of other compounds by MnO_2 (e.g. Stone 1987). For steric effects, the much smaller size of PP molecules likely enables their access to more available active surface sites, as indicated by the higher adsorption percentage of 47 % for PP versus 34 % for cipro at pH 6. For electronic effects, the multiple electron-withdrawing substituents on the aromatic heterocyclic ring in FQs (versus the benzene ring in PP) would definitely exert a retarding effect on the oxidation reactions of the FQs (Wang and Sayre 1992).

The oxidation of FQs at the N1 position may be considered to be similar to the oxidation of aniline, in which FQs could be viewed as N,N-disubstituted anilines. Aniline oxidation by Mn oxides proceeds by producing anilinium radicals followed by coupling reactions of the radicals (e.g., Laha and Luthy 1990). By analogy, FQs (and their corresponding dealkylated products) may be oxidized by Mn oxide through a radical coupling pathway, though likely at a much slower rate than aniline due to the retardation effects by the electron-withdrawing substituents on the aromatic heterocyclic ring. This deduction can also explain the slow decrease in the fully dealkylated product ($M\text{-}NH_2$) over extended reaction time. However, products from radical coupling were not detected in this study and that could be caused by: (1) only supernatants were analyzed for

products, and (2) dimeric products might adsorb strongly to Mn oxide and thus were difficult to extract for analyses. Based on the observations that FQs reacted about 3-fold slower than PP at pH 6, and that aniline reacted about 3-fold slower than PP at pH 5 (Tables 3.1 and 3.2), we would expect FQs and aniline to react with MnO_2 at similar rates. However, as discussed earlier, theoretical assessment of the N1 reactivity does not yield such a conclusion. This contradiction provides another evidence that the reactivity of FQs with MnO_2 cannot be explained solely by the N1 oxidation through radical coupling reactions, i.e., other parallel oxidation pathways must be involved.

3.4.2 Surface Reaction Pathways

On the basis of the reaction kinetics, product identification, literature on the photodegradation of FQs, and literature on the oxidation of substituted anilines by metal oxides and other oxidants (e.g., Stone 1987, Laha and Luthy 1990, Burhenne et al. 1997, Fasani et al. 1999, Iley and Tolando 2000), a surface reaction scheme for the oxidation of FQs by Mn oxide has been developed (Figure 3.9). In summary, the redox reaction is initiated by generating a surface complex between the FQ and MnO_2. Within the surface complex, one electron is transferred from the FQ N1 atom to the surface-bound Mn^{IV} to yield a radical intermediate and a Mn^{III} ion that can be further reduced to Mn^{II}. The formed radical intermediate can be stabilized by the neighboring aromatic ring via resonance effects. Organic oxidation products and Mn^{2+} are then released from the oxide surfaces. The surface complex formation and electron transfer are likely rate-limiting. Any factors that may affect either of them will potentially influence the overall reaction rate. Among the possible factors are properties of FQs. For example, electron-

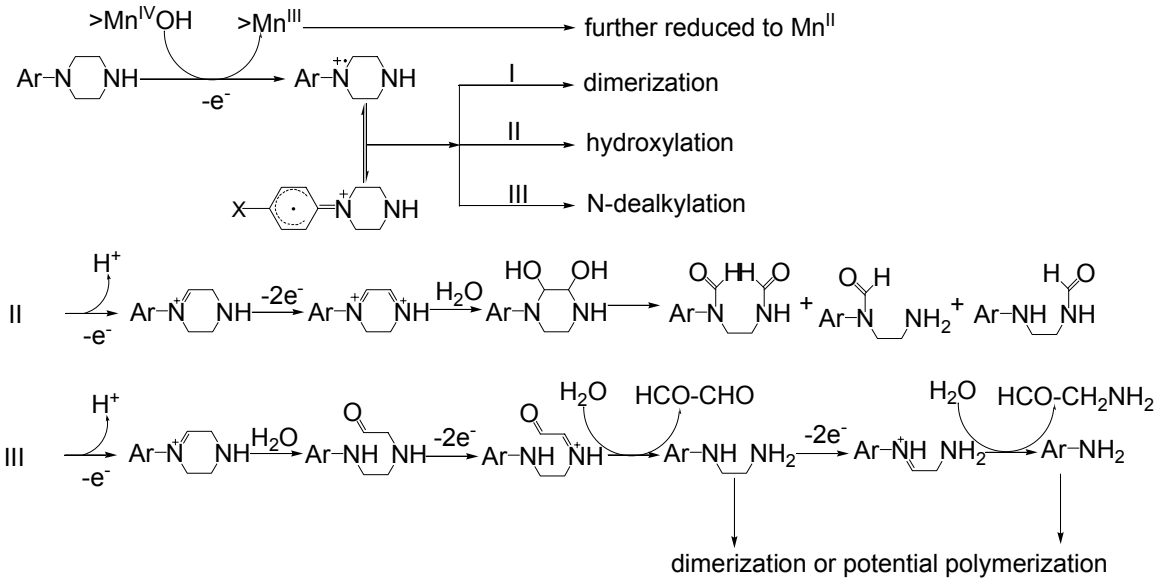

Figure 3.9. Proposed reaction scheme for oxidation of FQs by MnO_2.

withdrawing substituents on FQs would interfere with electron transfer from the FQ to the surface-bound Mn^{IV} and thus lead to a slower oxidation rate (Laha and Luthy 1990). Additionally, the relatively larger FQ molecules (than the model compounds) would obstruct more active surface sites, limit the number of surface complexes and thus achieve surface saturation faster. For instance, in our earlier study on the oxidation of the phenolic antibacterial agent triclosan with MnO_2, the surface saturation was not observed at a triclosan to MnO_2 molar ratio of 10 : 100 (Zhang and Huang 2003). In contrast, a cipro to MnO_2 molar ratio of 3 : 100 was already enough to render the surface saturation in this study (Figure 3.4).

The strong pH dependence of the reaction rate (Figure 3.3) can be attributed to the effects of pH on the rate-limiting step(s). For surface complex formation, experiments showed that the adsorption of cipro increased with decreasing pH (Figure 3.3b), suggesting that lowering the solution pH provides a greater number of surface species that favor interaction with cipro. A similar effect of pH on resulting in more surface favorable species has already been observed in the oxidation of chloroanilines by Mn oxides (Pizzigallo et al. 1998). For electron transfer, the reduction potential of MnO_2 increases from 0.76 V to 0.99 V (Stumm and Morgan 1996) when pH is decreased from 8 to 4. Our previous study on the oxidation of triclosan and chlorophene (also a phenolic antibacterial agent) by MnO_2 yielded reaction orders of 0.46 - 0.50 for H^+ (Zhang and Huang 2003), highly comparable to the reaction order of 0.49 observed in the oxidation of cipro by MnO_2. The fact that the reaction order for H^+ did not vary when different organic reductants were involved indicates that the effect of pH in these cases is mainly on the Mn oxide, i.e., on affecting the reduction potential of MnO_2.

Three major pathways are likely involved in the generation of FQ oxidation products (Figure 3.9). Pathway I is dimerization of the radical intermediates. The coupling reaction most likely occurs at the inner N1 position because of blockage at the *para* position in the aromatic heterocyclic ring (Stassen and Hambitzer 1997). Polymerization of the radicals is unlikely due to the strong steric hindrance in the FQ molecules. Pathway II involves one-electron transfer of the radical intermediate to Mn^{IV}/Mn^{III} yielding an iminium ion (Smith and Mortimer 1986, Seto and Guengerich 1993, Bietti et al. 1998, Cuppoletti et al. 1999, Iley and Tolando 2000). The outer N6 in the piperazine ring then undergoes a similar 2-electron transfer generating another iminium ion at the same ethylenediamine edge as the N1 (Wang and Sayre 1992). This ion is then quickly hydrolyzed to a 1,2-diol intermediate (i.e., M+32) (Carey and Sundberg 2000, Smith and March 2001). In the presence of MnO_2, the 1,2-diol intermediate is readily oxidized to yield a di-aldehyde product (i.e., M+30) (Adler and Becker 1961, Ohloff and Giersch 1973). The two M+2 products are also believed to be produced in the process of the diol oxidation, although further confirmatory study is necessary. On the basis of pathway II and experimental results, the likely oxygen source for the diol and >C=O groups in the hydroxylation products is the -OH groups closely associated with the Mn oxide skeleton.

Pathway III resembles pathway II initially on the formation of an iminium ion. However, hydrolysis of the iminum ion follows. Although hydrolysis of an iminium ion with the N atom connecting to an aromatic ring is a relatively slow process (Carey and Sundberg 2000, Smith and March 2001), it may still kinetically compete with the electron transfer reaction. In this case, the outer N6 in the hydrolyzed intermediate then loses two

electrons to the surface-bound Mn^{IV} yielding another iminium ion, also at the same ethylenediamine edge as the N1 (Wang and Sayre 1992). Further hydrolysis leads to the production of the M-26 product. In a similar fashion, the M-26 product is oxidized to its corresponding iminium ion at its inner N1, and finally hydrolyzed to the M-NH_2 product (Wang and Sayre 1992). Due to their substituted aniline-like structures (Figure 3.5), both M-26 and M-NH_2 products may further oxidize and form dimeric products in the presence of excess amounts of MnO_2 (Laha and Luthy 1990, Stassen and Hambitzer 1997).

The extents of the aforementioned three pathways will be affected by both steric and electronic effects. Similar steric hindrance is expected among the FQs examined in this study due to their common base structure. However, different electronic effects from the aromatic ring neighboring to the piperazine moiety exist among the FQs and may exert a dominant influence on the stability of the radical intermediates, and hence affect the reaction kinetics and product distributions. For example, the electron-withdrawing substituents in oflox, lome and PA can slow the electron transfer within the surface complex precursors to form anilinium radical intermediates, and thus cause slower reaction rates for these compounds as observed in Table 3.1 (note: the reaction rate of oflox is faster than lome and PA most likely due to the higher reactivity of its tertiary N6). It's also plausible that the stability of the anilinium radicals is more critical for the dimerization pathway than for the other two pathways. Since the electron-withdrawing substituents in oflox, lome and PA make the radical intermediates less stable, less dimeric products and more hydroxylated products will be expected. Indeed oflox, lome, and PA yielded higher percentages of the hydroxylated products (i.e., the M+30 products) than

cipro, enro, and nor (Table 3.9). Reaction pathways other than the three proposed in Figure 3.9 cannot be excluded; for example, one of which could be a pathway leading to a trace amount of the *N*-oxide product (i.e., M+16). Due to the high complexicity of these surface reactions, the inability to detect any FQ dimeric products, and the general low mass balance in the product analyses, the relative contribution from each reaction pathway cannot be concluded with the current data. Nevertheless, the product distribution shown in Table 3.9 provides some indication as to the contribution of major pathways to the overall reaction. For example, N-dealkylation accounts for approximately 10% in the overall reaction for all of the FQs. Hydroxylation, on the other hand, accounts for approximately 10% (for cipro, enro and nor) to 25% (for oflox, lome, and PA) in the overall reaction.

3.5 Conclusions

Manganese oxides commonly found in soils are known to facilitate degradation of organic contaminants. Recent research reported that unintentional release of fluoroquinolone antibacterial agents (FQs) into aquatic environments could pose health and ecological threats. In this study, FQs including ciprofloxacin (cipro), enrofloxacin (enro), norfloxacin (nor), ofloxacin (oflo), lomefloxacin (lome), and pipemidic acid (PA) were found to be readily oxidized by Mn dioxide (δ-MnO_2). A comparison of k_{obs} values for the FQs showed that the former four FQs reacted with MnO_2 at very similar rates while lome and PA reacted much more slowly, likely due to the presence of electron-withdrawing substituents in their aromatic rings (i.e., 5-fluorine substituent in lome and two ring N's in PA) which reduced the bacisity and reactivity of the N1 atom via

resonance and electronic effects. These interfacial reactions exhibited complex reaction kinetics. The initial reactions were first-order with respect to FQs and MnO_2 (applicable within the employed experimental conditions), whereas later reactions exhibited more complicated kinetics which was consistent with the limited available active surface sites. The reaction rate and adsorption of the FQs to MnO_2 both increased as pH decreased, which can be attributed to the effects of pH on both precursor complex formation and electron transfer between FQs and Mn oxide surfaces. Comparison among the FQs demonstrated that the piperazine ring within the FQs is the reactive site toward oxidation by Mn oxides.

To facilitate elucidating the reaction mechanisms, oxidation of structurally-related aniline and alicyclic amines including 1-phenylpiperazine (PP), N-phenylmorpholine (PM), and 4-phenylpiperidine (PD) by Mn oxides has also been investigated. The reactivity of these model compounds further confirms that the N1 atom of the piperazine ring is the rate-limiting reactive site. Additionally interactions likely exist between the piperazine N1 and N6 atoms during oxidation and affect the overall reaction rate. Similar product patterns as those of FQs were observed for PP oxidation by both LC/MS and GC/MS analyses. FTIR spectra provide strong evidence for the presence of the >C=O group in PP oxidation products. Dimerization and possibly polymerization were observed in the oxidation of these model compounds by Mn oxides.

The compound reactivity comparison by HPLC and the product identification by LC/MS, GC/MS and IR indicate that three major reaction pathways are involved. The reaction is initiated by formation of a common radical intermediate that is centered at the inner N1 on the piperazine moiety, followed by three pathways to form the reaction

products. Pathway I is the coupling reaction of the radical intermediates to form dimeric products, most likely at the inner N1 position. In pathway II, the radical intermediates are further oxidized to form iminium ions which are then subject to hydrolysis leading to generation of 1,2-diol. In the presence of MnO_2, 1,2-diol is readily oxidized to yield mono-aldehyde and di-aldehyde products. In pathway III, the piperazine ring of the radical intermediate is broken upon hydrolysis and oxidation to yield dealkylated products. Due to the substituted aniline-like structures, these dealkylated products could further oxidize to form dimeric products in the presence of excess amounts of MnO_2.

In addition to chemical reactivity, the product distribution of FQs is also affected by the substituents on the aromatic heterocyclic ring linked to the piperazine moiety via electronic and resonance effects. Electron-withdrawing substituents can reduce the stability of the anilinium radicals and inhibit pathway I most significantly. Thus the electron-withdrawing substituents in oflox, lome and PA lead to the generation of less dimeric products and more hydroxylated products compared to the cases of cipro, enro, and nor.

Based on the mass balance of the product formation, N-dealkylation accounts for approximately 10% in the overall reaction for all of the FQs. Hydroxylation accounts for approximately 10% (for cipro, enro and nor) to 25% (for oflox, lome, and PA) in the overall reaction. The contribution from other reaction pathways is possible and cannot be determined based on the current data, and warrants further studies.

3.6 Environmental Significance

This investigation shows fast degradation of fluoroquinolone antibacterial agents in the presence of Mn oxides. Due to the strong adsorption of FQs toward soils and sediments (Tolls 2001), reactions with Mn oxides will likely play an important role in the attenuation of FQs at soil-water interfaces. An earlier study reported that the carboxylic acid moiety is the sorption site of FQs towards clay minerals (Nowara et al. 1997). However, this study found that FQs did not adsorb to MnO_2 any more strongly than the model compounds (e.g., 47 % for PP versus 34 % for cipro at pH 6) and that FLU adsorbed poorly to MnO_2 (~10% at pH 6), indicating that MnO_2 may behave quite differently from clay minerals in adsorptive interactions with the FQs and model compounds. Additionally, much poorer adsorption to MnO_2 was observed with PD and N-ethylformanilide compared to the other model compounds. Because the model compounds lack the carboxylic acid group, PD lacks the N1 atom in the piperazine ring and N-ethylformanilide possesses alkyl substituents on the N1 atom, the piperazine moiety and mostly likely the N1 atom of the piperazine may be more active than the carboxylic acid group in the adsorption to MnO_2. It can also be anticipated that the oxidation products of FQs may have different adsorption capability from the parent FQs, which in turn will affect their bioavailability and toxicity. For example, the hydroxylation products may be less adsorptive and the dimerization products may be more adsorptive.

In comparison to the reaction facilitated by Mn oxides, photodegradation is another important degradation pathway for FQs in shallow waters (e.g., Mella et al. 2001). Dealkylated products similar to those found in this study have been identified in the FQ photodegradation mixtures (Burhenne et al. 1997, Mella et al. 2001). Several

groups have examined the antibiotic activity of FQ photodegradation products (Phillips et al. 1990, Sunderland et al. 1999, Sunderland et al. 2001). No detectable antibiotic activity was observed for the photodegradation products of cipro. In contrast, antimicrobial activity against *E. coli*, *E. cloacae* and *K. oxytoca* was statistically significant with increased levels of photodegradation for oflox and levofloxacin (Sunderland et al. 2001). Fasani et al. (1999) reported that photodegradation of oflox was much slower than that of cipro, enro and nor due to its 5-oxygen electron-withdrawing substituent (versus 5-hydrogen substituent in the others), and underwent primarily defluorination while the other three FQs underwent primarily dealkylation. Thus the dealkylated products might lose their antibiotic activity while the defluorinated products might not. If the above reasoning was indeed correct, the dealkylated oxidation products of FQs with Mn oxide would also lose their antibiotic activity. Information regarding the antibiotic activity of the dimerization and hydroxylation products of FQs is currently not available and thus necessitates further investigation.

CHAPTER 4

ADSORPTION AND OXIDATIVE TRANSFORMATION OF FLUOROQUINOLONES AND STRUCTURALLY RELATED AMINES IN THE PRESENCE OF GOETHITE

4.1 Introduction

The widespread presence and the potential toxicities of fluoroquinolone antibacterial agents (FQs) in the environment (Volmer et al. 1997, Hartmann et al. 1999, Golet et al. 2001, Kolpin et al. 2002, Golet et al. 2002, Renew and Huang 2004) necessitate further investigation on their fate and transformation in order to properly evaluate their risks. In addition to the extensive studies on biodegradation (e.g, Parshikov et al. 1999, Wetzstein et al. 1999) and photodegradation (e.g., Burhenne et al. 1999, Mella et al. 2001, Fasani et al. 2001) of FQs, strong adsorption of FQs to soils and sediments has been well documented in the literature (Nowara et al. 1997, Tolls 2001). The favorable interactions of FQs with soils and sediments point to the potentially significant role of minerals in the environmental fate of these compounds. Of particular interest in this regard is the metal oxide (e.g., Mn oxides or Fe oxides) facilitated oxidation. A previous study has investigated the reaction kinetics and mechanism of Mn oxide-facilitated oxidation of FQs (Zhang and Huang 2004). Here, the FQs in question were found to be readily oxidized by Mn dioxide (δ-MnO_2) through a surface process and the overall reactions exhibited complex kinetics. The reaction rate and adsorption of the FQs to MnO_2 were highly pH dependent and both increased as pH decreased. The reactivity comparison among the FQs and the product identification indicated that (i) the

piperazine ring within the FQs was the adsorptive and reactive site toward Mn oxides, and (ii) three major reaction pathways were likely involved in the oxidation of FQs by MnO_2 (dimerization, hydroxylation, and N-dealkylation), sharing a common radical intermediate which was most probably centered at the inner N on the piperazine moiety.

In the present study, the oxidation reaction of FQs by Fe oxides was studied as a potential means for natural attenuation of FQs at the mineral-water interface. Fe oxides, a common component in clay minerals, are known to facilitate abiotic reactions of organic pollutants via redox reactions. Fe oxides have lower reducing power than Mn oxides (reduction potentials of 0.67 V and 1.23 V for FeOOH and MnO_2, respectively (Stone 1987)); however, they are more important in a practical sense due to their widespread abundance in soils and sediments. For example, in recognition of more amine loss than the amount of Mn(III/IV) reduced to Mn(II) in the presence of whole soils, Li et al. (2003) proposed that Fe reduction did contribute to the further oxidation of the more reactive amines when all readily reducible Mn was consumed. Fe oxides have also been shown to be effective oxidants for a wide range of pollutants including phenolic compounds (McBride 1987, Pizzigallo et al. 1995), hydroquinone (e.g. Kung and McBride 1988), and chloroanilines (Pizzigallo et al. 1998).

In addition to their oxidation ability in the dark, iron oxides were also recognized for their special photochemical properties of oxidizing organic compounds in natural waters and atmospheric and surface droplets (Wu and Deng 2000). Amino- and chlorophenols (Pulgarin and Kiwi 1995, Bandara et al. 2001) and organic acids (Cunningham et al. 1988, Goldberg et al. 1993, Pehkonen et al. 1995) have all been

successfully photolyzed in the presence of goethite and the reaction kinetics of the surface photolysis were much faster than those without light.

The study described here investigated the specific effects of Fe oxides in degrading FQs including ciprofloxacin (cipro), enrofloxacin (enro), flumequine (FLU), norfloxacin (nor), ofloxacin (oflox), lomefloxacin (lome), and pipemidic acid (PA) (structures are shown in Table 4-1). Two types of Fe oxides were selected for surface comparison: goethite chemically synthesized in our lab and goethite from the commercial supplier Aldrich. Experiments were conducted to determine adsorption isotherms, reaction kinetics and product formation. Effects of O_2 and light on the reaction kinetics were also evaluated. On the basis of these results, adsorptive and reactive sites were identified and reaction schemes were proposed. Parallel studies involving oxidation of structurally-related anilines and alicyclic amines including 1-phenylpiperazine (PP), N-phenylmorpholine (PM), and 4-phenylpiperidine (PD) (structures are shown in Table 4-2) were also conducted to assess compound reactivities and illustrate reaction mechanisms.

4.2 Materials and Methods

4.2.1 Chemical Reagents

Reagent-grade water (18.3 MΩ-cm resistivity) was prepared by a Millipore Nanopure water system. Cipro, enro, nor, oflox, and FLU were purchased from ICN (Irvine, CA). Lome and PA were purchased from Sigma (St. Louis, MO). The purity of the above compounds was not specified. Aniline, *N,N'*-dimethylaniline, PP and PM were obtained from Aldrich (St. Louis, MO) at greater than 98% of purity. PD was purchased from Acros (Fairlawn, NJ) at 98% of purity. Other employed chemical reagents

Table 4-1. Kinetic comparison among fluoroquinolones [a].

Compound	Structure	pK_{a1} [b]	pK_{a2} [b]	pK_{a3} [b]	k_{obs} (h^{-1})	Adsorption (%)[c]
Ciprofloxacin [85721-33-1] (cipro)	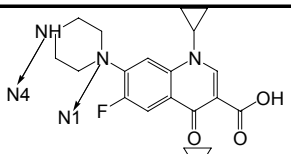	5.46	7.67	-0.84	$0.45 \pm 0.30 \times 10^{-3}$	62 ± 1
Enrofloxacin [93106-60-6] (enro)	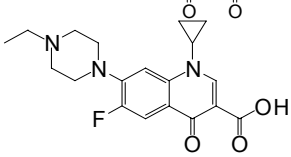	5.46	7.03	-0.84	$0.30 \pm 0.40 \times 10^{-3}$	54 ± 1
Norfloxacin [70458-96-7] (nor)	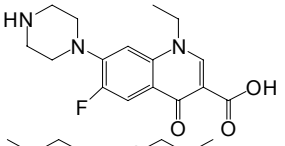	5.46	7.67	-0.84	$1.65 \pm 1.10 \times 10^{-3}$	65 ± 1
Ofloxacin [83380-47-6] (oflox)	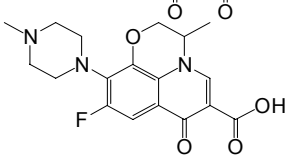	5.41	7.08	0.79	$0.22 \pm 0.40 \times 10^{-3}$	50 ± 2
Lomefloxacin [98079-51-7] (lome)	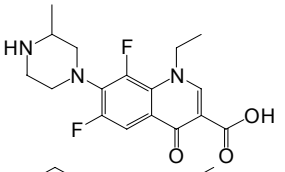	5.38	7.85	-1.48	$0.11 \pm 0.20 \times 10^{-3}$	54 ± 1
Pipemidic Acid [51940-44-4] (PA)	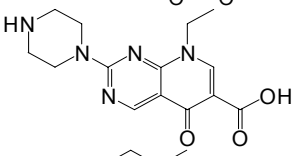	5.20	6.38	-5.28	$0.45 \pm 0.10 \times 10^{-3}$	59 ± 1
Flumequine [42835-25-6] (FLU)	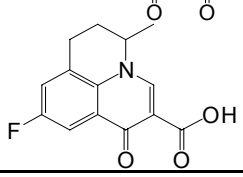	5.45	-	-	0[d]	76 ± 4

[a] Reaction conditions: 1.5 μM FQs, 0.44 g/L Syn-FeOOH, 0.01 M pH 5 buffer, 0.1 M NaCl, 22°C. Reported experimental data are in the format of average pseudo-first order rate constant ± 95% confidence level (n=2). k_{obs} for 1-phenylpiperazine under the identical conditions was $0.45 \pm 0.30 \times 10^{-3}$ h^{-1}. [b] Estimated based on the computer program SPARC. [c] Adsorption % = C_{ads}/C_{total} %. [d] No reaction was observed for up to 19 days.

Table 4-2. Kinetic comparison among model compounds[a].

Compound	Structure	pK_{a1} [b]	pK_{a2} [b]	k_{obs} (h^{-1})
Dimethylaniline	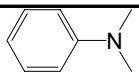	5.15[c]	-	$3.76 \pm 0.96 \times 10^{-2}$
N-phenylmorpholine (PM)	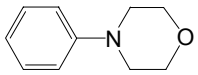	3.32	-	$0.66 \pm 0.48 \times 10^{-2}$
Aniline	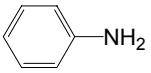	4.6[d]	-	$0.37 \pm 0.17 \times 10^{-2}$
1-phenylpiperazine (PP)	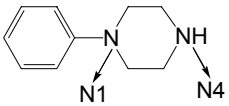	4.49	8.63	$0.12 \pm 0.06 \times 10^{-2}$
4-phenylpiperadine (PD)	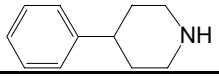	10.44	-	0[e]

[a] Reaction conditions: 10 μM amines, 10 g/L Ald-FeOOH, 0.1 M pH 5 buffer, 0.1 M NaCl, 22°C. Negligible adsorption was detected for all amines. Reported kinetic data are in the format of average pseudo-first order rate constant ± 95% confidence level (n=2). [b] Estimated based on SPARC. [c] Lide 1998. [d] Perrin, D. D. 1972. [e] No reaction was observed for up to 19 days.

including acetic acid, acetonitrile (ACN), 2-(cyclohexylamino)ethanesulfonic acid (CHES), $Fe(NO_3)_3 \bullet 9H_2O$, HCl, HNO_3, H_3PO_4, methylene chloride, methanol (MeOH), 4-morpholinepropanesulfonic acid (MOPS), NaCl, NaOH, and NaH_2PO_4 were obtained from Fisher Scientific (Fairlawn, NJ) or Aldrich (St. Louis, MO) at greater than 98% of purity (for solids) or of HPLC and GC/MS grade (for solvents), unless otherwise specified. All chemicals were used without further purification.

4.2.2 Oxide Preparation and Characterization

Goethite I was synthesized following the method of Moerup et al. (1983) in the acid system and was referred to as Syn-FeOOH throughout the paper. Briefly, 283 g (0.7 mol) of $Fe(NO_3)_3 \bullet 9H_2O$ was dissolved in 350 mL of 2 M HNO_3 in a 4-L polyethylene bottle and diluted with distilled water to 1.4 L. Then under vigorous stirring, 1.4 mol of NaOH (OH/Fe = 2.0) dissolved in 1.4 L water was added in a drop-wise fashion. The mixture (pH = 1.7 – 1.8) was aged 51 days at room temperature and the precipitate was repeatedly washed by centrifugation and replacing the supernatant with Nanopure water until the conductivity of the supernatant was below 2 μS/cm. The supernatant was decanted and the 0.5 L concentrated oxide slurry (20 g/L) was stored at 4°C for future usage. Reasonably well crystalline goethite has been proved to be very stable in suspension for long periods of time (years) (Schwertmann and Cornell 2000). A portion of the slurry was freeze-dried for later oxide characterization. Goethite II was purchased from Aldrich (Iron (III) oxide, hydrated FeOOH, catalyst grade, 30-50 mesh) and was referred to as Ald-FeOOH throughout the paper.

A nitrogen-based BET surface area (Micromeritics) of 159 ± 14 m^2/g was determined for Syn-FeOOH. A lower surface area, from 16 to 82 m^2/g, for Ald-FeOOH has been documented previously (Borggaard 1983). The mean diameter and effective diameter of Syn-FeOOH were measured to be 37.6 nm and 138.4 nm, respectively (ZetaPlus particle analyzer). The pH_{zpc} was reported to be 7.8 for goethite (Stumm 1992). Scanning electron microscopy (SEM) images were obtained for both goethites as shown in Figure 4-1. It is clearly evident that these two types of goethite have markedly different morphologies. Compared to Ald-FeOOH, Syn-FeOOH has a much smaller particle size, a different crystal shape (acicular versus nearly circular for Syn- and Ald-FeOOH respectively), and a smoother surface. The aforementioned different surface properties of Syn-FeOOH and Ald-FeOOH imply their likely different reactivities toward FQs. Surface elemental compositions for Syn- and Ald-FeOOH were obtained by energy dispersive X-ray spectroscopy (EDX) (Figure 4-2). Since the employed instrumentation can not detect any elements smaller than fluorine, the abundance of surface oxygen and hydrogen atoms was not measured. Nevertheless, Fe was shown to be the only metal species on the Syn-FeOOH surface (the different Fe peaks in Figure 4-2 correspond to surface Fe atoms with different energies). There is a trace amount of other metal species such as Ca, Mg, Na and Si on the Ald-FeOOH surface, although the abundance of Fe accounts for more than 99%. These results suggest that any subsequent interactions (particularly redox reactions) between Ald-FeOOH and FQs would most likely be due to the activity of the Fe species on the surface.

a) Ald-FeOOH

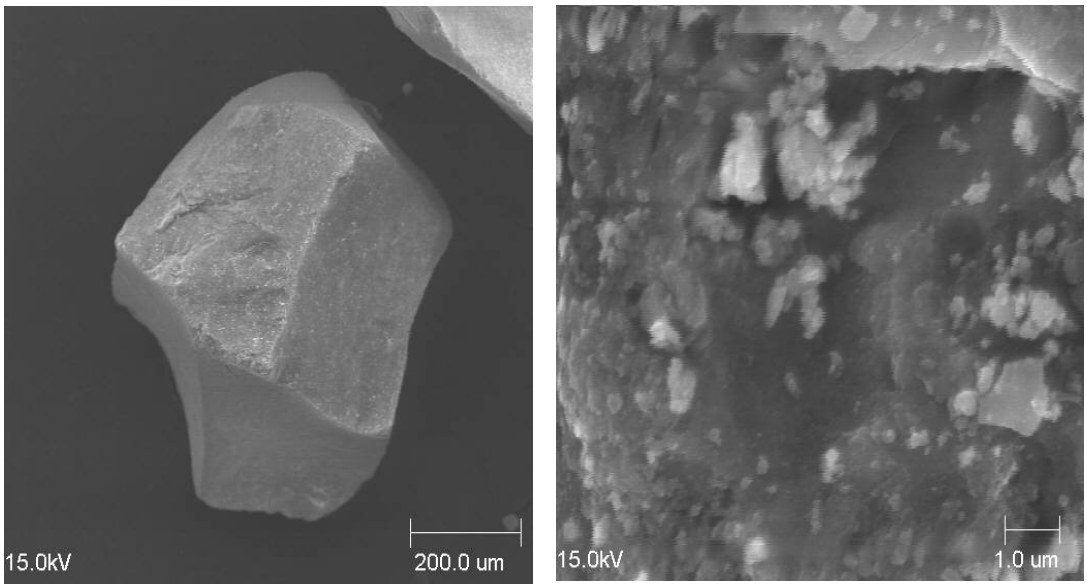

b) Syn-FeOOH

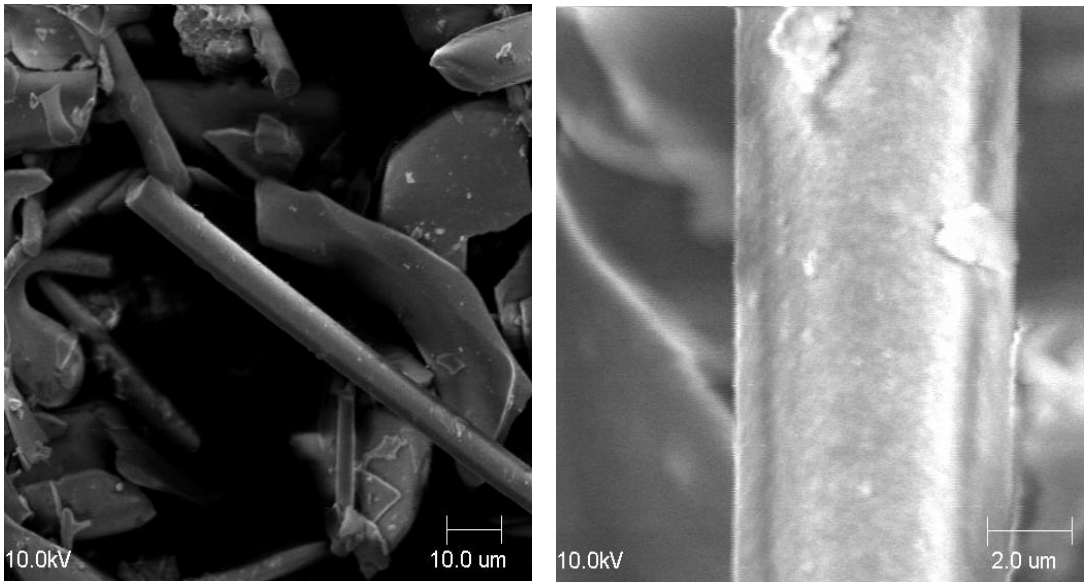

Figure 4-1. SEM images of a) Ald-FeOOH and b) Syn-FeOOH.

a) Ald-FeOOH

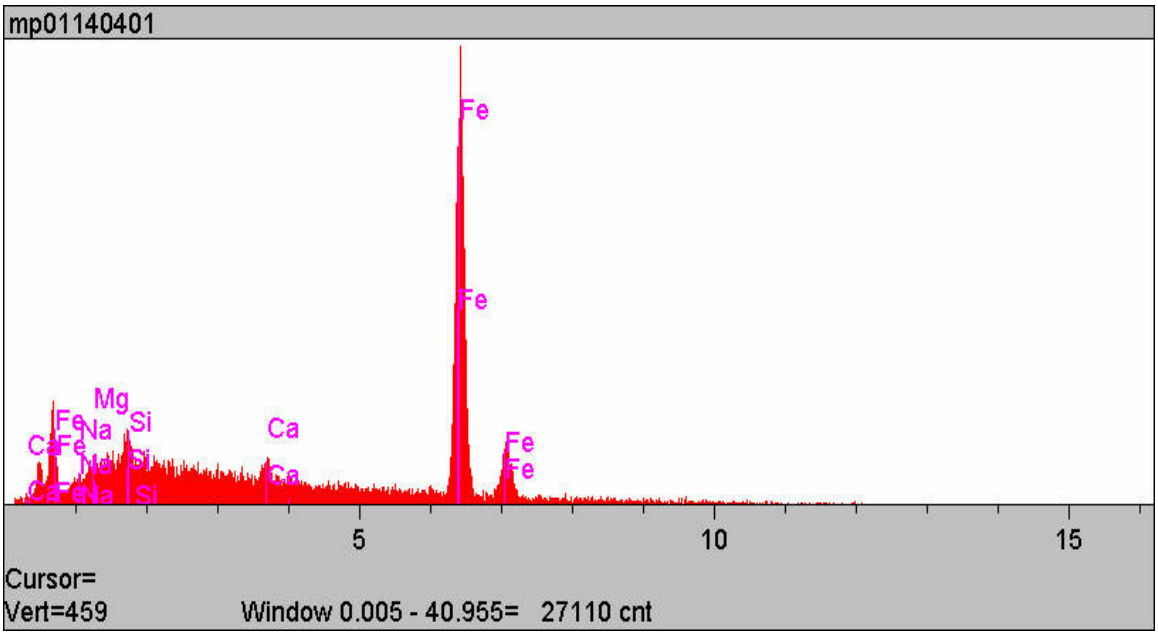

b) Syn-FeOOH

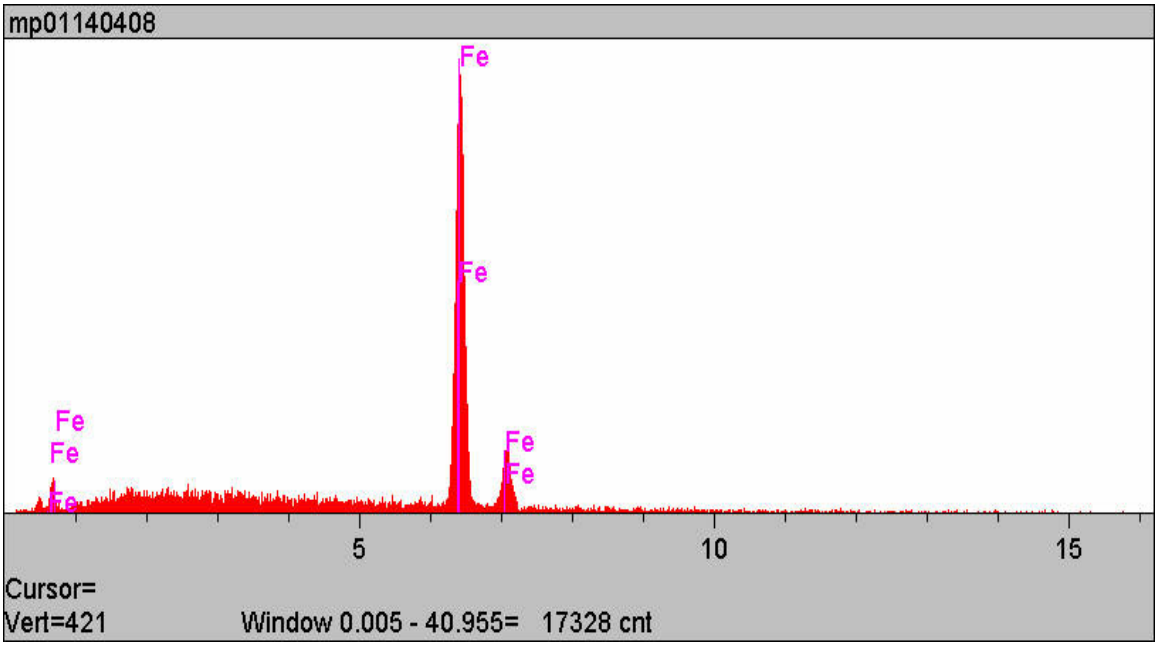

Figure 4-2. Surface elemental compositions of a) Ald-FeOOH and b) Syn-FeOOH.

4.2.3 Adsorption and Reaction Setup

All glassware was soaked in 5 N HNO_3 and rinsed thoroughly with reagent-grade water prior to use. All experiments were conducted in 25-120 mL screw-cap amber glass bottles with Teflon septa. The reaction bottles were placed on a magnetic stir plate in a 22^{o}C water basin and were continuously stirred. Reaction solutions were maintained at constant pH with 10-100 mM of appropriate buffer: acetic acid/sodium acetate for pH 4-5, MOPS and its sodium salt for pH 6-8, and CHES and its sodium salt for pH 9. Solution ionic strength was maintained by adding 10-100 mM of NaCl. FQ stocks were prepared in methanol/H_2O (10/90, v/v) at 100-120 mg/L, while the model compound stocks were prepared in Nanopure water at 100-120 mg/L. All stocks were stored at 4 °C and used within a month of preparation. Adsorption and reaction experiments were initiated by adding an appropriate amount of organic stocks to pre-equilibriated solutions containing goethite, buffer, and constant ionic medium.

The monitoring time of 48 hours for adsorption or 2 - 3 weeks for oxidation reactions was selected based on the results of preliminary experiments. Negligible association (neither adsorption nor oxidation) of FQs with goethite at pH above 10 was confirmed by preliminary experiments. In those experiments, FQ/goethite suspensions prepared at pHs below 10 were added with strong base to raise the pH to above 10 after less than 24 hours of reaction time, and an average recovery of 99.7 ± 2.9 % (based on 95% confidence level, n = 12) for the parent FQs was obtained. Thus in monitoring the subsequent experiments, sample aliquots were periodically collected and quenched immediately by centrifugation (at 12000 rev/min for 20 min) for adsorption studies, and by NaOH (1 M) addition (to adjust pH to above 10 to desorb the unreacted FQs on the

oxide surfaces) followed by centrifugation for oxidation reaction studies. 100 μL of 1 M H_3PO_4 was added to each quenched sample (1 mL) for the purpose of maintaining the stability of FQs to obtain the best analytical results for the parent compounds. Separate experiments had confirmed that the addition of H_3PO_4 after quenching did not alter the nature of the oxidation reaction of FQs.

To study the effect of O_2 on the reaction kinetics, reaction mixtures were also prepared under anoxic conditions in 100 mL crimped-top glass bottles wrapped with aluminum foil. The pre-equilibrated solutions containing goethite, buffer, and constant ionic medium were purged with nitrogen gas for 15 minutes and 500 - 800 μL of organic stocks were added to the mixture inside a glove box (N_2/H_2 = 95/5). Then the reaction bottles were sealed, placed on a magnetic stir plate in a 22^{o}C water basin, and continuously stirred. 3 mL of N_2 gas was injected into the headspace of the reaction bottle (to over-pressurize the headspace) each time before sampling (1 mL each). Parallel to the anoxic experiments, tests with identical conditions but under air (oxic) conditions were also conducted for comparison.

4.2.4 Analysis of FQs, FQ Oxidation Products and Model Compounds

Decrease in the concentrations of FQs and structurally-related model compounds were monitored by a reverse-phase high performance liquid chromatography (HPLC) system with a Zorbax RX-C18 column (4.6 × 250 mm, 5 μm), a fluorescence detector and a diode-array UV/Vis detector (1100, Agilent Technology). The respective excitation and emission wavelengths of the fluorescence detector were: 210 nm and 360 nm for PP, PD, and PM; 235 nm and 365 nm for FLU; 278 nm and 450 nm for cipro,

enro, nor, lome, and PA; 298 nm and 490 nm for oflox. Aniline and *N*,*N*'-dimethylaniline were detected at 210 nm by the UV detector. The mobile phase consisted of a solution containing 20 mM H_3PO_4 and 20 mM NaH_2PO_4 (eluent A, pH ~ 2.4) and acetonitrile (eluent B) at a flow rate of 1 mL/min. The mobile phase began with 0.5 minute isocratic 2% B (98% A), increased to 10% B in 0.5 minutes, increased to 80% B till 10 minutes, then the column was flushed thoroughly under these conditions for 4 minutes followed by a 5-min post time which allowed re-equilibration of the column. The generation of oxidation products from cipro was also monitored by the HPLC with fluorescence detection (278 nm of excitation wavelength and 450 nm of emission wavelength). The employed HPLC conditions were the same as the above.

4.3 Results and Discussion

4.3.1 Adsorption Isotherms and Effect of pH on Adsorption

Under typical adsorption conditions (5 g/L goethite, pH 5), cipro concentration in the supernatant decreased rapidly within the initial 4 - 6 hours and then leveled off (Figure 4-3a). By adjusting pH to above 10 before centrifugation for each sample, more than 95% of cipro could be recovered (desorbed), indicating that reversible adsorption was responsible for this rapid loss (Figure 4-3a). Thus the adsorption amount was calculated by extrapolating the flat line to time zero and subtracting the intercept from the corresponding initial concentration. For Syn-FeOOH and Ald-FeOOH, respectively, adsorption isotherm was obtained at pH 5 by fixing the oxide loading at 5 g/L and varying cipro concentration from 1 μM to 1 mM. The Langmuir isotherm (Schwarzenbach et al. 2003) was used to interpret the adsorption data:

$$C_s = \frac{C_{max} \cdot K_L \cdot C_w}{1 + K_L \cdot C_w} \qquad (1)$$

where C_s is the adsorbed concentration in mmol/g, C_w is the dissolved concentration in mmol/L, K_L is the Langmuir constant in $L \cdot mmol^{-1}$ (i.e., the equilibrium constant of the sorption reaction), and C_{max} is the maximum achievable surface concentration in mmol/g. The Langmuir isotherm can also be linearized as shown in equation (2):

$$\frac{1}{C_s} = \frac{1}{C_{max} \cdot K_L} \times \frac{1}{C_w} + \frac{1}{C_{max}} \qquad (2)$$

By plotting $1/C_s$ versus $1/C_w$, C_{max} (reciprocal of the intercept) and K_L (the intercept over the slope) could be obtained.

As shown in Figure 4-3b, adsorption isotherms for both goethites fit into the Langmuir equation very well. The C_{max} are 0.15 and 0.10 mmol cipro/g (or 9.03×10^{19} and 6.02×10^{19} molecules/g) for Syn-FeOOH and Ald-FeOOH, respectively. The K_L are 79.96 and 4.19 $L \cdot mmol^{-1}$ for Syn-FeOOH and Ald-FeOOH, respectively. If taking the specific surface areas of the two oxides into account (159 ± 14 m^2/g for Syn-FeOOH and 16 – 82 m^2/g for Ald-FeOOH), the surface site per area for cipro adsorption is calculated to be 0.57 molecules/nm^2 for Syn-FeOOH and 0.73 – 3.76 molecules/nm^2 for Ald-FeOOH. These numbers suggest that these two goethites do not differ greatly in the surface site density despite their significant difference in the surface area. In contrast to the adsorption site densities observed above with cipro, the surface Fe atom density for goethite/hematite mixture was reported to be more than 1.5 orders of magnitude higher (3 mmole/600mg or 3.01×10^{21} molecules/g, Kung and McBride 1988). The lower adsorption site density of either goethite for cipro in the current study (than the surface Fe atom density) may be due to the relatively large size of cipro molecules in occupying

more than one surface Fe atom per molecule. However, differences in the oxide structures in the two studies may also play a role and cannot be ruled out.

Adsorption interactions can be significantly affected by solution pH. Goethite surface sites are positively charged ($>FeOH_2^+$) when solution pH is below the pH_{zpc}, but negatively charged ($>FeO^-$) when solution pH is above the pH_{zpc}. Cipro also undergoes protonation and deprotonation with varying pH as shown in Figure 4-4a. Depending on the solution pH, cipro exists predominantly as a cation (H_2Q^+), a neutral/zwitter ion ($HQ/HQ^{\pm}$) or an anion (Q^-). Based on the pH_{zpc} of goethite (~ 7.8) (Stumm 1992) and the pK_a values of cipro (pK_{a1} = 5.46 and pK_{a2} = 7.67, Table 4-1), speciation of both adsorbent and adsorbate is plotted in Figure 4-4b. Because the neutral and zwitter ionic species of cipro cannot be distinguished by the analytical techniques used in this study, the two macroscopic pK_a values that treat the neutral and zwitter ionic species as one species are used. Additionally, the concentration products of $[>FeOH_2^+]*[HQ/HQ^{\pm}]$ and $[>FeOH_2^+]*[Q^-]$ are also included in Figure 4-4b to facilitate the following discussion.

In general, adsorption of cipro to both Syn-FeOOH and Ald-FeOOH was strong and showed similar pH dependence (Figure 4-5a). The adsorption achieved its maximum at the pH slightly above 6 and decreased with either increasing or decreasing pH from this range. This maximum adsorption appears to coincide with the highest value of the $[>FeOH_2^+]*[HQ/HQ^{\pm}]$ concentration product (Figure 4-5a). The $>FeOH_2^+$ form of Fe oxides has been widely suggested as the active surface species in adsorbing organic contaminants (e.g., Pizzigallo et al. 1998). The experimental results also evidently identify that the neutral and zwitter ionic forms of cipro ($HQ/HQ^{\pm}$) are the dominant adsorptive species to goethite. Under the same experimental conditions (pH 5), other

FQs including enro, nor, oflox, lome and PA showed comparable adsorption to Syn-FeOOH as cipro (50 – 65 %, Table 4-1). These results are expected since these FQs have comparable pK_{a1} and pK_{a2} values (i.e., similar pH speciation) and share closely related structures.

Experiments were also conducted to examine the adsorption of FLU to Ald-FeOOH at various pH values (Figure 4-5b). The adsorption of FLU to Ald-FeOOH was also strong and showed similar pH dependence as the case of cipro. Speciation of goethite surface and FLU is also depicted in Figure 4-5b. FLU has only one pK_a value of 5.45 for its carboxylic acid group and does not have the second pK_a as the other FQs due to the lack of the piperazine ring (see Table 4.1). In other words, FLU speciates as a simple monoprotic acid with the neutral form dominant at $pH < pK_a$ and the anionic form dominant at $pH > pK_a$. The adsorption of FLU to Ald-FeOOH appears to follow the trend of the $[>FeOH_2^+]$*[FLU anion] concentration product, highest at around pH 6 and lower with either increase or decrease in the solution pH. These results evidently point to the anionic species of FLU as the dominant species for adsorption to the $>FeOH_2^+$ surface sites.

FLU adsorbs to goethite more strongly than cipro, with the adsorption extent of 76 ± 4 % for FLU versus 62 ± 1 % for cipro at pH 5 (Table 4-1). This difference may be explained by the effects of speciation and molecular size. In terms of speciation, at $pH <$ 5.45 the oxide surface is predominantly positively charged ($pH_{zpc} \sim 7.8$), cipro is in the cationic form of H_2Q^+, while FLU is in the neutral form. The neutral FLU will surely adsorb more favorably to positively-charged surface sites than the positively-charged H_2Q^+. In terms of molecular size, the additional piperazine ring would increase the

molecular size of cipro compared to that of FLU, and thus the larger molecular size may obstruct more surface active sites per molecule basis, rendering a lower surface coverage capability. FLU also carries negative charge at a lower pH (at pH >5.45) than cipro does (at pH > 7.67). The faster drop-off in the adsorption of FLU than that of cipro as pH increased (Figure 4-5) was likely caused by the stronger electrostatic repulsion between the negatively charged FLU anion and the surface >FeO^-.

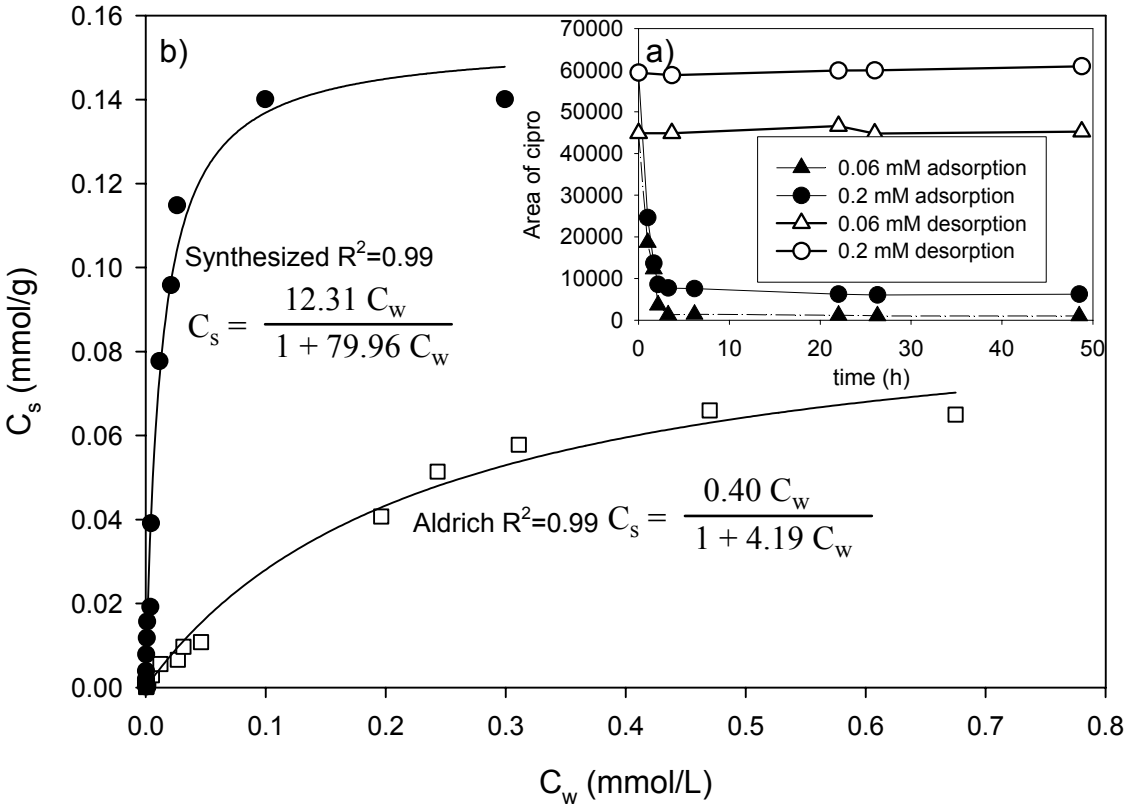

Figure 4-3. a) Typical time course of cipro adsorption and desorption in the presence of goethite; b) isotherm data and best-fit Langmuir equations for adsorption of cipro by Syn-FeOOH or Ald-FeOOH.

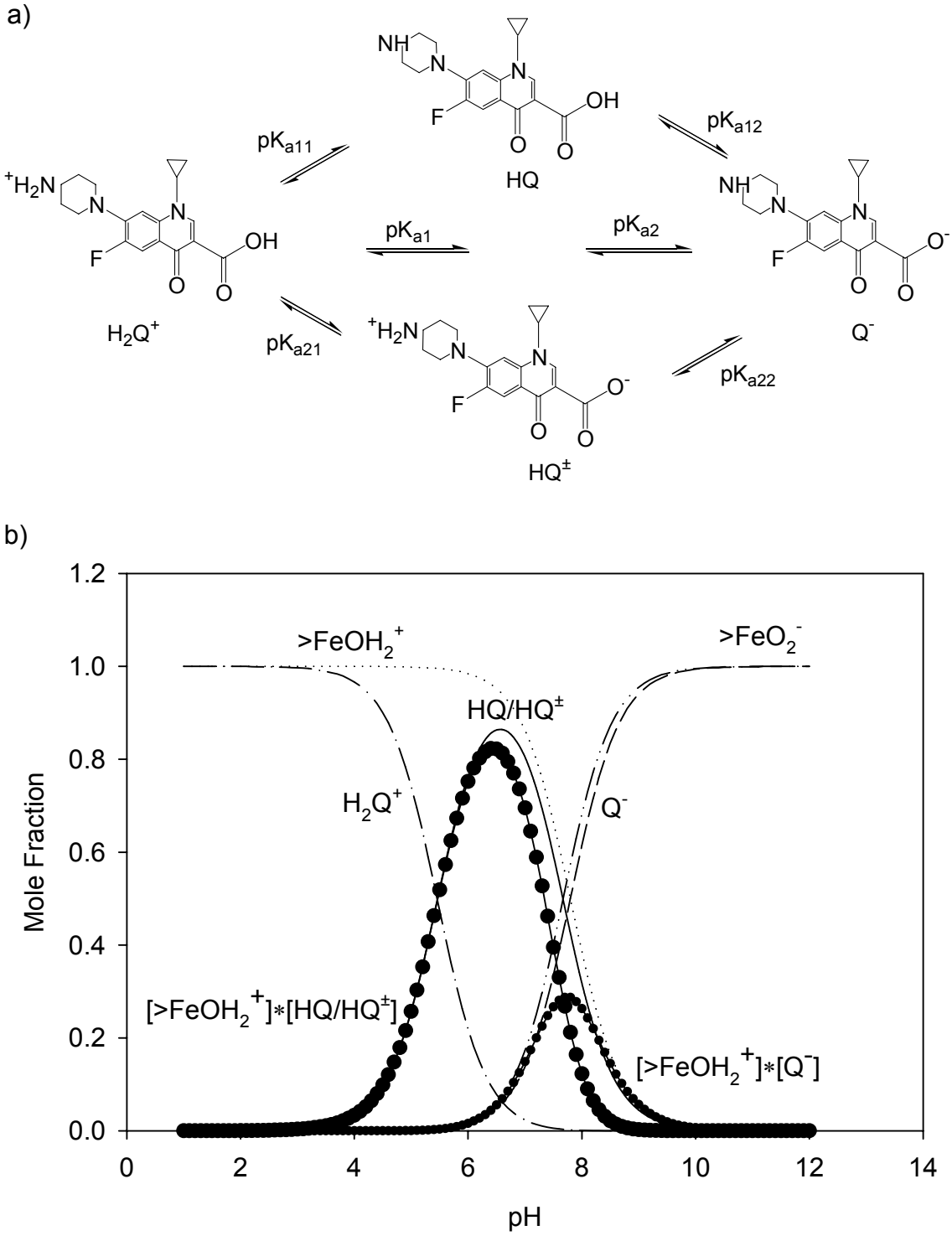

Figure 4-4. a) Speciation of cipro; b) speciation diagram of cipro and goethite (cipro: pK_{a1} = 5.26, pK_{a2} = 7.67; goethite: pH_{zpc} = 7.8).

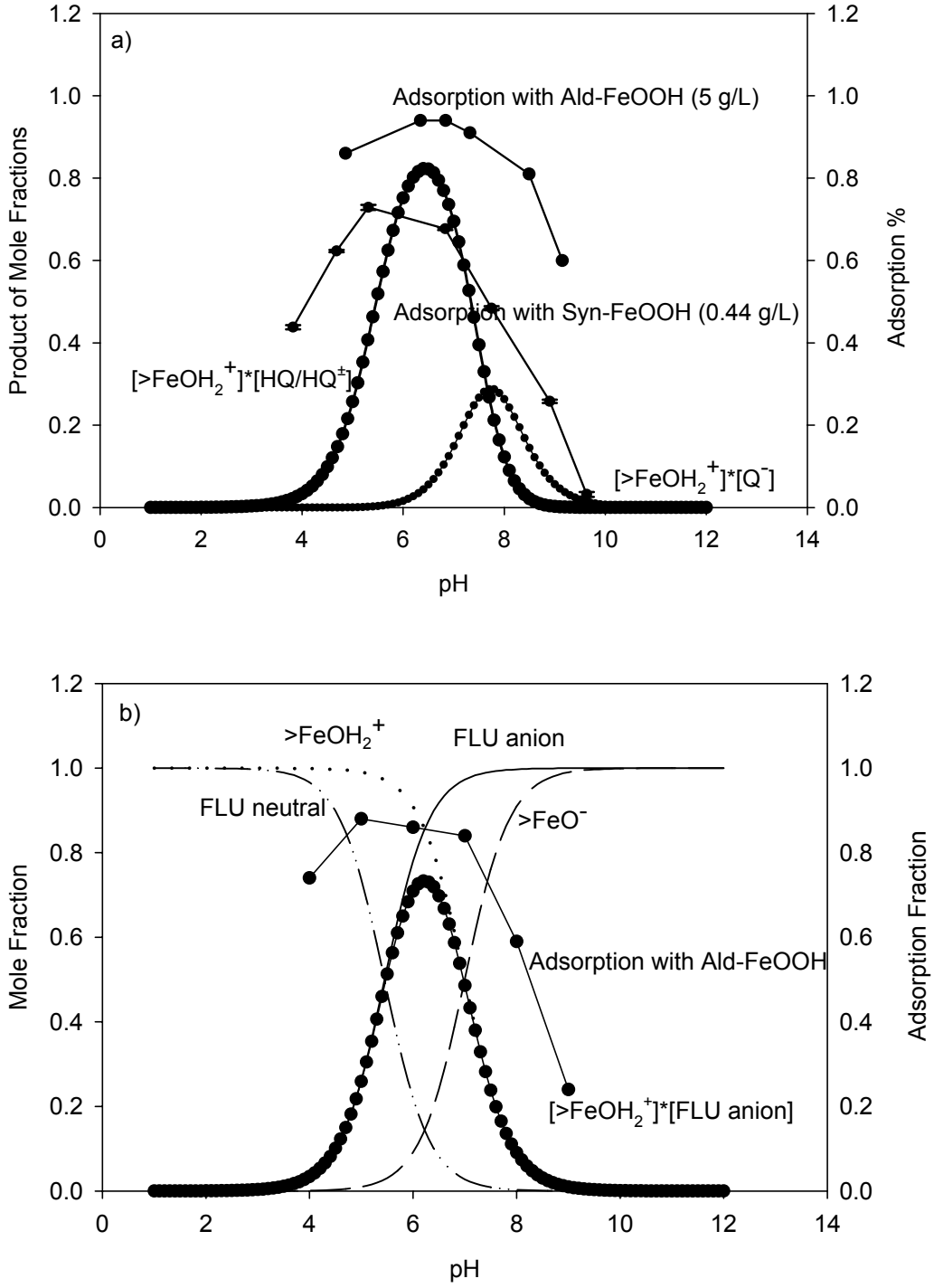

Figure 4-5. Effect of pH on adsorption. a) cipro; b) FLU (pK_a = 5.45). Adsorption conditions: a) 1.5μM cipro with 5g/L Ald-FeOOH or 10 μM cipro with 0.44 g/L Syn-FeOOH, b) 1.5μM FLU with 1 g/L Ald-FeOOH, 0.1 M pH buffer, 0.1 M NaCl, 22°C.

The earlier work by Nowara et al. (1997) pointed out that the carboxylic acid moiety of FQs is the sorptive site toward clay minerals via IR spectroscopic analysis and experiments with decarboxylated FQs. Compared to cipro, FLU contains a similar carboxylic acid moiety but lacks the piperazine moiety. The fact that FLU showed similarly strong adsorption as cipro to goethite in this study supports the importance of the carboxylic acid moiety in the FQ adsorption to iron oxides. Furthermore, the results that the anionic form of FLU (in which the carboxylic acid group is deprotonated) is the dominant species in adsorbing to the $>FeOH_2^+$ surface sites would imply that the zwitter ion ($HQ^{\pm}$) of cipro is likely more effective in adsorbing to goethite than the neutral form (HQ) of cipro because the carboxylic acid group is deprotonated in the zwitter ion from. Deprotonation of the carboxylic acid group increases the Lewis bacisity of the O atom, rendering it a stronger ligand to coordinate with the surface-bound Fe(III) atoms. Coordination of the carboxylate O atoms with dissolved and surface-bound metal species has been shown with various carboxylate-containing compounds in many previous studies (e.g., McBride 1987, Henderson 2003). Thus the FQs most likely adsorb to goethite surfaces through coordination between the carboxylic acid group and the surface-bound Fe(III).

4.3.2 Kinetics of FQ Oxidation by Syn-FeOOH

In the absence of goethite, all tested FQs were stable under the experimental conditions and no measurable loss of the parent compounds could be detected after 2 to 3 weeks. In contrast, significant degradation occurred in the presence of goethite for all of the FQs except FLU. Typical time course of cipro and nor oxidation by goethite is

shown in Figure 4-6. Note that a much lower oxide loading was employed in the kinetic studies than in the adsorption studies (0.44 g/L versus 5 g/L of FeOOH) while the same initial FQ concentration (10 μM) was used to reduce the extent of adsorption. Furthermore, a desorption procedure for FQs was utilized in the kinetic monitoring (see section 4.2.3 in Materials and Methods), thus the data shown in Figure 4-6 reflect only the loss due to oxidative degradation and do not include adsorption loss.

Three apparent stages of oxidation are evident from the data in Figure 4-6: the decrease in the concentration of cipro or nor proceeded relatively fast in the first stage, slowed down in the second stage, and then resumed approximately to the initial rate in the third stage. A similar kinetic behavior was also observed with the other FQs except FLU (which did not degrade over time, see later discussion). Because of this complicated kinetic behavior, reaction kinetics were evaluated, for the sake of comparison, based upon (i) the initial reaction rate in $\mu M\text{-}h^{-1}$ (i.e., the slope over the first few time increments in stage 1), (ii) the fraction of breakdown (i.e, C_{break}/C_{total}) at a certain reaction time, and (iii) the initial reaction rate constant k_{obs} in h^{-1} (i.e., the initial reaction rate divided by the initial FQ concentration). All the kinetic data are expressed based on the 95% confidence level (Table 4-1) and are statistically significantly greater than the detection limit (0.10×10^{-3} h^{-1}). The detection limit for rate constants was estimated by first calculating the standard deviation (STD) of the FQ concentrations in the control over a 2-week reaction period and then estimating the rate of FQ disappearance in h^{-1} from the initial concentration C_0 to the amount of ($C_0 - 3 \times STD$). This approach yields the minimum rate that is statistically greater than the experimental errors. Because slower reaction rates were observed in the oxidation of cipro with Ald-FeOOH (e.g., $k_{obs} = 0.95$

$\times 10^{-3}$ h^{-1} with 10 g/L of Ald-FeOOH versus $k_{obs} = 1.8 \times 10^{-3}$ h^{-1} with 4.4 g/L of Syn-FeOOH at cipro initial concentration of 1.5 μM and pH 5), later studies on the FQ degradation were conducted with Syn-FeOOH only.

As shown in Figure 4-7, pH markedly affected the reaction rate of cipro oxidation by goethite. The maximum oxidation rate occurred at pH near 6, and decreased with increasing or decreasing pH values. This trend is remarkably similar to the pH dependence of adsorption (Figure 4-5a), strongly suggesting that adsorption and the corresponding speciation (i.e., $HQ/HQ^{\pm}$ and $>FeOH_2^+$) play a critical role in determining the overall oxidation rate.

A series of experiments with varying cipro loadings (1.5 – 10 μM) but a fixed Syn-FeOOH loading (0.44 or 4.4 g/L) were conducted to assess the initial reaction order with respect to cipro. Overall the initial reaction rate increased linearly with cipro concentration. Plotting the log of the initial reaction rate versus the log of cipro loading yielded lines with a slope of 0.69 ± 0.03, indicating that the reaction order of cipro in oxidation by Syn-FeOOH is about 0.69 (Figure 4-8). This result is not surprising if the fact was realized that goethite was maintained at a great excess relative to cipro in the experiments (i.e., the surface cipro loading in the range of 3.4×10^{-4} to 2.3×10^{-2} mmol/g is far less than the observed C_{max} of 0.15 mmol/g).

The investigation showed appreciable degradation of all the FQs except FLU by Syn-FeOOH within two weeks at pH 5 (Table 4-1). No degradation was observed for FLU for up to 19 days. The comparison between FLU and the rest of FQs strongly indicates that the piperazine ring of the FQs is the reactive moiety toward oxidation by goethite. Due to experimental errors associated with slow reactions, relatively high

confidence levels (95%) were calculated for all rate constants. Despite that, comparison of the initial reaction rate constants (i.e., k_{obs}'s) of the FQs showed that all FQs except nor reacted at a very similar rate. The somewhat higher reaction rate of nor than the rates of all other FQs (by a factor of less than 15) is not expected and could be a result of greater experimental errors.

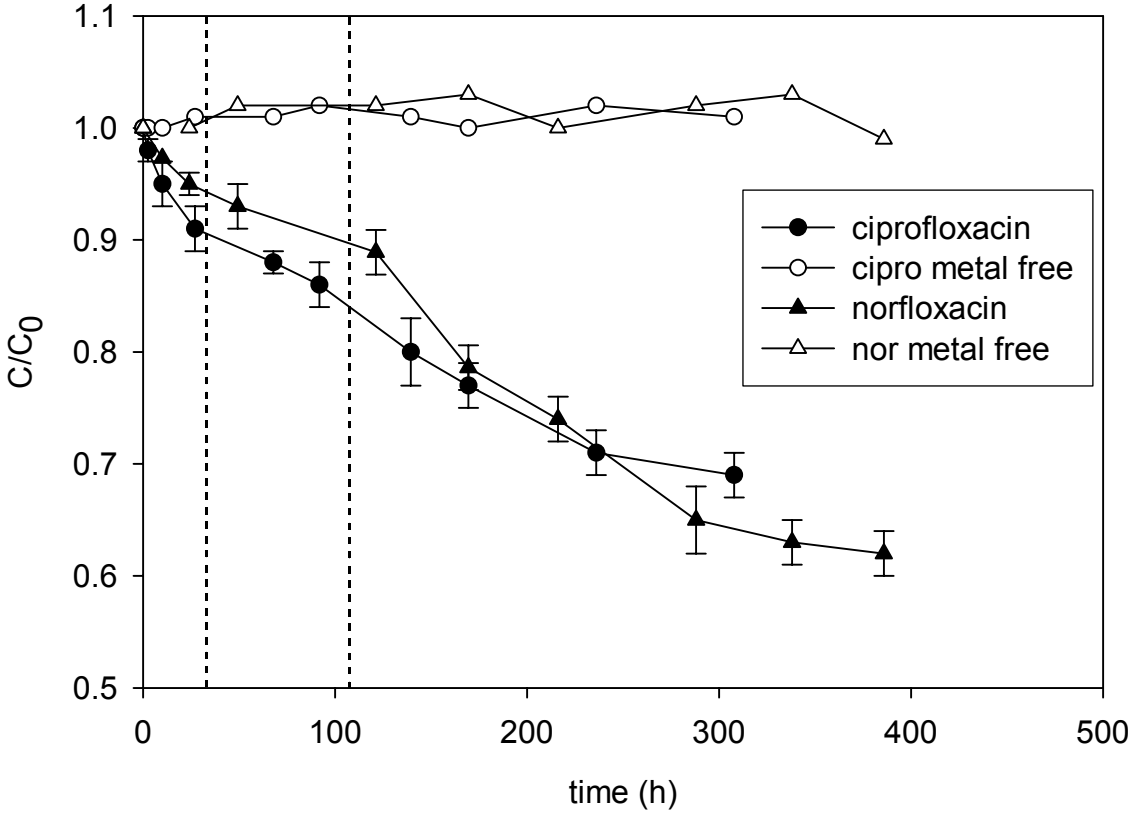

Figure 4-6. Time course of FQ oxidation by Syn-FeOOH. Typical reaction conditions: 1.5 μM FQ, 0.44 g/L Syn-FeOOH, 0.01 M pH 5 buffer, 0.01 M NaCl, 22°C.

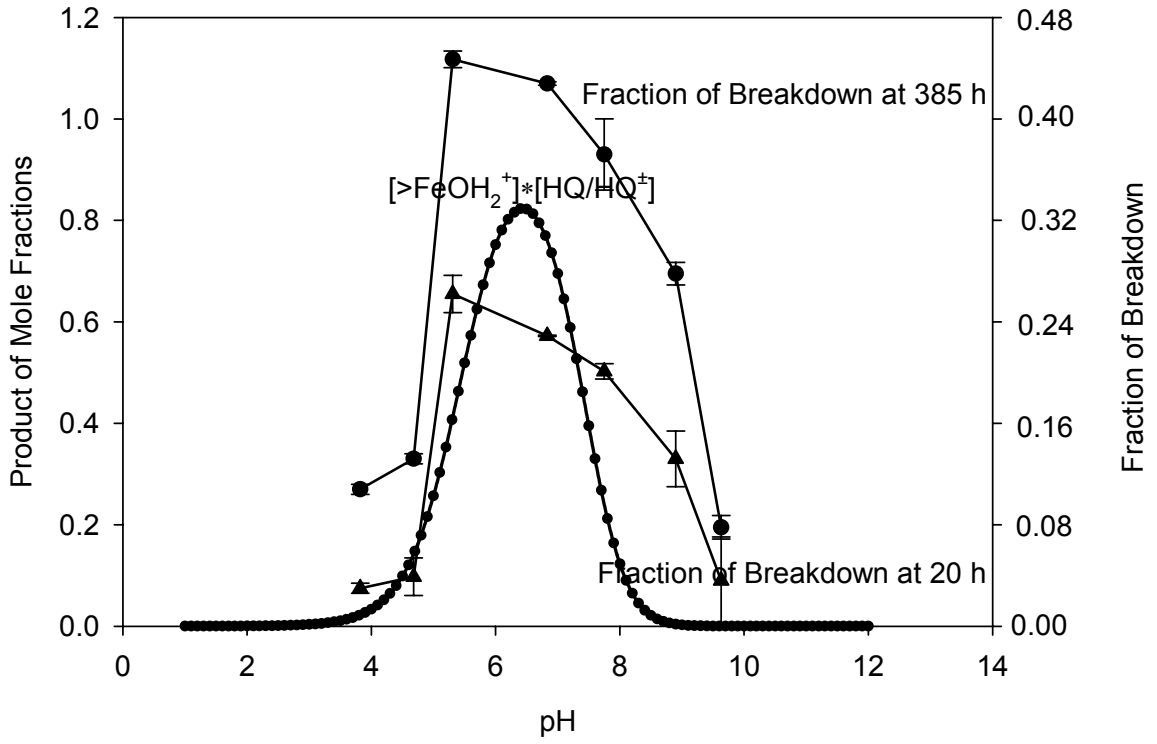

Figure 4-7. Effect of pH on cipro reaction kinetics. Typical reaction conditions: 1.5 μM cipro with 0.44 g/L Syn-FeOOH, 0.01 M pH buffer, 0.01 M NaCl, 22°C.

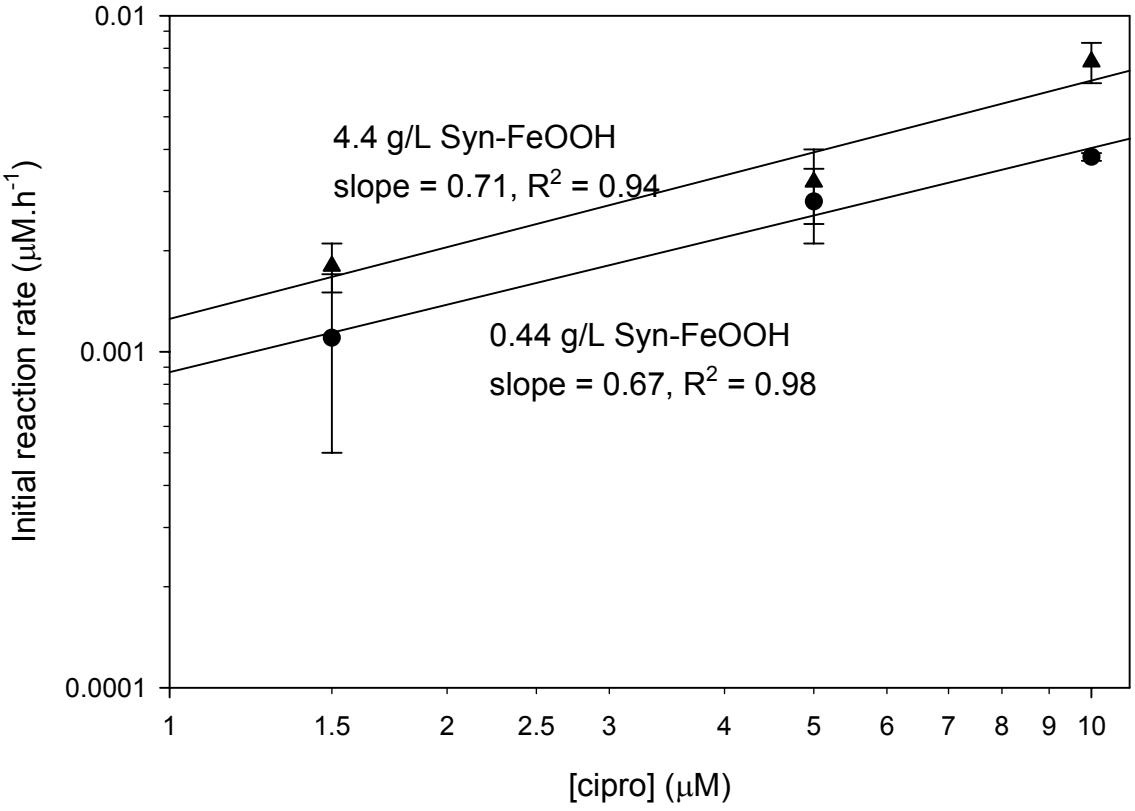

Figure 4-8. The reaction order with respect to cipro. Typical reaction conditions: 1.5 – 10 μM cipro with 0.44 – 4.4 g/L Syn-FeOOH, 0.01 M pH buffer, 0.01 M NaCl.

4.3.3 Kinetics of Model Compound Oxidation by Goethite

Because the piperazine ring of FQs is indicated by the experimental results to be the reactive moiety to oxidation by goethite, a range of model compounds that are structurally related to the piperazine ring of FQs (PP, PM, PD, aniline and *N,N'*-dimethylaniline) were also investigated for comparison (Table 4.2). In the absence of goethite, all model compounds were stable under the experimental conditions and no measurable loss of the compound could be detected after two weeks. In contrast, significant degradation of PP, PM, aniline and *N,N'*-dimethylaniline occurred in the presence of goethite.

A typical time course of PP oxidation by either Ald- or Syn-FeOOH is shown in Figure 4-9. The kinetic trend of PP (i.e., also three apparent stages of oxidation) was generally similar to those of FQs in the presence of either goethite, although the second stage (where a slowing in the reaction occurred) was more pronounced in the case of PP with Syn-FeOOH. Under the same reaction conditions, PP reacted with Syn-FeOOH at a rate ($k_{obs} = 0.45 \pm 0.30 \times 10^{-3}$ h^{-1}) similar to those of the FQs ($k_{obs} = 0.11$ - 1.65×10^{-3} h^{-1}, Table 4-1).

The oxidation of PP by goethite was investigated over the pH range of 4 to 10 and the maximum reaction rate was observed at pH 4 (Figure 4-10b). The two N atoms of PP can be protonated as pH decreases, with the pK_a values of 4.49 and 8.63 for the N_1 and N_4 atoms, respectively (Table 4-2). As the pH decreases from high to low, PP can be present as a neutral, +1 (cation I), or +2 (cation II) species (Figure 4-10a). As shown in Figure 4-10, there is no apparent correlation between the reaction rate and the speciation over the studied pH range.

A notable difference between PP and the FQs is that adsorption of PP to goethite was negligible, further supporting the earlier conclusion that the carboxylic acid group of FQs is key to the adsorption to goethite. The weak adsorption of PP to goethite makes it suitable for assessing the reaction order with respect to goethite. A series of experiments with varying goethite loadings (0.2 – 50 g/L) but a fixed PP loading (10 μM) were conducted to assess the initial reaction order with respect to goethite (Figure 4-11). Plotting the log of the initial reaction rate versus the log of goethite loading yielded lines with slopes of 0.29 and 0.54 for Aldrich-FeOOH and Syn-FeOOH, respectively, indicating the reaction order of goethite is about 0.29 – 0.54.

The comparison among the related amine compounds showed that the reactivities followed the trend of *N,N'*-dimethylaniline > PM > aniline > PP >> PD (Table 4-2). *N,N'*-Dimethylanine, PM and aniline reacted about 30-fold, 5-fold and 3-fold faster than PP, respectively. PD did not react to any significant extent after 2 weeks. Similar to PP, these related amine compounds also showed negligible adsorption to goethite.

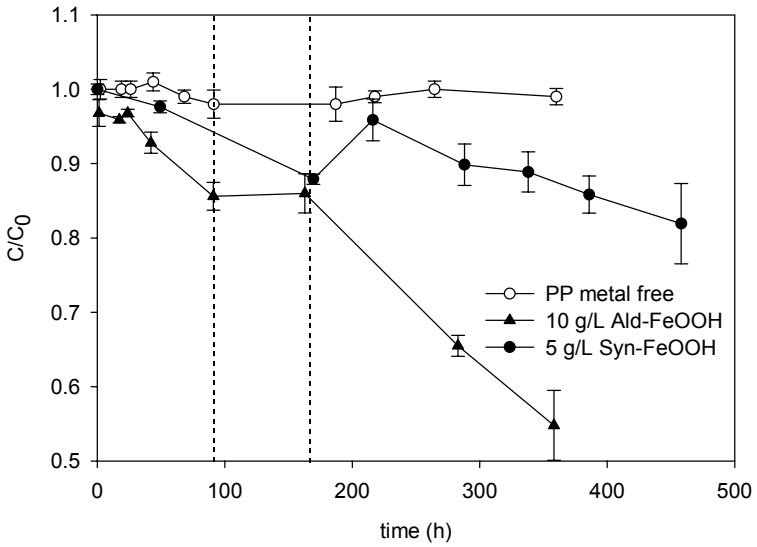

Figure 4-9. Time course of PP oxidation by goethite. Typical reaction conditions: 10 μM PP, 0.1 M pH 5 buffer, 0.1 M NaCl, 22°C.

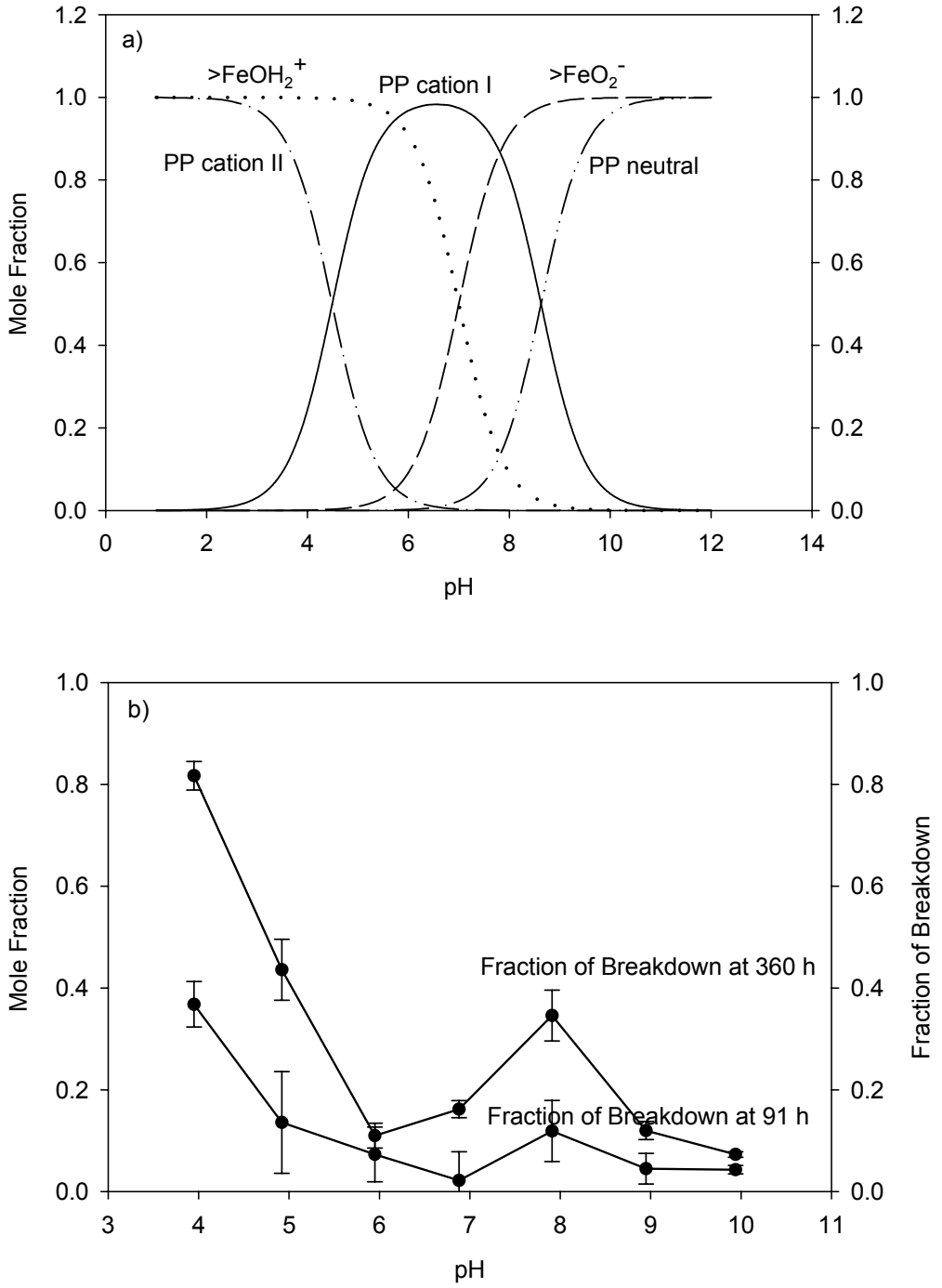

Figure 4-10. a) Speciation of PP and FeOOH; b) effect of pH on PP reaction kinetics. Typical reaction conditions: 10 μM PP with 10 g/L Ald-FeOOH, 0.1 M pH buffer, 0.1 M NaCl; 22°C.

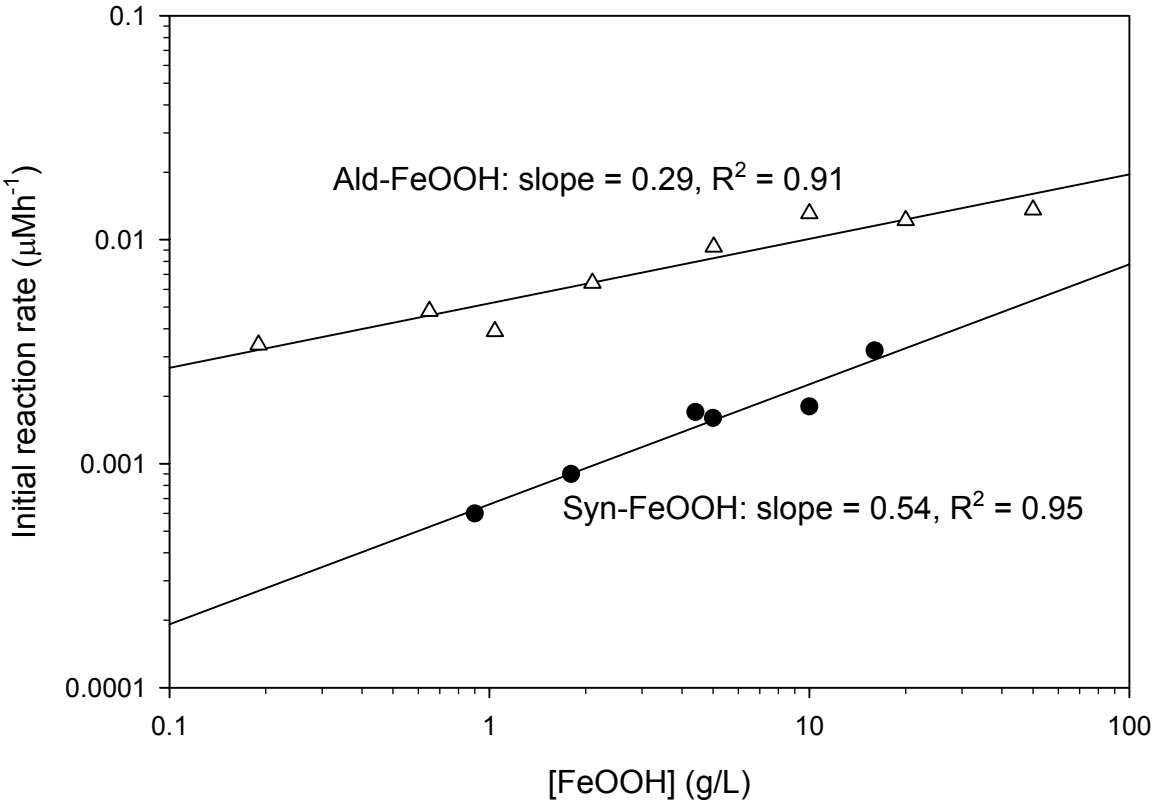

Figure 4-11. The reaction order of goethite in the reaction with PP. Typical reaction conditions: 10 μM PP, 0.01 M pH 5 buffer, 0.01 M NaCl, 22°C.

4.3.4 Product Identification

Analyses of cipro reaction mixtures by HPLC with fluorescence detection indicated the presence of primarily five products with retention times of 6.50 min, 7.30 min, 7.47 min, 7.94 min, 8.59 min, respectively (the retention time of cipro was 6.83 min). In these experiments, desorbing cipro and its oxidation products from goethite was also applied by raising the pH to above 10 prior to analysis (see section 4.2.3 Materials and Methods). The retention times and the UV and fluorescence spectra of these products matched closely with those of the products that have been identified previously in the oxidation of FQs by Mn dioxide (Zhang and Huang 2004). Details for the characterization of these products have been described in the previous study and will not be repeated here. The example of cipro and its oxidation products is shown in Figure 4-12 and comparable patterns apply to the oxidation of other FQs by MnO_2 as well (Zhang and Huang 2004). In summary, these products are the M-26, M+2a, M+2b, M+30 and M-NH_2 products with respective molecular ions of m/z 306, 334, 334, 360, and 263 (Figure 4-12, the molecular ion of cipro is m/z 332 and is represented by M). Although not analyzed in this study, the oxidation products of other FQs with goethite are expected to be similar to those of cipro, as in the case of oxidation by MnO_2.

Because the oxidation products are structurally similar to the parent cipro and all possess the adsorptive carboxylic acid moiety (Figure 4-12), they are likely desorbed as much as cipro by the experimental procedure (raising the pH to above 10). As shown in Figure 4-13, analyzing the generation of cipro oxidation products over time showed that the fluorescence peak areas of all products continuously increased along with the degradation of cipro (the increase in the products which had lower abundances is better

shown in the upper corner plot). In the second stage of the reaction when the rate of cipro oxidation slowed down, the formation of some of the products (i.e., the M+30 product) appeared to be more gradual than that in the first stage. Despite that, the small abundances of the products generally prohibited a more in-depth interpretation of the product generation kinetics during the early stage of the reaction. Furthermore, a similar trend in the product evolution was observed across the studied pH range ($4 < pH < 10$, data not shown), suggesting that the same reaction mechanism is operative regardless of the solution pH.

It is interesting to note that the amount of the M-26 product increased steadily over a period of more than 400 hours in this study, while the amount of the same product increased sharply initially then decreased slowly until disappearance in the oxidation of cipro by Mn oxide (Zhang and Huang 2004). In other words, the M-26 product was an intermediate in the oxidation of cipro by Mn oxide (Zhang and Huang 2004). This difference can be most likely explained by the much higher oxidation power of Mn oxides than Fe oxides (reduction potentials of 0.67 V and 1.23 V for FeOOH and MnO_2, respectively (Stone 1987)). Because Fe oxides are less oxidative, the M-26 product reacted with the oxide at a much slower rate and thus could survive longer in the current study.

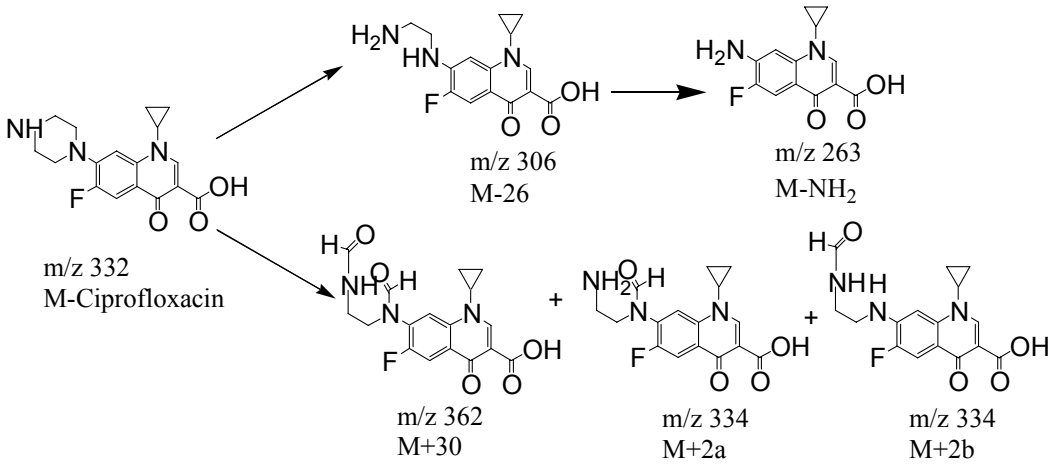

Figure 4-12. Reaction products of cipro oxidation by Syn-FeOOH.

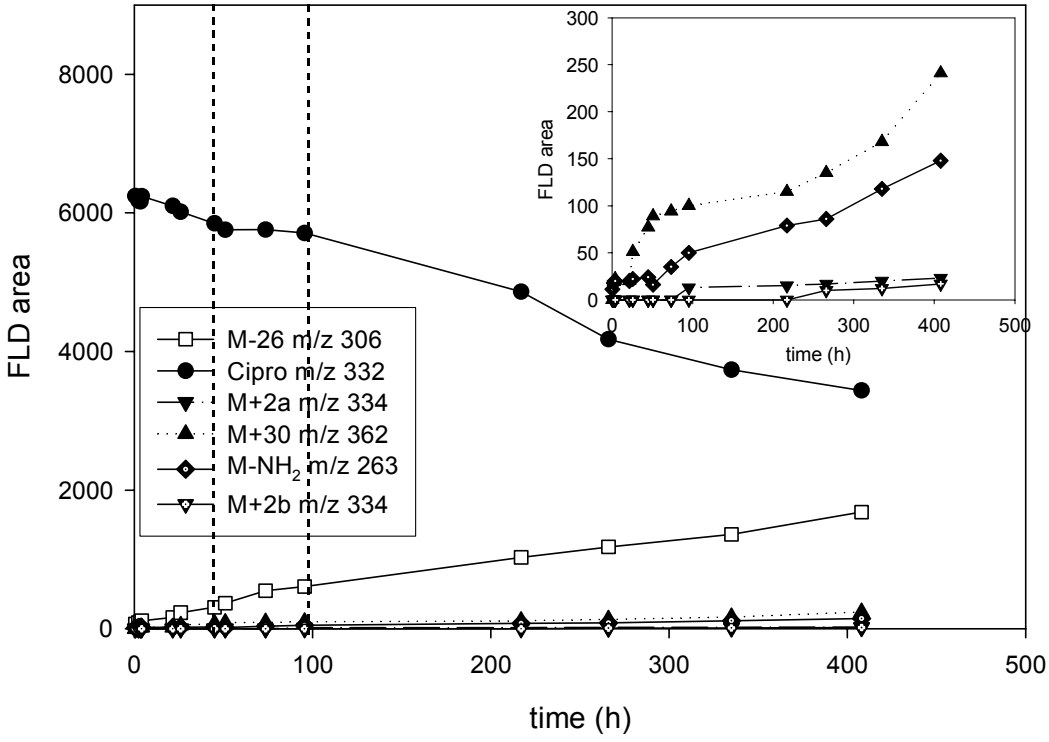

Figure 4-13. Time course of oxidation products of cipro reaction with Syn-FeOOH. Typical reaction conditions: 10 μM cipro, 0.44 g/L Syn-FeOOH; 0.01 M pH 5 buffer, 0.01 M NaCl, 22°C. Note: FLD = Fluorescence detection.

4.3.5 Delayed Redox Reaction

A similar three-stage kinetic behavior has been documented by Kung and McBride on the oxidation of hydroquinone (HQ) by iron oxide (goethite-ferrihydrite mixture or hematite) (Kung and McBride 1988). In the first stage, the concentration of HQ decreased to a minimum and the concentration of the product *p*-benzoquinone (Q) increased to a maximum. In the second stage, Q concentration began to decrease whereas HQ concentration increased, indicating a reversal of the HQ oxidation. In the third stage, both HQ and Q concentrations decreased. The authors attributed this reversal of HQ oxidation to the delayed release of Fe^{2+} into solution as the reduction of Fe oxide proceeded. The accumulation of Fe^{2+} ions on the oxide surface would lead to a distribution of a reduced state over Fe atoms on the surface, which in turn would lead to the cease of the HQ oxidation. Additionally, the Fe^{2+} ions, once released into solution, appeared to reduce the quinone product back to HQ, contributing to the increase in the HQ concentration in the second stage. The decrease in both HQ and Q concentrations in the third stage was believed to be associated with polymerization and/or adsorption of the organics on the oxide surface.

By analogy, the first stage of the reaction observed in this study in which cipro degraded rapidly was most likely caused by a rapid oxidation of cipro with surface Fe(III) (Figure 4-6). The delayed release of Fe^{2+} from the goethite surface may be the reason for the slower reaction rate of cipro observed in the second stage of kinetics. As the oxidation of cipro proceeded, the oxide surface must have become more and more reduced by the accumulated Fe^{2+} and this reduced state may have been distributed over the surface and shared by Fe atoms as suggested by Kung and McBride (1988). This

reduced state of Fe oxide caused by the delayed release of Fe^{2+} could lead to the slowed oxidation of cipro. Unlike the case in which hydroquinone and quinone are involved (Kung and McBride 1988), the cipro oxidation products (either hydroxylated or dealkylated products) are unlikely to be reduced back to the parent compound by the released Fe^{2+} ions, thus increase in the cipro concentration did not occur in the second stage. In other words, the delayed release of Fe^{2+} only slowed or ceased the oxidation of cipro for a period of time and did not reverse the oxidation reaction. Once Fe^{2+} ions were released to solution and the surface recovered its oxidation state, cipro was continuously degraded by oxidation by the Fe oxide (i.e., stage 3). Dimerization or polymerization of cipro and its hydroxylated or dealkylated oxidation products on the oxide surface is believed not to play an important role in the third stage of the reaction because the abundances of the hydroxylated and dealkylated oxidation products were observed to increase constantly (Figure 4-13). However, dimerization of cipro oxidation intermediates cannot be ruled out and may be partly responsible for the decrease in cipro concentration throughout the whole reaction (Zhang and Huang 2004).

The delayed release of Fe^{2+} from the goethite surface can also explain the kinetic slow-down in the oxidation of PP by goethite (Figure 4-9). The more pronounced second stage in PP oxidation with Syn-FeOOH than with Ald-FeOOH might be due to the larger surface area of the former, which could adsorb the generated Fe^{2+} more strongly and thus lead to a more pronounced delayed release of Fe^{2+}.

4.3.6 Chemical Reactivities and Reactive Sites

Based on the results shown in Table 4-2, the inertness of PD in the presence of goethite versus the rapid oxidation of PP indicates that the reactivity of the outer N (i.e., N_4) is very low and the inner N (i.e., N_1) in the piperazine ring is the reactive site. These results are consistent with the previous study on the oxidation of FQs with Mn dioxide (Zhang and Huang 2004).

In studying aliphatic amine oxidation by aqueous $(batho)_2Cu^{II}$, Wang and Sayre (1992) observed that the reactivity of amines followed the trend of primary amines < secondary amines < tertiary amines, and that tertiary amines reacted at an average 4-fold and 110-fold faster rate than secondary amines and primary amines, respectively. The observed faster rate of *N,N'*-dimethylaniline compared to that of aniline is consistent with the tertiary versus primary amine effect, though the difference in reactivity is of a smaller magnitude, which may be due to the involvement of aromatic amines (instead of aliphatic amines) in this case. Conversely, PP (with a tertiary N_1) reacted slower than aniline (with a primary N). For PP, the steric hindrance of the alicyclic ring may be more pronounced than the inductively accelerating effect, thus overall lowering the reactivity.

The higher reaction rate of PM than PP was opposite to what was found in their oxidation with Mn dioxide (in which PP reacts with MnO_2 significantly faster than PM) (Zhang and Huang 2004). As demonstrated in the study by Wang and Sayre (1992) on aliphatic amine oxidation, *N*-substitution with electron-donating substituents would increase the reaction rate while *N*-substitution with electron-withdrawing substituents would decrease the reaction rate. A morpholine moiety is generally less reactive than a piperazine moiety to oxidation because, compared to piperazine, its O atom is not reactive to oxidation and the electronegativity of the O atom may reduce the reactivity of

the N_1 atom. Furthermore, the potential interactions between the two N atoms in the piperazine ring may also render its reactivity to be significantly higher than that of the morpholine ring (Zhang and Huang 2004). The experimental results of PM with goethite apparently contradict with the prediction and could not be explained by the current data. More studies are necessary in order to better understand the mechanism for PM reaction with Fe oxides.

The potential surface PP loadings were between 0.20×10^{-3} and 0.05 mmol/g in studying the reaction orders with respect to both goethites (Figure 4-11). These surface PP loadings were lower than the maximum adsorption capacity of Syn-FeOOH (0.15 mmol cipro/g) and Ald-FeOOH (0.10 mmol cipro/g). The observed constant reaction order with respect to goethite (Figure 4-11) thus reflects that (1) although adsorption of PP to goethite is negligible, the oxidation of PP by goethite is still dependent on the amount of available surface sites; and (2) the number of active surface sites for oxidation is likely much lower than those for adsorption and thus the reactivity increases steadily with increasing goethite loadings.

The experimental results showed that Ald-FeOOH reacted more slowly with FQs but faster with the model compounds than Syn-FeOOH. This comparison indicates that there is no direct correlation between the oxide reactivity and the surface area or the available surface sites, since Ald-FeOOH has a smaller surface area but a similar surface site density compared to those of Syn-FeOOH (see section 4.3.1 in Results and Discussion). Further study is needed to better understand the dominant factors in affecting the redox activity of Fe oxides.

The comparison between FLU and the other FQs provides the evidence that the piperazine ring (especially the N_1 atom) is the reactive site for oxidation and the carboxylic acid moiety (especially the carboxylate oxygen) is the adsorptive site in FQs. Considering the negligible adsorption of PP and its similar reactivity to that of FQs in the presence of goethite (Tables 4-1 and 4-2), it seems that adsorption is not necessary in the overall oxidation of PP by Fe oxide. However, in the oxidation of FQs by goethite, surface adsorption is still believed to facilitate the reaction for the following reasons. Firstly, the study results have indicated that the steric hindrance of the alicylic ring in PP retards its oxidation compared to aniline (Table 4-2). The much bulkier molecules of the FQs would experience an even greater steric hindrance and thus react with iron oxide more slowly than PP if there were no other accelerating factors (note the similar reactivity of FQs and PP as shown in Table 4-1). Secondly, the adsorption of FQs through its carboxylic acid moiety, though not directly associated with the reaction center, would bring the piperazine ring closer to the surface and hence speed up the reaction. The fact that the oxidation rate and adsorption extent of cipro shared very similar pH dependence (Figures 4-5a and 4-7 in sections 4.3.1 and 4.3.2) strongly supports the hypothesis. In other words, the adsorption step in which a surface complex precursor is formed between cipro and the surface-bound Fe prior to the electron-transfer step significantly affects the overall oxidation rate. In the case of PP (and other model amines as well), in order for oxidation to occur, the amines may attack the oxide surface to form a surface complex temporarily for further reactions to occur. This surface complex formation must be very slow; once it is formed, the redox reaction occurs right away. As a result, only degradation but no significant adsorption was observed.

4.3.7 Effect of pH on Reaction Kinetics

The effect of pH on the reduction potential (E_h) of goethite is demonstrated by the following calculation. Using the half-reaction (3) (Stone 1987) and the Nernst equation (4):

$$Fe^{III}OOH(s) + 3H^+ + e^- = Fe^{2+}(aq) + 2H_2O \quad (3)$$

$$E^0_h = + 0.67 \text{ V}$$

$$E_h = E^0_h - \frac{0.059}{1} \log \frac{[Fe^{2+}]}{a_{FeOOH}[H^+]^3} \quad (4)$$

and assuming that the activity of FeOOH is 1.0 and $[Fe^{2+}] = 10^{-6}$ M (Kung and McBride 1988), the pH dependence of E_h is shown in equation (5):

$$E_h = 1.02 - 0.18 \text{ pH} \quad (5)$$

Clearly the reduction potential and hence the reducing power of FeOOH decreases with increasing pH. For example, E_h = 0.30, 0.12, -0.06, and -0.78 at pH = 4, 5, 6, and 9, respectively. The linear dependence of E_h on pH would most likely be responsible for the drastic decrease in PP reaction rate from pH 4 to pH 6 (Figure 4-10b). Between pH 6 and 10, however, instead of continuing to decrease, the PP reaction rate increased to a local maximum at pH near 8 (Figure 4-10b). A radical mechanism was believed to be involved in the oxidation of FQs and related amines by Mn oxide (Zhang and Huang 2004), and in the oxidation of hydroquinone by iron oxides (Kung and McBride 1988). Faster hydroquinone oxidation by Fe oxides was observed at pH 9 than at pH 6 in the study by Kung and McBride (1988) and was attributed to the higher stability of radical intermediates at the higher pH condition. Because higher pH is favorable for more stable radical intermediates while lower pH is favorable for a higher reduction potential, these

two opposite trends likely lead to the observed bell-shaped pH dependency for PP reaction rate within the pH range of 6 to 10.

The role of pH in affecting the overall reaction rate may look different for PP and cipro at first sight; however, there is little conflict after careful examination of various factors. Of particular importance is the fact that cipro has strong adsorption toward iron oxide surface through its carboxylic acid moiety but PP does not, which renders speciation and precursor complex formation most critical in determining the overall reaction rate in the case of cipro. In other words, the effect of pH on speciation and precursor complex formation (section 4.3.1) overrides the effect of pH on the reduction potential of Fe oxide and the stability of cipro radical intermediates. As a result, cipro reaction rate reached maximum at around pH 6 instead of pH 4, and decreased with increasing pH without a local maximum at the higher pH region (Figure 4-7).

4.3.8 Effect of Oxygen and Light on Reaction Kinetics

O_2 was believed to be the ultimate oxidizing agent in the iron oxide-involved reactions because it could rapidly oxidize the generated Fe^{2+} ions back to Fe(III) oxide (McBride 1987). The effect of O_2 on the oxidation of cipro and PP with goethite was investigated in this study. Comparable rate constants (for cipro, k_{obs} (oxic) = 0.45 ± 0.30 × 10^{-3} h^{-1} and k_{obs} (anoxic) = 0.50 ± 0.30 × 10^{-3} h^{-1}; for PP, k_{obs} (oxic) = 1.2 ± 0.6 × 10^{-3} h^{-1} and k_{obs} (anoxic) = 1.5 ± 0.2 × 10^{-3} h^{-1}) were obtained under oxic versus anoxic but otherwise identical conditions (0.44 g/L Syn-FeOOH, 5.8 μM cipro or 10 μM PP, 0.01 M pH 5 acetate buffer, 0.01 M NaCl and 22°C). The negligible effect of O_2 on the reaction kinetics could be explained by the fact that Fe oxide was maintained at a great excess to

the organic reactant in the experiments and that oxidation of Fe^{2+} to Fe(III) oxide by dissolved O_2 only occurred readily after Fe^{2+} ions were released to solution. It is also plausible that the oxidized form of the released Fe^{2+} (by O_2) is not as active as goethite in facilitating the redox reaction of cipro or PP. Thus whether Fe^{2+} was re-oxidized back to Fe(III) oxide did not affect the oxidation rate of cipro or PP.

Surface photolysis involving iron oxides has been documented (Cunningham et al. 1988, Goldberg et al. 1993, Pulgarin and Kiwi 1995, Wu and Deng 2000, Bandara et al. 2001, Bandara et al. 2001), though iron oxides are generally not considered to be good light conductors. FQs were also reported to readily undergo photodegradation (Fasani et al. 1999, Burhenne et al. 1999, Phillips et al. 1990, Fasani et al. 2001, Mella et al. 2001). Thus it would be interesting to know what actually happens to FQs in the presence of both light and iron oxides. To avoid direct photolysis of FQs, only office light was employed in the present study by using two different types of reactors: amber bottles versus clear bottles. It turned out that surface photolysis did promote the overall degradation of cipro (preliminary tests confirmed the stability of cipro in the presence of office light without iron oxides). For example, the reaction rate of cipro was more than two times faster in clear bottles ($k_{obs} = 0.98 \pm 0.02 \times 10^{-3}$ h^{-1}) than in amber bottles ($k_{obs} = 0.43 \pm 0.19 \times 10^{-3}$ h^{-1}) (typical reaction conditions: 0.44 g/L Syn-FeOOH, 1.5 μM cipro, 0.01 M pH 5 buffer, 0.01 M NaCl, 22°C). This surface photolysis involving iron oxide and FQs merits further studies; however such investigation is beyond the scope of the current study and thus is not covered here.

4.3.9 Reaction Mechanism

A likely reaction mechanism that is consistent with the above experimental results and relevant previous studies (e.g., Zhang and Huang 2004, Kung and McBride 1988, Pizzigallo et al. 1998) is proposed as follows for the oxidation reaction of FQs with iron oxides:

Step 1. FQs are adsorbed to the Fe oxide surface through the carboxylic acid moiety forming an inner-sphere precursor complex:

$$>Fe^{III}\text{-}OH_2^{+} + HO\text{-}Ar\text{-}X \rightleftharpoons >Fe^{III}\text{-}O\text{-}Ar\text{-}X + H_2O + H^{+} \quad (6)$$

The abundance and stability of the precursor complex are largely affected by pH, primarily due to the effect of pH on the speciation and charge of both reactants.

Step 2. The formation of the precursor complex brings the piperazine moiety in FQs close to the surface. When the two are close enough at some point (forming either inner- or outer-sphere complex), one electron is transferred from the N_1 of the piperazine ring to surface $>Fe^{3+}$ generating a structural $>Fe^{2+}$ and a FQ radical intermediate. The radical intermediate is stabilized most likely via resonance with the neighboring aromatic ring:

$>Fe^{III}$-O-Ar-X ⟶ $>Fe^{II}$ + 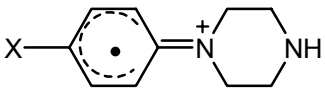 (7)

Both Steps 1 (adsorption) and 2 (electron-transfer) play a critical role in determining the overall reaction rate, with the slower one to be the rate-limiting step.

Step 3. The formed radicals are released to solution and undergo various oxidation reactions such as dimerization (forming dimeric products), hydroxylation (forming mono-

aldehyde and di-aldehyde products), dealkylation (forming the M-26 and the M-NH_2 products), and others (Zhang and Huang 2004).

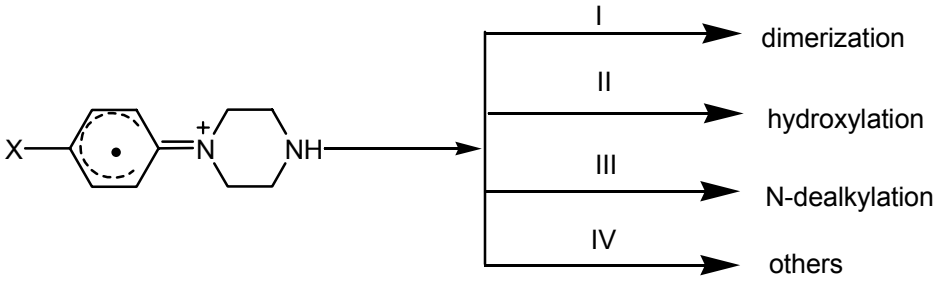

(8)

Step 4. Structural Fe^{2+} is released from the oxide surface and oxidized immediately by dissolved O_2. With the release of the $>Fe^{2+}$, more active surface is available for further adsorption and oxidation of FQs by Fe oxide.

$$>Fe^{II} \longrightarrow Fe^{2+}(aq) \xrightarrow{O_2(aq)} Fe(OH)_3(ppt) \quad (9)$$

4.4 Conclusions

Iron oxides are widely present in various soils and sediments, and are the most abundant metallic oxides in most soils. Iron oxides have been shown to be effective oxidants for a wide range of pollutants including phenols and anilines. Goethite is the most thermodynamically stable form of Fe oxides under aerobic conditions. This study found that adsorption and oxidation were both involved in the reaction of fluoroquinolones (FQs) with goethite. Adsorption isotherms for ciprofloxacin adsorption to two types of goethite were developed and fitted well to the Langmuir model.

In the reaction kinetics, three apparent stages of oxidation were observed: (i) stage 1 proceeded with a fast degradation, (ii) stage 2 involved a slowed reaction which was believed to result from the delayed release of Fe^{2+} ions generated during the reduction of goethite, and (iii) stage 3 involved a fast reaction rate similar to that in stage 1. The

reaction order of cipro in oxidation by Syn-FeOOH was about 0.69. The reaction orders of Ald-FeOOH and Syn-FeOOH were determined to be 0.29 and 0.54, respectively.

The adsorption and oxidation kinetics of FQs were examined extensively at varying pH and initial concentration of reactants, and with different types of goethite. Adsorptive and reactive sites were assessed based upon the speciation analyses and the kinetic comparisons among FQ antibacterial agents and model compounds. The neutral/zwitter ion form of FQs (i.e, $HQ/HQ^{\pm}$), especially the zwitter ion ($HQ^{\pm}$) form, and the positively charged Fe oxide surface (i.e., $FeOH_2^+$) played an important role in determining the overall adsorption. The carboxylic acid group of FQs is the reactive site in adsorption to the goethite surface, most likely via coordination between the carboxylate oxygen and the structural Fe(III). The piperazine ring of FQs is proven by the experimental results to be the reactive moiety toward oxidation by goethite

Owing to the large ratio of Fe oxide to antibacterial agent employed in the experiments, O_2 was found to have negligible influence on the reaction kinetics. Office light, on the other hand, increased the reaction rate by a factor of 2 to 3, which can be attributed to the surface photo-catalytic properties of goethite.

Oxidation products of the FQs were identified to be the same as the products formed in the oxidation of FQs by MnO_2. Reaction schemes were delineated based on the experimental results. In summary, FQs are initially adsorbed to the Fe oxide surface through their carboxylic acid moiety forming an inner-sphere precursor complex. The formation of the precursor complex brings the piperazine moiety in FQs close to the surface and one electron is transferred from the N_1 in the piperazine ring to surface $>Fe^{3+}$, generating a structural $>Fe^{2+}$ and a FQ radical intermediate. The formed radicals are then

released to solution and undergo various oxidation reactions such as dimerization (forming dimeric products), hydroxylation (forming mono-aldehyde and di-aldehyde products), dealkylation (forming the M-26 and the M-NH_2 products), and others. Structural Fe^{2+} is finally released from the oxide surface and oxidized immediately by dissolved O_2.

Results of this study indicate that Fe oxides in aquatic sediments may well play an important role in the natural attenuation of FQ antibacterial agents. The examination of the reaction kinetics and reaction mechanisms of Fe oxide-facilitated oxidation of FQs has yielded important insight into predicting the abiotic fate of structurally-related pharmaceutical compounds at the soil-water interface in the natural environment.

CHAPTER 5

REACTIVITY AND TRANSFORMATION OF AROMATIC *N*-OXIDES IN THE PRESENCE OF MANGNAESE DIOXIDE

5.1 Introduction

Quinoline-*N*-oxides and quinoxaline-*N,N'*-dioxides represent a structural class of aromatic *N*-oxides that are common in many pharmaceuticals, agrochemicals and industrial chemicals (Albini and Pietra 1991, Katritzky and Lagowski 1971). Aromatic *N*-oxide structures have also been observed in metabolites of many drugs and xenobiotics, as well as in intermediates of synthetic chemical processes because N atoms can undergo hydroxylation or oxidation to form *N*-oxides (Gorrod and Beckett 1978). Several quinoxaline-*N,N'*-dioxides have been developed as potent antibacterial agents to promote growth and prevent dysentery and bacterial enteritis in farm animals (FAO/WHO 1990, JECFA 1991, Hutchinson et al. 2002). Among those, carbadox (methyl-3-(2-quinoxalinylmethylene)carbazate-*N,N'*-dioxide) (see Table 5-1 for structure) is most widely used. Olaquindox (2-methyl-3-[N-(2-hydroxyethyl)carbamoyl]quinoxaline N,N'-dioxide) (see Table 5-1 for structure) is another example of aromatic *N*-oxide antibacterial agents and is used solely as a growth promoter (JECFA 1991). Recently it was found that carbadox and desoxycarbadox (Table 5.1), one of its metabolites, are suspected carcinogens and mutagens (JECFA 1991, FAO/WHO 1990). For this reason, carbadox has been banned in animal feedings in Europe (Commission Regulation No. 2788/98 1998).

The common uses of many aromatic *N*-oxides in various applications and their potential toxicities to humans and animals necessitate a better understanding of the environmental fate of these compounds in order to properly evaluate their risks. A comprehensive literature search revealed extremely limited information regarding abiotic or biotic transformation of aromatic *N*-oxides under environmental conditions. In particular the potential transformation of aromatic *N*-oxides with metal oxides in soils is essentially non-existent. So far most of the published studies focused on the photolytic reactions of aromatic *N*-oxides. For example, photolytic activity of carbadox and desoxycarbadox has been observed in the process of sample preparation, i.e., fresh tissue samples were spiked with these compounds followed by extraction and cleanup and the whole process lasted about 2 hours (MacIntosh and Neville 1984). The study showed that a minimal incandescent light in the hood reached the samples and caused degradation especially of desoxycarbadox, as indicated by their poorer recoveries (at 50 ± 8.8 % and 54 ± 10.8 % with light while 53 ± 13.6 % and 61 ± 7.2 % in near darkness for carbadox and desoxy-carbadox, respectively). In addition, a considerable amount of information has been published on the photochemical reactions of heterocyclic *N*-oxides in water or organic solvent media (reviewed in Katritzky and Lagowski 1971 and Kurasawa et al. 1995). Therefore photolysis of aromatic *N*-oxides can be expected in most sun-lit environments. Mild sorption of olaquindox to various soil types with distribution coefficients K_d in the range of 0.7 to 1.7 ml/g was documented (Rabolle and Spliid 2000). The possible biodegradation of olaquindox (50-5000 μg/L) both aerobically and anaerobically was also reported, with a slower degradation rate under anaerobic conditions (Ingerslev et al. 2001).

In a recent occurrence study, no carbadox was detected in 104 samples from various locations in the United States at the method detection limit of 0.1 μg/L (Kolpin et al. 2002). Veterinary *N*-oxides such as carbadox may enter soils, e.g., in pig sludge or through food wastes, while industrial *N*-oxides may enter aquatic systems through wastewater treatment plants. These *N*-oxides will likely end up in surface or ground waters and have contacts with soils and sediments. The likely moderate interactions of these compounds with soils and sediment (similar to that of olaquindox) point to the potentially significant role of minerals in their environmental fate. Among the most important naturally-occurring oxidants in facilitating organic pollutant transformation in soils and sediments, Mn oxides deserve particular attention due to their high reduction potentials. In fact, Mn oxides have been shown to be effective oxidants for a wide range of pollutants including substituted phenols (e.g. Stone 1987, Zhang and Huang 2003) and anilines (e.g. Laha and Luthy 1990, Pizzigallo et al. 1998). As will be discussed later, this study demonstrates that aromatic *N*-oxides are highly susceptible to Mn dioxide-facilitated oxidation.

In this study, experiments were conducted to examine the reactivity and transformation of a variety of quinoline and quinoxaline *N*-oxides toward an important soil oxidant Mn dioxide. To the authors' knowledge, this is the first study that reports the abiotic transformation of these aromatic *N*-oxide compounds with metal oxides. Environmentally relevant antibacterial agents carbadox (CDX), olaquindox (ODX), and desoxycarbadox (desoxy-CDX) were investigated along with model compounds quinoline-*N*-oxide (QNO), quinoxaline-*N*-oxide (QXO), quindoxin (or quinoxaline-*N,N'*-dioxide) (QDX), and quinoxaline (QX) (structures are shown in Table 5-1). Reaction

Table 5-1. Kinetic comparison among aromatic *N*-oxides and related model compounds.[a]

Compound	Structure	r_{init} (μM-h^{-1})[b]	Adsorption%[c]
Quindoxin (QDX)	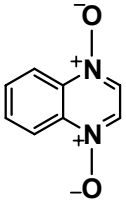	6.9 ± 0.6	<10
Quinoxaline *N*-oxide (QXO)	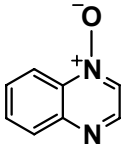	3.8 ± 0.2	<14
Quinoline *N*-oxide (QNO)	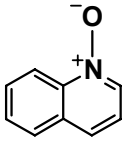	3.1 ± 0.1	0
Carbadox (CDX)	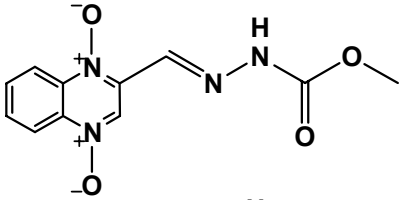	3.0 ± 0.2	<10
Desoxycarbadox (Desoxy-CDX)	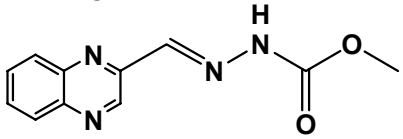	3.5 ± 0.8 × 10^{-2}	-
Quinoxaline (QX)	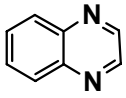	0	0
Olaquindox (ODX)	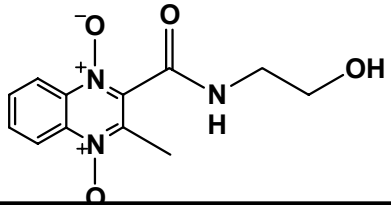	0	0

[a] Typical reaction conditions: 1mM MnO_2, 10 μM organic compound, 0.01 M pH 4 buffer, 0.01 M NaCl, 22°C. [b] r_{init} is in the format of initial reaction rate ± 95 % confidence level. [c] Adsorption % = C_{ads}/C_{total} %.

kinetics and product formation were characterized. Based on the results from this series of aromatic *N*-oxides, compound reactive sites and reaction schemes were delineated.

5.2 Materials and Methods

5.2.1 Chemical Reagents and Preparation

CDX was purchased from Sigma (St. Louis, MO). ODX was obtained from ICN Biomedicals (Irvine CA). QNO, QX, 2-hydroxyquinoline, 4-hydroxyquinoline, quinoxaline-2,3-diol, and methyltrioxorhenium were purchased from Aldrich (St. Louis, MO). All the above chemicals were at greater than 97% of purity. $H_2{}^{18}O$ was obtained from Cambridge Isotope (Andover, MA) at 95% of purity. Other employed chemical reagents including acetic acid, acetonitrile, ammonia acid, L-ascorbic acid, 2-(cyclohexylamino)ethanesulfonic acid (CHES), HCl, HNO_3, H_2O_2, methylene chloride, methanol, 4-morpholinepropanesulfonic acid (MOPS), NaCl, NaOH, Na_2SO_4, toluene, were obtained from Fisher Scientific (Fairlawn, NJ) or Aldrich (St. Louis, MO) at greater than 98% of purity (for solids) or of HPLC and GC/MS grade (for solvents), unless otherwise specified. All chemical reagents were used directly without further purification.

Reagent grade water (18.3 MΩ-cm resistivity) was prepared by a Millipore Nanopure water system. Mn dioxide (δ-MnO_2, similar to the naturally occurring birnessite) was synthesized based on the method by Murray (1974) and has been reported in our previous study (Zhang and Huang 2003).

QDX was synthesized following the method from Coperet et al. (1998). Briefly, QX (1.302 g, 10 mmol) and methyltrioxorhenium (MTO 25 mg, 0.1 mmol) were first

mixed in 4 mL of methylene chloride ($MeCl_2$), followed by addition of 4 mL of 30 % aqueous H_2O_2 solution (40 mmol, 4 equivalents to QX). The resulting biphasic reaction mixture was continuously stirred for more than 16 h at 24°C before being treated with a catalytic amount (2.5 mg) of MnO_2 and stirred for another hour until oxygen evolution ceased. Stirring was then ceased and the reaction mixture was allowed to undergo phase separation. Afterwards, the water layer was extracted with two times of 4 mL of $MeCl_2$. The combined organic layers were dried over Na_2SO_4, filtered through glass fiber filters (47 mm, Pall Corporation), and concentrated under a gentle stream of nitrogen gas to give predominantly QDX and a trace amount of QXO. The mixture was then dissolved in approximately 2 mL of methanol and subjected to HPLC fraction collection. The HPLC mobile phase consisted of Nanopure water (eluent A) and acetonitrile (eluent B) at a flow rate of 1 mL/min. The mobile phase began with 5% B (95% A), increased to 60% B in 10 minutes, increased to 95% B till 11 minutes, then the column was flushed thoroughly under these conditions for 4 minutes followed by a 4-min post time which allowed re-equilibration of the column. The major fraction corresponding to QDX was collected and subsequently evaporated to dryness using a rotary evaporator. A small amount of QXO was also purified in a similar fashion. The purified QDX and QXO were kept in the freezer for storage.

Desoxy-CDX was synthesized following the method by Massy and McKillop (1996). Briefly, carbadox (6.0 g, 22.9 mmol) was dispersed in 120 mL of acetic acid by refluxing the mixture briefly and cooling rapidly to 26°C. $Na_2S_2O_4$ (85 %, 10.56 g, 51.5 mmol) was dissolved in 60 mL of cold water and the solution was immediately added to the stirred dispersion, accompanied by a temperature rise to 33°C. After stirring for 1 h,

the mixture was placed in a rotary evaporator to evaporate to dryness. Toluene (50 mL) was added in the final evaporation to assist in the removal of acetic acid. After the sample was dried, 60 mL of water was added to the residue, and the resulting mixture was cooled to 4°C in a refrigerator overnight. The mixture was filtered through glass fiber filters (47 mm, Pall Corporation) and the collected solids were washed with water (3 × 6 mL). After vacuum drying, brown crystalline desoxy-CDX was obtained, pure based on HPLC as indicated by a single distinct peak with high peak purity by a diode-array UV/Vis detector (detailed HPLC conditions are discussed in section 5.2.3).

Stocks of *N*-oxides and related model compounds were prepared in pure methanol at 100-120 mg/L. All stocks were stored at 4 °C and used within a month of preparation.

5.2.2 Reactor Setup

The experimental setup for the reaction of *N*-oxides with Mn dioxide is similar to that used in the study by Zhang and Huang (2003). Briefly, all experiments were conducted in 25 ml screw-cap amber glass bottles with Teflon septa. The reaction bottles were placed on a magnetic stir plate in a 22^{o}C water basin and were continuously stirred. Reaction solutions were maintained at constant pH with 10 mM of appropriate buffer: acetic acid/sodium acetate for pH 4-5, 4-morpholinepropanesulfonic acid (MOPS) and its sodium salt for pH 6-8, and 2-(cyclohexylamino)ethanesulfonic acid (CHES) and its sodium salt for pH 9-10. Reactions were initiated by adding a certain amount of organic stock solutions to solutions containing manganese oxide, buffer, and constant ionic medium. Aliquots were periodically collected and reactions were quenched immediately for analyses either by centrifugation (at 12000 rev/min for 20 min) or by ascorbic acid

(0.1 M) addition. Typical reaction times were from hours to several days. Controls with *N*-oxides alone and with reaction media alone were prepared simultaneously with each batch of reaction.

5.2.3 Analysis of *N*-Oxides, Model Compounds and Mn^{II} Ions

Decrease in the concentrations of *N*-oxides and other structurally related compounds was monitored by a reverse-phase high performance liquid chromatography (HPLC) system with a Zorbax RX-C18 column (4.6 × 250 mm, 5 μm) and a diode-array UV/Vis detector (1100, Agilent Technology). CDX and desoxy-CDX were detected at 308 nm, and ODX was detected at 262 nm by the UV detector. All the other compounds were detected at 230 nm. The mobile phase consisted of a solution containing 20 mM ammonia acetate (eluent A) and acetonitrile (eluent B) at a flow rate of 1 mL/min. The mobile phase began with 5% B (95% A), increased to 60% B in 10 minutes, increased to 95% B till 11 minutes, then the column was flushed thoroughly under these conditions for 4 minutes followed by a 4-min post time which allowed re-equilibration of the column.

Generation of Mn^{II} ions from reductive dissolution of Mn dioxide was monitored using an inductively coupled plasma (ICP) spectrometer (Thermo Jarrell Ash Trace Analyzer) (for details of the analytical procedure, see Zhang and Huang 2003). Controls with only Mn oxide, electrolytes and pH buffers revealed that dissolution of Mn dioxide did not occur in the absence of the *N*-oxides.

5.2.4. Analysis of Organic Products

Reaction products were analyzed by a HPLC/MS system with a Zorbax SB-C18 column (2.4 × 150 mm, 5 μm) and a mass spectrometer (1100/1100MSD, Agilent Technology). Typically 20 mL of reaction suspensions containing 0.1 mM of *N*-oxides and 1 mM of MnO_2 were prepared at pH 4. Product analyses were also conducted in $H_2{}^{18}O$ by preparing reaction suspensions with $H_2{}^{18}O$ (at 95% purity) and adjusting pH with 0.1 M HCl, while keeping other conditions identical. The $H_2{}^{18}O$ reaction suspensions were equilibrated overnight before adding the *N*-oxide stock to initiate the reaction. Reactions were quenched after 1-7 days by centrifugation (at 12000 rev/min for 20 min) and the supernatants were analyzed by LC/MS. Gradient elution was conducted using pure acetonitrile (eluent B) and 0.02% acetic acid in 90/10 water/acetonitrile (v/v, eluent A) at a flow rate of 0.20 mL/min. The gradient was as follows: B started at 10% for the first minute, increased to 60% by 10 minute, increased to 80% by 25 minute. Then the column was flushed by 100% B for 10 minutes followed by a 15-min post time which allowed re-equilibration of the column. The MS analysis was conducted by electrospray positive ionization at the fragmentation voltage 80-120 V with mass scan range 50-1000 m/z. The drying gas was operated at 10 mL/min at 325 °C. The nebulizer pressure was 30 psig and the capillary was set at 4000 V.

5.3 Results and Discussion

5.3.1 Reaction Kinetics

In the absence of Mn oxide, all of the *N*-oxides investigated in this study (see Table 5-1) were stable under the experimental conditions and no measurable loss of the compounds could be detected after a week. In contrast, significant degradation of *N*-

oxides (CDX, QDX, QXO and QNO) occurred in the presence of Mn dioxide. Among the investigated *N*-oxides, only ODX was found to be stable in the presence of MnO_2, with no detectable degradation for up to a week. Typical time course of CDX reaction with MnO_2 is shown in Figure 5-1. Similar kinetic behavior was observed for all the other *N*-oxides. As shown in Figure 5-1, the reaction kinetics deviated from the pseudo-first-order kinetics even over the first few time increments, thus for the sake of comparison, reaction kinetics were evaluated based upon initial reaction rates r_{init} in μM-h^{-1} (i.e., the slopes over the first few time increments in plotting concentration versus time, r_{init} = - dC/dt). Similar kinetic behavior involving Mn oxide surfaces has been observed in many previous studies (e.g., Zhang and Huang 2003). All kinetic data are expressed based on the 95% confidence level (Table 5-1).

Investigation with a range of *N*-oxides showed rapid degradation of all *N*-oxides except ODX by MnO_2 at pH 4 (Table 5-1). QDX reacted the fastest, followed by similar initial reaction rates measured for QXO, QNO and CDX. Desoxy-CDX was found to react 2 orders of magnitude slower than other *N*-oxides. Furthermore, no appreciable degradation was observed for ODX and QX within a week.

A series of experiments with varying CDX loadings (5 – 50 μM) but a fixed MnO_2 loading (1 mM or 3 mM) or with varying Mn oxide loadings (0.1 – 3 mM) but a fixed CDX loading (10 μM) were conducted to assess the initial reaction orders with respect to CDX and Mn oxide (Figure 5-2). When CDX loading was below 20 μM, plotting the log of the initial reaction rate r_{init} versus the log of CDX loading yielded lines with slopes of 0.56 – 0.58. However, when CDX loading was above 20 μM, the curves appeared to level off, resembling Langmuir behavior which ascertained surface saturation

effect in the presence of large amount of adsorbates. Previous work by Zhang and Huang (2003) has shown the limited number of reactive sites on the Mn dioxide surfaces, in which a slowed increase in the reaction rate was observed when an increasing amount of triclosan was oxidized by a fixed excess amount of Mn dioxide. This present study further demonstrated that MnO_2 surfaces, even at an over 20-fold excess, could be saturated by small amounts of CDX molecules. For MnO_2, a slope of 0.54 was obtained by plotting log of r_{init} versus the log of MnO_2 loading across the range of the investigated MnO_2 loadings. These results demonstrated that the reaction order with respect to either CDX or MnO_2 was constant and quite comparable within a suitable concentration range of either reactant. To minimize further complication of the surface kinetics, subsequent studies were conducted within the concentration range where the constant reaction order of either reactant could be applied.

The initial reaction rate constant k_{obs} in $\mu M_{CDX}^{-0.56} \cdot h^{-1}$ (i.e., the initial reaction rate divided by the initial CDX concentration to the power of 0.56, r_{init} = - dC/dt = - k_{obs} × $[CDX]^{0.56}$) was also estimated in order to evaluate the reaction order with respect to $[H^+]$ ($k_{obs} = k_{pH} \times [H^+]^a$). Least-square fitting of Figure 5-3 data gives an average reaction order of 0.16 for H^+. As shown in Figure 5-3, pH exerted a marked influence on the reaction rate of CDX oxidation by Mn oxide, with log k_{obs} decreasing linearly with the increasing pH (CDX degradation rate at pH > 7 was too slow to be observed within 2 weeks). Adsorption of CDX to Mn oxide surfaces under different pH values was evaluated by comparing the experimental results from two different quenching methods (i.e., centrifugation and ascorbic acid addition) as described in our previous study (Zhang and Huang 2003). By adding ascorbic acid, Mn oxide was readily reductively dissolved

yielding Mn^{2+} ions and thus the adsorbed yet unreacted CDX on the oxide surface could be released and measured (control experiments have verified the stability of CDX in the presence of ascorbic acid). In contrast, only the non-adsorbed CDX could be detected in the centrifugation supernatant. This comparison showed that <10 % of CDX was adsorbed to MnO_2 at pH 4 (Table 5-1). Similar low adsorption extent (<10 %) was observed for CDX at other pH values (5 < pH < 9). Low adsorption extent (<14 %) for other examined *N*-oxides was also obtained by the same approach (data are shown in Table 5-1).

Based upon the above kinetic results, the initial rate of CDX oxidation by MnO_2 can be described by the following kinetic expression:

$$\text{Initial rate} = -\frac{d[\text{CDX}]}{dt} = -k_{obs}[\text{CDX}]^{0.56} = -k_{\text{exp}}[\text{CDX}]^{0.56}[\text{MnO}_2]^{0.54}[\text{H}^+]^{0.16} \qquad (1)$$

From the values of r_{init} at various initial MnO_2 loadings and pH's, the third-order rate constant k_{exp} (applicable within the employed experimental conditions) was computed to be $2.98 \pm 0.48 \times 10^5$ $M_{CDX}^{0.44} \cdot M_{MnO_2}^{-0.54} \cdot M_{H^+}^{-0.16} \cdot h^{-1}$ (n = 30) for CDX.

Production of Mn^{2+} ions from reductive dissolution of MnO_2 by QDX or QNO was monitored and an increase in Mn^{2+} concentration was observed as breakdown of the *N*-oxides proceeded (Figure 5-4). Despite that, it was difficult to accurately determine the kinetics of the Mn^{2+} generation, particularly at the initial stage of the reaction, due to strong adsorption of Mn^{2+} to MnO_2. Experiments showed that greater than 90% of 10 μM Mn^{2+} was adsorbed to 1 mM MnO_2 at various pH values (4 < pH < 7). Nevertheless, the increase in Mn^{2+} corresponding to the loss of either QDX or QNO provides the evidence that Mn oxide was reductively dissolved by *N*-oxides yielding Mn^{2+}. Visual inspection of the slopes in Figure 5-4 as an indication of the magnitude of the redox

reactions further revealed that Mn dioxide was consumed at a similar rate as the *N*-oxides.

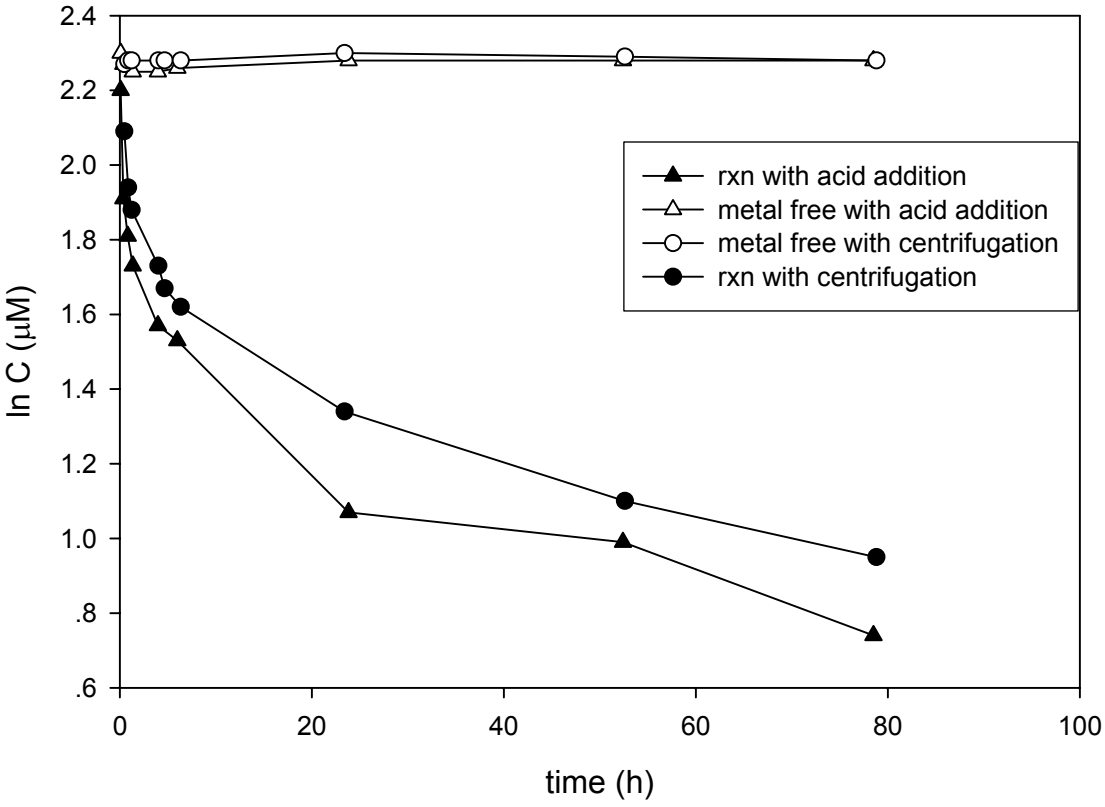

Figure 5-1. Time course of CDX oxidation by MnO_2. Reactions contained 1 mM MnO_2 and 10 μM CDX initially with pH 4 acetate buffer at 22 °C.

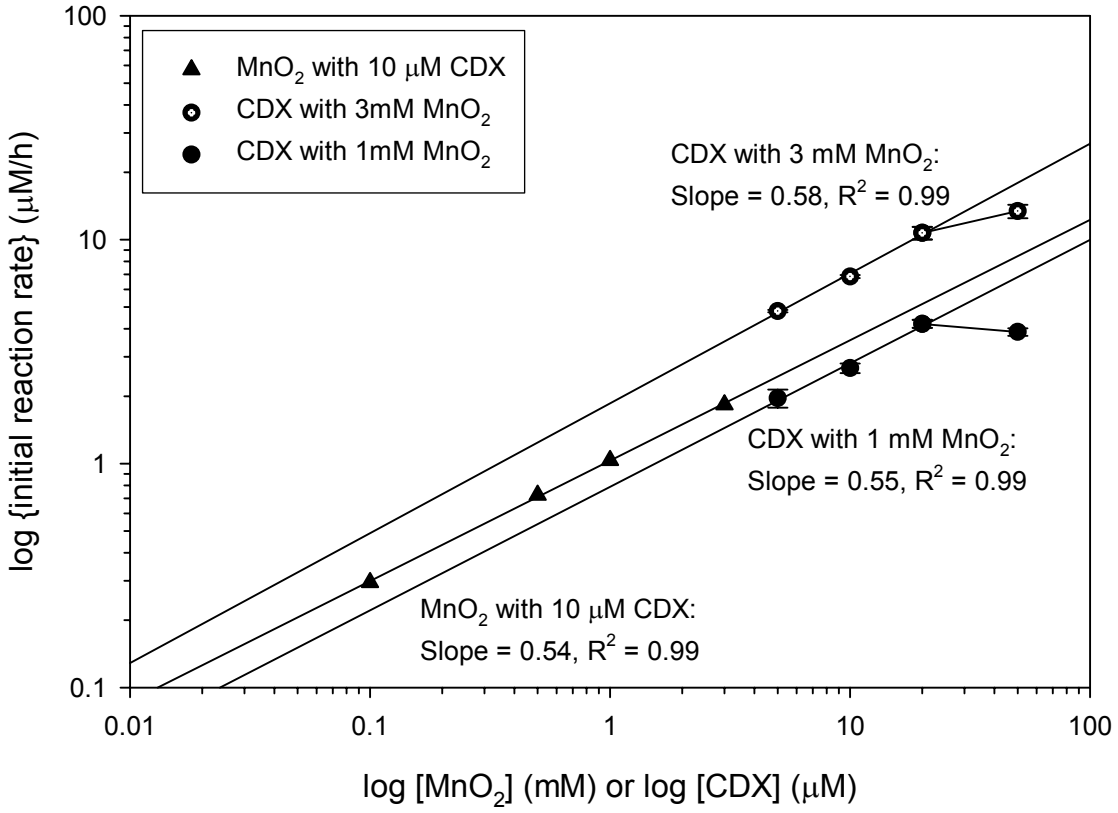

Figure 5-2. Reaction orders with respect to CDX and MnO_2. Typical reaction conditions: 5 – 50 μM CDX, 0.1 – 3 mM MnO_2, 0.01 M pH 4 buffer, and 0.01 M NaCl at 22°C.

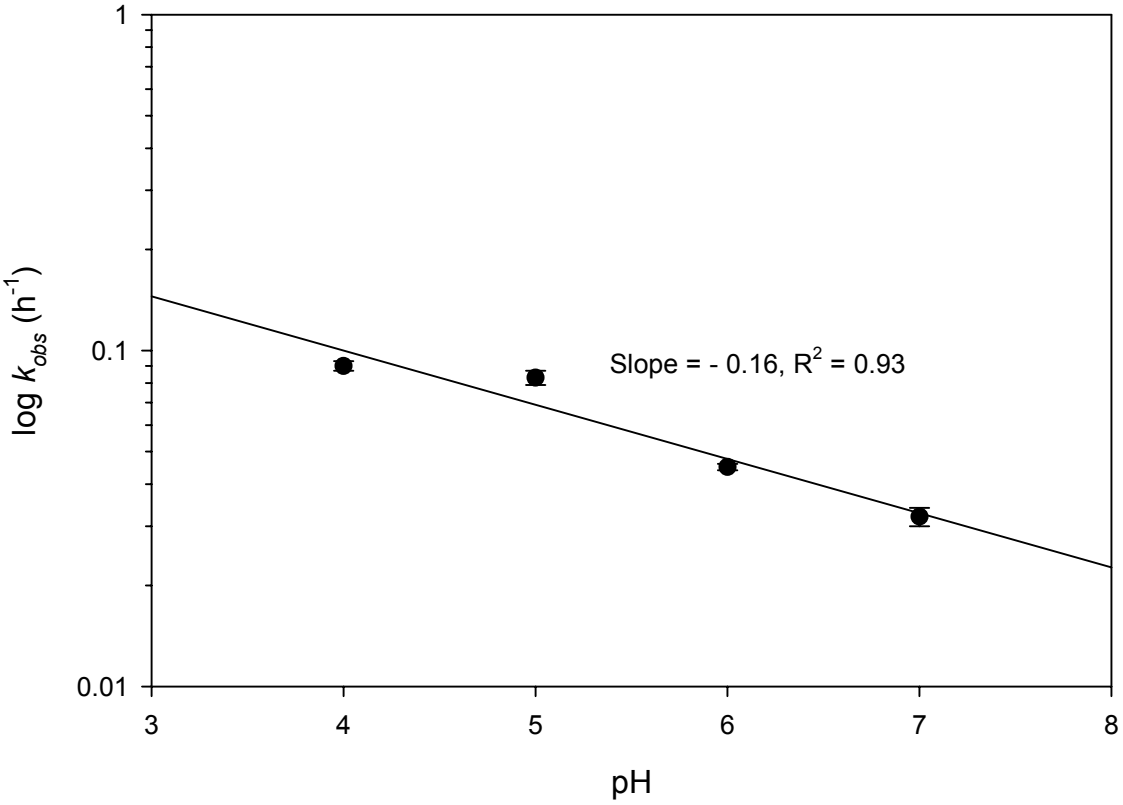

Figure 5-3. Effect of pH on CDX oxidation by MnO_2. Reactions contained 3 mM MnO_2 and 10 μM CDX initially with pH 4 acetate buffer at 22 °C.

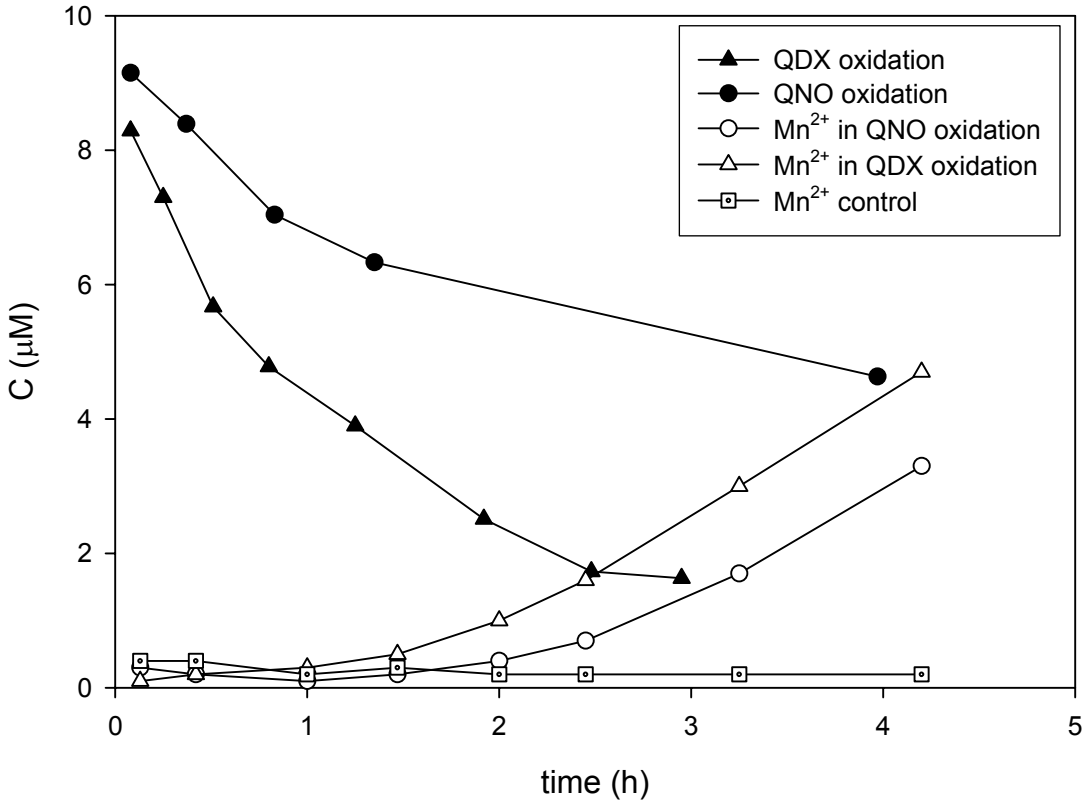

Figure 5-4. Kinetic comparison between Mn^{2+} and QDX or QNO. Typical reaction conditions: 10 μM QDX or QNO, 1 mM MnO_2, 0.01 M pH 4 buffer and 0.01 M NaCl at 22°C.

5.3.2 Oxidation products of QNO and QDX

Electrospray LC/MS analysis of the QNO (m/z 146) reaction mixture exhibited the existence of one major product (m/z 146) and one minor product (m/z 305) (Table 5-2a). The parent QNO and its major reaction product had the same molecular weight but exhibited different fragmentation patterns. The parent QNO fragmented by the loss of OH from the *N*-oxide position (i.e., - m/z 17), consistent with the previous work by Miao et al (2003) in which detailed fragmentation pathways of QNO were documented. In contrast, the major product of QNO fragmented by the loss of H_2O (i.e., - m/z 18) – a fragmentation pattern often involves a hydroxyl substituent on the compound. Authentic standards of 2-hydroxyquinoline and 4-hydroxyquinoline (both are of m/z 146; see Figure 5-5 for structures) were also analyzed by electrospray LC/MS under the same conditions. 2-Hydroxyquinoline and 4-hydroxyquinoline exhibited the same mass spectrum but had different retention times. The LC retention time and MS spectrum of 2-hydroxyquinoline matched closely with those of the major product of QNO, confirming the major product to be 2-hydroxyquinoline. For the minor product, the molecular ion of 305 was assigned based on the difference of 22 in m/z 327 ($[M+Na]^+$) and m/z 305 ($[M+H]^+$). There were two fragments, m/z 146 and m/z 160, in the minor product, suggesting that the minor product could be a dimeric product of QNO and one of its reaction intermediates.

Analyses of the oxidation products of QNO (at pH 4) over the period of 39 hours (Figure 5-6) showed that the MS peak area of the m/z 305 product increased slightly in the very beginning and then quickly decreased until disappearance. This kinetic behavior indicates that the m/z 305 product is a reaction intermediate. The product evolution study

showed that the abundance of the m/z 146 product (i.e., 2-hydroxylquinoline) consistently increased over time (Figure 5-6), suggesting it being a stable end product. Separate experiments with 2-hydroxyquinoline also confirmed that this compound is stable in the presence of Mn oxide. Moreover, at any reaction time the sum of QNO and the 2-hydroxylquinoline product accounts for more than 95% of the initial QNO, indicating that 2-hydroxylquinoline is the dominant product.

LC/MS analysis of the *N,N'*-dioxide QDX (m/z 163) reaction mixture indicated the presence of primarily two products: m/z 163 and m/z 197. The molecular ions of these two products were assigned based on the observation of the sodiated ions $[M + Na]^+$ and the molecular ions $[M + H]^+$ (Table 5-2c). Similar to the case of QNO, QDX and its major m/z 163 product had the same molecular weight but different fragmentation patterns. QDX exhibited the characteristic loss of OH (i.e. –m/z 17) from one of its *N*-oxide groups, while the m/z 163 product yielded very different fragments. By analogy to the 2-hydroxyquinoline product of QNO, the m/z 163 product of QDX was suspected to be quinoxaline-2,3-diol (structure shown in Figure 5-5). Comparison of this product with the authentic standard of quinoxaline-2,3-diol based on LC/MS analyses confirmed that the above conclusion is indeed correct. The structure of the minor product of m/z 197 could not be determined based on its LC/MS spectrum information.

Product evolution study of QDX (Figure 5-7) revealed that quinoxaline-2,3-diol and m/z 197 products were stable end products. Quinoxaline-2,3-diol was present at an abundance almost twice as much as the m/z 197 product. The inertness of quinoxaline-2,3-diol toward Mn oxide under the reaction conditions was further confirmed by kinetic experiments that lasted up to 5 days. As shown in Figure 5-7, the sum of QDX,

quinoxaline-2,3-diol and the m/z 197 products gradually decreased over time. For example, only 75% of mass balance was obtained at reaction time of 72 hours, indicating that other unknown product(s) could also be present but were undetectable by the current approach. Thus, the oxidation of *N,N'*-dioxide QDX appeared to be more complex than the oxidation of *N*-monooxide QNO.

Information regarding chemical oxidation of *N*-oxides is rather limited. Published results on the photoreactions of *N*-oxides were reviewed to gain insights into the products observed in this study. Previous work proposed that photoreaction of QDX in water proceeded via an intermediate with a three-membered ring among O, N, and the neighboring C atoms on QDX, followed by rearrangement of the three-membered ring to form a 2-hydroxyl substituent on the product (reviewed in Kurasawa et al. 1995). To discern whether the same type of rearrangement was the mechanism behind the formation of 2-hydroxyquinoline (m/z 146) from QNO, isotope experiments in $H_2{}^{18}O$ were conducted to test this hypothesis. If the oxidation of QNO in $H_2{}^{18}O$ yielded the same m/z 146 product, it would be evident that the O atom of the *N*-oxide rearranged to form the –OH substituent in 2-hydroxyquinoline. In fact the oxidation of QNO by Mn oxide in $H_2{}^{18}O$ yielded one major product of m/z 148 and one minor product of m/z 309, with the same retention times as the previous m/z 146 and m/z 305 products, but 2 and 4 masses higher, respectively (Table 5-2b). The m/z 148 product had the same major fragment (m/z 128) as that of m/z 146, corresponding to the loss of $H_2{}^{18}O$ (-20) from ^{18}O-labeled 2-hydroxyquinoline (Figure 5-5). The molecular ion of 309 was assigned based on the observation of the sodiated ion (m/z 331) and the molecular ion (m/z 309). The m/z 309 product also had two major fragments: m/z 148 and m/z 162. Each of the fragments was

2 masses higher than the corresponding fragment in the m/z 305 product, which corresponded to the presence of one ^{18}O atom in each fragment. The tentative structures of the m/z 305 and m/z 309 products are postulated in Figure 5-5. Thus the isotope experiments confirmed that rearrangement of the *N*-oxide group was not involved in the production of 2-hydroxyquinoline from QNO. Instead, the loss of the O atom from the *N*-oxide group and the formation of the 2-OH substituent are likely two separate steps. The source of the 2-OH substituent is likely from either the bulk water or –OH groups associated with the Mn oxide skeleton, which is discussed further in a later section.

5.3.3 Oxidation Products of CDX and Desoxy-CDX

LC/MS analysis of CDX reaction mixture indicated the presence of primarily four products with molecular ions of m/z 281, 279, 205 and 197, respectively (Table 5-2d). The molecular ion of CDX is m/z 263, and its main fragment (m/z 231) corresponds to the loss of $–OCH_3$ (i.e., - m/z 32) from the side chain (detailed fragmentation pathways were proposed in Miao et al. 2003). Most molecular ions of the products were identified based on the difference of 22 in m/z's between $[M + Na]^+$ and $[M + H]^+$ ions. For the m/z 279 product of CDX, the major fragment m/z 263 corresponded to the loss of one O atom (i.e., - m/z 16) from the molecular ion. Two other fragment ions m/z 247 and m/z 231 corresponded to the loss of $–OCH_3$ (i.e., - m/z 32) from the molecular ion (i.e., m/z 279) and the main fragment m/z 263, respectively. These results indicated that the m/z 279 product could be a parent CDX analog with an O atom addition. All of the other three products (m/z 281, 205 and 197) had small MS responses and the structure identification could not be achieved based on their spectra. In addition to the above four products, UV

detection (220 nm) of CDX reaction mixtures revealed the presence of two extra products without any MS responses, despite the fact that the following range of LC/MS conditions was tried: (i) using formic acid instead of acetic acid in the mobile phase; (ii) changing the electrospray positive ionization mode to negative mode; and (iii) applying either positive or negative atmospheric pressure chemical ionization (APCI) instead of electrospray ionization. These results suggested a complicated product pattern in CDX oxidation.

Analyzing the oxidation products of CDX (at pH 4) over several hours further revealed that the m/z 279 product was an intermediate, with its MS area increasing slightly in the very beginning followed by a fast disappearance (resembling the kinetic trend of the m/z 305 product from the oxidation of QNO as shown in Figure 5-6). All other products displayed their small MS/UV responses throughout the reaction period for up to 1 week.

The same fragmentation pattern as that of CDX was observed for desoxy-CDX, with the molecular ion m/z 231 and the major fragment m/z 199 (i.e., - m/z 32, the loss of $–OCH_3$) (Table 5-2e). No appreciable products were detected in desoxy-CDX oxidation mixtures for up to 1 week owing to the fact that less than 10 % of the parent compound was degraded under the experimental conditions employed.

Table 5-2. LC/MS spectra for the aromatic *N*-oxides and corresponding oxidation products [a].

a. Quinoline *N*-oxide (QNO)

m/z	MS Fragments
146[b]	147(75), **146**(42), 129(100), 103(60), 102(8), 76(5)
146	**146**(60), 128(100)
305	327(20), **305**(70), 160(65), 146(100)

b. Quinoline *N*-oxide (QNO) rxn in H_2O^{18}

m/z	MS Fragments
146[b]	147(75), **146**(42), 129(100), 103(60), 102(8), 76(5)
148	**148**(60), 128(100)
309	331(20), **309**(70), 162(65), 148(100)

c. Quindoxin (QDX)

m/z	MS Fragments
163[b]	**163**(32), 146(100), 135(20), 118(60), 99(20), 91(65), 61(5)
163	185(48), **163**(100), 61(5)
197	219(32), **197**(100), 158(20), 99(15)

d. Carbadox (CDX)

m/z	MS Fragments
?	303(100), 305(10), **281**(10), **263**(5), 245(10), 235(40), 217(10), 205(25), 190(5), 163(5), 117(6), 99(12), 6
263[b]	285(10), 264(18), **263**(100), 231(40)
279	303(45), 301(100), 285(30), **279**(95), 263(80), 247(38), 231(25), 217(20), 204(15), 163(15), 99(15), 61(3(
?	303(50), 263(10), 245(30), **205**(100), 177(10), 99(10), 61(40)
?	**197**(35), 165(100), 163(10), 148(28), 135(65), 99(30), 81(45), 66(25)

e. Desoxycarbadox (Desoxy-CDX)

m/z	MS Fragments
231[b]	231(10), 199(40), 172(25), 171(5), 143(100), 130(35), 116(12), 102(10)

[a] MS fragments are expressed in the form of m/z (abundance%). [b] the parent compound.

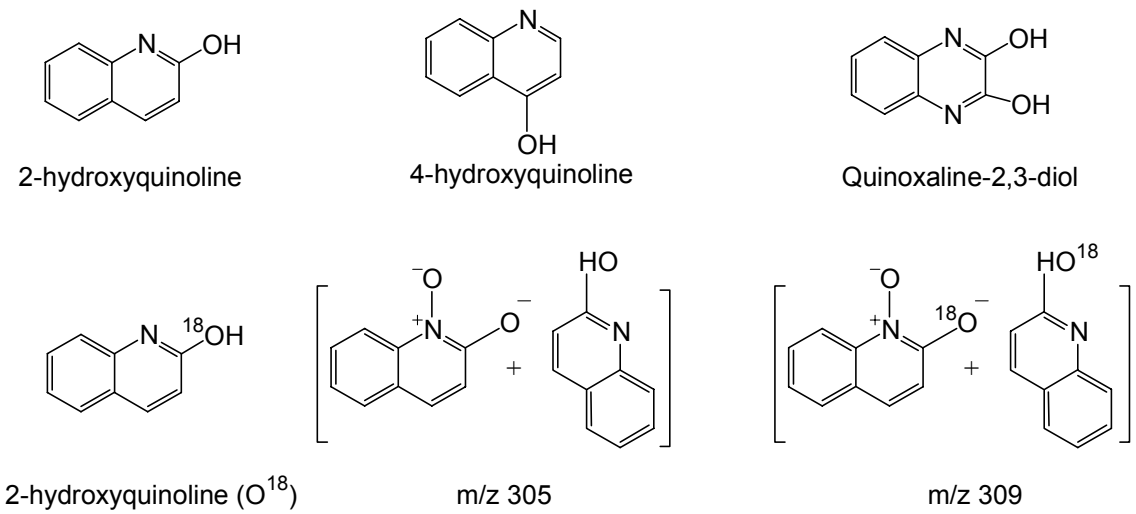

Figure 5-5. Structures of the oxidation products of QNO and QDX.

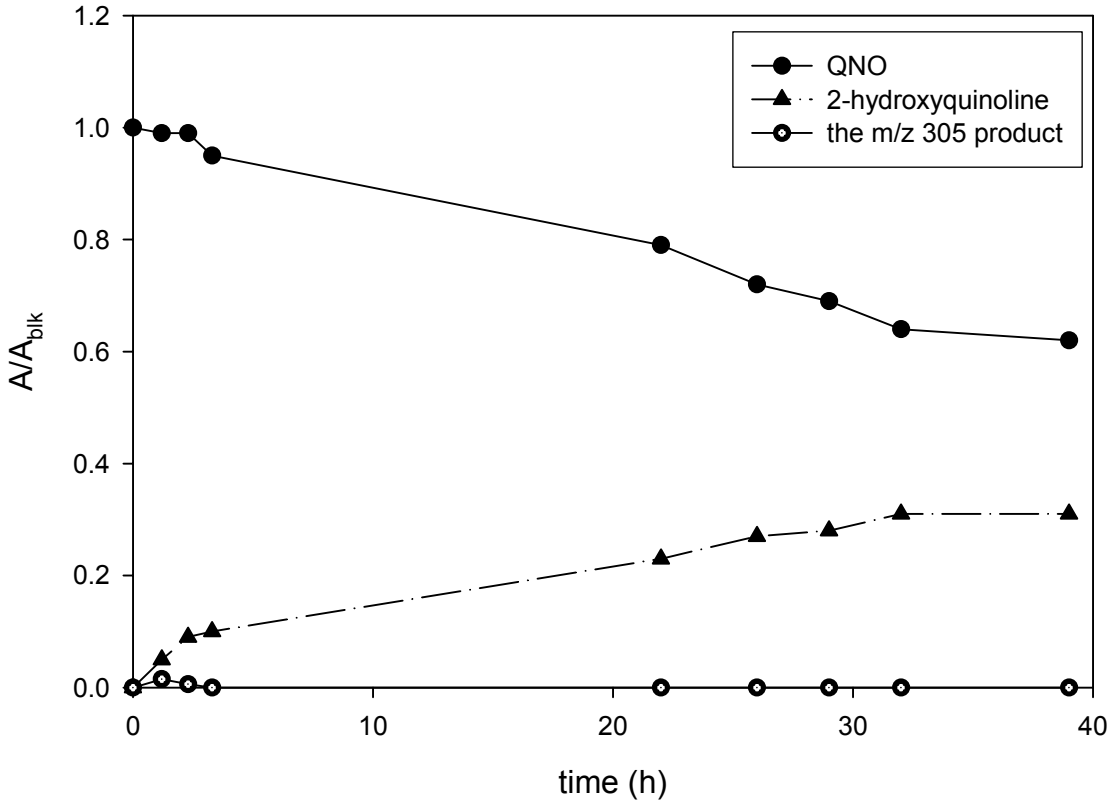

Figure 5-6. Time evolution of the oxidation products of QNO (A = LC/MS area of each compound in the reaction suspension at a certain reaction time; A_{blk} = LC/MS area of the parent QNO control at the certain reaction time).

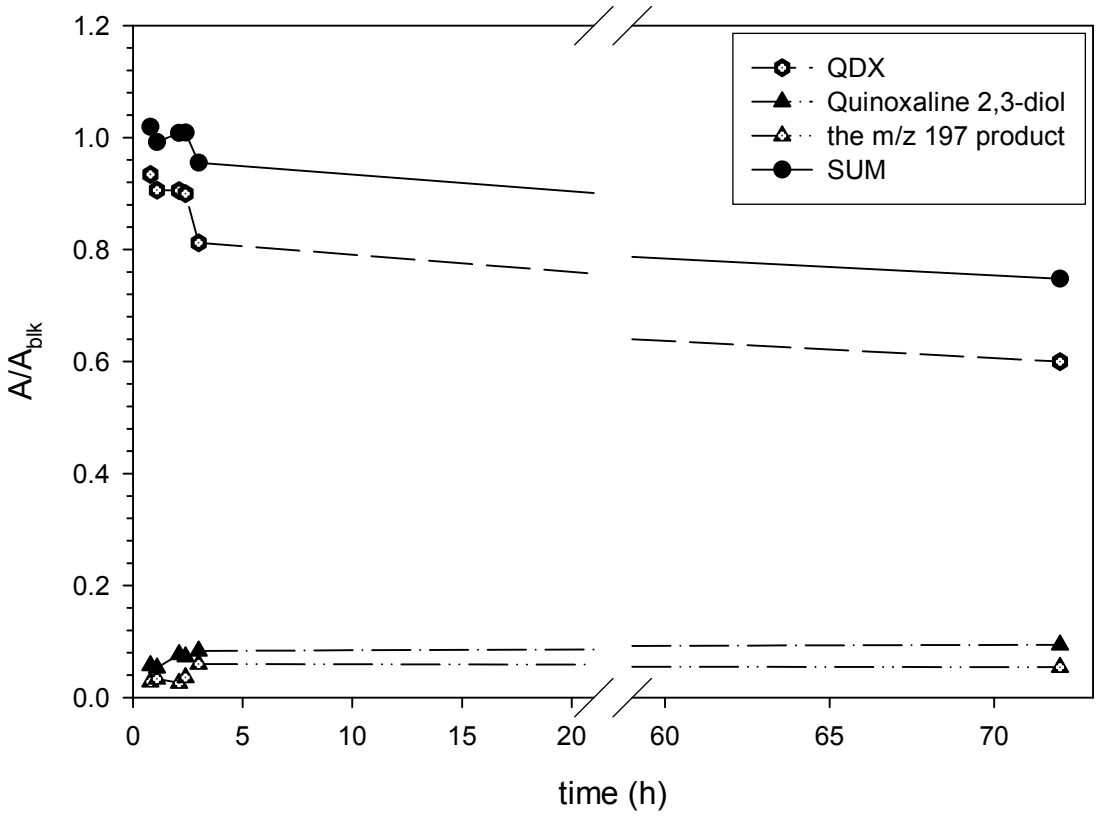

Figure 5-7. Time evolution of the oxidation products of QDX (A = LC/MS area of each compound in the reaction suspension at a certain reaction time; A_{blk} = LC/MS area of the parent QDX control at the certain reaction time).

5.3.4 Chemical Reactive Sites and Reactivities

The much higher reactivity of the *N*-oxide compounds (QDX, QNO, DXO, CDX) versus the non-*N*-oxide compounds (QX, desoxy-CDX) in Table 5-1 indicates that the *N*-oxide functional group is the reactive site in the oxidation with MnO_2. The average 2-fold higher reactivity of QDX (*N*,*N*'-dioxide) versus QNO and QXO (*N*-oxide) also supports the above conclusion, with the presence of two versus one reactive *N*-oxide moieties, respectively. The slow reaction rate of desoxy-CDX versus the inactivity of QX indicates that the side chain of CDX and desoxy-CDX can also react with MnO_2, but with a much lower reactivity than the *N*-oxide moiety. This observation is consistent with the susceptibility of hydrazide (-CO-NH-N<) or hydrazone (>CH=N-N<) moieties toward oxidation reactions (Bhatnagar and George 1968, Haksar et al. 1979).

Both CDX and ODX contain two *N*-oxide functional groups, however CDX has reactivity similar to *N*-oxide (rather than *N,N*'-dioxide) while ODX does not react with MnO_2 at all. Compared to QDX, CDX has one substituted side chain neighboring to one of its *N*-oxide groups, while ODX has one substituted side chain and one methyl substituent next to either of its *N*-oxide functional groups, respectively. The carbamate (-CO-NH-) side chain of ODX is not expected to undergo redox reaction with MnO_2. As discussed in the preceding sections, characterization of the *N*-oxide oxidation products revealed the involvement of the α-C and α-H atoms neighboring to the *N*-oxide group; i.e., the oxidation of the *N*-oxide group requires at least one H substituent in its neighboring position. In other words, the reactivity of one of the *N*-oxide groups in CDX, and both of the *N*-oxide groups in ODX was retarded due to the blockage and replacement of an α-H substituent by an alkyl side chain or substituent.

5.3.5 Surface Reactions

A general surface reaction mechanism involving Mn oxides has been extensively reported (e.g., Stone 1987, Zhang and Huang 2003, Laha and Luthy 1990). In summary, the organic compound in question is adsorbed to the oxide surface, forming a precursor complex. Electrons are transferred within the precursor complex, followed by the release of organic oxidation products and Mn^{2+}. The precursor complex formation and electron transfer are likely rate-limiting. Oxidation of *N*-oxides by MnO_2 is likely to follow this surface reaction mechanism as do many other organic contaminants. For example, the reaction kinetics of CDX observed in this study supports this conclusion as discussed below.

The initial reaction orders of CDX, MnO_2 and H^+ were determined to be 0.56, 0.54 and 0.16, respectively (Equation 1). The linear dependence of CDX oxidation rate on pH is mainly due to the linear dependence of the reduction potential of MnO_2 on pH. In other words, the oxidizing power of MnO_2 decreases with the increase in pH, which leads to the observed pH dependence of the reaction rate in Figure 5-3. Such a phenomenon was also seen in many previous studies (e.g., Stone 1987, Laha and Luthy 1990, Zhang and Huang 2003).

Higher reaction orders with respect to reactants were found by the authors in a previous study, in which oxidation of two phenolic antibacterial agents, triclosan and chlorophene, by Mn oxides was examined (Zhang and Huang 2003). In that study, the reaction orders were about 1, 1 and 0.5 for triclosan, MnO_2 and H^+, respectively. A much higher adsorption of triclosan toward Mn oxide was also observed. For example, over 55% of triclosan (initial concentration of 10 μM) was adsorbed to 0.1 mM of MnO_2 at pH

5. In contrast, less than 10 % of CDX (initial concentration of 10 μM) was adsorbed to 1 mM of MnO_2 within the pH range of 4-9. Low adsorption to MnO_2 was also found for all the other *N*-oxides as shown in Table 5-1. Thus the smaller reaction orders observed in the current study than those in the previous one could be due to the weak adsorption of the *N*-oxides to Mn dioxide. As illustrated in much of the earlier work, precursor complex formation and electron transfer are likely rate-limiting (e.g., Stone 1987, Laha and Luthy 1990, Zhang and Huang 2003), and the overall dependence of the reaction rate on each of the reactants (i.e., the reaction order of each reactant) would be influenced by the reaction rates of these two steps. Adsorption of the organic reductant to MnO_2 has a significant impact on the overall surface oxidation rate through affecting the precursor complex formation (e.g., Stone 1987, Laha and Luthy 1990, Zhang and Huang 2003). Weaker adsorption would lead to poorer precursor complex formation, a slower reaction rate, and thus less sensitivity of the reaction rate to the change in the reactant concentration. Such an effect would be reflected as smaller reaction orders for the reactants in the first elementary reaction (i.e., precursor complex formation) and hence in the overall reaction rate. A similar phenomenon was also observed in the oxidation of fluoroquinolone antibacterial agents and related amine compounds by goethite (α-FeOOH) (Chapter 4). In this particular study by the authors, 1-phenylpiperazine had a smaller reaction order (0.54) than ciprofloxacin (0.67-0.71), presumably due to the much higher adsorption of ciprofloxacin to goethite. Additionally, 1-phenylpiperazine exhibited different reaction orders toward two types of goethite with a greater reaction order (0.54 versus 0.29) in reaction with the goethite that has a higher specific surface area (159 m^2/g versus 10-86 m^2/g).

The same reaction order of CDX and MnO_2 indicates that these two reactants react at a similar rate, with an average of two electrons transferred from CDX to MnO_2 to generate Mn^{2+} ions. The fact that the rate of Mn^{2+} generation is comparable to that of QDX or QNO degradation is also consistent with the observed reaction orders, and supports the above conclusion (Figure 5-4).

5.3.6 Reaction Schemes

Studies have shown that deoxygenation of QDX in the presence of nucleophiles such as $S_2O_4^-$ or AcO^- starts with their attack at the α–C atom neighboring to one of the *N*-oxide groups, followed by loss of the *N*-oxide oxygen atom, and upon hydrolysis produces an α–OH substituent (Ahmed et al. 1987, Kurasawa et al. 1995). Other studies generally believed that radicals of *N*-oxides are involved in the oxidation of QDX by photolytic, enzymatic, or electrochemical means (Shukun and Hanqing 1986, Geletii et al. 1989, Ganley et al. 2001, Inbaraj et al. 2003). Radical intermediates are also involved in many Mn oxide-mediated oxidation systems (e.g., Stone 1987, Laha and Luthy 1990, Zhang and Huang 2003). For example, oxidation of triclosan by Mn oxides was carefully elucidated by Zhang and Huang (2003), where it was found that phenoxy radical intermediates were critical in forming the subsequent oxidation products through coupling, further oxidation and breakdown of the radicals.

It has been reported that substantial oxygen exchange occurs between hydroxyl groups in water and the oxygen anions on the α-Fe_2O_3 surface; and the mechanism for this oxygen exchange likely involves the interchange of terminal and bridging OH groups on the surface with hydroxyl groups in water (Henderson et al. 1998). A similar

exchange is expected in MnO_2/water mixtures. In oxidation experiments conducted in $H_2{}^{18}O$, we would expect Mn oxide surfaces being covered by $-{}^{18}OH$ groups via the above oxygen exchange processes. Since surface reaction is involved in the oxidation of *N*-oxides by MnO_2, the observed ^{18}O isotopes in the oxidation products of QNO most likely come from the surface-bound $-{}^{18}OH$ groups.

Based on the above relevant studies and the experimental results, an oxidation scheme of QNO by Mn oxide is proposed in Figure 5-8. In analogy to triclosan and other substituted phenols, QNO could be viewed as a phenoxy anion which, after forming a precursor complex with the oxide surface, would lose an electron to Mn oxide generating a *N*-oxide radical. *N*-oxide radicals are most likely centered at the α-C rather than at the O atom, due to the stronger electronegativity of O than C. Similar to phenoxy radicals, *N*-oxide radicals could undergo further oxidation leading to the generation of the 2-hydroxyquinoline major product and the intermediate m/z 305 product (an overall 2-electron transfer). The m/z 305 product may degrade further to eventually yield 2-hydroxyquinoline. Radical coupling leading to the production of dimeric products was observed to be the dominant pathway in the oxidation of triclosan by Mn oxides (Zhang and Huang 2003). However, no appreciable amount of dimeric products could be detected in the current study. There are two possible reasons for this result. First, QNO and hence the corresponding QNO radicals do not adsorb strongly to the oxide surfaces. The low radical density at the surfaces would make it unlikely for radicals to couple with each other. Once radicals are released into the bulk solution, they are highly unstable under the mildly acidic experimental conditions (Kung and McBride 1988), and thus could not survive long enough to undergo any coupling reactions.

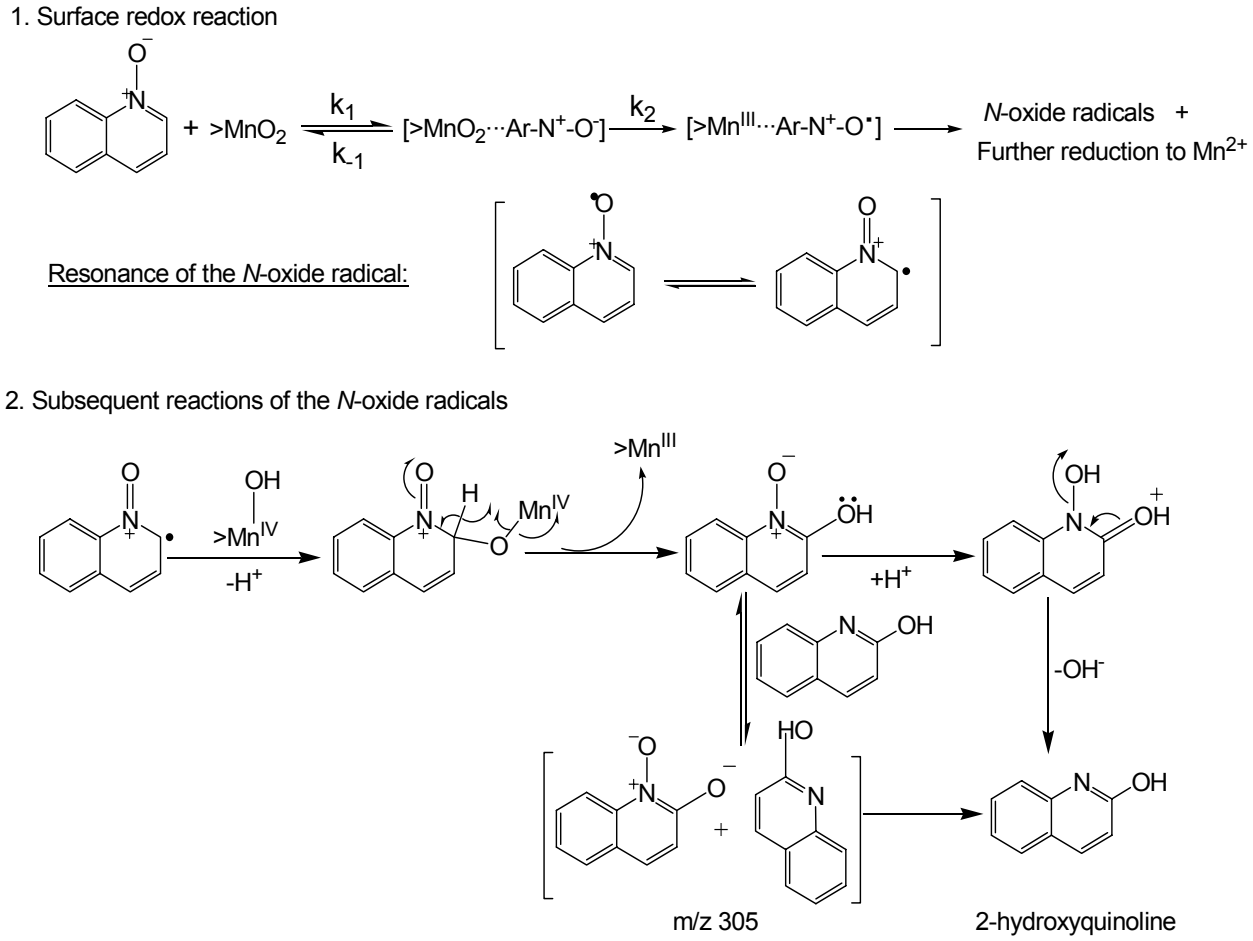

Figure 5-8. The reaction scheme of QNO.

Second, the positive charge on the N atom of QNO radicals may lead to the formed dimeric products very unstable due to the accumulation of double positive charges.

Although only a small amount of QXO was synthesized and purified for the kinetic study and thus was not included in the isotope investigation, the oxidation mechanism of QXO is expected to resemble that of QNO. Other *N*-oxides would also follow the above reaction scheme in oxidation by Mn dioxide. If two *N*-oxide groups are both reactive as in the case of QDX, other reaction pathways may also play a role, likely due to the interactions between the two *N*-oxide groups through the resonance structure within the heterocyclic ring (Katritzky and Lagowski 1971). As shown in Figure 5-8, the α-H is critical in the further oxidation of *N*-oxide radicals, in which it hops to the neighboring $O^{\bullet}$ on MnO_2 (Chauhan et al. 1999) followed by the leaving of Mn^{III} ions. The above mechanism very well explains the inertness of ODX with both *N*-oxide neighboring α-positions occupied by substituents other than H. The inertness of 2-hydroxyquinoline and quinoxaline-2,3-diol products toward oxidation by MnO_2 may appear to be somewhat surprising, based on the knowledge of fast oxidation of some phenols and catechol by Mn oxides (Stone 1987, McBride 1987, Liu and Huang 2001, Zhang and Huang 2003). The strong electron-withdrawing effect of the heterocyclic nitrogen atom in the pyridine ring was demonstrated previously to be similar to that of a nitro group (Iqbal et al. 1997), and it is known that electron-withdrawing substituents retard the oxidation of phenols by Mn oxides (e.g., Stone 1987, Zhang and Huang 2003). Therefore the heterocyclic nitrogen atoms present in 2-hydroxyquinoline and quinoxaline-2,3-diol likely resulted in their very low reactivity toward oxidation by Mn oxides. Our study also shows that only 2-hydroxyquinoline, rather than 4-

hydroxyquinoline, is formed from the oxidation of QNO by MnO_2. This result suggests that QNO likely interacts with the oxide surface via its *N*-oxide group, rendering the attack at the *ortho*-position of the radical intermediate much more likely at the oxide surfaces.

Hydrazines (-NH-NH-) and hydrazides (-CO-NH-NH-) have been oxidized to azo compounds (-N=N-) by several oxidizing agents, including MnO_2 (Bhatnagar and George 1968, Haksar et al. 1979, Smith and March 2001), silver (I) oxide (Iqbal et al. 1997), cobalt salts (Jacobs 1977), phenylseleninic acid (Bath et al. 2003), and enzymes (Johnsson and Schultz 1994). The formed azo compounds would lose N_2 to generate radicals. Ketone hydrazones (>C=N-NH_2) were also documented to undergo similar oxidation resulting in diazo (>C=N^+=N^-) intermediate (Nishinaga et al. 1986, Smith and March 2001). Particular to our interest is the study on the oxidation of phenylhydrazone ($(Ph)_2$C=N-NH-Ph) with active Mn dioxide in benzene solvent (Bhatnagar and George 1967). In that study, a pseudo allylic radical (-Ċ-N=N-) was generated after losing one electron to Mn oxide. This radical then combined with a –OH group from the oxide skeleton, lost another electron at the O atom, finally lost N_2 resulting in the generation of the corresponding ketone and biphenyl.

Based on the experimental results and the discussion to this point, a reaction scheme of CDX by Mn oxide is proposed in Figure 5-9. In light of the comparable reaction rates between CDX and QXO, and the very slow reaction of desoxy-CDX, the oxidation of the *N*-oxide group of CDX should be much faster than any reactions on the side chain. Thus compound I is postulated to be an intermediate, in analogy to the oxidation of QNO and QDX. Any further reactions would proceed from I. The oxidation

on the side chain would be mainly at the hydrazone substituent (-CH=N-NH-) in its unprotonated form (Hongekar and Patil 1998). By analogy to the oxidation of phenylhydrazone with Mn dioxide (Bhatnagar and George 1967), Mn oxide produces the pseudo allylic radical II, with the C-centered resonance structure being dominant due to the lower electronegativity of C than that of N. The radical II would then abstract a hydroxyl group from the oxide surface resulting in the observed m/z 279 intermediate. The m/z 279 intermediate is not stable in the presence of Mn oxide and undergoes further oxidation to generate N_2 and other unknown products (Table 5-2d).

Unfortunately the compound I intermediate could not be detected by the electrospray LC/MS analyses. In fact, the inability to detect this intermediate is not expected based on the fact that the structurally similar parent CDX exhibits a strong response in electrospray LC/MS. Some possible reasons for the inability to detect the compound I intermediate are offered in the following: (1) the overall electronic effect of the side chain is electron-donating, which could increase the stability of the formed *N*-oxide radicals as shown in Figure 5-8. Instead of undergoing further oxidation to compound I, the more stabilized radicals may undergo radical coupling to form dimeric products; (2) the electron-donating effect of the side chain could also lead to relatively fast oxidation at the formed 2-OH substituent (in a manner similar to the oxidation of substituented phenols by MnO_2), which keeps I at a trace level; and (3) the hydrazone side chain in CDX could be more reactive than the side chain in desoxy-CDX owing to the strong electron-withdrawing effect of the two heterocyclic quinoxaline nitrogen atoms in desoxy-CDX (Iqbal et al. 1997). In CDX the electron-withdrawing effect of the

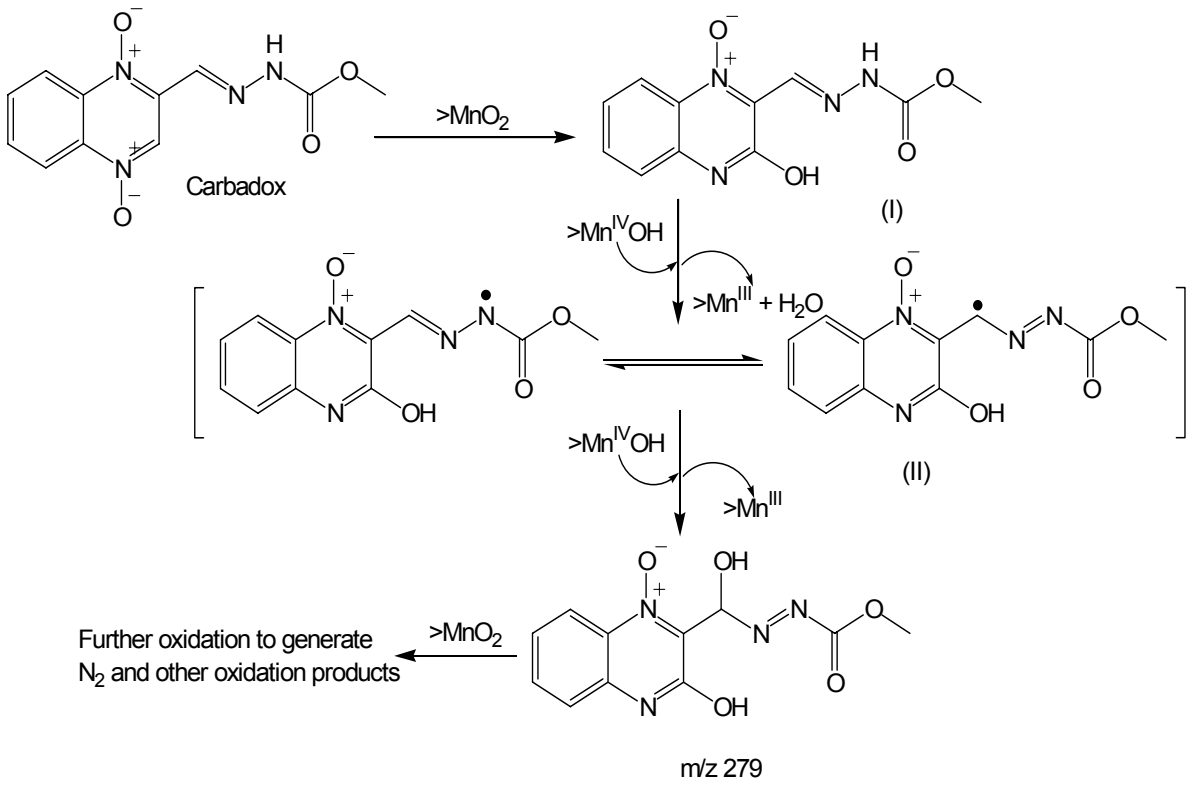

Figure 5-9. The reaction scheme of CDX.

heterocyclic nitrogen atoms is considerably reduced by the electron-donating effect of the *N*-oxide oxygen atoms. Thus compound I, once generated from CDX, may undergo further oxidation at the side chain. Further investigation on the products of CDX with different analytical approaches is needed and may shed more light on the CDX oxidation mechanism.

5.4 Conclusions

Aromatic *N*-oxides represent a structural class in many pharmaceuticals and agrochemicals, and little is known about their potential transformation at the sediment-water interfaces. Experimental results with a variety of aromatic *N*-oxides including quinoline-*N*-oxide, quinoxaline-*N,N'*-dioxide, carbadox and olaquindox revealed surprisingly high reactivity toward MnO_2 with the exception of olaquindox. In contrast, quinoxaline and desoxycarbadox showed little or much lower reactivity toward MnO_2. The above kinetic comparison among the *N*-oxides and their non-*N*-oxide analogs confirms that the *N*-oxide moiety is the reactive site.

Complex surface kinetics were observed in the oxidation of aromatic *N*-oxides with MnO_2, a phenomenon consistent with much of the previous studies on the oxidative reactions with MnO_2. However, considerably lower adsorption of aromatic *N*-oxides to Mn oxide, in contrast to the significant adsorption of other pollutants in previous studies, was observed. The initial reaction rate constant of carbadox increased as pH decreased, likely due to the higher reduction potential of Mn oxides and the generation of a greater number of surface species that favored the interactions with carbadox under lower pH

values. The apparent reaction orders with respect to carbadox, MnO_2, and H^+ were determined to be 0.56, 0.54 and 0.16, respectively.

The oxidation of aromatic *N*-oxides by MnO_2 is likely to follow the general surface reaction mechanism as do many other organic contaminants. In summary, the *N*-oxide is adsorbed to the oxide surface, forming a precursor complex. Electrons are transferred within the precursor complex, followed by the release of organic oxidation products and Mn^{2+}. The precursor complex formation and electron transfer are likely rate-limiting.

2-Hydroxyquinoline and quinoxaline-2,3-diol were determined to be the dominant stable end-products in the oxidation of quinoline-*N*-oxide and quindoxin (i.e., quinoxaline-*N,N'*-dioxide) by MnO_2, respectively. Experiments of the ^{18}O isotope effect indicated that the 2-hydroxyl substituent in the products come from $-^{18}OH$ groups associated with MnO_2 or the bulk $H_2{}^{18}O$. Other unknown products were also generated in the case of quindoxin, yielding a poorer mass balance between the detectable products and the parent compound. The more complex reaction of *N,N'*-dioxides may be due to the interactions between the two *N*-oxide groups through the resonance structure within the heterocyclic ring. Overall, the investigation results indicate that the *N*-oxide oxidation by MnO_2 likely generates a *N*-oxide radical intermediate, followed by the loss of the oxygen atom from the *N*-oxide moiety and the formation of a hydroxyl group at the α-C atom adjacent to the *N*-oxide moiety. Hence, the reactivity of aromatic *N*-oxides is highly dependent on the presence of neighboring proton(s) (α-H). A complicated pattern of oxidation products was observed with carbadox, likely due to both fast oxidation at one of its *N*-oxide groups (the one that has an neighboring α-H) and a relatively slow

reaction at its hydrazide side chain. The inactivity of olaquindox toward MnO_2 is also well explained by the proposed reaction scheme, in which both α-H atoms adjacent to the *N*-oxide groups of olaquindox were replaced with alkyl substituents thus blocking the possibility of the oxidation reaction. This investigation strongly indicates that under appropriate conditions, Mn oxide-facilitated oxidation will likely play an important role in the abiotic degradation of aromatic *N*-oxides at the mineral-water interfaces.

5.5 Environmental Significance

To the authors' knowledge, this is the first study reporting the high reactivity of organic *N*-oxides toward oxidation by Mn oxides. Results of this study offer a new degradation pathway for this group of compounds in relevant natural systems, as well as in potential industrial and chemical applications. The reactive sites, compound reactivity and reaction pathways have been carefully assessed based on the investigation with a suite of structurally-related compounds and the characterization of reaction products. The mechanistic information obtained in this study provides the basis for predicting the reactivity and transformation of other organic *N*-oxide compounds in the mineral-water environment. Results of this study also warrant further investigation on the potential reactions of organic *N*-oxides with other environmentally important minerals.

As far as the abiotic attenuation of organic *N*-oxides in the sediment-water interface is concerned, although the adsorption of these compounds is typically low toward pure Mn dioxide, their moderate sorption to soils and sediments with the aid of organic matter in presence may enable their interactions and thus degradation by minerals in the soil-water environment. Although the overall initial reaction rate expression in

equation 1 does not consider the complicated nature of subsequent surface reactions, and it only provides estimations under ideal reaction conditions, it could still offer a relatively good approximation of the maximum reactivity of CDX, and likely other *N*-oxides as well, because of the comparable initial reaction rates observed for all *N*-oxides, toward Mn oxides under environmental conditions. Any other degradation pathways with reaction rates higher than this prediction will dominate the degradation of *N*-oxides. Otherwise, Mn oxide-facilitated oxidation of *N*-oxides will play an important role in the overall fate and transformation of *N*-oxides in the environment.

CHAPTER 6

CONCLUSIONS

This study has provided systematic information on the transformation and product formation of antimicrobial agents with pure metal oxides. The examination of the reaction kinetics and mechanisms of Mn and Fe oxide-facilitated oxidation of three groups of antibacterial agents has yielded important insight into predicting the abiotic transformation of structurally related emerging contaminants at the soil-water interfaces in natural environments. By pinpointing the reactive moieties in the antibacterial agent structures, environmentally "greener" chemicals can be designed.

6.1 Overall Reaction Kinetics of Oxidation of Antibacterial Agents by Metal Oxides

The three groups of antibacterial agents examined in this study (i.e., phenolic triclosan and chlorophene, fluoroquinolones, and aromatic *N*-oxides) all possess functional groups (i.e., phenol, amine, and *N*-oxide, respectively) that are susceptible to oxidation by Mn and Fe oxides. Reductive dissolution of Mn and Fe oxides resulted in the generation of Mn^{2+} and Fe^{2+} ions, respectively. These interfacial reactions exhibited complex reaction kinetics.

In oxidation with MnO_2, the reaction rates generally increased linearly as pH decreased, a phenomenon that can be attributed to the effect of pH on the rate-limiting steps (i.e., precursor complex formation and electron transfer between organic reductants and Mn oxide surfaces). Decreasing pH increases the oxidation potential of MnO_2 and generates reactant species that favor their adsorptive interactions. Dissolved metal ions

(Mn^{II}, Zn^{II} and Ca^{II}) and natural organic matter decreased the reaction rate by competitively adsorbing and/or reacting with MnO_2. The initial reactions were first-order with respect to triclosan, chlorophene, FQs and MnO_2 (applicable within the employed experimental conditions), while later reactions exhibited more complicated kinetics which was consistent with the limited number of available active surface sites. The apparent reaction orders of H^+ were determined to be 0.46, 0.50, and 0.49 in oxidation of triclosan, chlorophene, and FQs, respectively. In the oxidation of the *N*-oxide carbadox by MnO_2, lower initial reaction orders, however, were observed for carbadox, MnO_2 and H^+ (0.56, 0.54, and 0.16, respectively), likely due to the much weaker adsorption of carbadox to Mn oxide surfaces.

In the oxidation of FQs with FeOOH, the maximum oxidation rate occurred at pH around 6 and decreased with either increasing or decreasing pH values. This trend is remarkably similar to the pH dependence of adsorption, suggesting the importance of adsorption and the significance of certain reactant species (i.e., $HQ/HQ^{\pm}$ for FQs and $>FeOH_2^+$ for FeOOH) in determining the overall oxidation rate. Three apparent stages of oxidation were observed: (i) stage 1 proceeded with a fast degradation, (ii) stage 2 involved a slowed reaction which was believed to be resulted from the delayed release of Fe^{2+} ions generated during reduction of goethite, and (iii) stage 3 involved a resumed reaction rate similar to that in the stage 1. The delayed release of Fe^{2+} ions would lead to (i) accumulation of Fe^{2+} ions on the oxide surfaces that would result in spread of reduced oxidation state on the oxide surfaces and in turn lead to the cease of FQ oxidation, and (ii) Fe^{2+} occupying and obstructing a large amount of surface sites and preventing further adsorption of FQ from the bulk solution which would lead to a slowing in the FQ

oxidation. Reaction orders of ciprofloxacin and goethite were 0.69 and 0.29-0.54, respectively. A smaller reaction order (0.29) was observed for the Ald-FeOOH than that of the Syn-FeOOH (0.54), a result that is likely associated with the much lower surface area in the former oxide.

Compared to structurally related substituted phenols, amines, or aromatic *N*-oxides, triclosan and chlorophene, FQs and quinoxaline *N*,*N*'-dioxides respectively exhibited comparable or higher reactivities toward oxidation by metal oxides. The higher reactivities were likely affected by factors including electronic and steric effects of substituents and compound hydrophobicity. For example, electron-donating substituents increased the susceptibility of organic reductants toward oxidation while electron-withdrawing substituents exerted the opposite effect. The steric hindrance was probably greater for antibacterial agents than model compounds due to their larger substituents. Furthermore, the higher hydrophobicity of antimicrobes may contribute to higher adsorption to metal oxide than the related compounds, which in turn may lead to more surface precursor complex formation and thus the faster reaction rates.

6.2 Adsorption of Antibacterial Agents to Metal Oxide Surfaces

This study found that triclosan, chlorophene and FQ antibacterial agents exhibited rapid and strong adsorption toward Mn oxides and goethite (α-FeOOH). The phenolic moiety is likely the adsorption site for triclosan and chlorophene toward Mn oxides; while the piperazine ring and carboxylic acid group (especially the OH moiety) are the potential adsorption sites of FQs toward Mn and Fe oxides, respectively. Little adsorption (< 10 %) by Mn oxides was observed for aromatic *N*-oxides, probably due to

the lack of a functional group that could have a strong interaction with the hydroxylated oxide surfaces.

In the presence of MnO_2, the percentage of adsorption of triclosan, chlorophene and FQs generally increased as pH decreased. The observed adsorption trend suggests that lowering the solution pH creates a greater number of surface species (i.e., the positively charged surfaces) that favor interaction with the protonated form of antibacterial agents.

The adsorption isotherms of FQs toward two types of goethite utilized could be fitted into the Langmuir model quite well. The zwitterions of FQs ($HQ/HQ^{\pm}$) were proved to be the predominant species involved in association with the positively charged Fe oxide surfaces ($>FeOH_2^+$). Thus adsorption of FQs achieved its maximum at pH around 6 when the product of [$HQ/HQ^{\pm}$] and [$>FeOH_2^+$] was the highest, but decreased with the decreasing and increasing pH when the product was low.

6.3 Mechanisms of Oxidation of Antibacterial Agents by Metal Oxides

The oxidation of antibacterial agents by metal oxides was consistent with the general mechanism for a surface reaction involving a precursor complex formation followed by a radical generation. In summary (Figure 6-1), the redox reaction was initiated by adsorption of the target compound to the oxide surface and generating a surface complex, then continued by one electron transfer from the reductant molecule to the surface bound Mn^{IV} or Fe^{III}, yielding a radical intermediate and Mn^{III} or Fe^{II} ion with the former being further reduced to Mn^{II}. After being formed, the radical intermediates can form resonance structures or be stabilized by the neighboring aromatic ring. Organic

oxidation products and Mn^{2+} or Fe^{2+} were then released from the oxide. The released Fe^{2+} was rapidly oxidized back to Fe^{3+} by dissolved oxygen while the released Mn^{2+} stayed in the solution within the studied time frame (days to weeks). The precursor complex formation and electron transfer were likely the rate-limiting steps.

There were many possible pathways in forming the final oxidation products following the generation of the radical intermediates. For triclosan, three pathways were proposed for the fate of the phenoxy radical intermediates. Pathway I was coupling of two phenoxy radicals to yield dimeric products. Pathway II involved one-electron oxidation of the phenoxy radical by manganese oxide to form hydroquinone. Further two-electron oxidation of hydroquinone yielded the quinone analog of triclosan. Pathway III involved cleavage of the ether bond of phenoxy radical, possibly via *o*-dealkylation, to yield 2,4-dichlorophenol and other products. Overall, the experimental results suggested that triclosan oxidation by manganese oxide occurred predominantly via pathway I and to a lesser degree pathway II. Pathway III was the least important in the overall reaction. Similar pathways were present for chlorophene except that pathway III could be excluded since breaking of the benzyl linkage of chlorophene did not occur. Chlorophene also exhibited higher complexity in coupling product formation, likely due to the fact that the *p*-Cl substituent of chlorophene was susceptible to substitution by hydroxide and consequently increased the variety of product formation.

For FQs, three major pathways likely followed the generation of radical intermediates which were most likely centered on the inner N in the piperazine ring. Pathway I was also the coupling reaction of the radical intermediates to form dimers. In pathway II, the radical intermediates were further oxidized to form iminium ions which

were then subject to hydrolysis leading to generation of 1,2-diol intermediates. In the presence of excess MnO_2, the 1,2-diol intermediates were readily oxidized to yield mono-aldehyde and di-aldehyde products. In pathway III, the piperazine ring of the radical intermediate was broken upon oxidation followed by dealkylation to yield dealkylated products. Other minor reaction pathways were also possible; one of which could be a pathway leading to the generation of a *N*-oxide product. The relative contribution of each pathway to the overall reaction could not be determined due to the complicated pattern of oxidation products and inability to detect some of the products. Nevertheless, pathway II (hydroxylation) accounts for approximately 10% (for cipro, enro and nor) to 25% (for oflox, lome, and PA) in the overall reaction. Pathway III (N-dealkylation) accounts for approximately 10% in the overall reaction for all of the FQs.

N-oxide radicals that were most likely centered at the C-atom neighboring to the *N*-oxide moiety was believed to be the reaction intermediate in oxidation of aromatic *N*-oxides by Mn oxides. For simple aromatic *N*-oxides such as quinoline-*N*-oxide, the following reactions of the radical intermediate were the loss of oxygen from the *N*-oxide moiety and the formation of a hydroxyl group at the C-atom adjacent to the *N*-oxide moiety. For aromatic *N*-oxides that posses more complicated structures including quindoxin and carbadox, other reaction pathways were also possible, including interactions among the *N*-oxide groups via resonance effect and oxidation of reactive hydrazide side chain of carbadox.

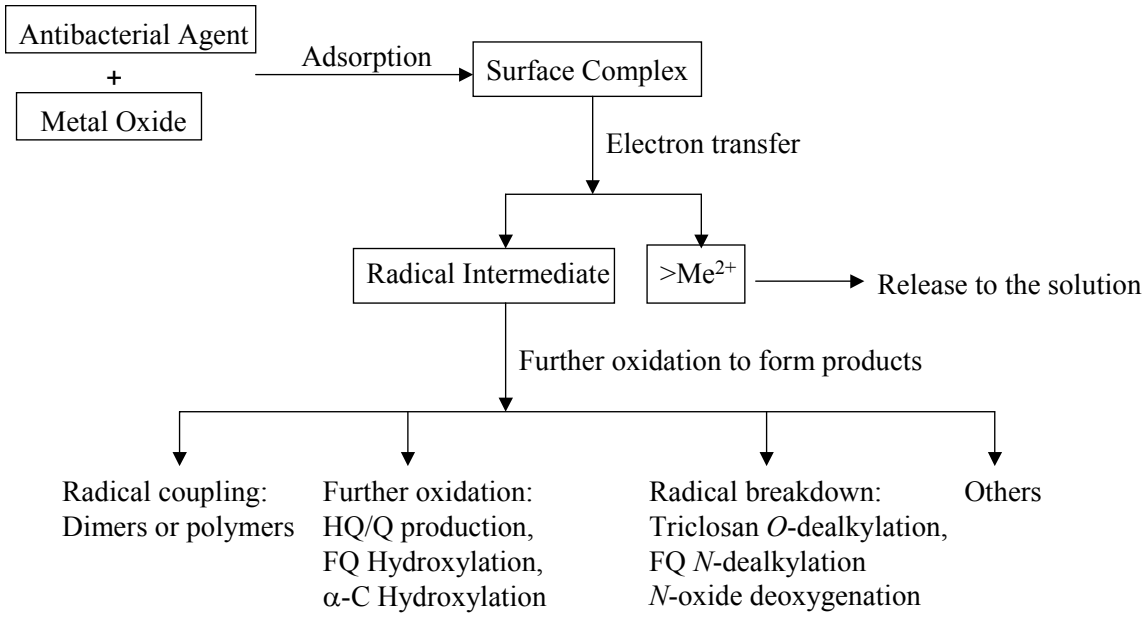

Figure 6-1. The reaction mechanism between antibacterial agents and Mn/Fe oxides is illustrated in the following simple schematic diagram.

6.4 Environmental Significance

Once released into the environment, partitioning of triclosan, chlorophene, FQs, and aromatic *N*-oxides to soils and sediments is expected due to their relatively hydrophobic nature and moderate to strong adsorption to pure metal oxides and soils documented in the current and other studies. Results of this study strongly indicate that metal oxides in soils and sediments will likely facilitate transformation of these antibacterial agents at the soil-water interfaces. Based on the kinetics developed in this study with pure metal oxides, a ballpark estimation of the upper-limit abiotic oxidation rate of these antibacterial agents in the soil-water environment can be made. Formation of heavier and more hydrophobic products via dimerization and polymerization will decrease the mobility of these antibacterial agents and potentially decrease the biological effects when the larger products become less available for aquatic organisms. Toxicities of much of the oxidation products found in this study remain unknown and warrant further investigation.

6.5 Future Work

6.5.1 Extension of the Current Research

Detailed reaction kinetics and mechanisms have been concluded in this research. However, the complex nature of surface reactions prohibits a complete understanding based on the current technology. For example, the reaction kinetics beyond the initial stage should be further studied; a kinetic model including surface parameters would be useful; and the overall mass balance should be closed through detection of all possible reaction products by other advanced analytical techniques such as NMR. Moreover,

various environmental factors should be considered in order to better estimate the fate of these antibacterial agents in the real environment.

6.5.2 Other Pharmaceutical Compounds

This study examined representative antibacterial agents from the phenol, aromatic amine, and aromatic *N*-oxide families. The oxidative reactivity toward metal oxides varied significantly among these three classes of compounds. Further research on additional compounds will improve understanding and strengthen predictive capability regarding oxidation kinetics and product generation of these classes of chemicals in the aquatic environment. The phenol, amine, and *N*-oxide functional groups are also prevalent among other common pollutants such as pesticides, industrial chemicals and other pharmaceuticals. The results from this research also constitute the basis for further investigation on other structurally related contaminants for their abiotic transformation with soil minerals.

6.5.3 Other Metal Oxides

Fe and Mn oxides are widely-existing natural oxidizing catalysts. The current study has ascertained their importance in degrading antibacterial pollutants in the aquatic environment. There are many different forms of Fe and Mn oxides in soils and sediments. The reactivity of various forms of Fe and Mn oxides may differ considerably due to their differences in oxidation states, structures, active surfaces, and involvement of other trace elements. More study is needed to correlate the reactivity of Fe or Mn oxide to their properties so that a systematic estimation of the fate of organic pollutants in

contact with these oxides could be achieved. Additionally, there are other metal oxides such as Al and Si oxides that are more abundant in the nature and may facilitate transformation and adsorption of organic pollutants. The potential effects of these metal oxides on the antibacterial agents are currently unclear and should be explored.

6.5.4 Actual Soil Samples

Whole soils generally have lower reduction potential, less available surface sites, but higher organic carbon contents than pure metal oxides. Because of these properties, whole soils may be less oxidative to antibacterial agents. On the other hand, they may have a stronger adsorption capacity due to the presence of organic contents, which also complicates the association between soils and organic pollutants. Thus considerable uncertainties exist in the attempt to extrapolate the current research to the real soil-water interface. Further research on the degradation and product formation of these antibacterial agents with well characterized whole soil samples is necessary.

6.5.5 Toxicity Assessment of Oxidation Products

The potential long-term adverse health effect and proliferation of bacterial drug-resistance are the two main concerns that have demanded investigation on the fate of antibacterial agents in the aquatic environment. The toxicity and health effect of different antibacterial compounds may also be quite different. This study demonstrated that various oxidation products can be generated in the abiotic degradation of antibacterial agents by metal oxides. On the basis of these research findings, more studies on the toxicity of the end products are necessary in order to evaluate the overall environmental

toxicity of antibacterial agents and to design environmentally “greener” compounds or apply environmentally sound treatment technologies.

APPENDICES

LC/MS SPECTRA OF ANTIBACTERIAL AGENTS AND THEIR CORRESPONDING OXIDATION PRODUCTS

LC/MS is commonly used to identify compound structures. Detailed operation conditions are discussed in individual chapters. The LC/MS spectra of triclosan and its oxidation products are shown in Figure A-I.1 to A-I.12. The LC/MS spectra of chlorophene and its oxidation products are shown in Figure A-II.1 to A-II.14. The LC/MS spectra of ciprofloxacin and its oxidation products are shown in Figure A-III.1 to A-III.8. The LC/MS spectra of quinoline *N*-oxide (QNO) and its oxidation products in H_2O are shown in Figure A-IV.1 to A-IV.4. The LC/MS spectra of quinoline *N*-oxide (QNO) and its oxidation products in $H_2{}^{18}O$ are shown in Figure A-IV.5 to A-IV.7.

Figure A-I.1. LC/MS chromatograph of triclosan reaction mixture.

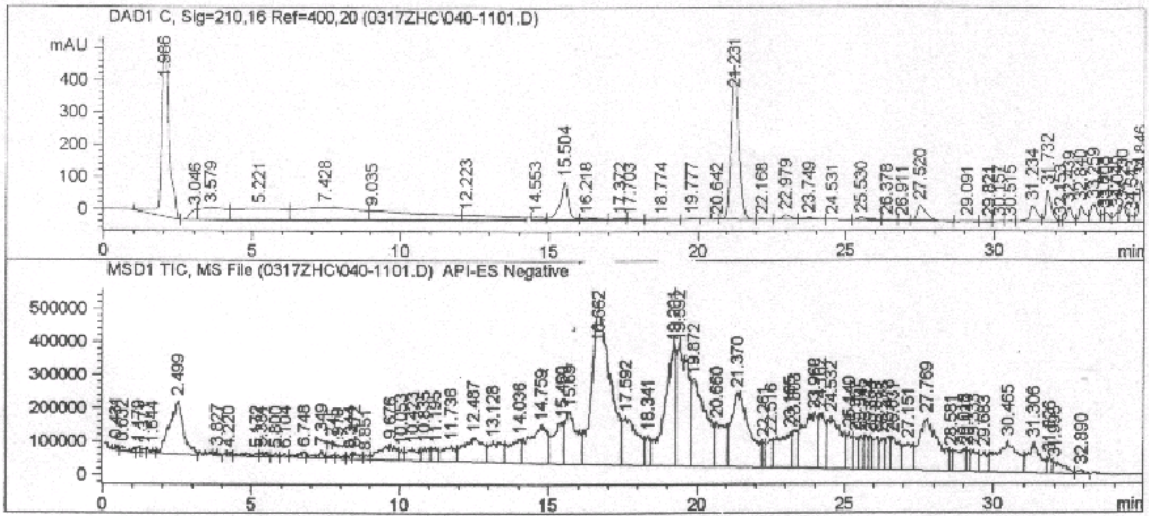

Figure A-I.2. LC/MS spectrum of the m/z 328 product of triclosan.

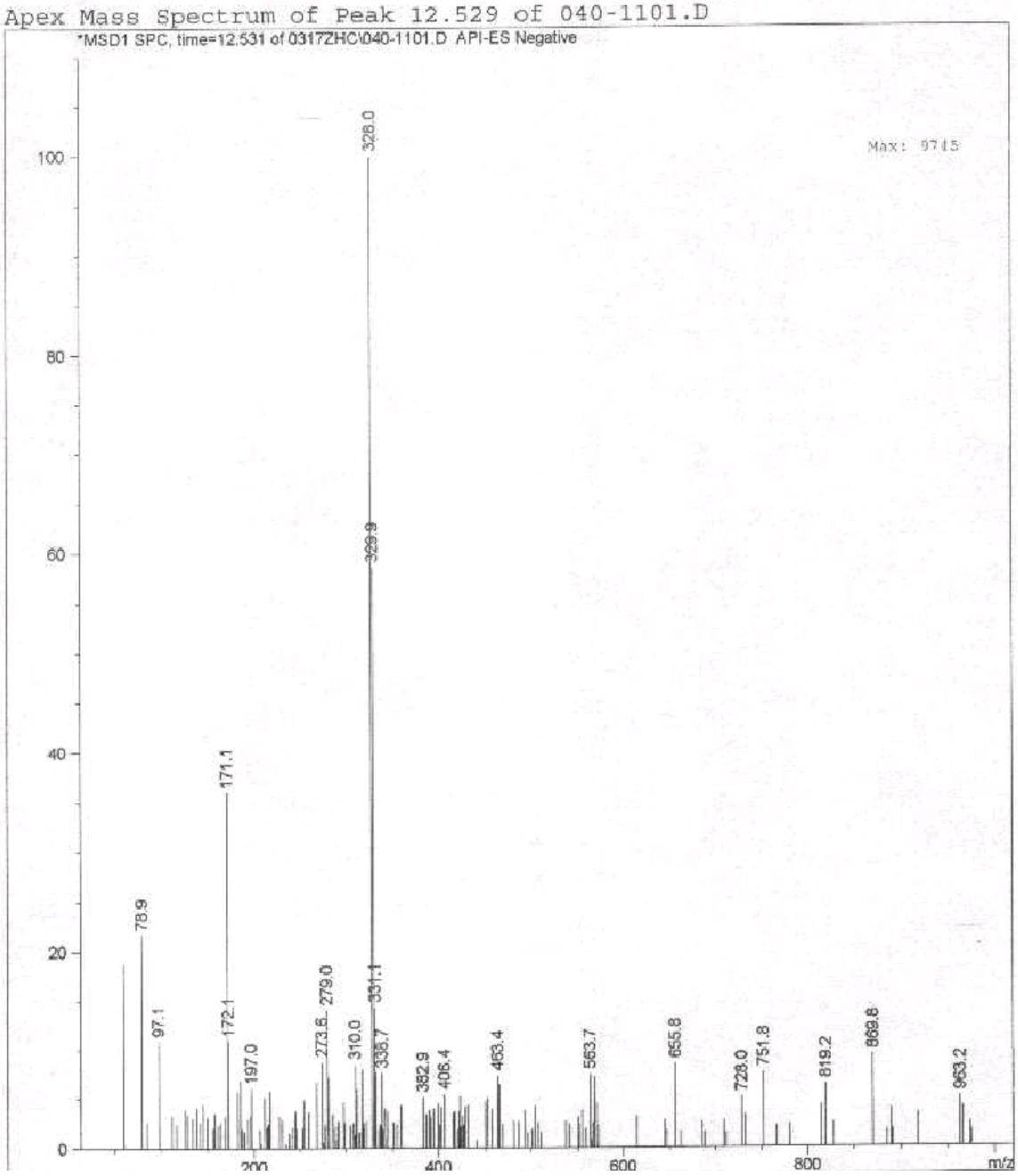

Figure A-I.3. LC/MS spectrum of the m/z 468 product of triclosan.

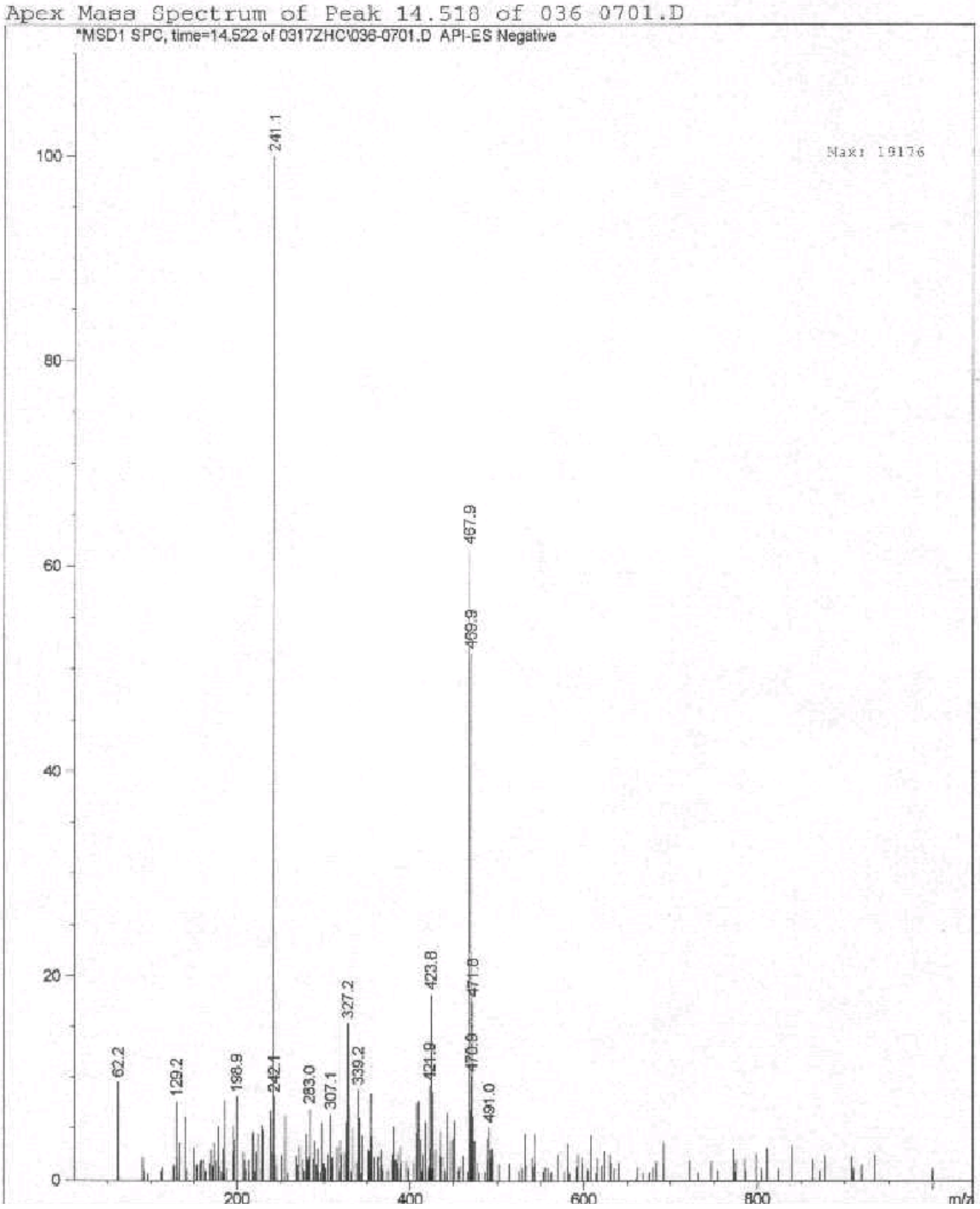

Figure A-I.4. LC/MS spectrum of 2,4-dichlorophenol (m/z 161).

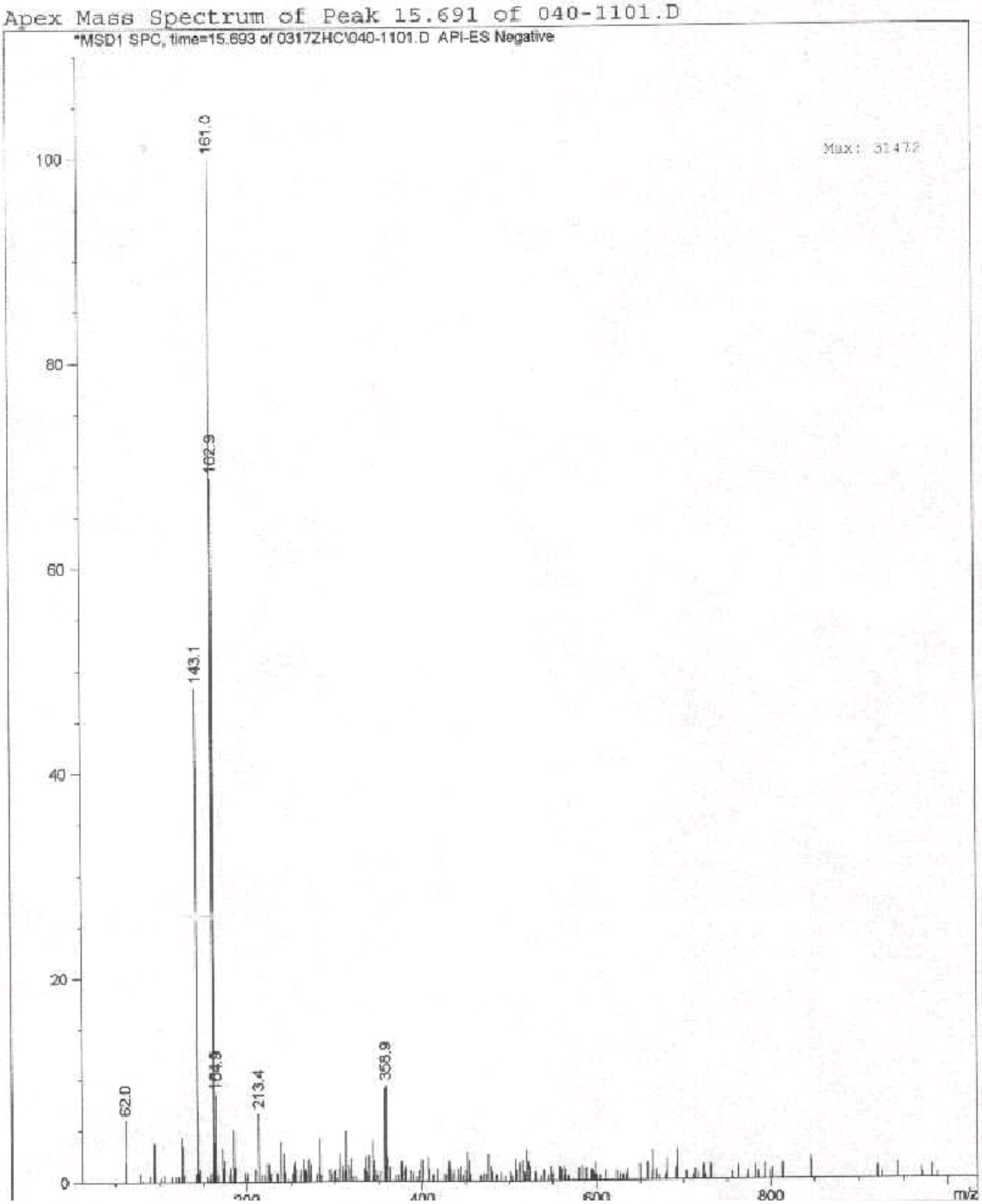

Figure A-I.5. LC/MS spectrum of the m/z 377 product of triclosan.

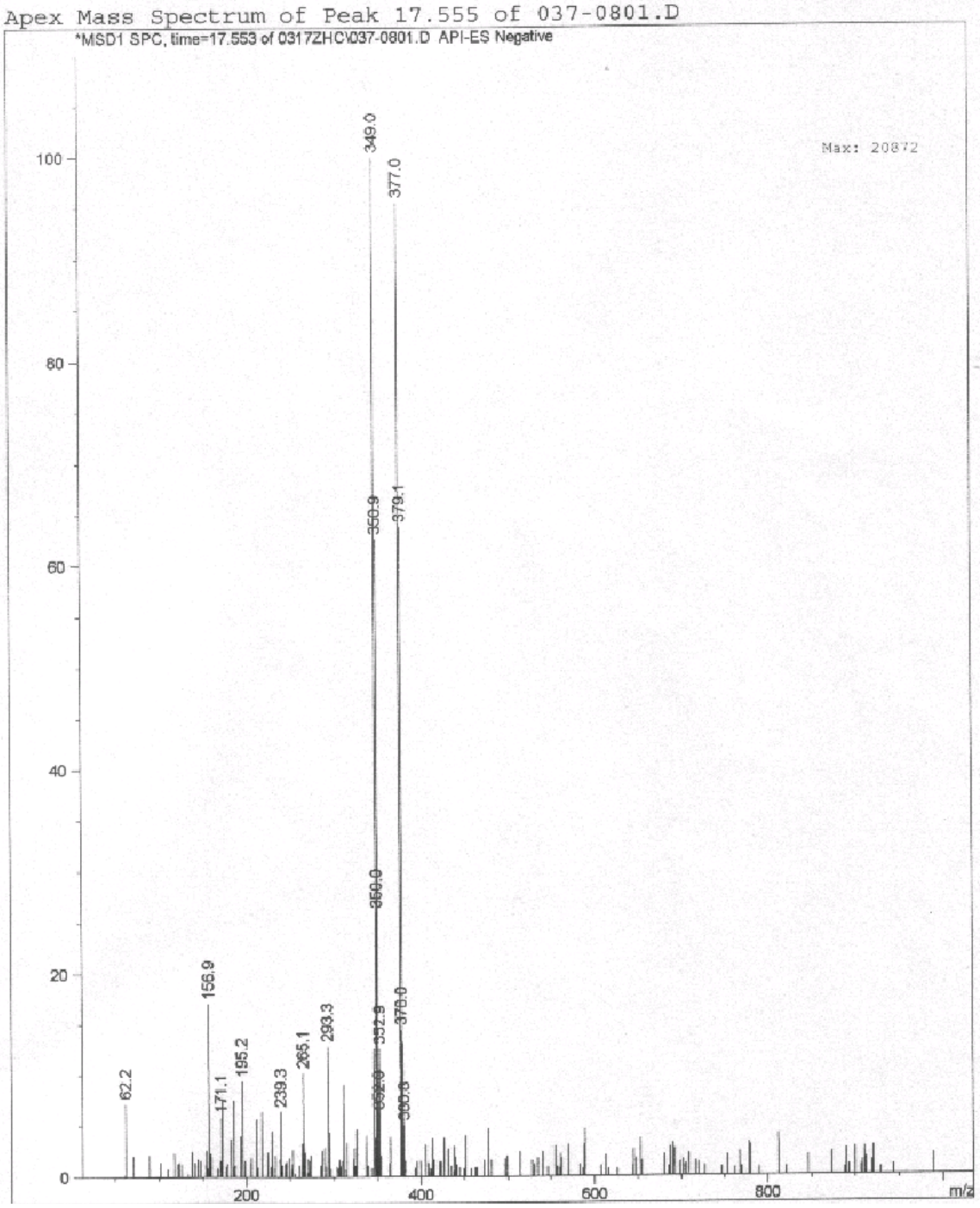

Figure A-I.6. LC/MS spectrum of the m/z 303 product (i.e., the product B) of triclosan.

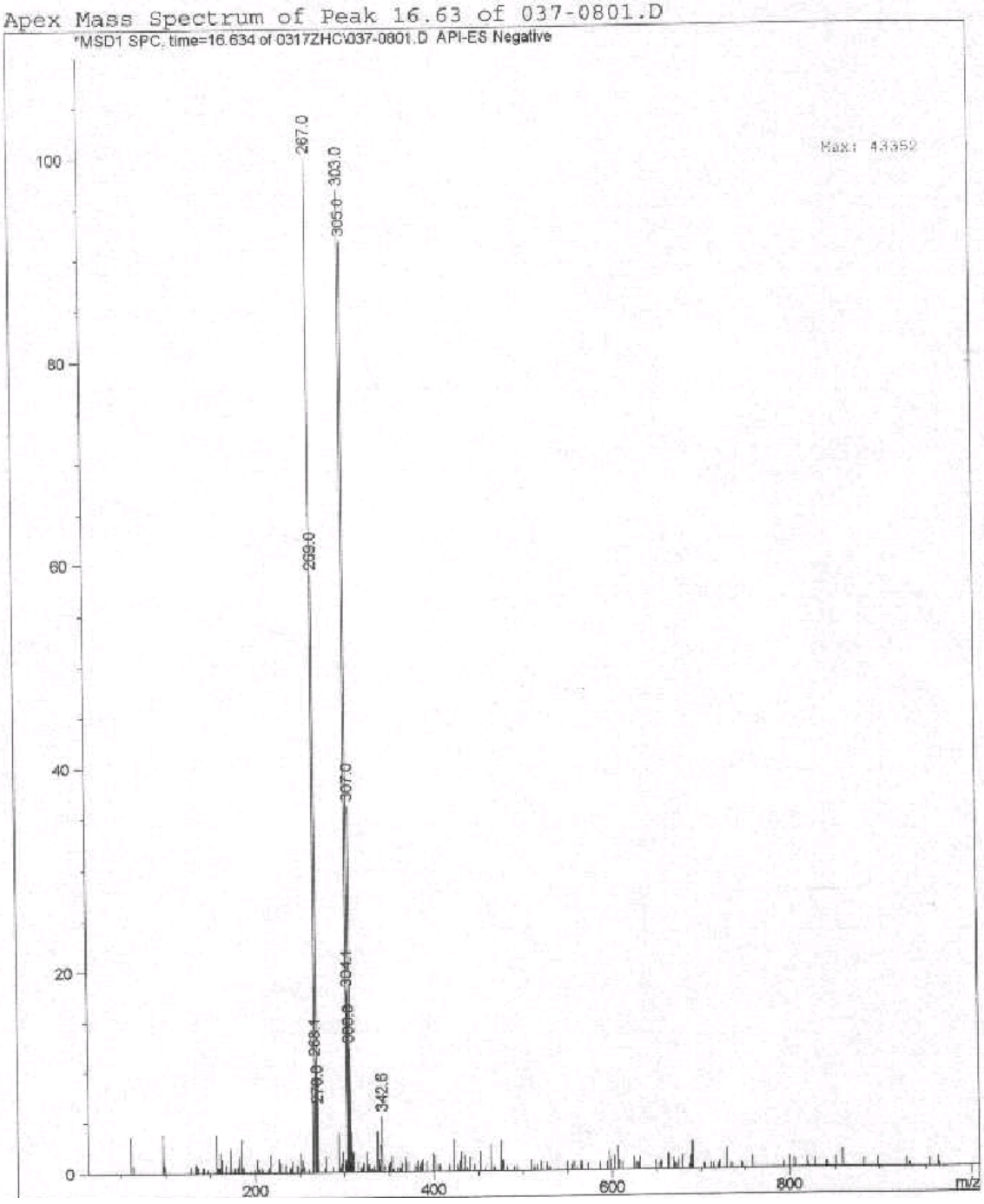

Figure A-I.7. LC/MS spectrum of the m/z 332 product of triclosan.

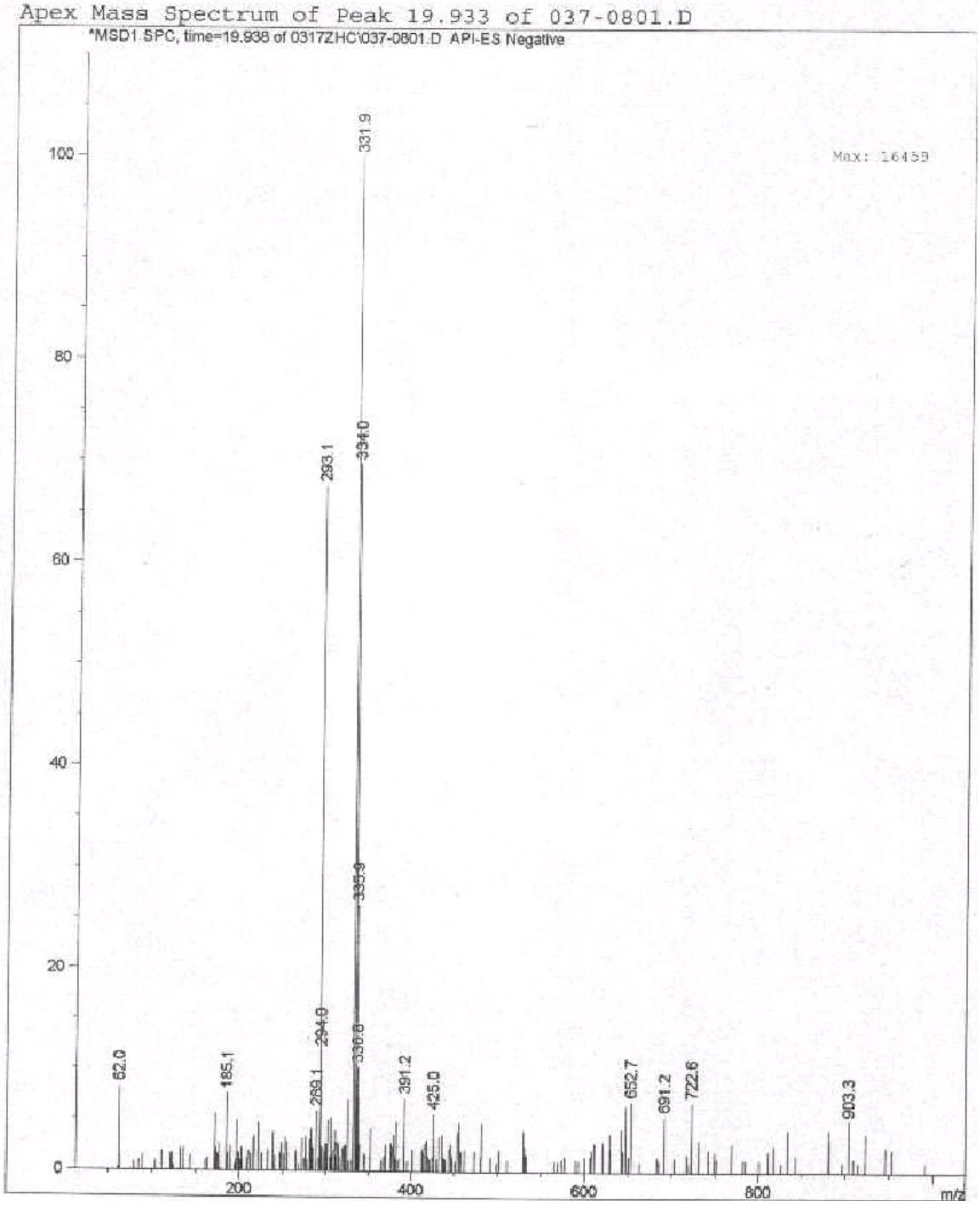

Figure A-I.8. LC/MS spectrum of triclosan.

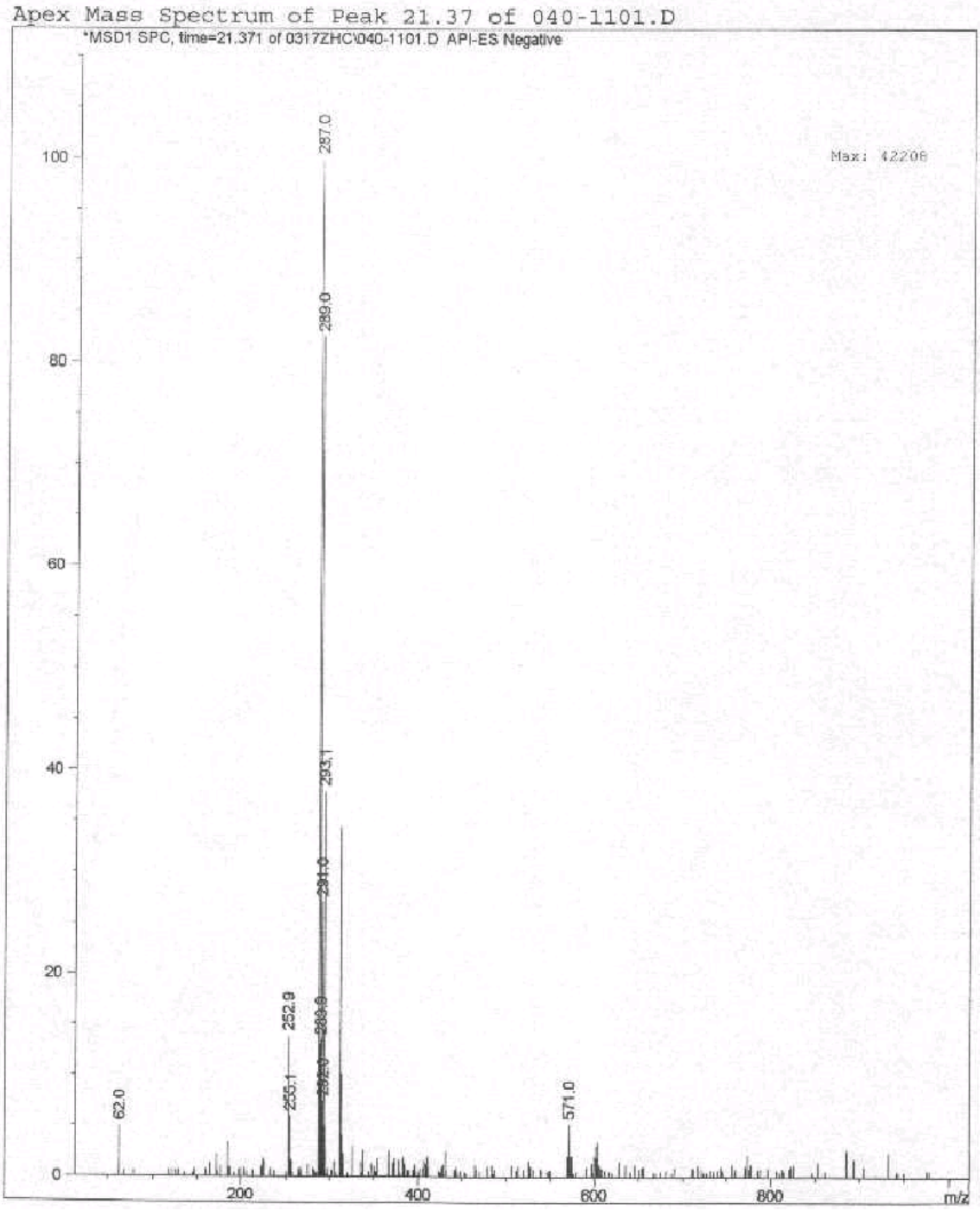

Figure A-I.9. LC/MS spectrum of the m/z 571 product of triclosan.

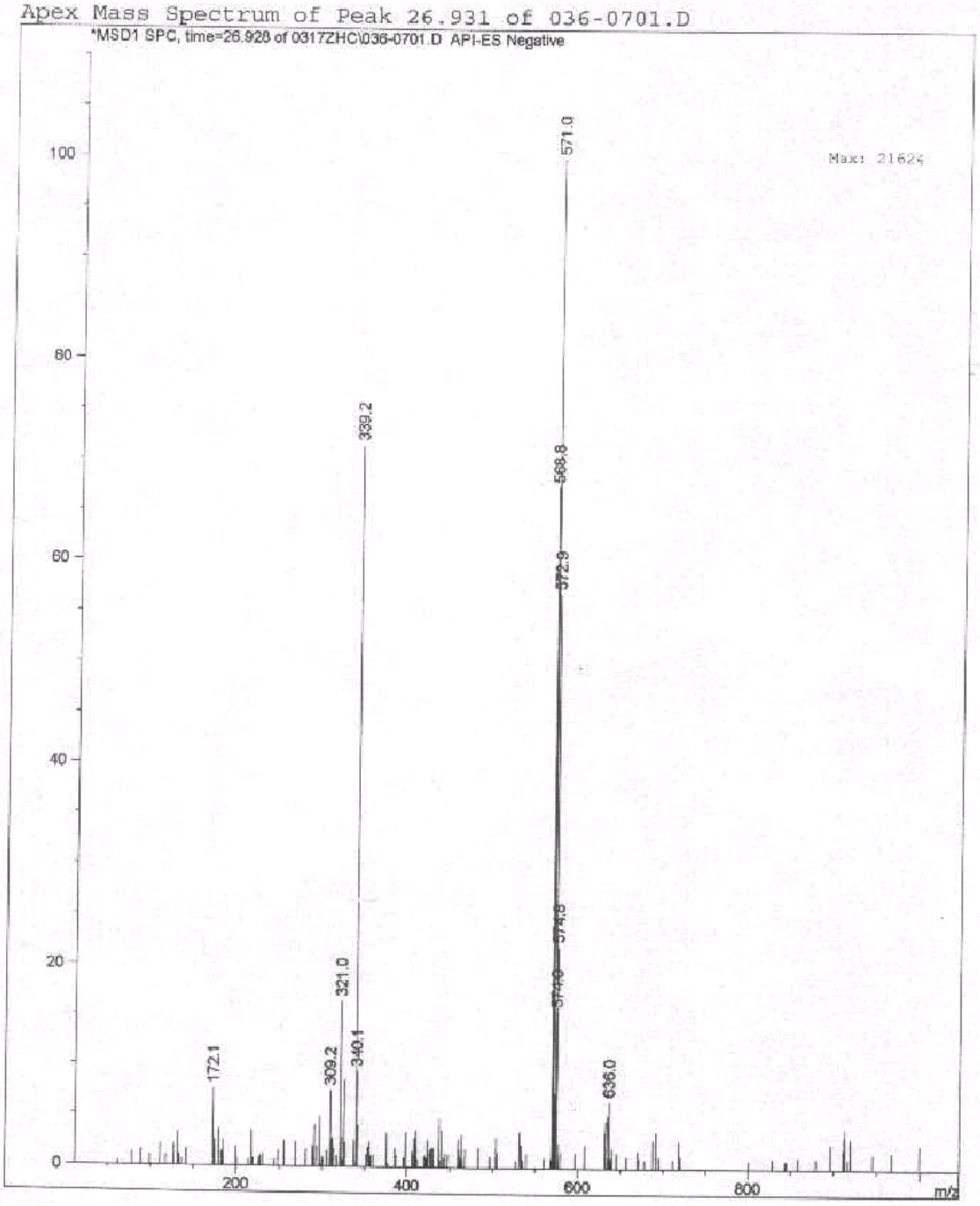

Figure A-I.10. LC/MS spectrum of the m/z 573a product of triclosan.

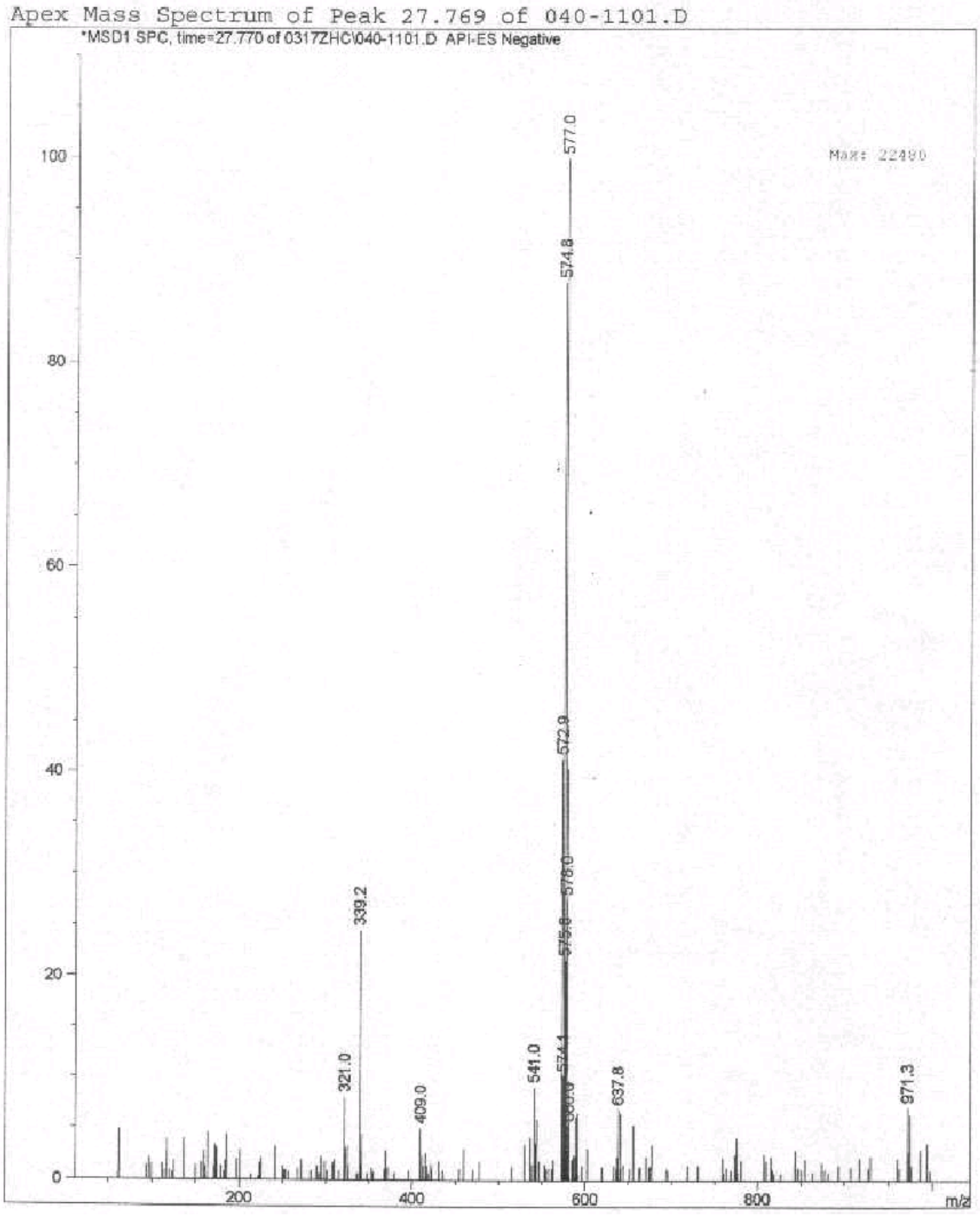

Figure A-I.11. LC/MS spectrum of the m/z 573b product of triclosan.

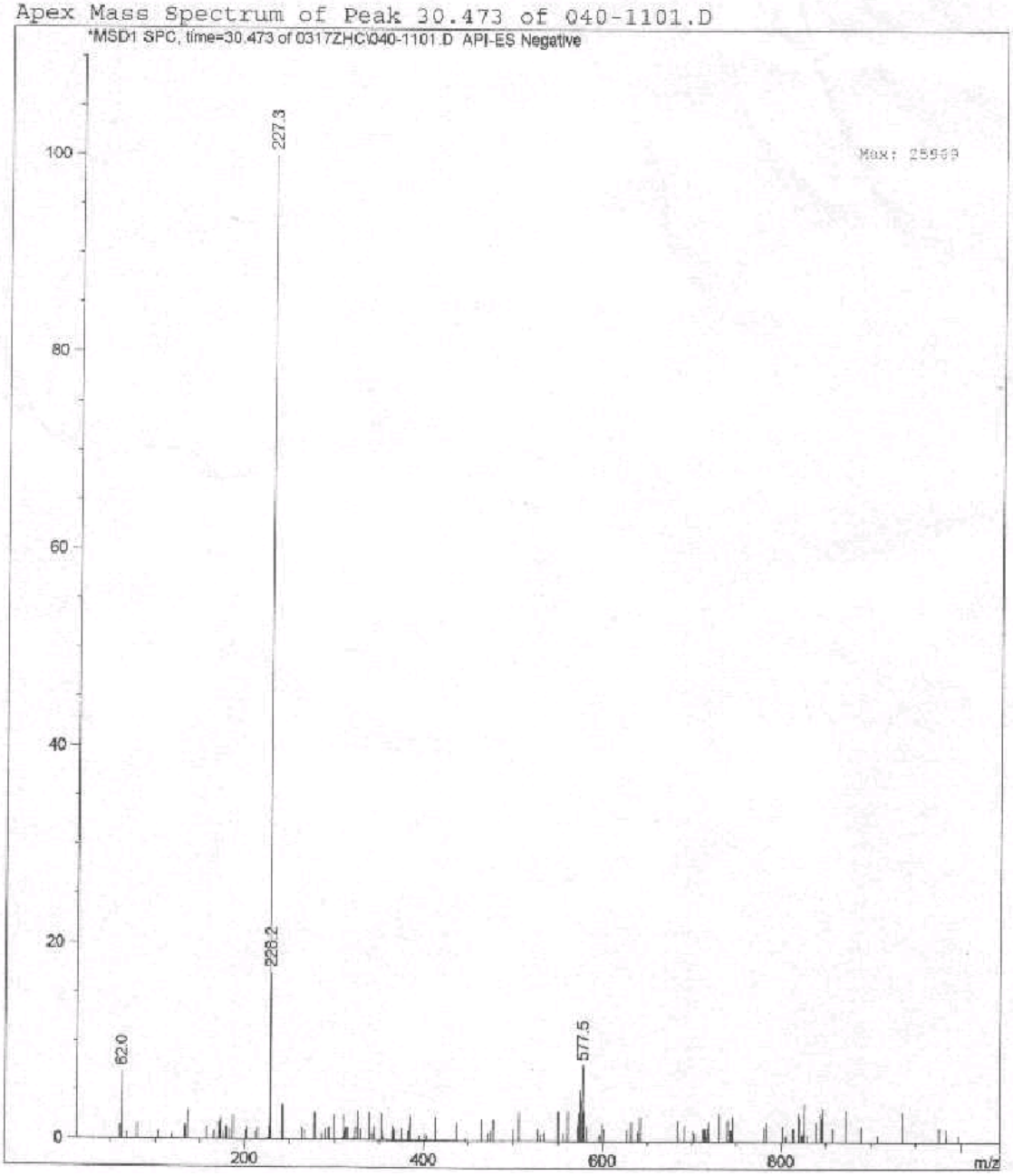

Figure A-I.12. LC/MS spectrum of the m/z 573c product of triclosan.

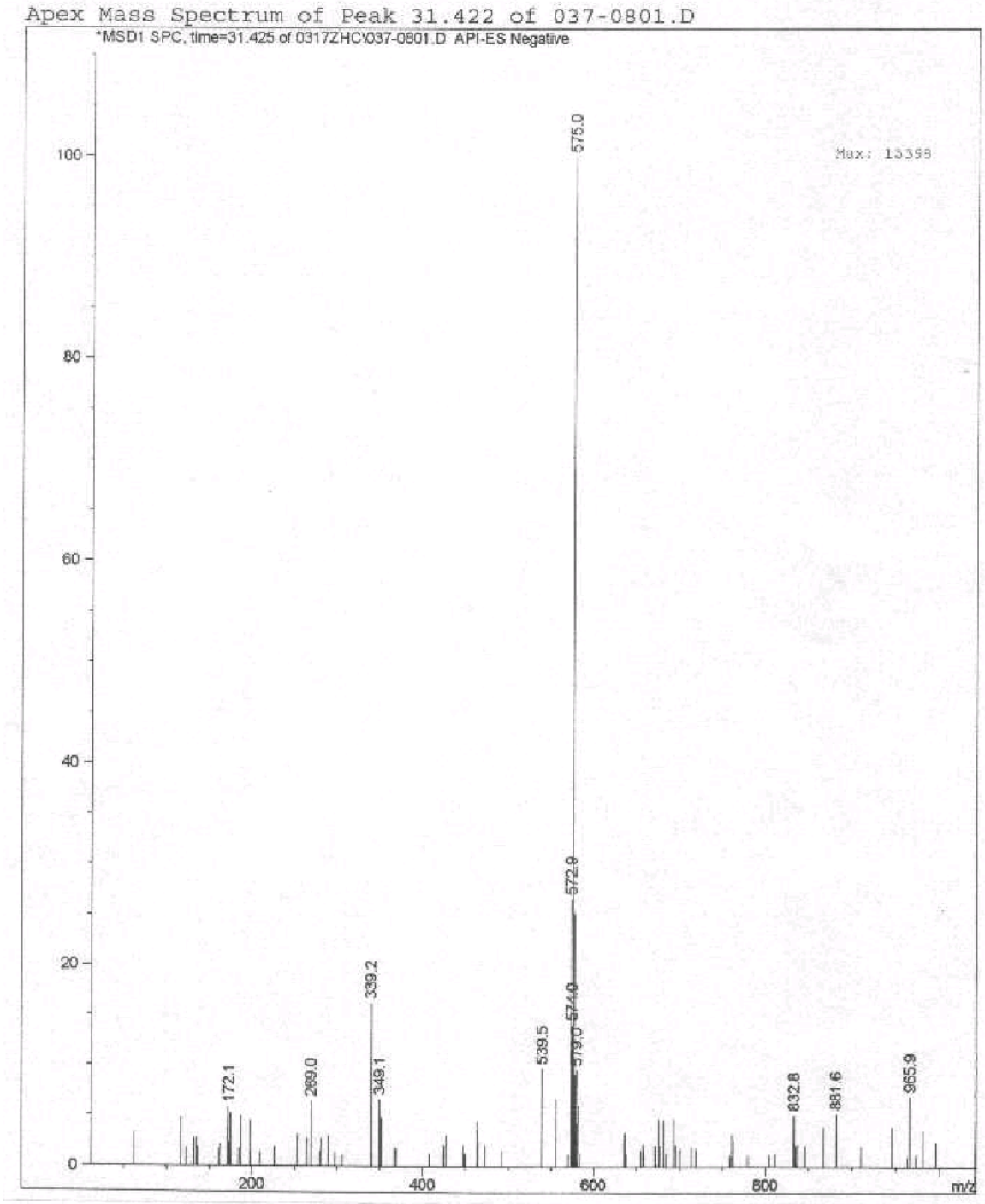

Figure A-II.1. LC/MS chromatograph of chlorophene reaction mixture.

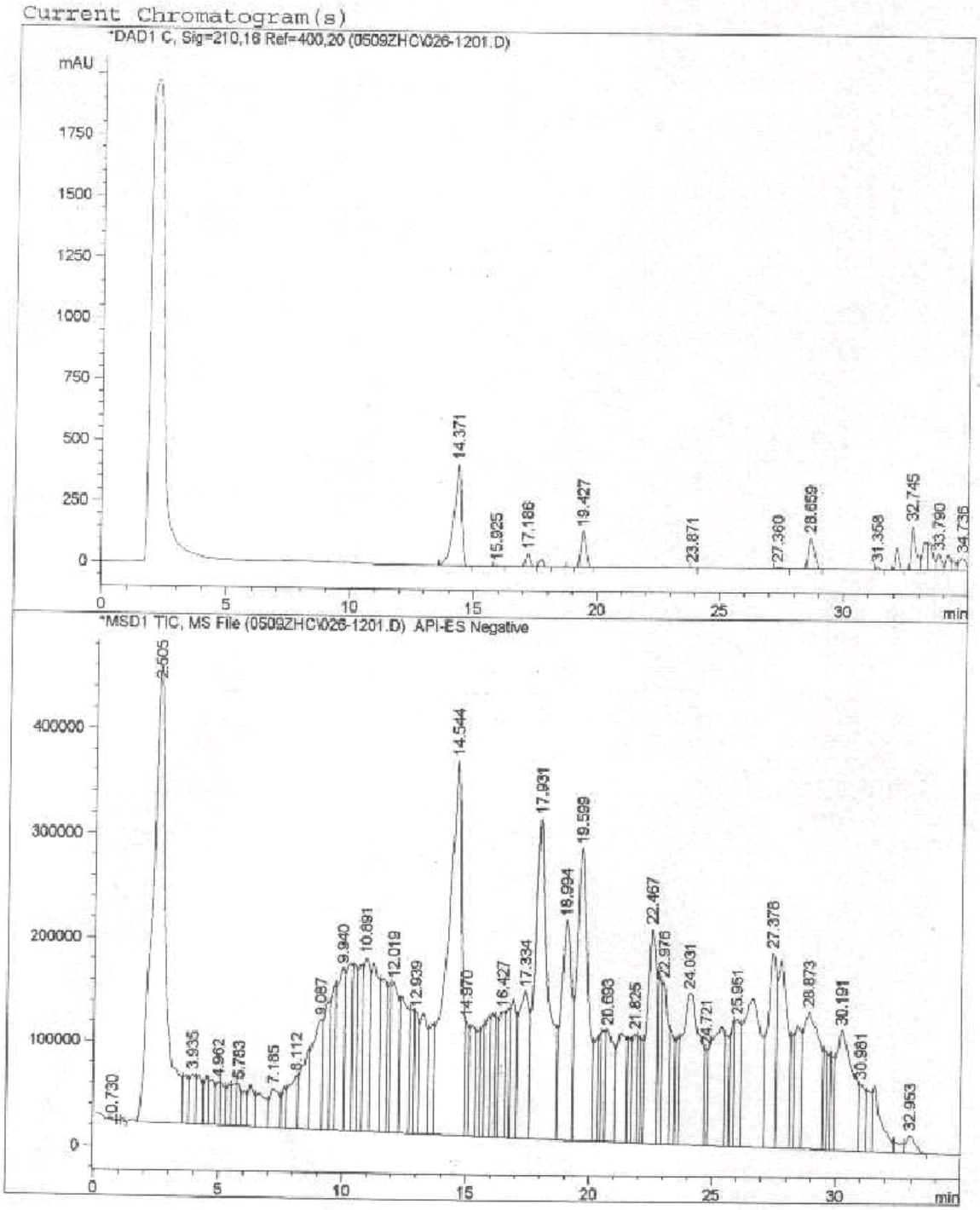

Figure A-II.2. LC/MS spectrum of the m/z 199 product (i.e., the product E) of chlorophene.

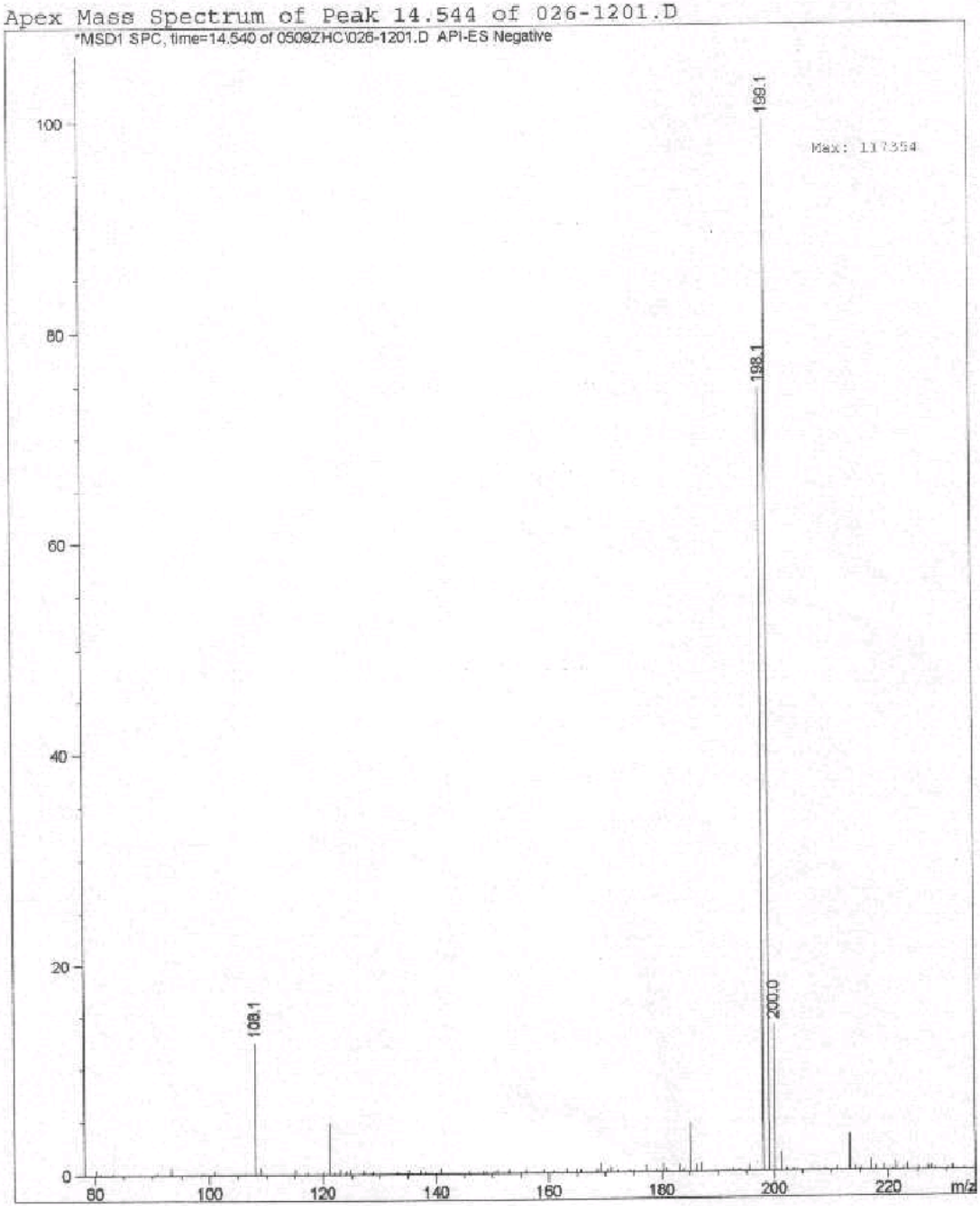

Figure A-II.3. LC/MS spectrum of the m/z 397 product of chlorophene.

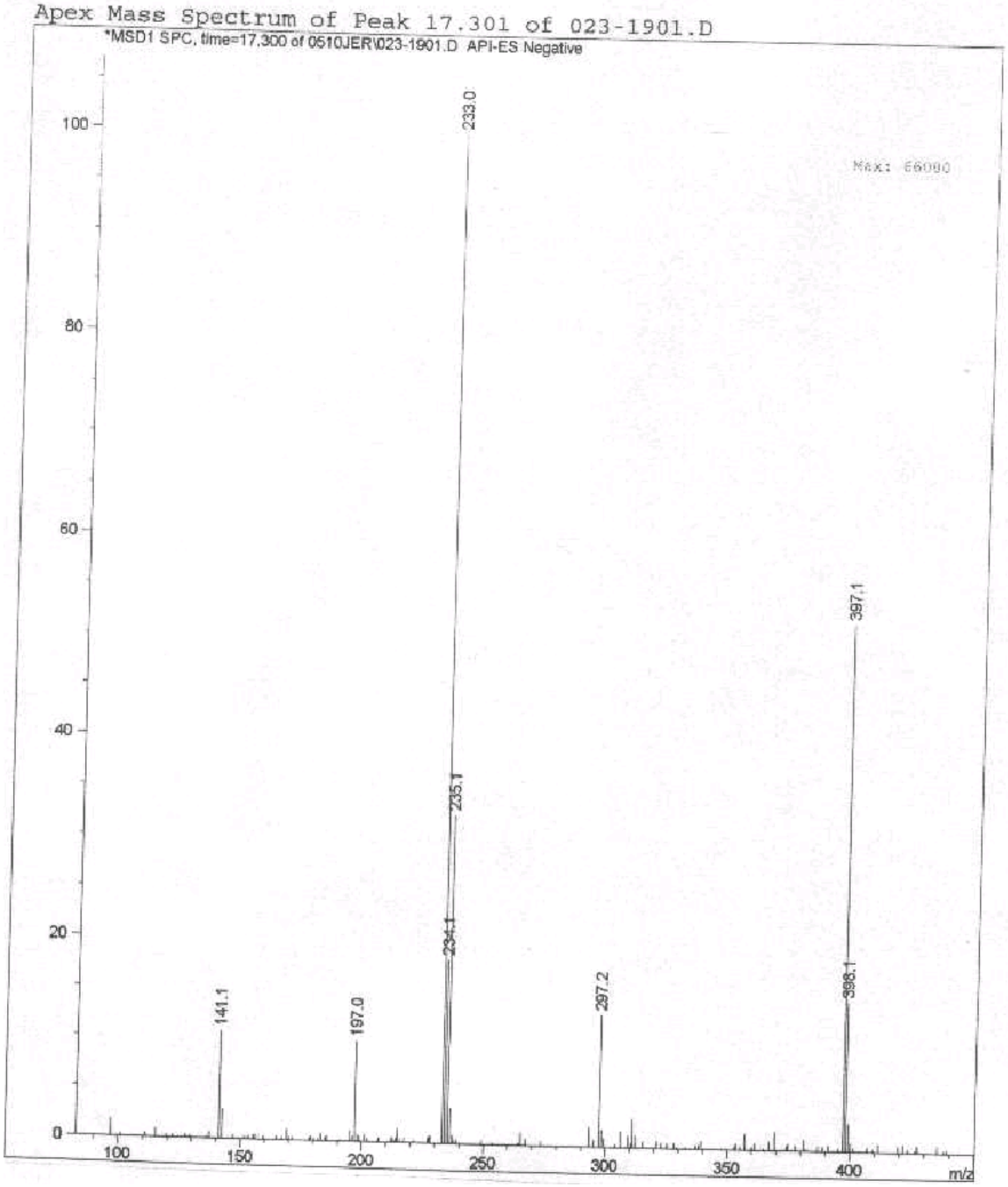

Figure A-II.4. LC/MS spectrum of the m/z 395 product of chlorophene.

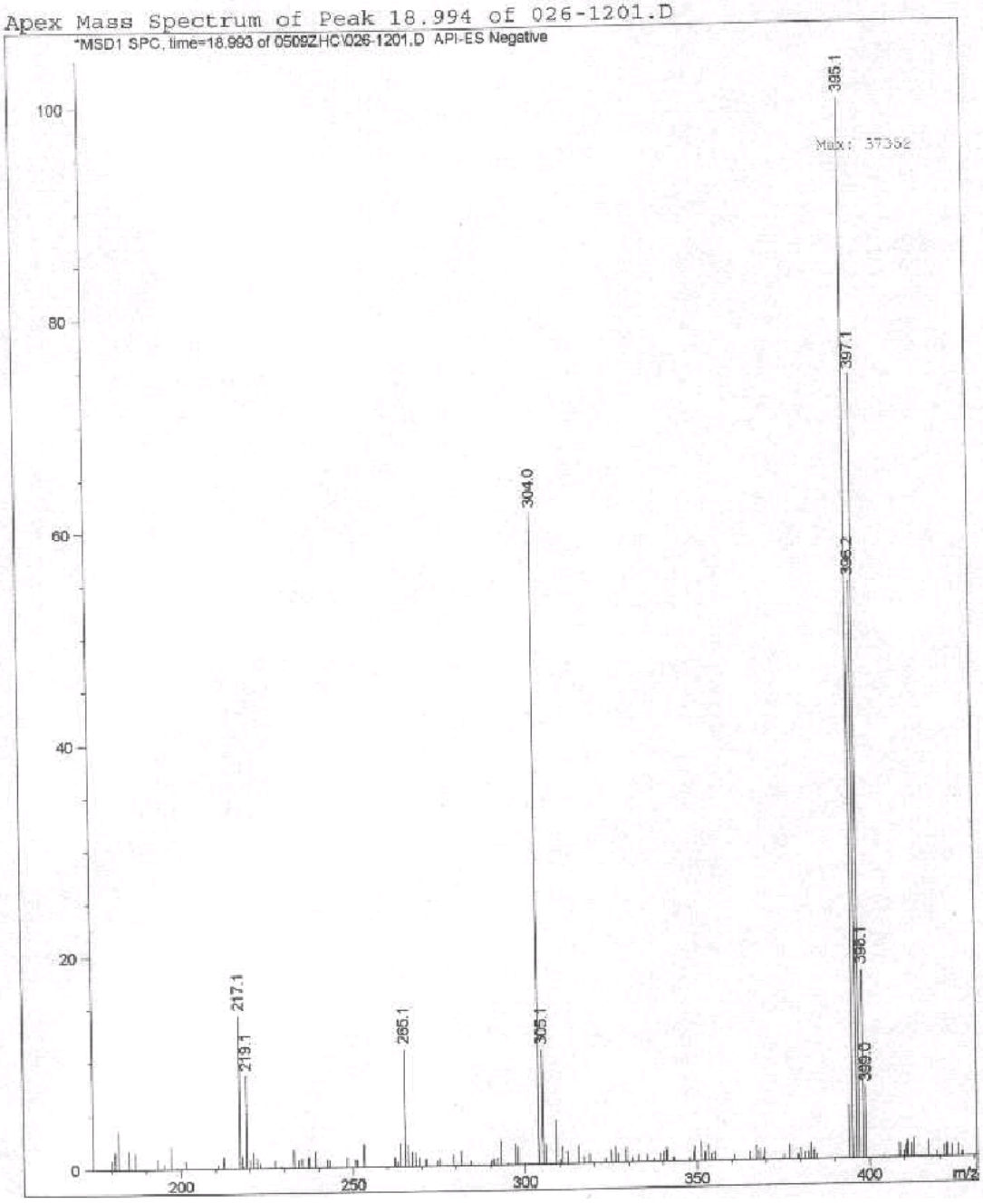

Figure A-II.5. LC/MS spectrum of chlorophene (m/z 217).

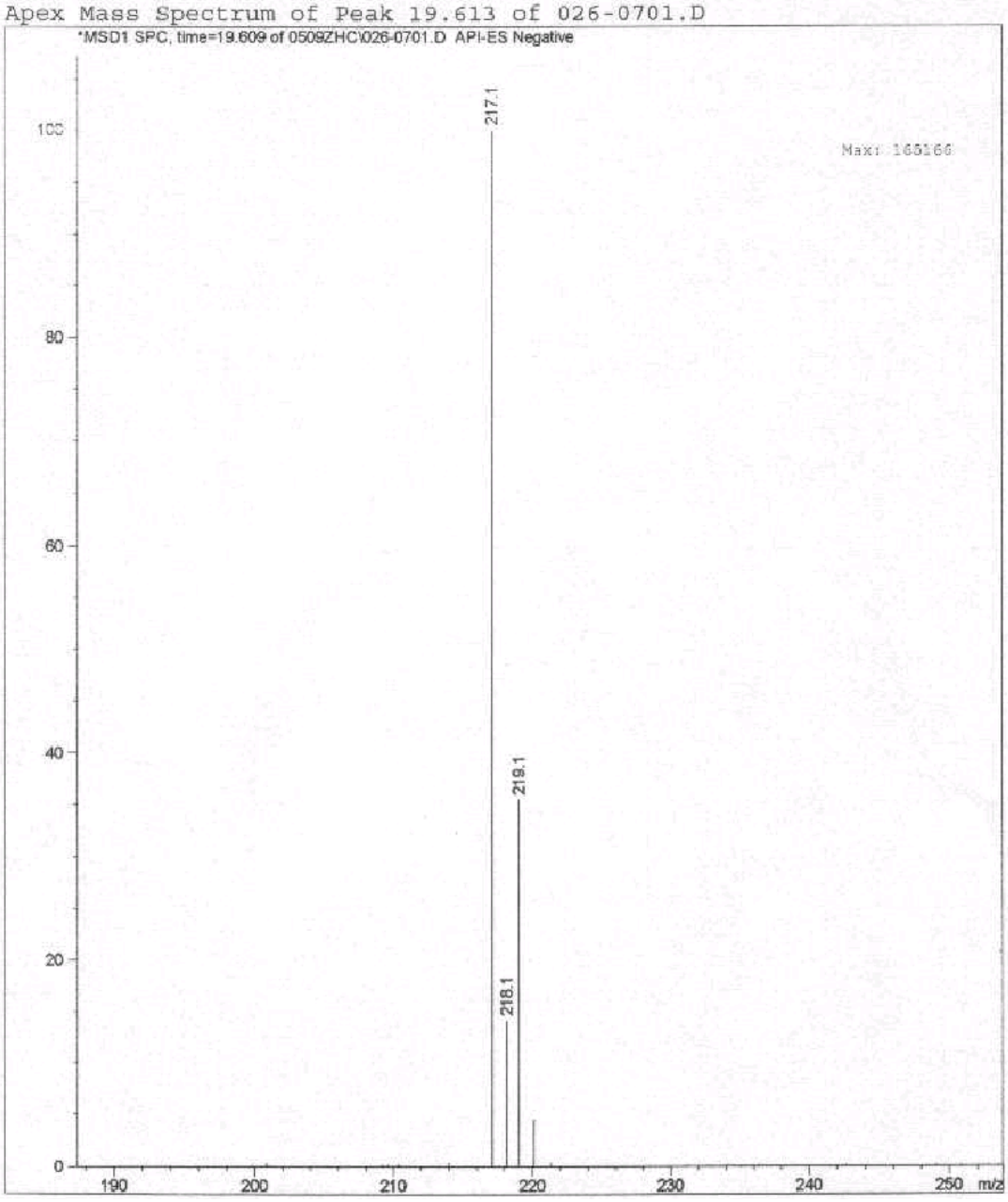

Figure A-II.6. LC/MS spectrum of the m/z 415a product of chlorophene.

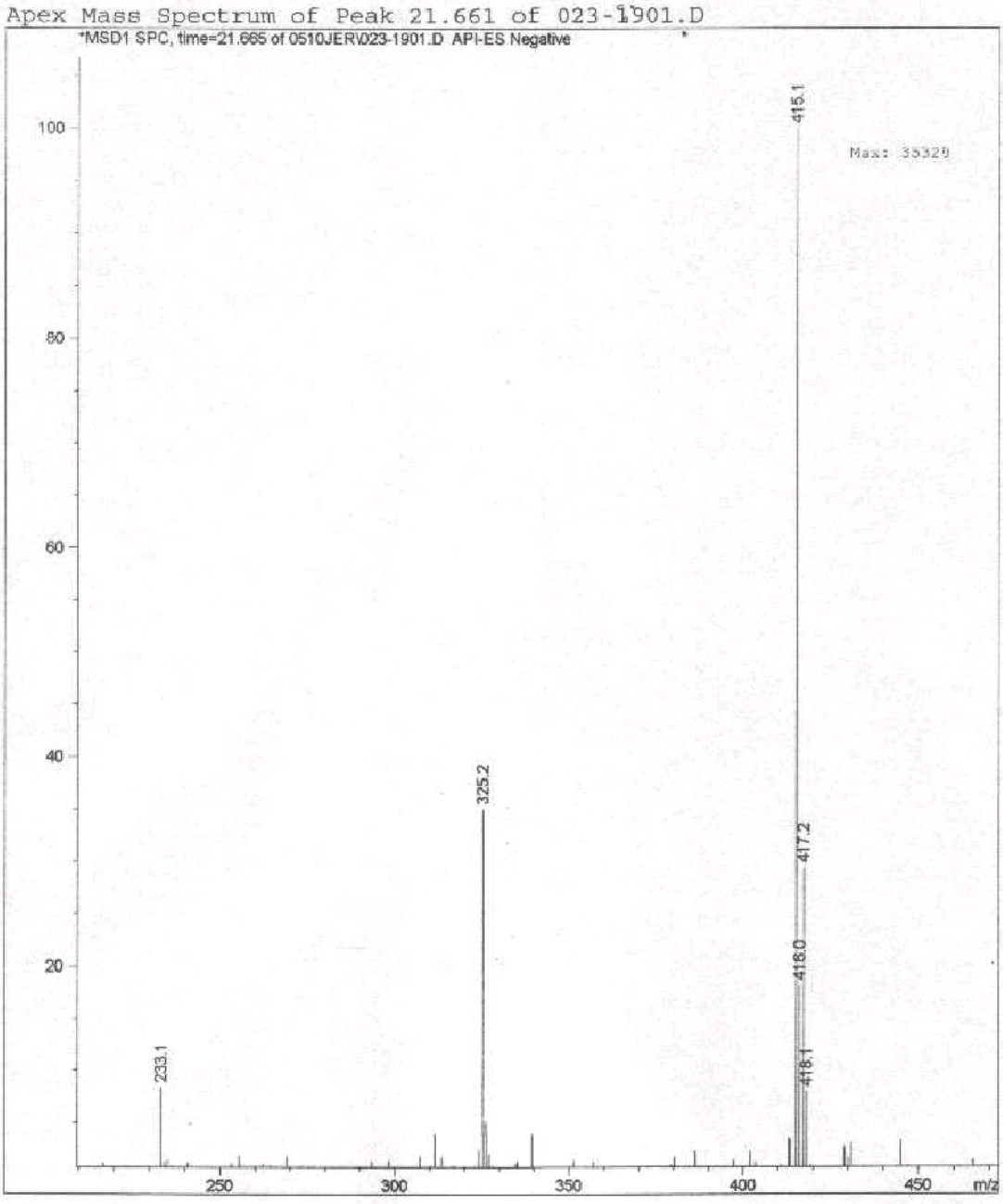

Figure A-II.7. LC/MS spectrum of the m/z 415b product of chlorophene.

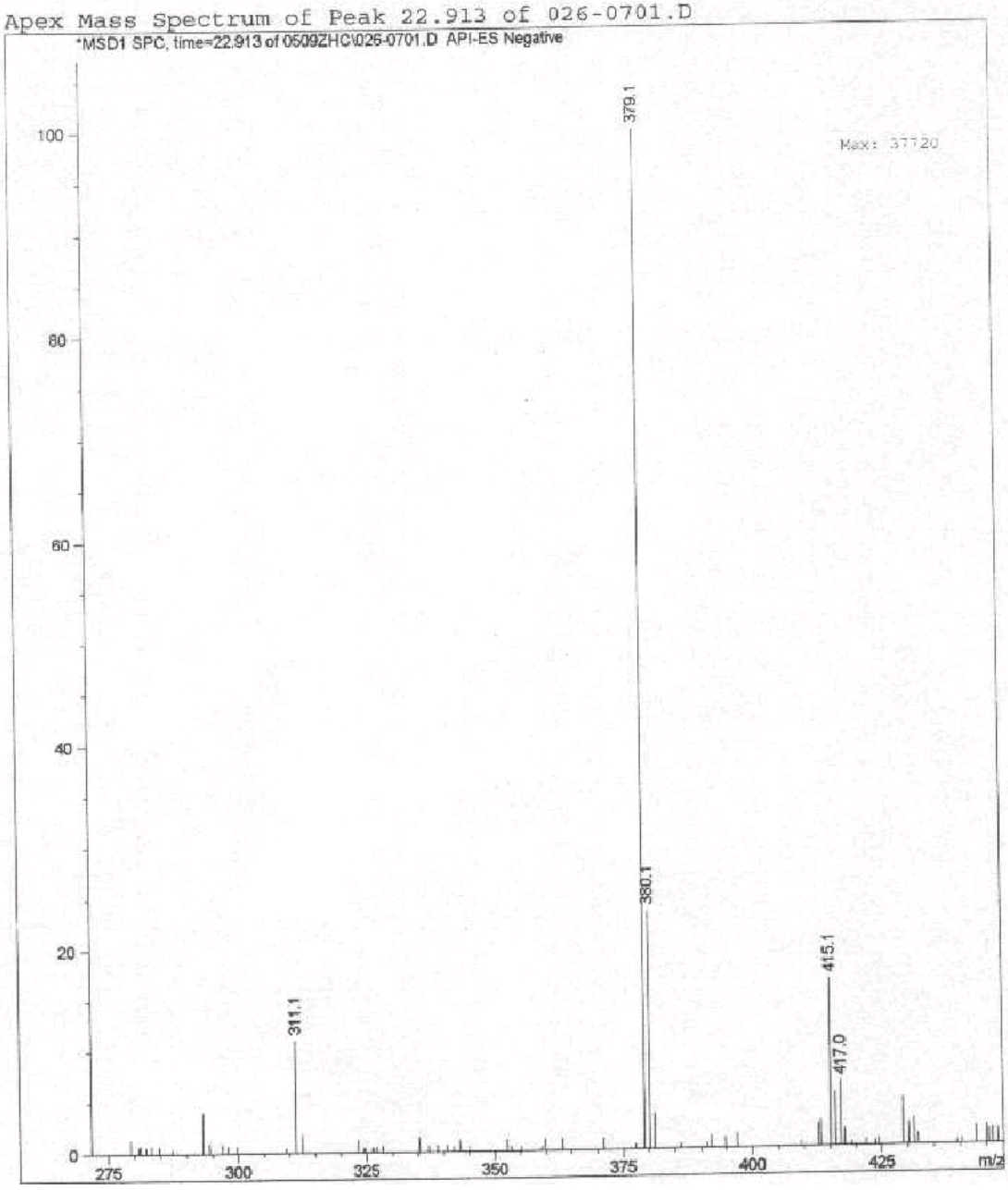

Figure A-II.8. LC/MS spectrum of the m/z 415c product of chlorophene.

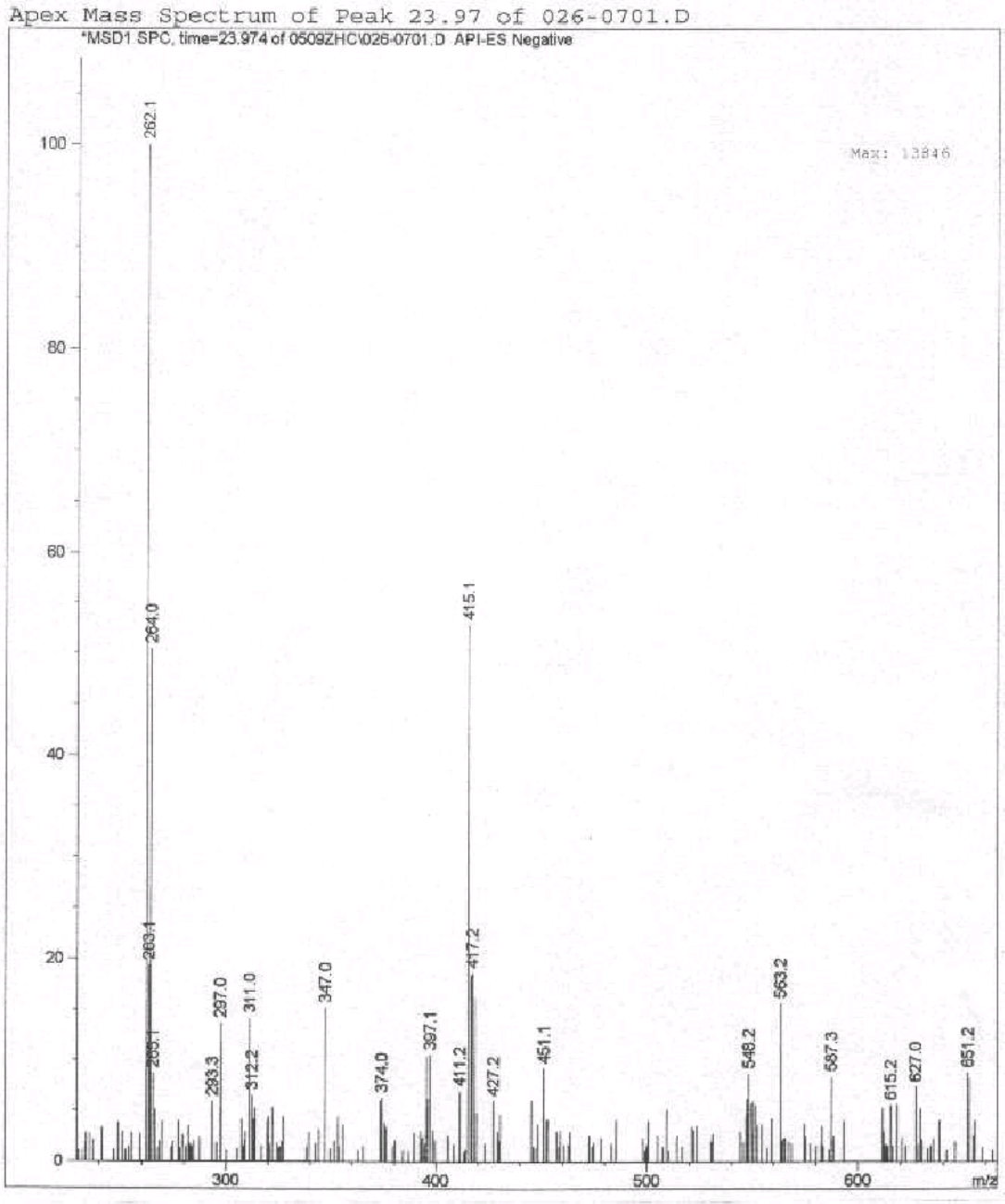

Figure A-II.9. LC/MS spectrum of the m/z 413a product of chlorophene.

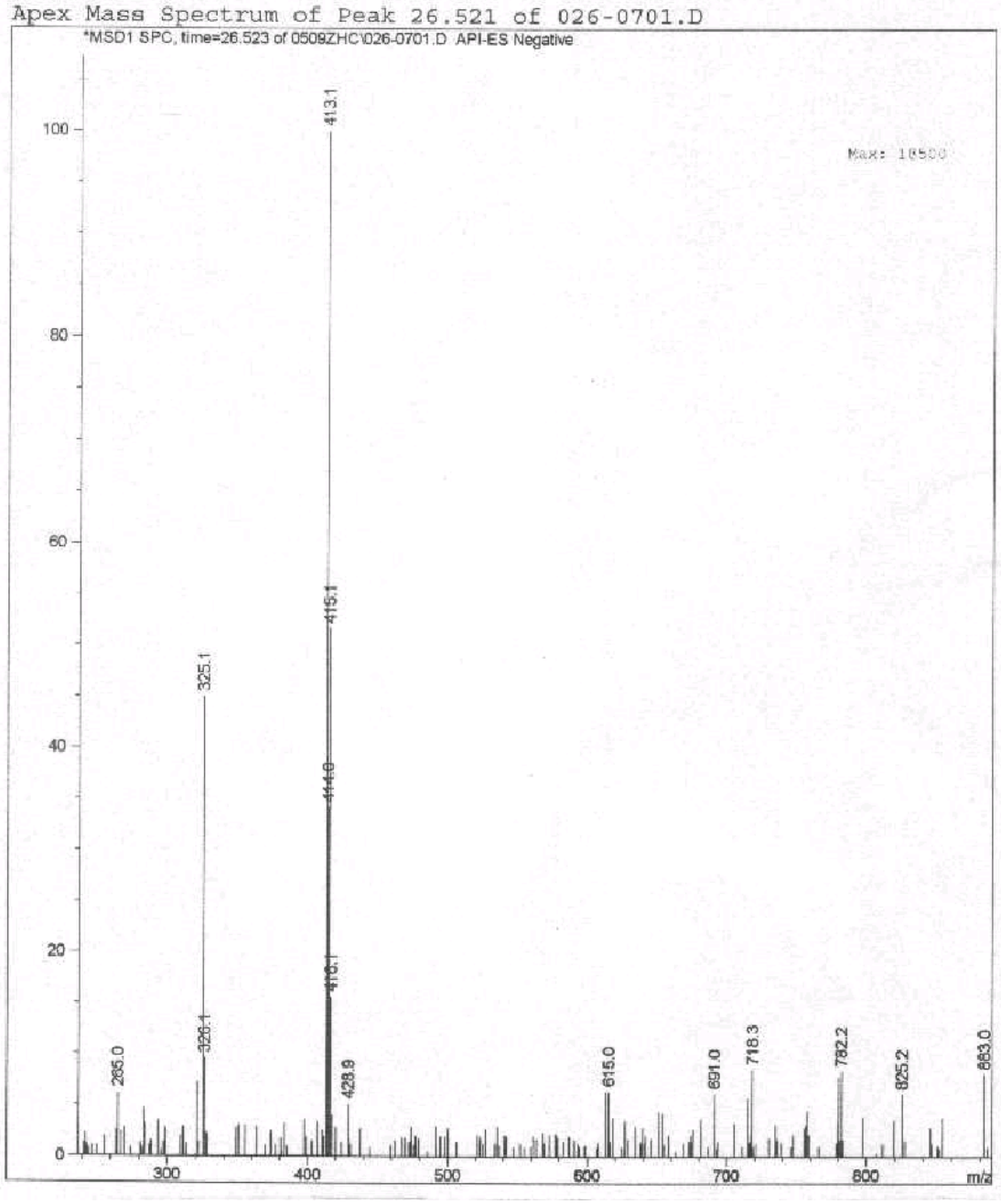

Figure A-II.10. LC/MS spectrum of the m/z 415d product of chlorophene.

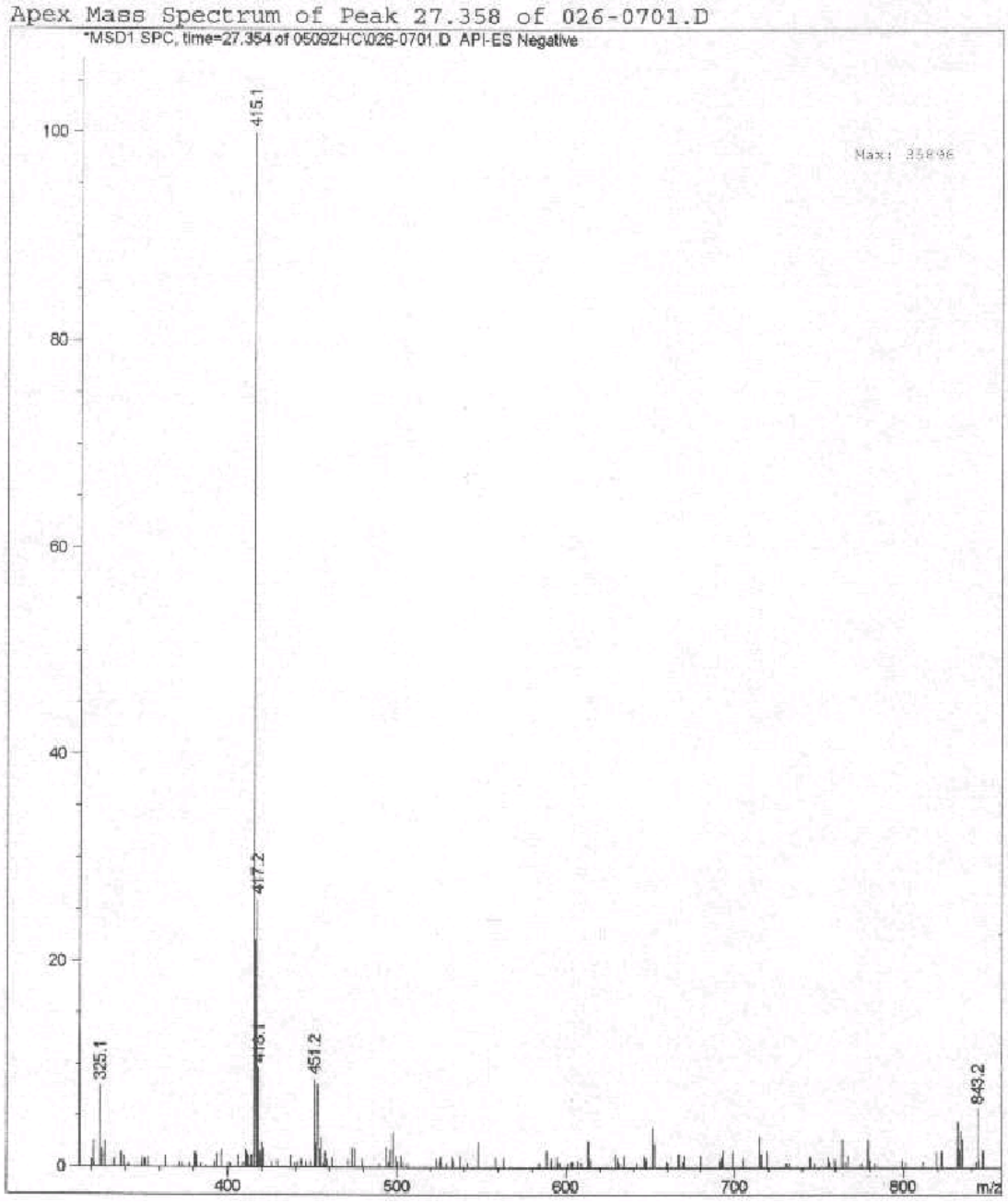

Figure A-II.11. LC/MS spectrum of the m/z 415e product of chlorophene.

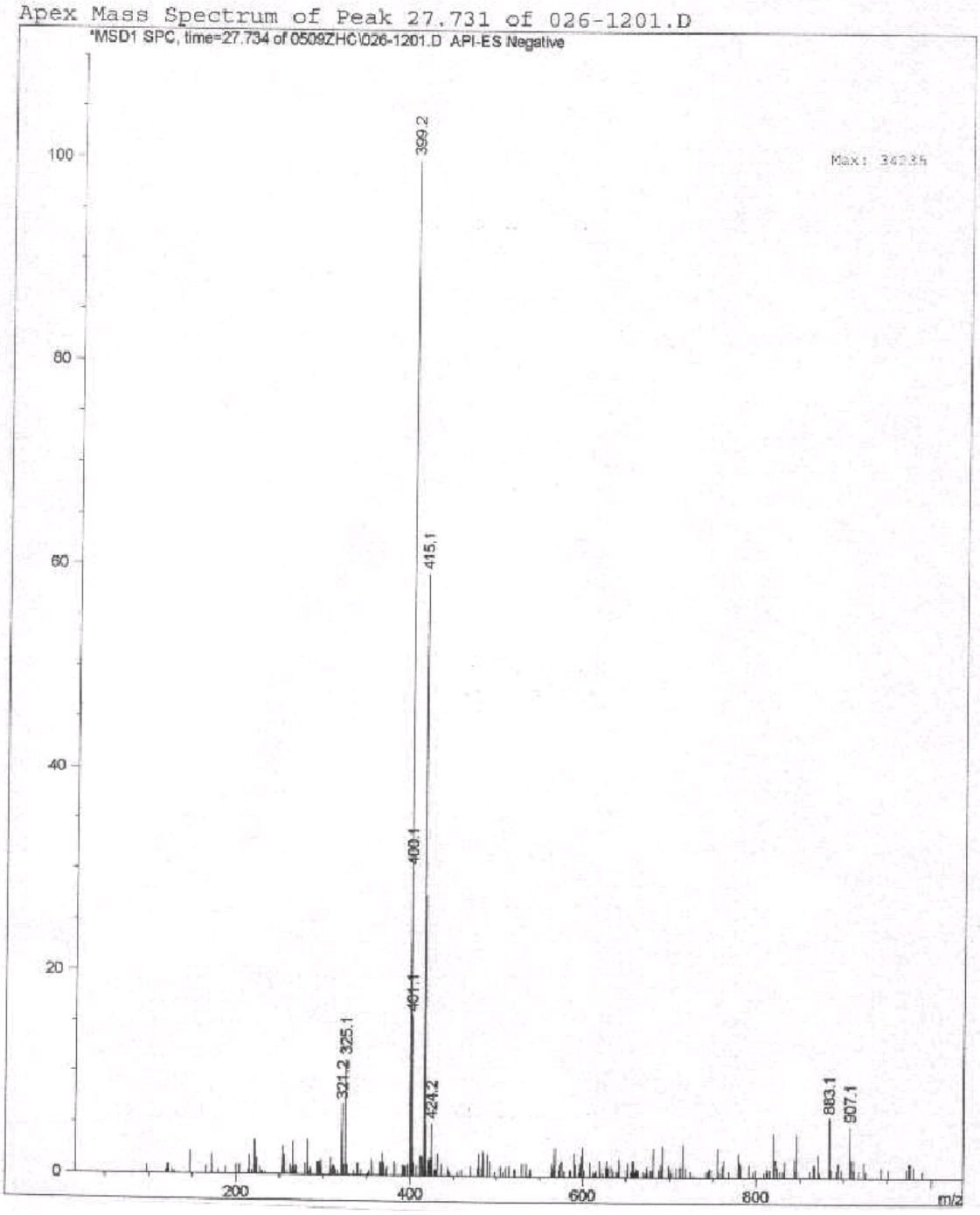

Figure A-II.12. LC/MS spectrum of the m/z 413b product of chlorophene.

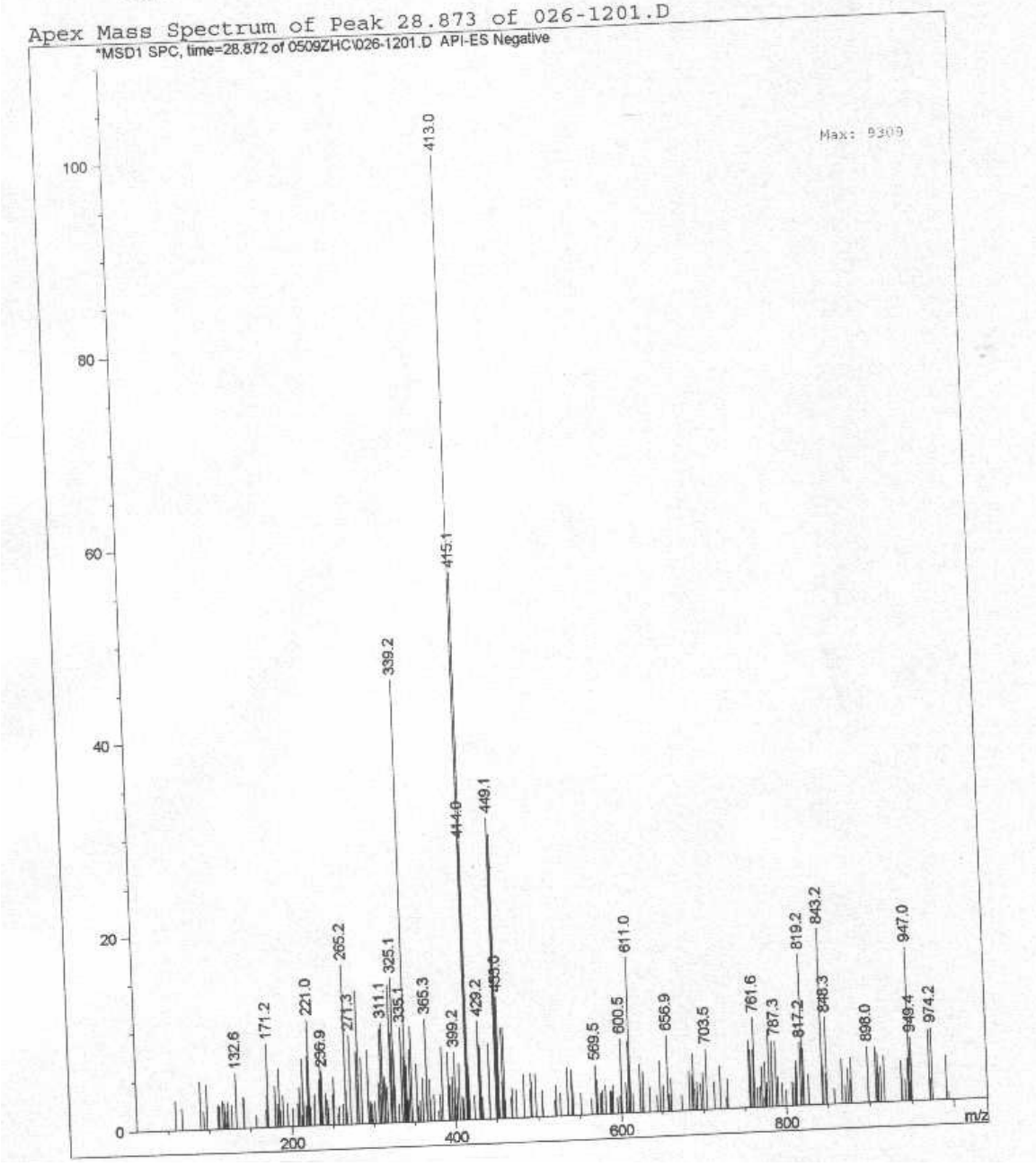

Figure A-II.13. LC/MS spectrum of the m/z 597 product of chlorophene.

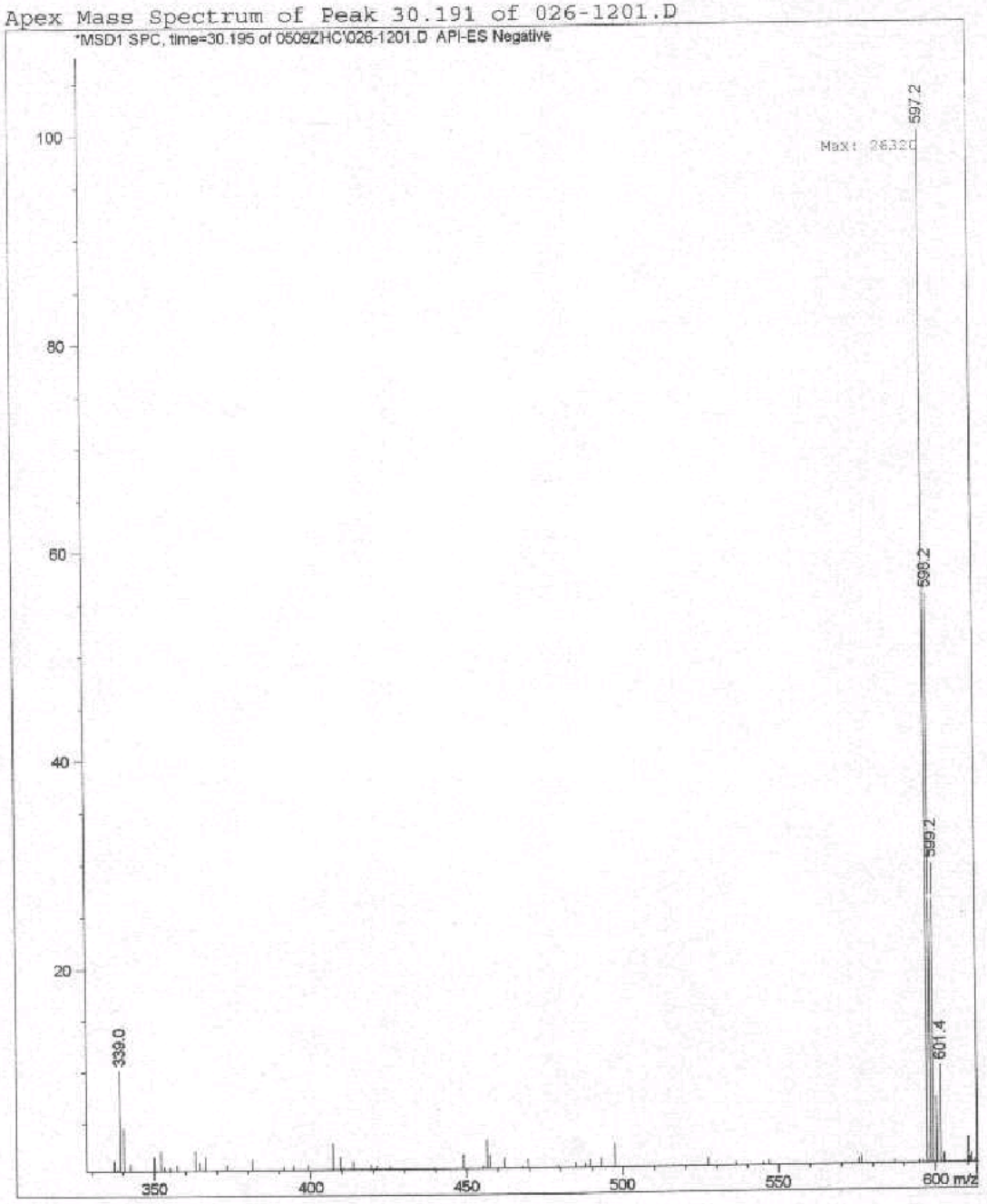

Figure A-II.14. LC/MS spectrum of the m/z 433 product of chlorophene.

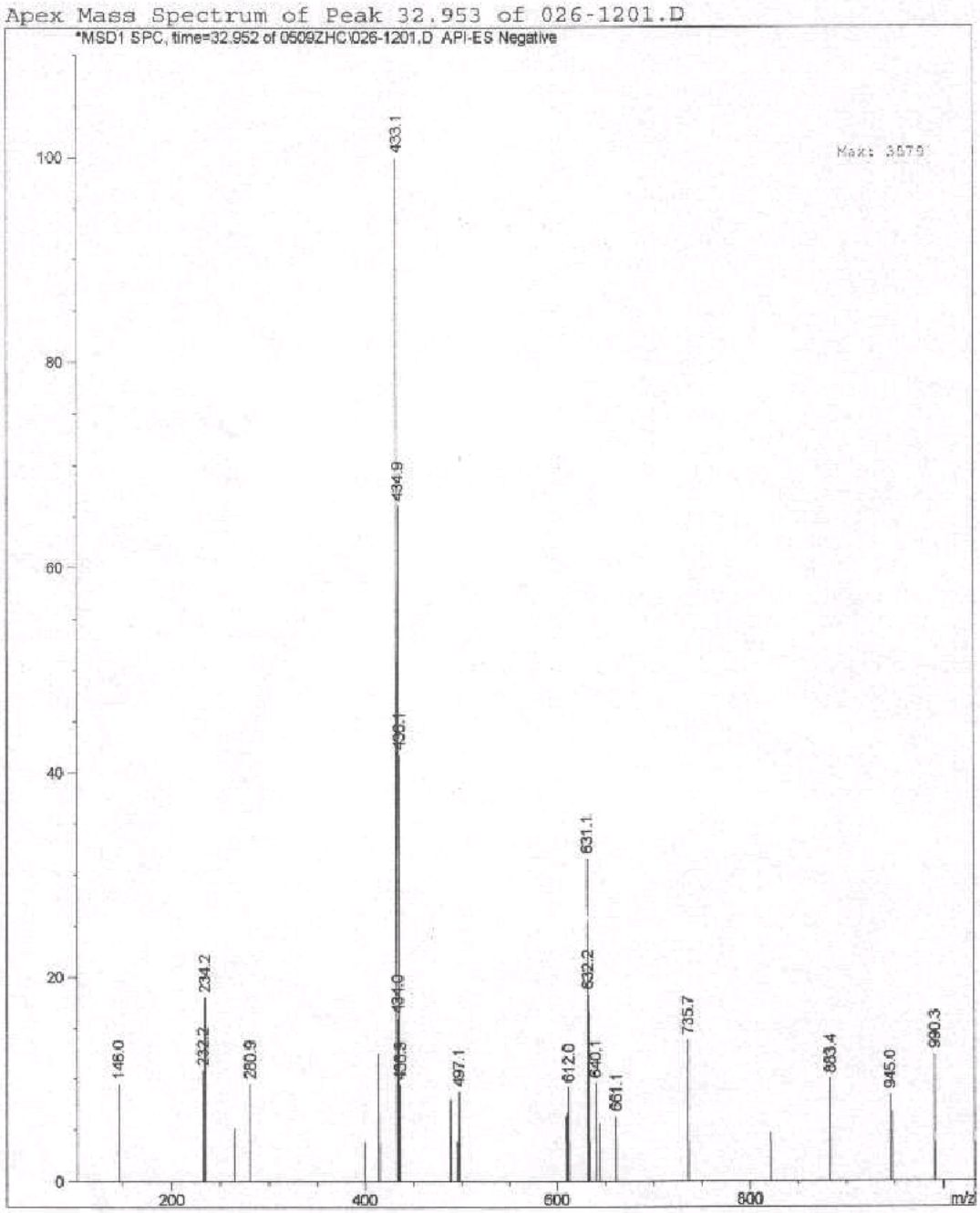

Figure A-III.1. LC/MS chromatograph of ciprofloxacin reaction mixture.

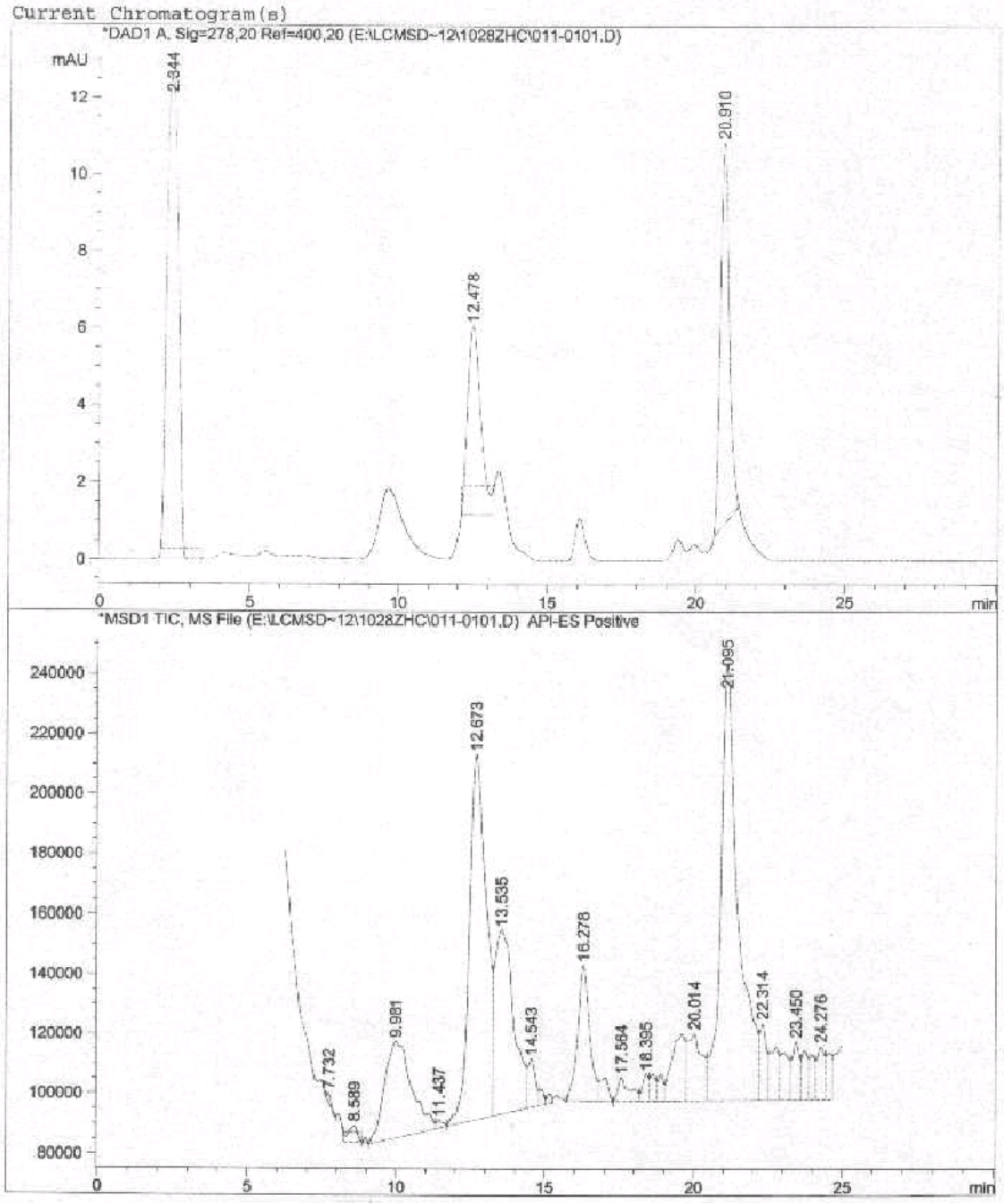

Figure A-III.2. LC/MS spectrum of the M+2a product (m/z 334) of cipro.

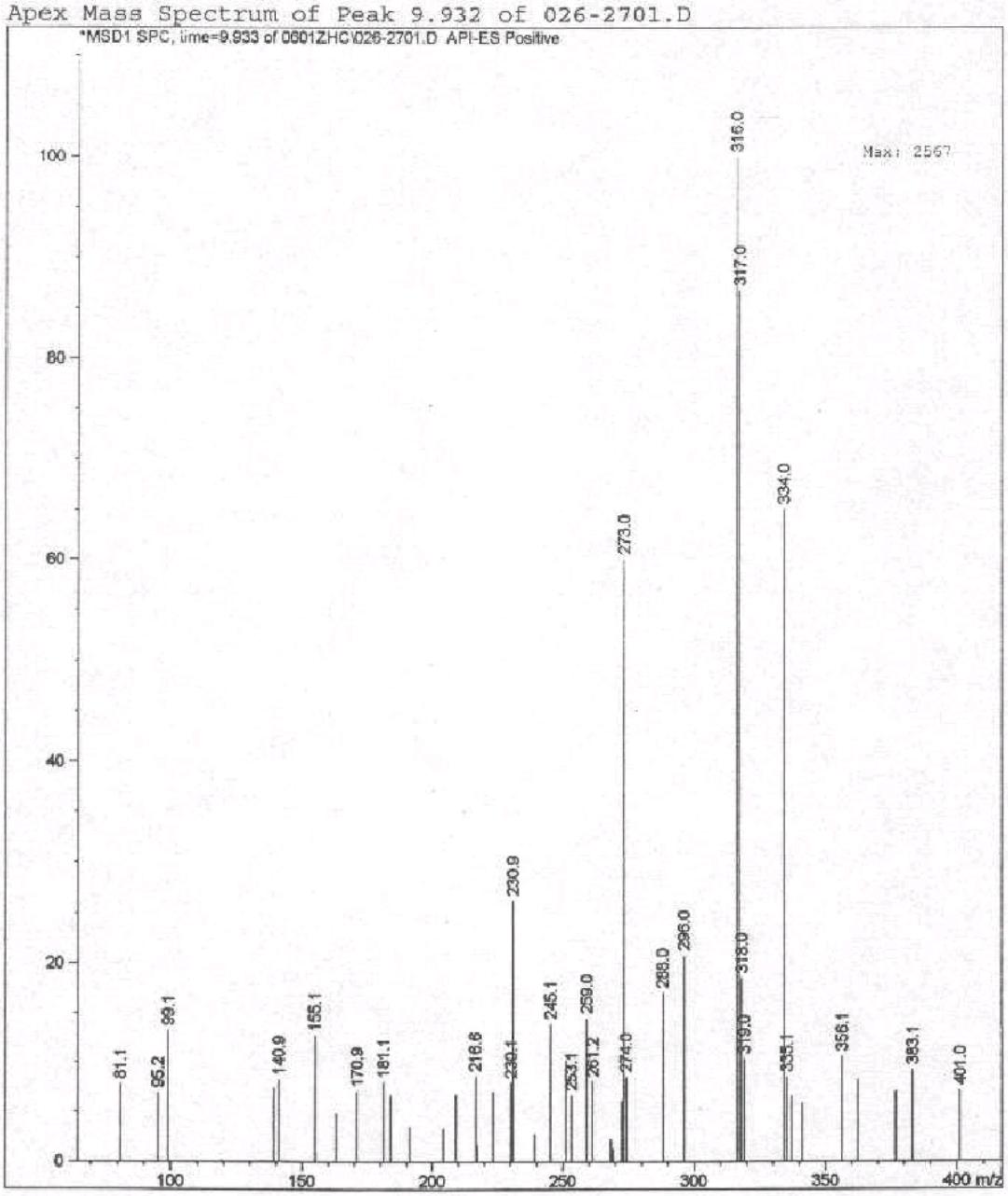

Figure A-III.3. LC/MS spectrum of the M-26 product (m/z 306) of cipro.

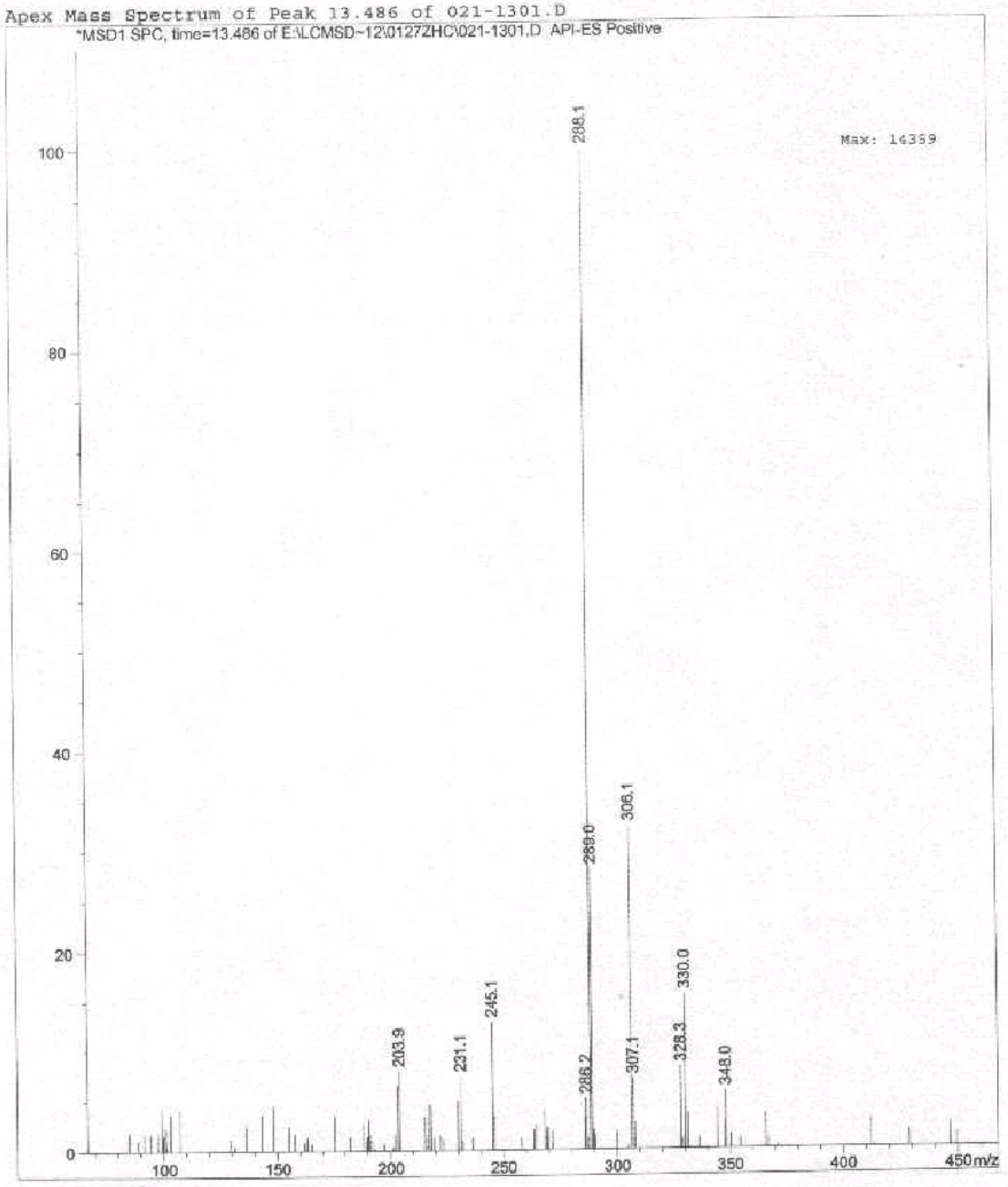

Figure A-III.4. LC/MS spectrum of ciprofloxacin (m/z 332).

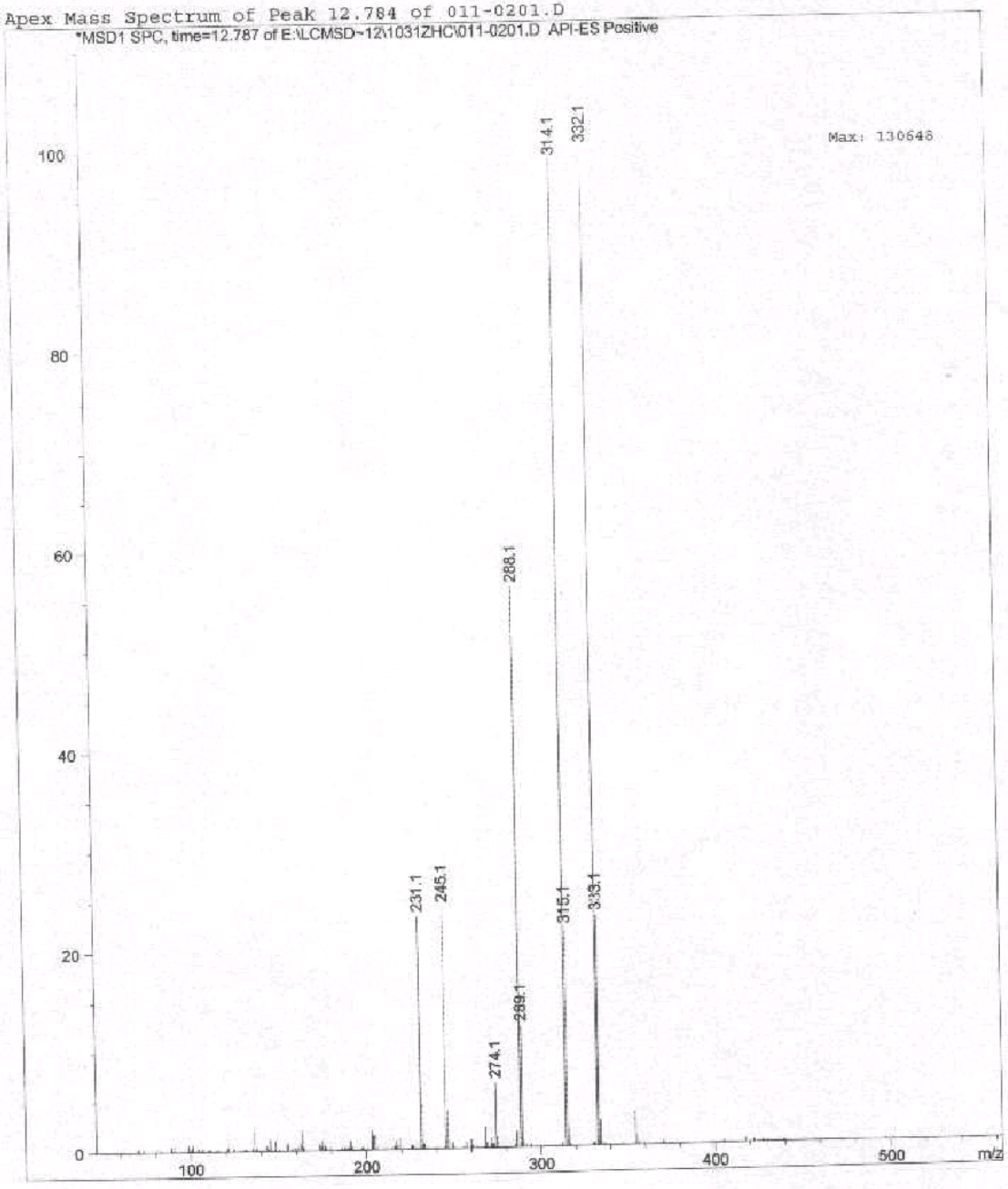

Figure A-III.5. LC/MS spectrum of the M+30 product (m/z 362) of cipro.

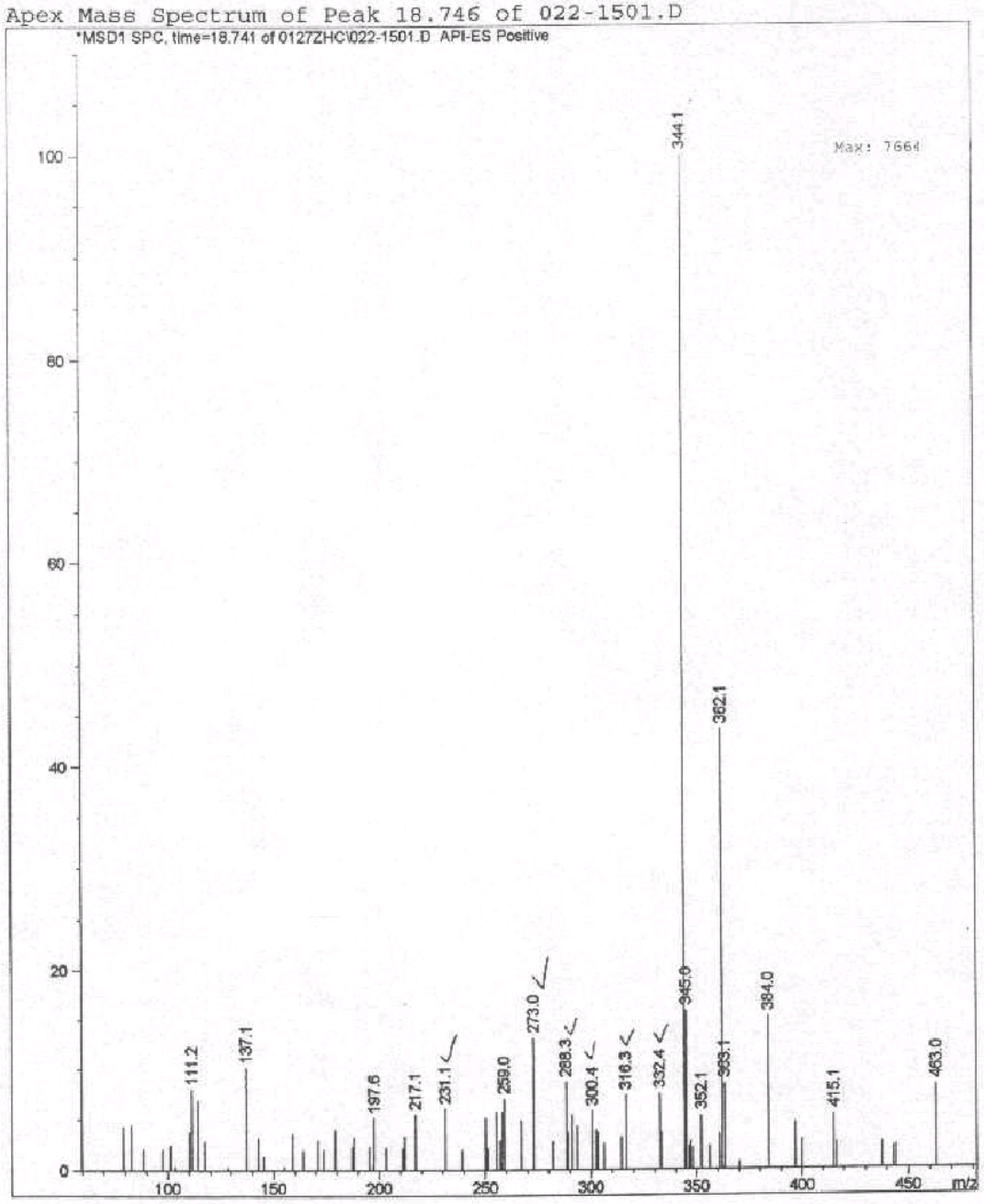

Figure A-III.6. LC/MS spectrum of the M+2b product (m/z 334) of cipro.

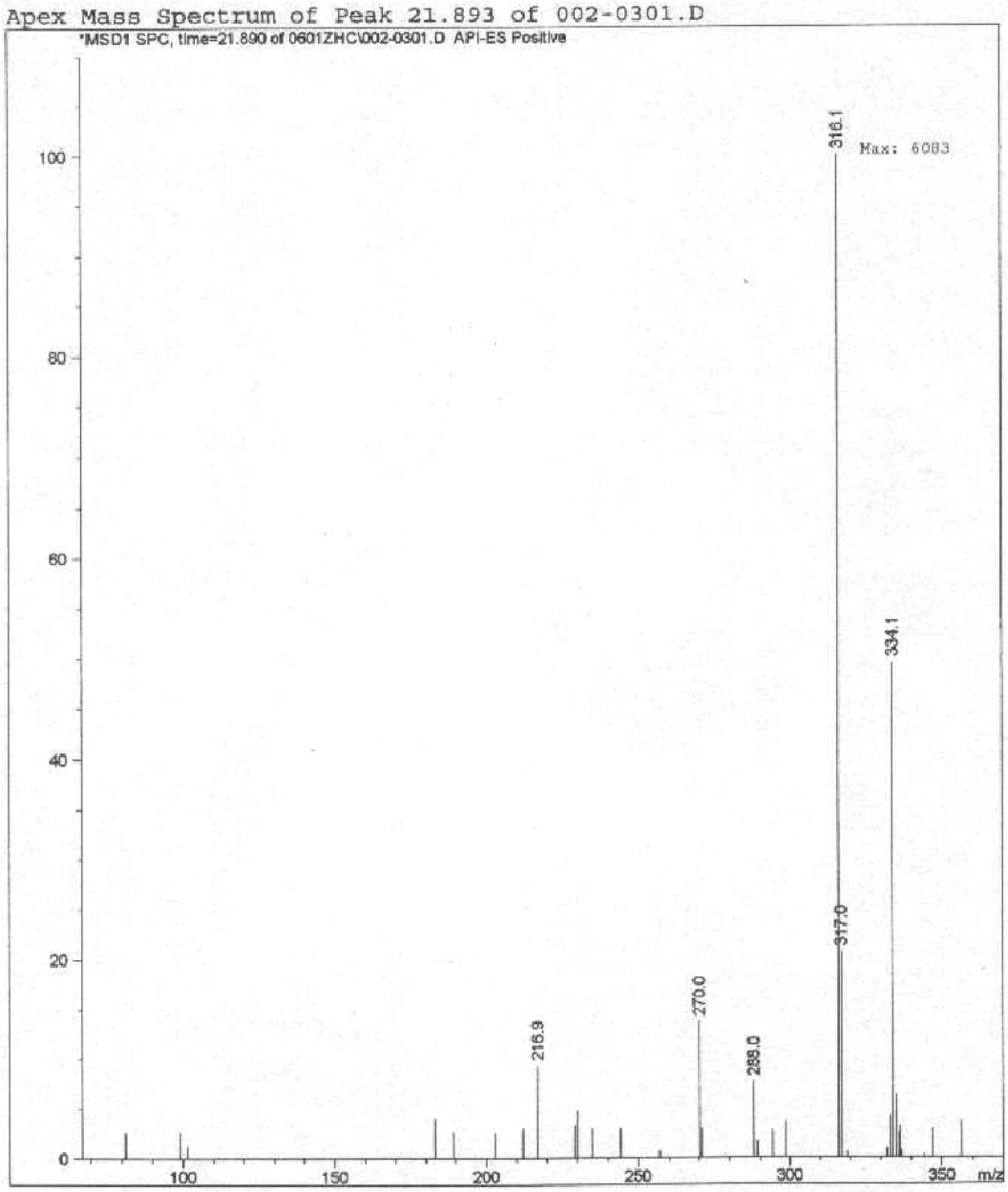

Figure A-III.7. LC/MS spectrum of the M-NH_2 product (m/z 263) of cipro.

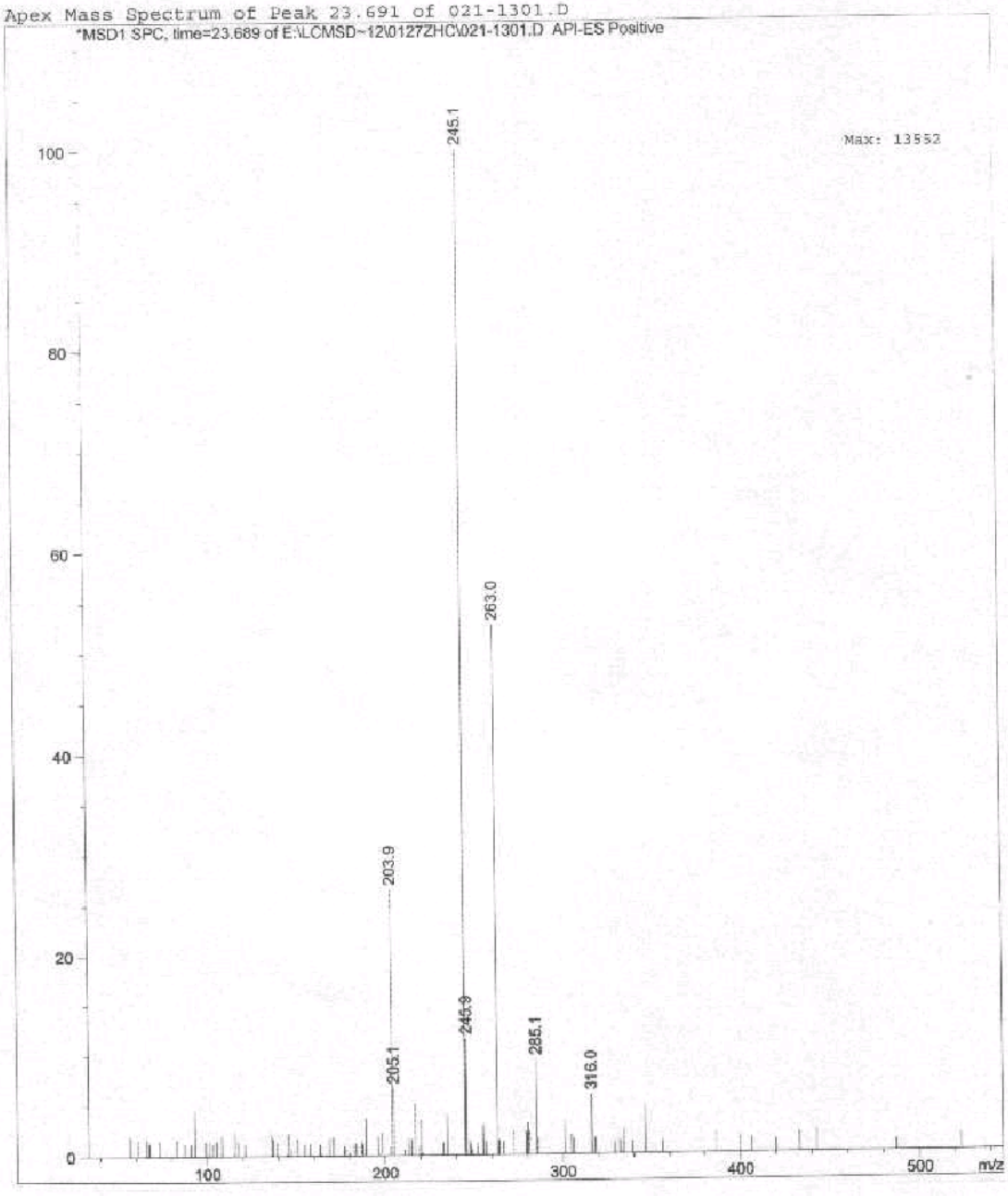

Figure A-III.8. LC/MS spectrum of the M+32 product (m/z 364) of cipro.

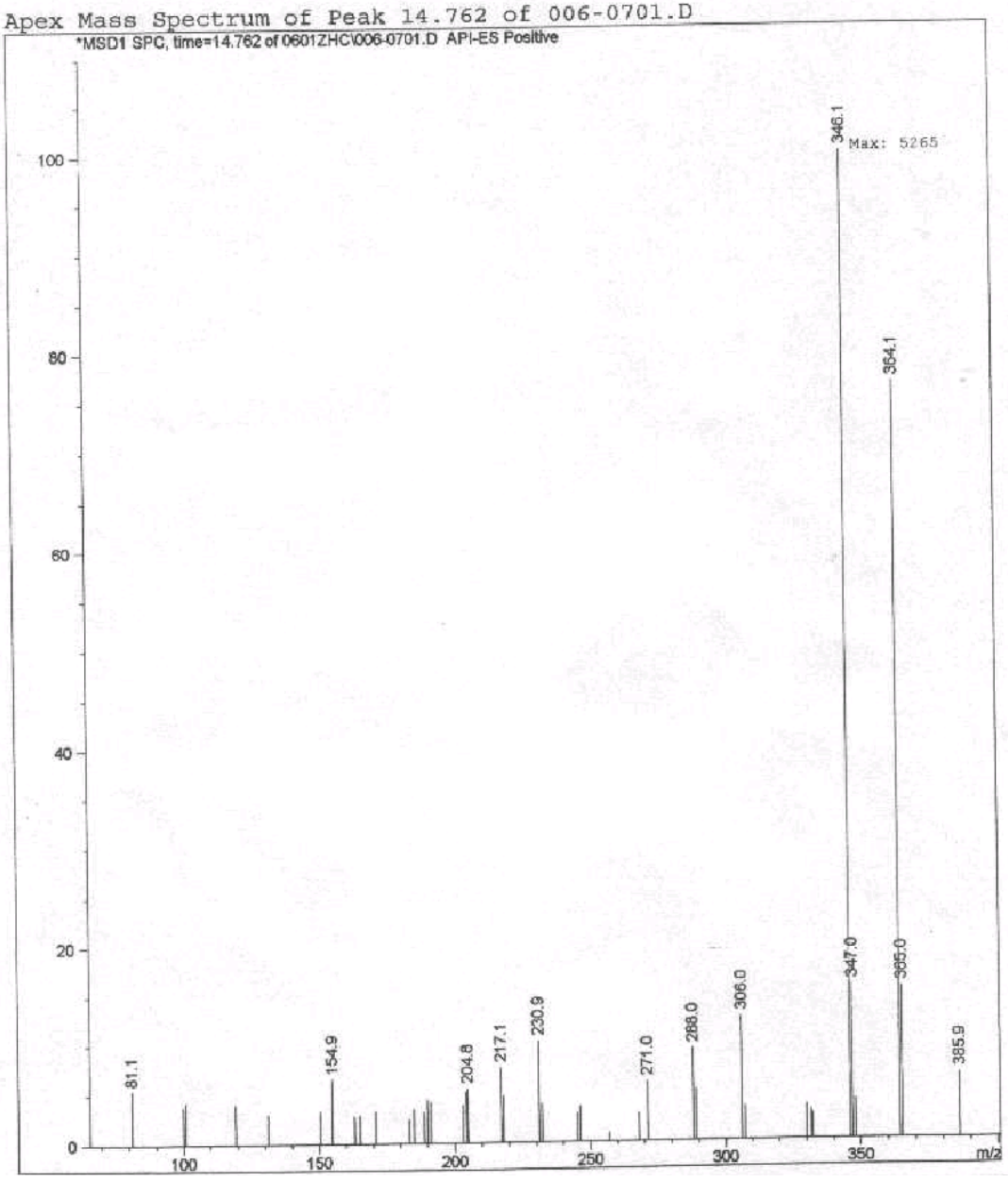

Figure A-IV.1. LC/MS chromatograph of QNO reaction mixture in H_2O.

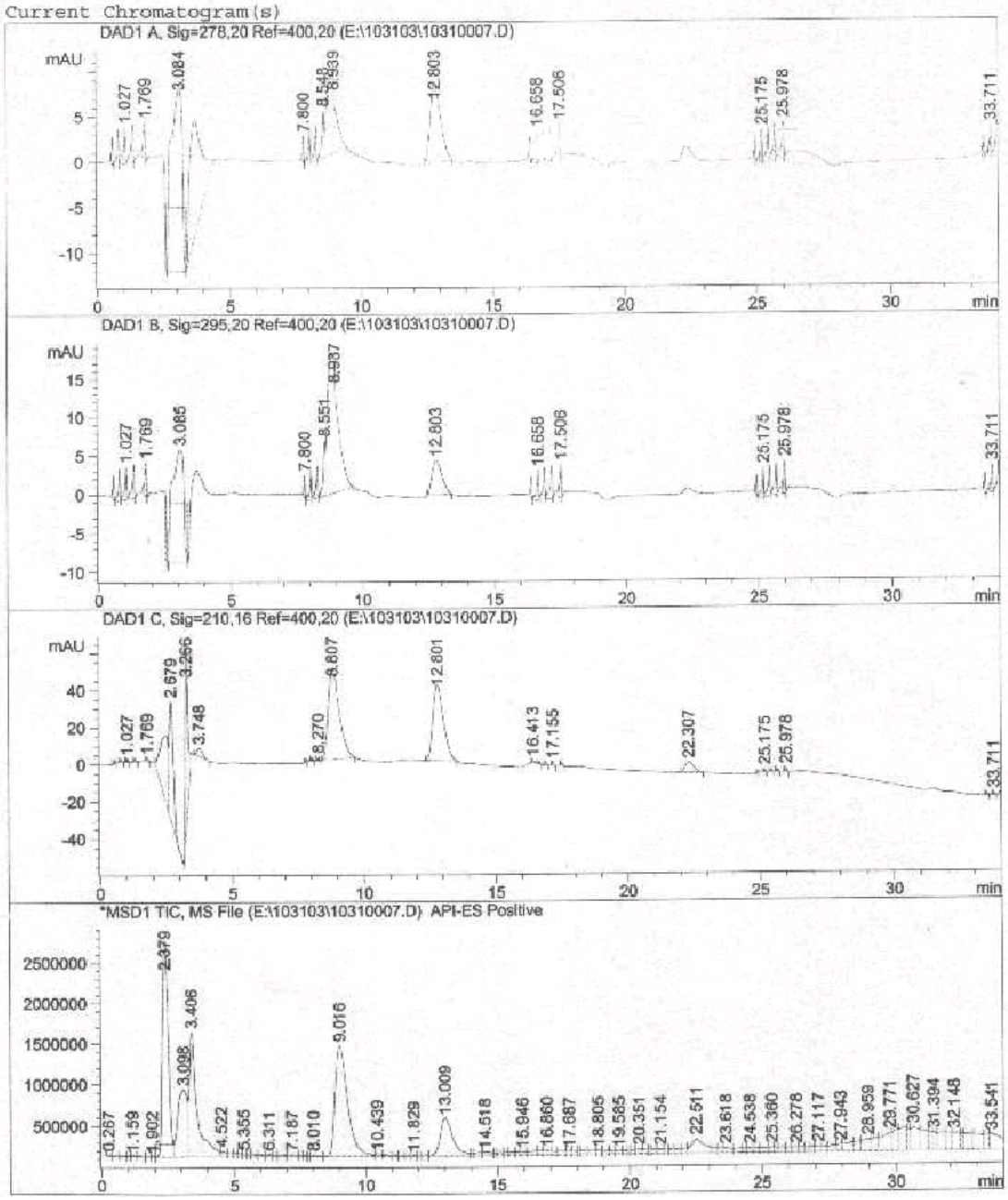

Figure A-IV.2. LC/MS spectrum of QNO (m/z 146).

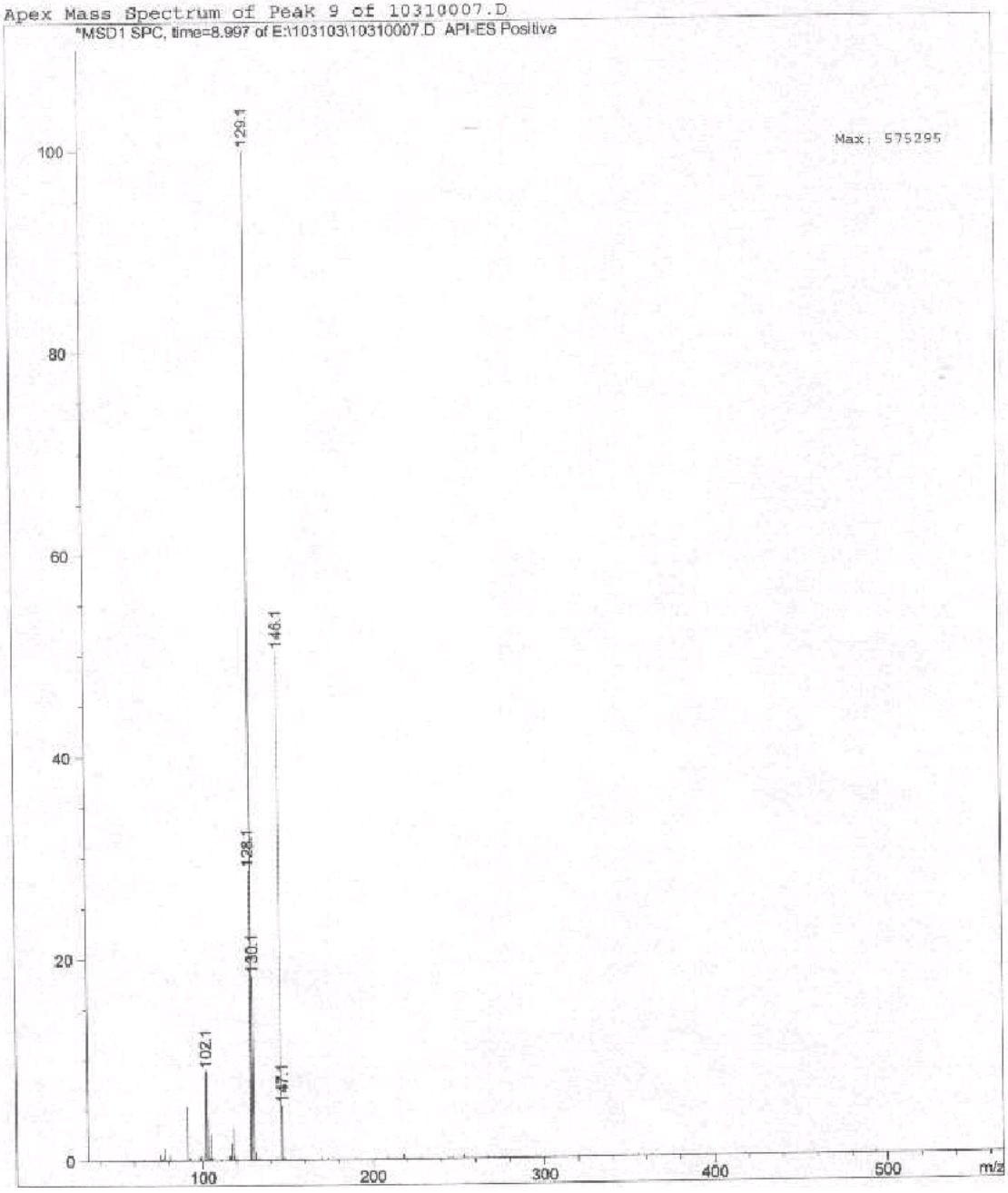

Figure A-IV.3. LC/MS spectrum of the m/z 146 product (i.e., 2-hydroxyquinoline) of QNO oxidation in H_2O.

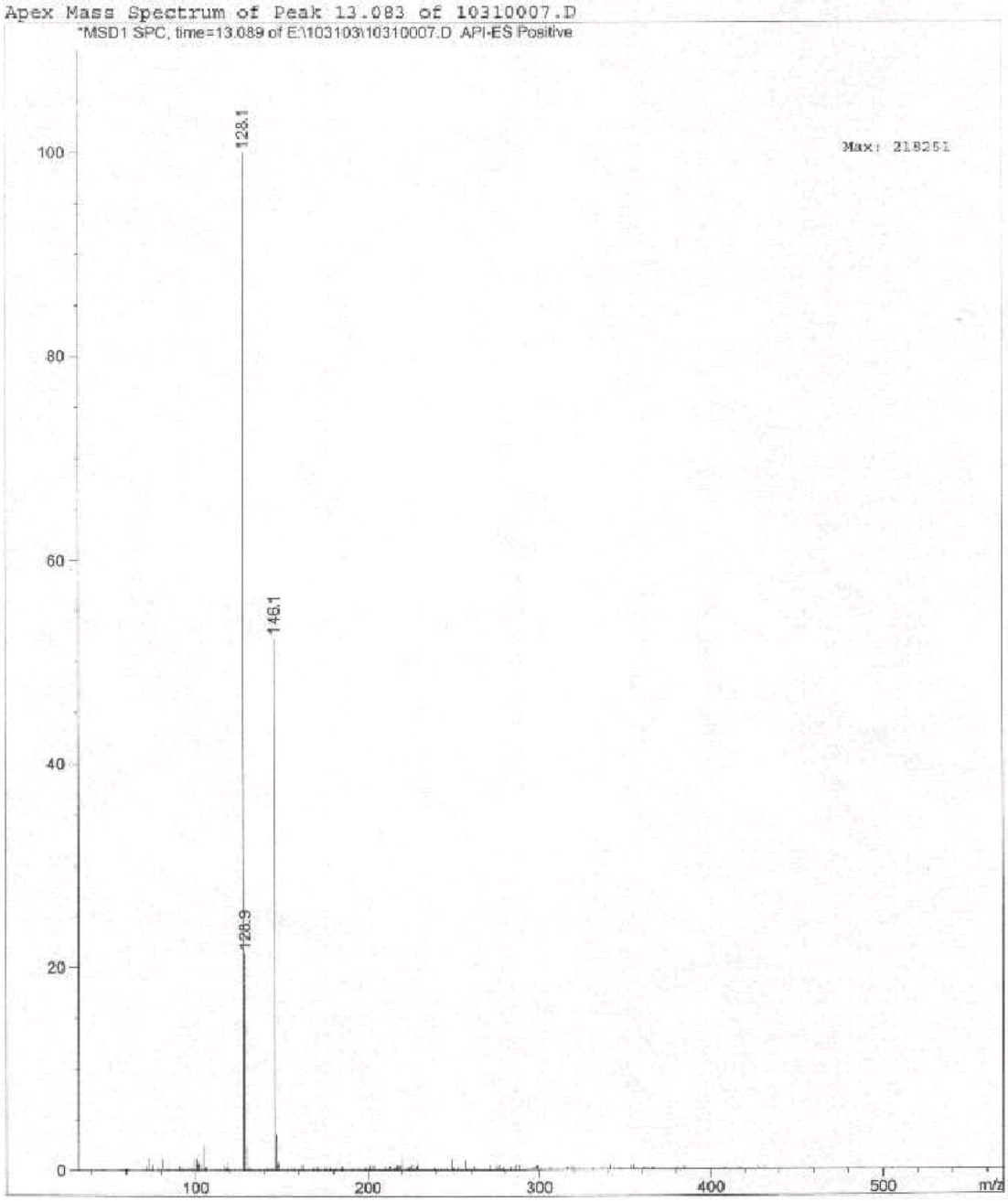

Figure A-IV.4. LC/MS spectrum of the m/z 305 product of QNO oxidation in H_2O.

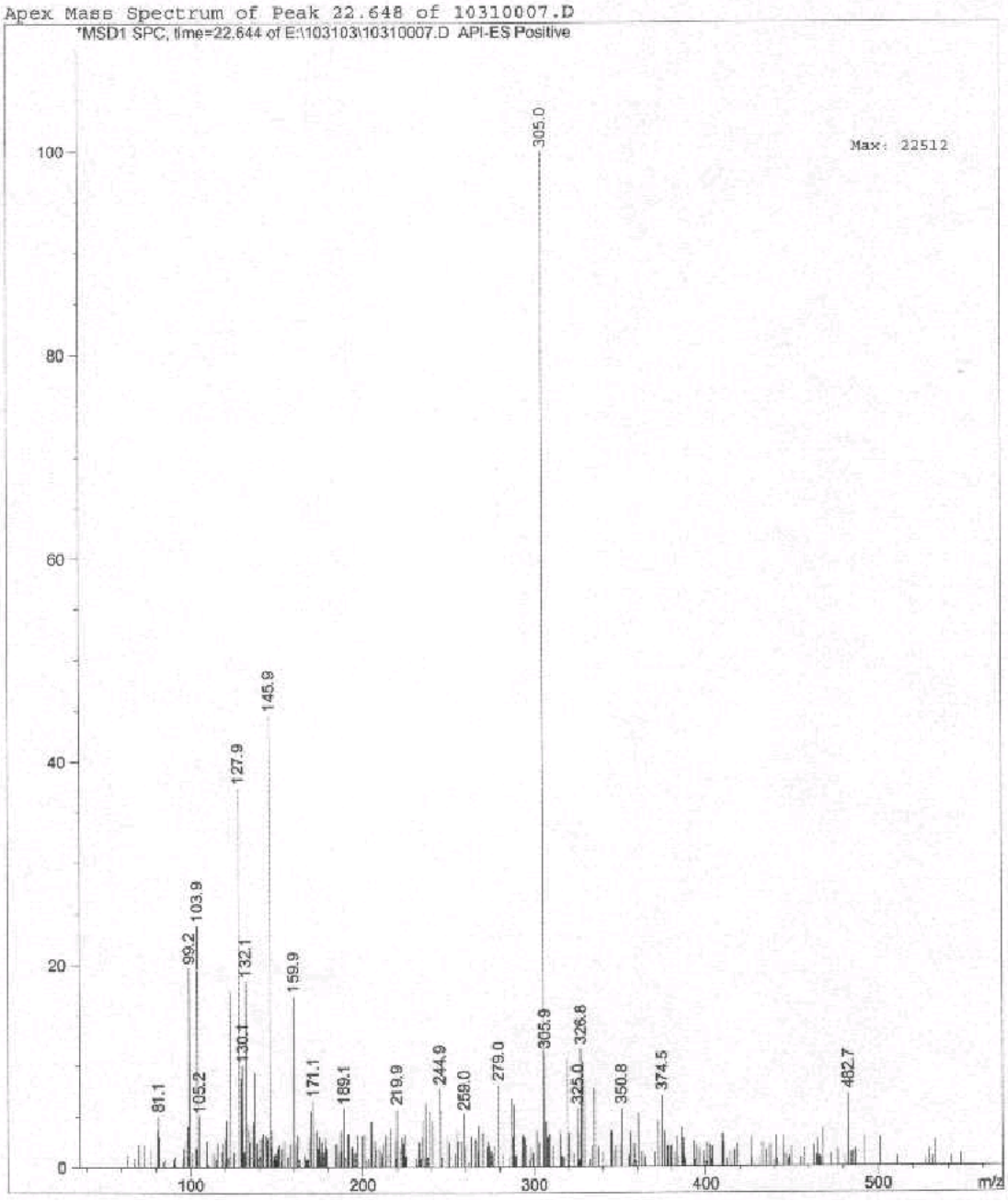

Figure A-IV.5. LC/MS chromatograph of QNO reaction mixture in $H_2{}^{18}O$.

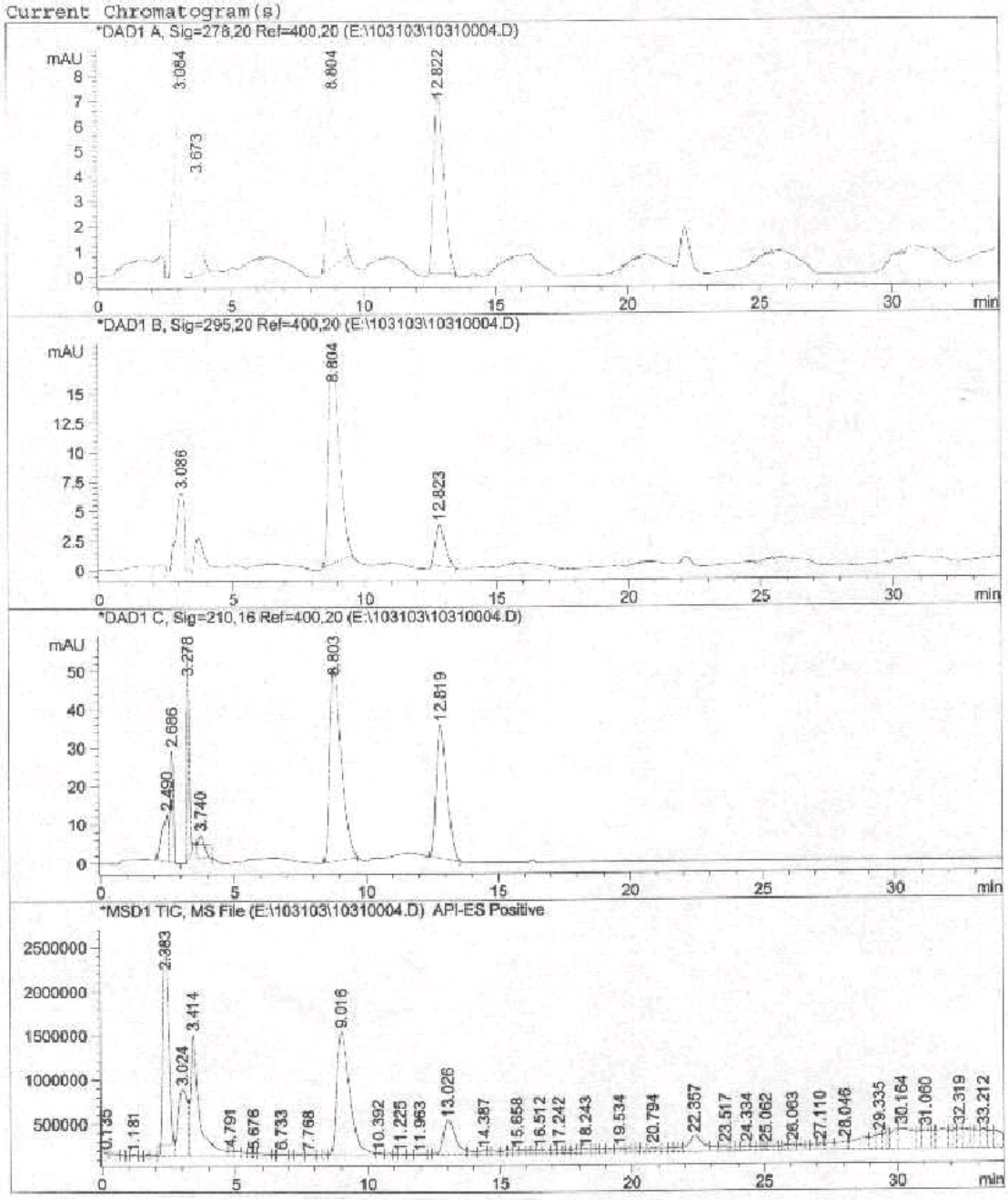

Figure A-IV.6. LC/MS spectrum of the m/z 148 product of QNO oxidation in $H_2{}^{18}O$.

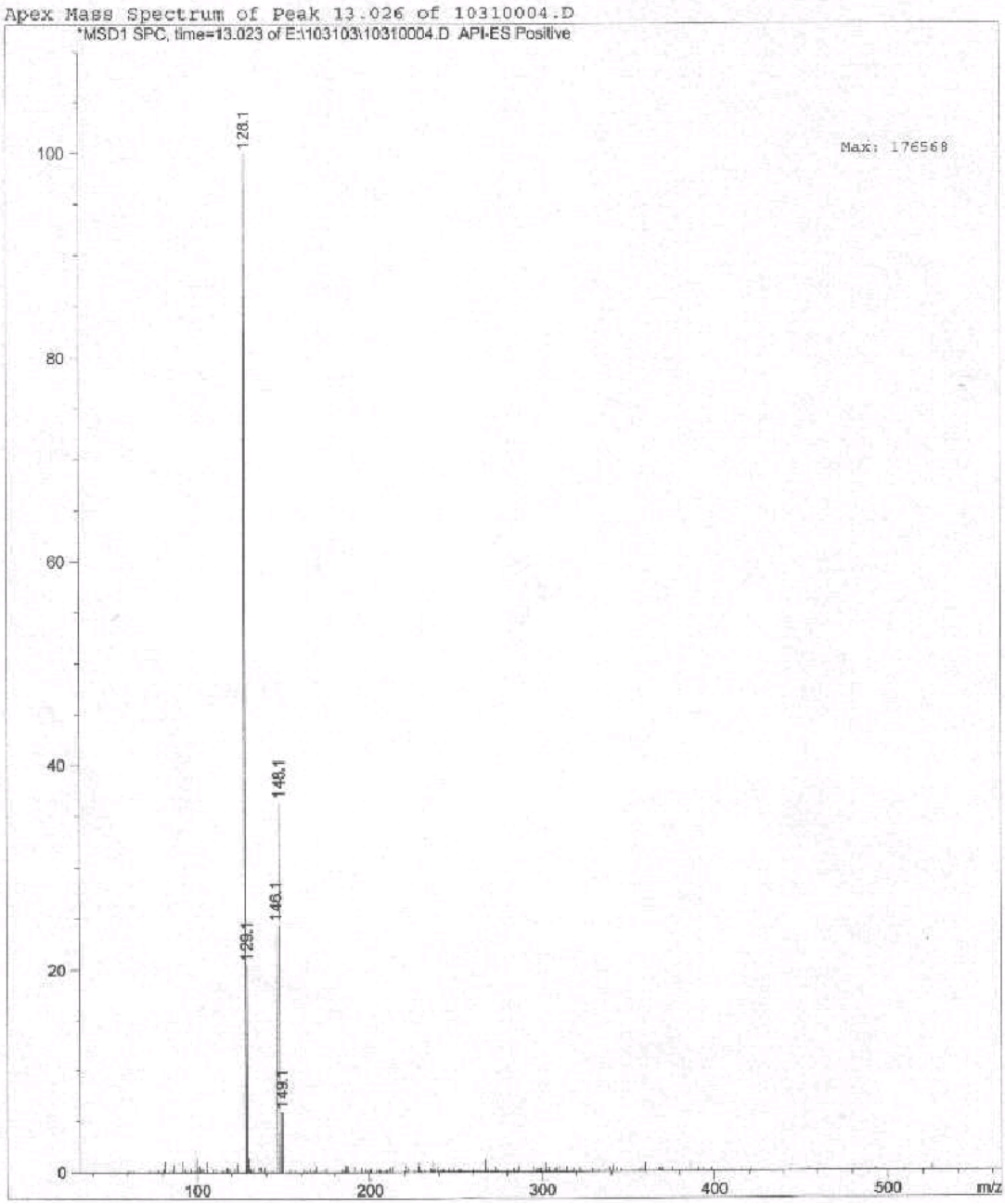

Figure A-IV.7. LC/MS spectrum of the m/z 309 product of QNO oxidation in $H_2{}^{18}O$.

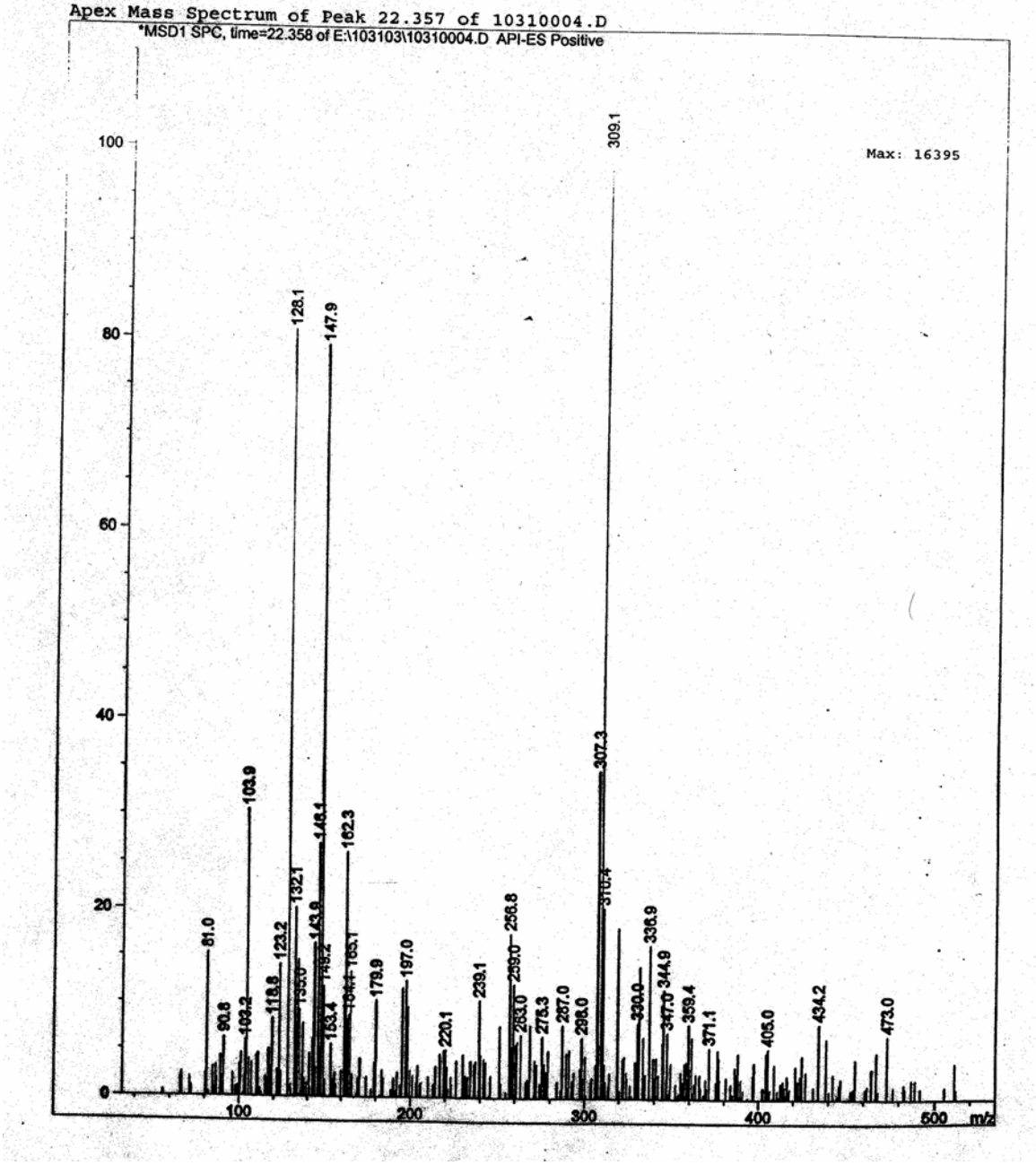

REFERENCES

Adler, E.; Becker, H.-D. 1961. Zur Selektiven Oxydation von Benzylalkoholen. *Acta Chemica Scandinavica*, *15,* 849-852.

Adolfsson-Erici, M.; Pettersson, M.; Parkkonen, J.; Sturve, J. 2000. Triclosan, a commonly used bactericide found in human milk and in the aquatic environment. *Organohalogen Compounds*, *48,* 83-86.

Ahmed, Y.; Qureshi, M. I.; Habib, M. S.; Farooqi, M. A. 1987. Quinoxaline derivatives. XII. The reactions of quinoxaline 1,4-dioxides with acetic anhydride. *Bulletin of the Chemical Society of Japan*, *60,* 1145-1148.

Al-Almad, A.; Daschner, F. D.; Kümmerer, K. 1999. Biodegradability of cefotiam, ciprofloxacin, meropenem, penicillin G, and sulfamethoxazole and inhibition of waste water bacteria. *Archives of Environmental Contamination and Toxicology*, *37,* 158-163.

Albini, A.; Pietra, S. 1991. *Heterocyclic N-oxides*; CRC Press: Boca Raton, Ann Arbor, Boston.

Al-Ghazali, M. R.; Jazrawi, S. F.; Al-Doori, Z. A. 1988. Antibiotic resistance among pollution indicator bacteria isolated from Al-Khair River, Baghdad. *Water Research*, *22,* 641-644.

Alfassi, Z. B. 1999. In *General Aspects of the Chemistry of Radicals*; Alfassi, Z. B., Ed.; John Wiley & Sons: New York, NY, pp 166-170.

Bath, S.; Laso, N. M.; Lopez-Ruiz, H.; Quiclet-Sire, B.; Zard, S. Z. 2003. A practical access to acyl radicals from acyl hydrazides. *Chemical Communications*, *2,* 204-205.

Bandara, J.; Mielczarski, J. A.; Lopez, A.; Kiwi, J. 2001. 2. Sensitized degradation of chlorophenols on iron oxides induced by visible light comparison with titanium oxide. *Applied Catalysis B: Environmental*, *34,* 321-333.

Bandara, J.; Tennakone, K.; Kiwi, J. 2001. Surface mechanism of molecular recognition between aminophenols and iron oxides surfaces. *Langmuir*, *17,* 3964-3969.

Bhargava, J. G.; Howes, D.; Rutherford, T. 1996. *American Journal of Infection Control*, *24,* 209-218.

Bhatnagar, I.; George, M. V. 1967. Oxidation of phenylhydrazones with manganese dioxide. *Journal of Organic Chemistry*, *32,* 2252-2256.

Bhatnagar, I.; George, M. V. 1968. Oxidation with metal oxides. III. Oxidation of diamines and hydrazines with manganese dioxide. *Journal of Organic Chemistry*, *33,* 2407-2411.

Bietti, M.; Cuppoletti, A.; Dagostin, C.; Florea, C.; Galli, C.; Gentili, P.; Petride, H.; Russo Caia, C. 1998. Stereoelectronic inhibition of deprotonation in the radical cation of

N-benzylpiperidine. A contribution to the debate on the mechanism of N-dealkylation of tertiary amines. *European Journal of Organic Chemistry*, *11,* 2425-2429.

Binnendijk, G. M.; Aerts, M. M. L.; Keukens, H. J.; Brinkman, U. A. T. 1991. Optimization and ruggedness testing of the determination of residues of carbadox and metabolites in products of animal origin: stability studies in animal tissues. *Journal of Chromatography*, *541,* 401-410.

Borggaard, O. K. 1983. Effect of surface area and mineralogy of iron oxides on their surface charge and anion-adsorption properties. *Clays and Clay Minerals*, *31,* 230-232.

Brooks, P. R.; Wirtz, M. C.; Vetelino, M. G.; Rescek, D. M.; Woodworth, G. F.; Morgan, B. P.; Goe, J. W. 1999. Boron trichloride/tetra-n-butylammonium iodide: a mild, selective combination reagent for the cleavage of primary alkyl aryl ethers. *Journal of Organic Chemistry*, *64,* 9719-9721.

Burhenne, J.; Ludwig, M.; Nikoloudis, P.; Spiteller, M. 1997. Photolytic degradation of fluoroquinolone carboxylic acids in aqueous solution. Part I. Primary photoproducts and half-lives. *Environmental Science and Pollution Research*, *4,* 10-15.

Burhenne, J.; Ludwig, M.; Spiteller, M. 1999. Polar photodegradation products of quinolones determined by HPLC/MS/MS. *Chemosphere*, *38,* 1279-1286.

Carey, F. A.; Sundberg, R. J. 2000. *Advanced organic chemistry. Part A. structure and mechanisms.*; Fourth Ed.; Kluwer Academic/Plenum Publishers: New York, Boston, Dordrecht, London, Moscow.

Chauhan, S. M. S.; Kalra, B.; Mohapatra, P. P. 1999. Oxidation of 1-naphthol and related phenols with hydrogen peroxide and potassium superoxide catalysed by 5,10,15,20-tetraarylporphyrinatoiron(III)chlorides in different reaction conditions. *Journal of Molecular Catalysis*, *137,* 85-92.

ChemProp - Chem 3D Ultra; 7.0.0 Ed.; 2002. CambridgeSoft: Cambridge, MA.

Chukhrov, F. V.; Gorshkov, A. I. 1981. Iron and manganese oxide minerals in soils. *Transactions of the Royal Society of Edinburgh: Earth Sciences*, *72,* 195-200.

Colarieti, M. L.; Toscano, G.; Greco, G., Jr. 2002. Soil-catalyzed polymerization of phenolics in polluted waters. *Water Research*, *36,* 3015-3022.

Colon, D.; Weber, E. J.; Baughman, G. L. 2002. Sediment-associated reactions of aromatic amines. 2. QSAR development. *Environmental Science and Technology*, *36,* 2443-2450.

Commission Regulation No. 2788/98. *Official Journal of European communication*, 1998.

Coperet, C.; Adolfsson, H.; Khuong, T.-A. V.; Yudin, A. K.; Sharpless, K. B. 1998. A simple and efficient method for the preparation of pyridine *N*-oxides. *Journal of Organic Chemistry*, *63,* 1740-1741.

Cornelis A. Kan; Petz, M. 2000. Residues of veterinary drugs in eggs and their distribution between yolk and white. *Journal of Agriculture and Food Chemistry*, *48,* 6397-6403.

Cox, A. R. 1987. Efficacy of the antimicrobial agent triclosan in topical deodorant products: recent developments in vivo. *Journal of the Society of Cosmetic Chemists*, *38,* 223-231.

Craig, W. A.; Dalhoff, A. 1998. *Pharmacodynamics of fluoroquinolones in experimental animals. Quinolone antibacterials*; Springer: New York.

Cunningham, K. M.; Goldberg, M. C.; Weiner, E. R. 1988. Mechanisms for aqueous photolysis of adsorbed benzoate, oxalate, and succinate on iron oxyhydroxide (Goethie) surfaces. *Environmental Science and Technology*, *22,* 1090-1097.

Cuppoletti, A.; Dagostin, C.; Florea, C.; Galli, C.; Gentili, P.; Lanzalunga, O.; Petride, A.; Petride, H. 1999. The oxidation of N-benzylaziridine catalyzed by iron porphyrin: radical versus electron transfer mechanism. *Chemistry--A European Journal*, *5,* 2993-2999.

Daughton, C. G.; Ternes, T. A. 1999. Pharmaceuticals and personal care products in the environment: agents of subtle change? *Environmental Health Perspectives Supplements*, *107,* 907-938.

DeSalva, S. J.; Kong, B. M.; Lin, Y. J. 1989. Triclosan: a safety profile. *American journal of dentistry*, *2,* 185-196.

Dixon, J. B.; Golden, D. C.; Uzochukwu, G. A.; Chen, C. C. 1990. Soil manganese oxides. *NATO ASI Series, Series B: Physics, 215(Soil Colloids Their Assoc. Aggregates)* 141-163.

Fabrega, J. R.; Jafvert, C. T.; Li, H.; Lee, L. S. 1998. Modeling short-term soil-water distribution of aromatic amines. *Environmental Science and Technology*, *32,* 2788-2794.

FAO/WHO. 1990. Joint expert committee on food additives: evaluation of certain veterinary drug residues in food. *Technical series*, *No. 799,* 45.

Fasani, E.; Mella, M.; Monti, S.; Albini, A. 2001. Unexpected photoreactions of some 7-amino-6-fluoroquinolones in phosphate buffer. *European Journal of Organic Chemistry*, *2,* 391-397.

Fasani, E.; Rampi, M.; Albini, A. 1999. Photochemistry of some fluoroquinolones: effect of pH and chloride ion. *Journal of the Chemical Society, Perkin Transactions 2: Physical Organic Chemistry*, *9,* 1901-1907.

Federle, T. W.; Kaiser, S. K.; Nuck, B. A. 2002. Fate and effects of triclosan in activated sludge. *Environmental Toxicology and Chemistry*, *21,* 1330-1337.

Fendorf, S. E.; Fendorf, M.; Sparks, D.; Gronsky, R. 1992. Inhibitory mechanisms of chromium(III) oxidation by d-manganese dioxide. *Journal of Colloid and Interface Science*, *153,* 37-54.

Feng, W.; Liu, H.; Chen, G.; Malchow, R.; Bennet, F.; Lin, E.; Pramanik, B.; Chan, T.-M. 2001. Structural characterization of the oxidative degradation products of an antifungal agent SCH 56592 by LC-NMR and LC-MS. *Journal of Pharmaceutical and Biomedical Analysis*, *25,* 545-557.

Ganley, B.; Chowdhury, G.; Bhansali, J.; Daniels, J. S.; Gates, K. S. 2001. Redox-activated, hypoxia-selective DNA cleavage by quinoxaline 1,4-di-*N*-oxide. *Bioorganic & Medicinal Chemistry*, *9,* 2395-2401.

Geletii, Y. V.; Strelets, V. V.; Shafirovich, V. Y.; Shilov, A. E. 1989. Cation radicals of heterocyclic *N*-oxides and their reactions. *Heterocycles*, *28,* 677-685.

Goldberg, M. C.; Cunningham, K. M.; Weiner, E. R. 1993. Aquatic photolysis: photolytic redox reactions between goethite and adsorbed organic acids in aqueous solutions. *Journal of Photochemistry and Photobiology, A: Chemistry*, *73,* 105-120.

Golet, E. M.; Alder, A. C.; Giger, W. 2002. Environmental exposure and risk assessment of fluoroquinolone antibacterial agents in wastewater and river water of the Glatt Valley Watershed, Switzerland. *Environmental Science and Technology*, *36,* 3645-3651.

Golet, E. M.; Alder, A. C.; Hartmann, A.; Ternes, T. A. G. W. 2001. Trace determination of fluoroquinolone antibacterial agents in urban wastewater by solid-phase extraction and liquid chromatography with fluorescence detection. *Analytical Chemistry*, *73,* 3632-3638.

Gorrod, J. W.; Beckett, A. H., Eds. 1978. *Drug metabolism in man*; Taylor & Francis LTD: London.

Haderleln, S. B.; Schwarzenbach, R. P. 1993. Adsorption of substituted nitrobenzenes and nitrophenols to mineral surf aces. *Environmental Science and Technology*, *27,* 316-326.

Haksar, C. N.; Malhotra, R. C.; Ramachandran, P. K. 1979. Oxidation of hydrazides of salicylic and substituted salicylic acids with active manganese dioxide. *Indian Journal of Chemistry, Section B: Organic Chemistry Including Medicinal Chemistry*, *17B,* 191-193.

Hansch, C.; Leo, A.; Hoekman, D. 1995. *Exploring QSAQ. Hydrophobic, electronic, and steric constants*; American Chemical Society: Washington, DC.

Hartmann, A.; Alder, A. C.; Koller, T.; Widmer, R. M. 1998. Identification of fluoroquinolone antibiotics as the main source of umuC genotoxicity in native hospital wastewater. *Environmental Toxicology and Chemistry*, *17,* 377-382.

Hartmann, A.; Golet, E. M.; Gartiser, S.; Alder, A. C.; Koller, T.; Widmer, R. M. 1999. Primary DNA damage but not mutagenicity correlates with ciprofloxacin concentrations in German hospital wastewaters. *Archives of Environmental Contamination and Toxicology*, *36,* 115-119.

Henderson, M. A. 2003. Surface stabilization of organics on hematite by conversion from terminal to bridging adsorption structures. *Geochimica et Cosmochimica Acta*, *67,* 1055-1063.

Henderson, M. A.; Joyce, S. A.; Rustad, J. R. 1998. Interaction of water with the (1 × 1) and (2 × 1) surfaces of α-Fe_2O_3(012). *Surface Science*, *417,* 66-81.

Hongekar, M. L.; Patil, J. B. 1998. Kinetics and mechanism of oxidation of n-butyric and iso-butyric acid hydrazides by hexacyanoferrate(III) in acidic medium. *Indian Journal of Chemistry, Section A: Inorganic, Bio-inorganic, Physical, Theoretical & Analytical Chemistry*, *37A,* 493-497.

Huang, C.-H.; Pinkston, K.; Renew, J. E.; Sedlak, D. L. 2004. Factors affecting the concentrations of pharmaceuticals released to the aquatic environment. M*anuscript in preparation*.

Huang, P. M.; Wang, M. K. 1997. Formation chemistry and selected surface properties of iron oxides [in soils]. *Advances in GeoEcology 30 (Soils and Environment)* 241-270.

Hutchinson, M. J.; Young, P. Y.; Hewitt, S. A.; Faulkner, D.; Kennedy, D. G. 2002. Development and validation of an important method for confirmation of the carbadox metabolite, quinoxaline-2-carboxylic acid, in porcine liver using LC-electrospray MS-MS according to revised EU criteria for veterinary drug residue analysis. *Analyst*, *127,* 342-346.

Iley, J.; Tolando, R. 2000. The oxidative dealkylation of tertiary amides: mechanistic aspects. *Perkin 2*, *11,* 2328-2336.

Inbaraj, J. J.; Motten, A. G.; Chignell, C. F. 2003. Photochemical and photobiological studies of tirapazamine (SR 4233) and related quinoxaline 1,4-di-*N*-oxide analogues. *Chemical Research in Toxicology*, *16,* 164-170.

Ingerslev, F.; Halling-Sorensen, B. 2001. Biodegradability of metronidazole, olaquindox, and tylosin and formation of tylosin degradation products in aerobic soil--manure slurries. *Ecotoxicology and environmental safety*, *48,* 311-320.

Ingerslev, F.; Torang, L.; Loke, M.-L.; Halling-Sorensen, B.; Nyholm, N. 2001. Primary biodegradation of veterinary antibiotics in aerobic and anaerobic surface water simulation systems. *Chemosphere*, *44,* 865-872.

Iqbal, R.; Ebrahim, S.; Ziaulhaq, M. 1997. Some oxidation reactions of isomeric pyridinecarboxylic acid hydrazides. *Turkish Journal of Chemistry*, *21,* 200-208.

Jacobs, R. L. 1977. Oxidation of p-toluenesulfonylhydrazide to 1,2-di(p-toluenesulfonyl)hydrazine. *Journal of Organic Chemistry*, *42,* 571-573.

Jazrawi, S. F.; Al-Doori, Z. A.; Haddad, T. A. 1988. Antibiotic resistant coliform and fecal coliform bacteria in drinking water. *Water, Air, and Soil Pollution*, *39,* 377-382.

JECFA. 1991. 36th meeting of the joint FAO/WHO expert committee on food additives. *WHO food additives series*, *No. 27,* 141.

Johnsson, K.; Schultz, P. G. 1994. Mechanistic Studies of the oxidation of isoniazid by the catalase peroxidase from mycobacterium tuberculosis. *Journal of the American Chemical Society*, *116,* 7425-7426.

Junta, J. L.; Hochella, M. F., Jr. 1994. Manganese(II) oxidation at mineral surfaces: a microscopic and spectroscopic study. *Geochimica et Cosmochimica Acta*, *58,* 4985-4999.

Kanetoshi, A.; Ogawa, H.; Katsura, E.; Kaneshima, H. 1987. Chlorination of Irgasan DP300 and formation of dioxins from its chlorinated derivatives. *Journal of Chromatography*, *389,* 139-153.

Kanetoshi, A.; Ogawa, H.; Katsura, E.; Kaneshima, H. 1988. Formation of polychlorinated bienzo-p-dioxin from 2,4,4'-trichloro-2'-hydroxydiphenyl ether (Irgasan DP300) and its chlorinated derivatives by exposure to sunlight. *Journal of Chromatography*, *454,* 145-155.

Kanetoshi, A.; Ogawa, H.; Katsura, E.; Kaneshima, H. 1988. Formation of polychlorinated dibenzo-p-dioxins upon combustion of commercial textile products containing 2,4,4'-trichloro-2'-hydroxydiphenyl ether (Irgasan DP300). *Journal of Chromatography*, *442,* 289-299.

Karthikeyan, K. G.; Chorover, J.; Bortiatynski, J. M.; Hatcher, P. G. 1999. Interaction of 1-naphthol and its oxidation products with aluminum hydroxide. *Environmental Science and Technology*, *33,* 4009-4015.

Katritzky, A., R.; Lagowski, J. M. 1971. *Chemistry of the heterocyclic N-oxides*; Academic Press: London and New York, Vol. 19.

Klausen, J.; Haderlain, S. B.; Schwarzenbach, R. P. 1997. Oxidation of substituted anilines by aqueous MnO_2: effect of co-solutes on initial and quasi-steady-state kinetics. *Environmental Science and Technology*, *31,* 2642-2649.

Kohler, B.; Karch, H.; Schmidt, H. 2000. Antibacterials that are used as growth promoters in animal husbandry can affect the release of Shiga-toxin-2-converting bacteriophages and Shiga toxin 2 from Escherichia coli strains. *Microbiology (Reading, England)*, *146,* 1085-1090.

Kolpin, D. W.; Furlong, E. T.; Meyer, M.; Thurman, E. M.; Zaugg, S. D.; Barber, L. B.; Buxton, H. T. 2002. Pharmaceuticals, hormones, and other organic wastewater contaminants in U.S. streams, 1999-2000: A national reconnaissance. *Environmental Science and Technology*, *36,* 1202-1211.

Krishnamurti, G. S. R.; Huang, P. M. 1988. Influence of manganese oxide minerals on the formation of iron oxides. *Clays and Clay Minerals*, *36,* 467-475.

Kuhlmann, J.; Dalhoff, A.; Zeiler, H.-J., Eds. 1998. *Quinolone Antibacterials*; Springer-Verlag Berlin Heidelberg: Berlin, Germany, Vol. 127.

Kümmerer, K.; Al-Ahmad, A.; Mersch-Sundermann, V. 2000. Biodegradability of some antibiotics, elimination of the genotoxicity and affection of wastewater bacteria in a simple test. *Chemosphere*, *40,* 701-710.

Kung, K. H.; McBride, M. B. 1988. Electron transfer processes between hydroquinone and iron oxides. *Clays and Clay Minerals*, *36,* 303-309.

Kurasawa, Y.; Takada, A.; Kim, H. S. 1995. Progress in the chemistry of quinoxaline N-oxides and N,N'-dioxides. *Journal of Heterocyclic Chemistry*, *32,* 1085-1114.

Laha, S.; Luthy, R. G. 1990. Oxidation of aniline and other primary aromatic amines by manganese dioxide. *Environmental Science and Technology*, *24,* 363-373.

Latch, D. E.; Packer, J. L.; Arnold, W. A.; McNeill, K. 2003. Photochemical conversion of triclosan to 2,8-dichlorodibenzo-p-dioxin in aqueous solution. *Journal of photochemistry and photobiology A-Chemistry*, *158,* 63-66.

Lee, L. S.; Nyman, A. K.; Li, H.; Nyman, M. C.; Jafvert, C. 1997. Initial sorption of aromatic amines to surface soils. *Environmental Toxicology and Chemistry*, *16,* 1575-1582.

Lehmann, R. G.; Cheng, H. H.; Harsh, J. B. 1987. Oxidation of phenolic acids by soil iron and manganese oxides. *Soil Science Society of American Journal*, *51,* 352-356.

Letzel, T.; Poschl, U.; Rosenberg, E.; Grasserbauer, M.; Niessner, R. 1999. In-source fragmentation of partially oxidized mono- and polycyclic aromatic hydrocarbons in atmospheric pressure chemical ionization mass spectrometry coupled to liquid chromatography. *Rapid Communications in Mass Spectrometry*, *13,* 2456-2468.

Levy, S. B.; Roujeinikova, A.; Sedelnikova, S.; Baker, P. J.; Stuitje, A. R.; Slabas, A. R.; Rice, D. W.; Rafferty, J. B. 1999. Molecular basis of triclosan activity. *Nature*, *398,* 383-384.

Li, H.; Lee, L. S.; Fabrega, J. R.; Jafvert, C. T. 2001. Role of pH in partitioning and cation exchange of aromatic amines on water-saturated soils. *Chemosphere*, *44,* 627-635.

Li, H.; Lee, L. S.; Jafvert, C. T.; Graveel, J. G. 2000. Effect of substitution on irreversible binding and transformation of aromatic amines with soils in aqueous systems. *Environmental Science and Technology*, *34,* 3674-3680.

Li, H.; Lee, L. S.; Schulze, D. G.; Guest, C. A. 2003. Role of soil manganese in the oxidation of aromatic amines. *Environmental Science and Technology*, *37,* 2686-2693.

Lide, D. R., Jr. 1998. *Properties of Organic Compounds CRCnetBASE 1999.*; Springer: Berlin, Germany.

Lindstrom, A.; Buerge, I. J.; Poiger, T.; Bergqvist, P.-A.; Muller, M. D.; Buser, H.-R. 2002. Occurrence and environmental behavior of the bactericide triclosan and its methyl derivative in surface waters and in wastewater. *Environmental Science and Technology*, *36,* 2322-2329.

Liu, C.; Huang, P. M. 2001. The influence of catechol humification on surface properties of metal oxides. *Special Publication - Royal Society of Chemistry*, *273(Humic Substances),* 253-270.

Loke, M.-L.; Tjornelund, J.; Halling-Sorensen, B. 2002. Determination of the distribution coefficient (log Kd) of oxytetracycline, tylosin A, olaquindox and metronidazole in manure. *Chemosphere*, *48,* 351-361.

Lützhøft, H.-C. H.; Vaes, W. H. J.; Freidig, A. P.; Halling-Sørensen, B.; Hermens, J. L. M. 2000a. 1-Octanol/water distribution coefficient of oxolinic acid: influence of pH and its relation to the interaction with dissolved organic carbon. *Chemosphere*, *40,* 711-714.

Lützhøft, H.-C. H.; Vaes, W. H. J.; Freidig, A. P.; Halling-Sørensen, B.; Hermens, J. L. M. 2000b. Influence of pH and other modifying factors on the distribution behavior of 4-quinolones to solid phases and humic acids studied by "negligible-depletion" SPME-HPLC. *Environmental Science and Technology*, *34,* 4989-4994.

MacIntosh, A. I.; Neville, G. A. 1984. Liquid chromatographic determination of carbadox, desoxycarbadox, and nitrofurazones in pork tissues. *Journal - Association of Official Analytical Chemists*, *67,* 958-962.

Marengo, J. R.; Kok, R. A.; Burrows, L. A.; Velagaleti, R. R.; Stamm, J. M. 2001. Biodegradation of ^{14}C-sarafloxacin hydrochloride, a fluoroquinolone antimicrobial by *Phanerochaete Chrysosporium*. *Journal of Scientific & Industrial Research*, *60,* 121-130.

Massy, D. J. R.; McKillop, A. 1996. Selective Monodeoxygenation of methyl 3-(2-quinoxalinylmethylene)carbazate N^1,N^4-dioxide (carbadox). *Synthesis* 1477-1480.

McArdell, C. S.; Stone, A. T.; Tian, J. 1998. Reaction of EDTA and related aminocarboxylate chelating agents with $Co^{III}OOH$ (heterogenite) and $Mn^{III}OOH$ (manganite). *Environmental Science and Technology*, *32,* 2923-2930.

McAvoy, D. C.; Schatowitz, B.; Jacob, M.; Hauk, A.; Eckhoff, W. S. 2002. Measurement of triclosan in wastewater treatment systems. *Environmental Toxicology and Chemistry*, *21,* 1323-1329.

McBride, M. B. 1987. Adsorption and oxidation of phenolic compounds by iron and manganese oxides. *Soil Science Society of America Journal*, *51,* 1466-1472.

McBride, M. B. 1994. *Environmental Chemistry of Soils*; Oxford University Press: New York.

McBride, M. B.; Sikora, F. J.; Wesselink, L. G. 1988. Complexation and catalyzed oxidative polymerization of catechol by aluminum in acidic solution. *Soil Science Society of America Journal*, *52,* 985-993.

McIlwain, H. 1943. Bacterial inhibition by metabolite analogs. V. Reactions and antibacterial properties of p-diazine di-*N*-oxides. *Journal of the Chemical Society* 322-325.

McKenzie, R. M. 1980. The manganese oxides in soils. *Geol. Geochem. Manganese, [Proc. Int. Symp.], 2nd. Meeting Date 1976*, *1*.

McKenzie, R. M. 1989. In *Minerals in soil environments*; 2nd Ed.; Dixon, J. B., Weed S. B., Eds.; Madison, Wis. : Soil Science Society of America, p 1244.

McMurry, L. M.; Oethinger, M.; Levy, S. B. 1998. Triclosan targets lipid synthesis. *Nature*, *394,* 531-532.

Mella, M.; Fasani, E.; Albini, A. 2001. Photochemistry of 1-cyclopropyl-6-fluoro-1,4-dihydro-4-oxo-7-(piperazin-1-yl)quinoline-3-carboxylic acid (ciprofloxacin) in aqueous solutions. *Helvetica Chimica Acta*, *84,* 2508-2519.

Miao, X.-S.; March, R. E.; Metcalfe, C. D. 2003. A tandem mass spectrometric study of the *N*-oxides, quinoline *N*-oxide, carbadox, and olaquindox, carried out at high mass accuracy using electrospray ionization. *International Journal of Mass Spectrometry*, *230,* 123-133.

Moerup, S.; Madsen, M. B.; Franck, J.; Villadsen, J.; Koch, C. J. W. 1983. A new interpretation of Moessbauer spectra of microcrystalline goethite: "super-ferromagnetism" or "super-spin-glass" behavior? *Journal of Magnetism and Magnetic Materials*, *40,* 163-174.

Morgan, J. J.; Stumm, W. 1964. Colloid-chemical properties of Mn dioxide. *Journal of Colloid Science*, *19,* 347-359.

Morrison, R. T.; Boyd, R. N. 1987. *Organic Chemistry*; 5th Ed.; Allyn and Bacon, Inc.: Newton, MA.

Munger, J. W.; Jacob, D. J.; Waldman, J. M.; Hoffmann, M. R. 1983. Fogwater chemistry in an urban atmosphere. *Journal of Geophysical Research, C: Oceans and Atmospheres*, *88,* 5109-5121.

Murray, J. W. 1974. Surface chemistry of hydrous manganese dioxide. *Journal of Colloid and Interface Science*, *46,* 357-371.

Naber, K. G. 2002. Lomefloxacin versus ciprofloxacin in the treatment of chronic bacterial prostatitis. *International Journal of Antimicrobial Agents*, *20,* 18-27.

Naidja, A.; Huang, P. M.; Bollag, J.-M. 1998. Comparison of reaction products from the transformation of catechol catalyzed by birnessite or tyrosinase. *Soil Science Society of America Journal, 62,* 188-195.

National Toxicology Program 1994. NTP toxicology and carcinogenesis studies of o-benzyl-p-chlorophenol (CAS No. 120-32-1) in F344/N rats and B6C3F1 mice (gavage studies). *National Toxicology Program Technical Report Series*, *424,* 1-304.

Nishinaga, A.; Yamazaki, S.; Matsuura, T. 1986. Novel oxidative cleavage of a carbon-carbon bond in hydrazones by oxygenation with cobalt Schiff base complex. *Tetrahedron Letters*, *27,* 2649-2652.

Nowack, B.; Stone, A. T. 2002. Homogeneous and Heterogeneous Oxidation of Nitrilotrismethylenephosphonic Acid (NTMP) in the Presence of Manganese(II, III) and Molecular Oxygen. *Journal of Physical Chemistry B*, *106,* 6227-6233.

Nowara, A.; Burhenne, J.; Spiteller, M. 1997. Binding of fluoroquinolone carboxylic acid derivatives to clay minerals. *Journal of Agriculture and Food Chemistry*, *45,* 1459-1463.

Nunoshiba, T.; Nishioka, H. 1989. Genotoxicity of quinoxaline 1,4-dioxide derivatives in Escherichia coli and Salmonella typhimurium. *Mutation Research*, *217,* 203-209.

Ohloff, G.; Giersch, W. 1973. Conversion of vicinal diols into dicarbonyl compounds by manganese dioxide. *Angewandte Chemie*, *12,* 401-402.

Okumura, T.; Nishikawa, Y. 1996. Gas Chromatography-mass spectrometry determination of triclosan in water sediment and fish samples via methylation with diazomethane. *Analytica Chimica Acta*, *325,* 175-184.

Orvos, D. R.; Versteeg, D. J.; Inauen, J.; Capdevielle, M.; Rothenstein, A.; Cunningham, V. 2002. Aquatic toxicity of triclosan. *Environmental Toxicology and Chemistry*, *21,* 1338-1349.

Pankow, J. F. 1991. *Aquatic Chemical Concepts*; Lewis Publishers: Chelsea, MI.

Parent, R. A. 2000. Acute toxicity data submissions. *International Journal of Toxicology*, *19,* 358-359.

Park, J.-W.; Dec, J.; Kim, J.-E.; Bollag, J.-M. 1999. Effect of humic constituents on the transformation of chlorinated phenols and anilines in the presence of oxidoreductive enzymes or birnessite. *Environmental Science and Technology*, *33,* 2028-2034.

Parshikov, I. A.; Freeman, J. P.; Lay, J. O. J.; Beger, R. D.; Williams, A. J.; Sutherland, J. B. 1999. Regioselective transformation of ciprofloxacin to *N*-acetylciprofloxacin by the fungus *Mucor ramannianus*. *FEMS Microbiology Letters*, *177,* 131-135.

Paxéus, N. 1996. Organic pollutants in the effluents of large wastewater treatment plants in Sweden. *Water Reseach*, *30,* 1115-1122.

Payne, L. 1998. Strength with safety - chlorophenolic disinfectants. *Specialty Chemicals*, *18,* 152-153.

Pehkonen, S. O.; Siefert, R. L.; Hoffmann, M. R. 1995. Photoreduction of iron oxyhydroxides and the photooxidation of halogenated acetic acids. *Environmental Science and Technology*, *29,* 1215-1222.

Perrin, D. D. 1972. *IUPAC. Dissociation constants of Organic Bases in Aqueous Solution: Supplement 1972*; Crane, Russak: New York, N. Y.

Phillips, G.; Johnson, B. E.; Ferguson, J. 1990. The loss of antibiotic activity of ciprofloxacin by photodegradation. *Journal of Antimicrobial Chemotherapy*, *26,* 783-789.

Pizzigallo, M. D. R.; Ruggiero, P.; Crecchio, C.; Mascolo, G. 1998. Oxidation of chloroanilines at metal oxide surfaces. *Journal of Agriculture and Food Chemistry*, *46,* 2049-2054.

Pizzigallo, M. D. R.; Ruggiero, P.; Crecchio, C.; Mininni, R. 1995. Manganese and iron oxides as reactants for oxidation of chlorophenols. *Soil Science Society of America Journal*, *59,* 444-452.

Pulgarin, C.; Kiwi, J. 1995. Iron oxide-mediated degradation, photodegradation, and biodegradation of aminophenols. *Langmuir*, *11,* 519-526.

Rabolle, M.; Spliid, N. H. 2000. Sorption and mobility of metronidazole, olaquindox, oxytetracycline and tylosin in soil. *Chemosphere*, *40,* 715-722.

Radtke, T. M.; Gist, G. L. 1989. Wastewater sludge disposal. Antibiotic resistant bacteria may pose health hazard. *Journal of Environmental Health*, *52,* 102-105.

Renew, J. E. 2003. Novel Analytical Method Development and Fate Assessment for Fluoroquinolone, Sulfonamide and Trimethoprim Antibiotics in Engineered Water Treatment Systems. *MS Thesis*. CEE, Georgia Tech. Atlanta, GA.

Renew, J. E.; Huang, C. H. 2004. Simultaneous Analysis of Fluoroquinolone, Sulfonamide and Trimethoprim Antibiotics in Wastewater using Tandem Solid-Phase Extraction and Liquid Chromatography Electrospray Mass Spectrometry. *Journal of Chromatography A*, accepted.

RxList "The internet drug index (The top 200 prescriptions: 1999 US prescriptions based upon more than 2.8 billion U.S. prescription)," cited June 10, 2000.

Sabaliunas, D.; Webb, S. F.; Hauk, A.; Jacob, M.; Eckhoff, W. S. 2003. Environmental fate of triclosan in the River Aire Basin, UK. *Water Research*, *37,* 3145-3154.

Schacht, P. 1998. Quinolone Antibacterials. *Handbook of Experimental Pharmacology*, *127,* 421-453.

Scheer, M. 1987. Studies on the antibacterial activity of Baytril. *Veterinary Medical Review*, *2,* 90-99.

Schwertmann, U.; Cornell, R. M. 2000. *Iron oxides in the laboratory. Preparation and characterization*; 2nd, Completely, Revised and Extended Ed.; WILEY-VCH: New York.

Schwertmann, U.; Fischer, W. R.; Taylor, R. M. 1974. New aspects of iron oxide formation in soils. *Tr. Mezhdunar. Kongr. Pochvoved., 10th*, *6,* 237-249.

Selig, H.; Keinath, T. M., II;; Weber, W. J., Jr. 2003. Sorption and manganese-induced oxidative coupling of hydroxylated aromatic compounds by natural geosorbents. *Environmental Science and Technology*, *37,* 4122-4127.

Seto, Y.; Guengerich, F. P. 1993. Partitioning between *N*-dealkylation and *N*-oxygenation in the oxidation of *N*,*N*-dialkylarylamines catalyzed by cytochrome P450 2B1. *Journal of Biological Chemistry*, *268,* 9986-9997.

Shindo, H.; Huang, P. M. 1982. Role of manganese(IV) oxide in abiotic formation of humic substances in the environment. *Nature*, *298,* 363-365.

Shukla, R. S.; Robert, A.; Meunier, B. 1996. Kinetic investigation of oxidative degradation of aromatic pollutant 2,4,6-trichlorophenol by an iron-porphyrin complex, a model ligninase. *Journal of Molecular Catalysis*, *113,* 45-49.

Shukun, L.; Hanqing, W. 1986. Radical mechanism in the photoreaction of organic *N*-oxides: some paradiazine N,N-dioxides. *Heterocycles*, *24,* 659-664.

Smith, J. R. L.; Mortimer, D. N. 1986. Model systems for cytochrome P450-dependent monooxygenases. Part 5. Amine oxidation. Part 17. Oxidative *N*-dealkylation of tertiary amines by metalloporphyrin-catalyzed model systems for cytochrome P450 monooxygenases. *Journal of the Chemical Society, Perkin Transactions 2: Physical Organic Chemistry (1972-1999)*, *11,* 1743-1749.

Smith, M. B.; March, J. 2001. *March's advanced organic chemistry*; 5th Ed.; John Wiley & Sons, INC.

SPARC (http://www.epa.gov/athens/research/projects/sparc/) 2003, US EPA, National Exposure Research Laboratory, Athens, Georgia.

Sparks, D. L. 1995. *Environmental Soil Chemistry*; Academic Press: San Diego.

Stassen, I.; Hambitzer, G. 1997. Anodic oxidation of aniline and *N*-alkylanilines in aqueous sulfuric acid studied by electrochemical thermospray mass spectrometry. *Journal of Electroanalytical Chemistry*, *440,* 219-228.

Stone, A. T. 1987. Reductive dissolution of manganese(III/IV) oxides by substituted phenols. *Environmental Science and Technology*, *21,* 979-988.

Stone, A. T.; Morgan, J. J. 1984. Reduction and dissolution of manganese(III) and manganese(IV) oxides by organics. 1. Reaction with hydroquinone. *Environmental Science and Technology*, *18,* 450-456.

Stone, A. T.; Morgan, J. J. 1984. Reduction and dissolution of manganese(III) and manganese(IV) oxides by organics: 2. Survey of the reactivity of organics. *Environmental Science and Technology*, *18,* 617-624.

Stone, A. T.; Ulrich, H.-J. 1989. Kinetics and reaction stoichiometry in the reductive dissolution of manganese(IV) dioxide and Co(III) oxide by hydroquinone. *Journal of Colloid and Interface Science*, *132,* 509-522.

Stumm, W. 1992. *Chemistry of the solid-water interface*; Wiley-Interscience: New York, NY.

Stumn, W.; Morgan, J. J. 1996. *Aquatic Chemistry*; 3rd Ed.; John Wiley and Sons, Inc.

Sunda, W. G.; Kieber, D. J. 1994. Oxidation of humic substances by manganese oxides yields low-molecular-weight organic substrates. *Nature*, *367,* 62-64.

Sunderland, J.; Tobin, C. M.; Hedges, A. J.; MacGowan, A. P.; White, L. O. 2001. Antimicrobial activity of fluoroquinolone photodegradation products determined by parallel-line bioassay and high performance liquid chromatography. *Journal of Antimicrobial Chemotherapy*, *47,* 271-275.

Sunderland, J.; Tobin, C. M.; White, L. O.; MacGowan, A. P.; Hedges, A. J. 1999. Ofloxacin photodegradation products possess antimicrobial activity. *Drugs*, *58,* 171-172.

Suter, W.; Rosselet, A.; Knuesel, F. 1978. Mode of action of quindoxin and substituted quinoxaline-di-*N*-oxides on Escherichia coli. *Antimicrobial Agents and Chemotherapy*, *13,* 770-783.

Sutherland, J. B.; Freeman, J. P.; Williams, A. J.; Cerniglia, C. E. 1994. *N*-oxidation of quinoline and isoquinoline by *Cunninghamella elegans*. *Experimental Mycology*, *8,* 271-274.

Taylor, R. M. 1968. The association of manganese and cobalt in soils; further observations. *Journal of Soil Science*, *19,* 77-80.

Taylor, R. M. 1990. Some observations on the formation and transformation of iron oxides. *NATO ASI Series, Series B: Physics (1990), 215(Soil Colloids Their Assoc. Aggregates)* 85-103.

Thomas, K. V.; Balaam, J.; Barnard, N.; Dyer, R.; Jones, C.; Lavender, J.; McHugh, M. 2002. Characterization of potentially genotoxic compounds in sediments collected from United Kingdom estuaries. *Chemosphere*, *49,* 247-258.

Tipping, E.; Heaton, M. J. 1983. The adsorption of aquatic humic substances by two oxides of manganese. *Geochimica et Cosmochimica Acta*, *47,* 1393-1397.

Tixier, C.; Singer, H. P.; Canonica, S.; Muller, S. R. 2002. Phototransformation of triclosan in surface waters: a relevant elimination process for this widely used biocide - laboratory studies, field measurements, and modeling. *Environmental Science and Technology*, *36,* 3482-3489.

Tolls, J. 2001. Sorption of veterinary pharmaceuticals in soils: A review. *Environmental Science and Technology*, *35,* 3397-3406.

Tucker, M. J. 1975. Carcinogenic action of quinoxaline 1,4-dioxide in rats. *Journal of the National Cancer Institute*, *55,* 137-146.

Ukrainczyk, L.; McBride, M. B. 1992. Oxidation of phenol in acidic aqueous suspensions of manganese oxides. *Clays and Clay Minerals*, *40,* 157-166.

Ukrainczyk, L.; McBride, M. B. 1993a. Oxidation and dechlorination of chlorophenols in dilute aqueous suspensions of manganese oxides: reaction products. *Environmental Toxicology and Chemistry*, *12,* 2015-2022.

Ukrainczyk, L.; McBride, M. B. 1993b. The oxidative dechlorination reaction of 2,4,6-trichlorophenol in dilute aqueous suspensions of manganese oxides. *Environmental Toxicology and Chemistry*, *12,* 2005-2014.

Ulrich, H.-J.; Stone, A. T. 1989. Oxidation of chlorophenols adsorbed to manganese oxide surfaces. *Environmental Science and Technology*, *23,* 421-428.

Urano, Y.; Higuchi, T.; Hirobe, M. 1996. Substrate-dependent changes of the oxidative o-dealkylation mechanism of several chemical and biological oxidizing systems. *Journal of the Chemical Society, Perkin Transactions 2: Physical Organic Chemistry*, *6,* 1169-1173.

Vasudevan, D.; Cooper, E. M.; Van Exem, O. L. 2002. Sorption-desorption of ionogenic compounds at the mineral-water interface: study of metal oxide-rich soils and pure-phase minerals. *Environmental Science and Technology*, *36,* 501-511.

Volmer, D. A.; Mansoori, B.; Locke, S. J. 1997. Study of 4-quinolone antibiotics in biological samples by short-column liquid chromatography coupled with electrospray ionization tandem mass spectrometry. *Analytical Chemistry*, *69,* 4143-4155.

Voogd, C. E.; Van der Stel, J. J.; Jacobs, J. J. J. A. A. 1980. The mutagenic action of quindoxin, carbadox, olaquindox and some other *N*-oxides on bacteria and yeast. *Mutation Research*, *78,* 233-242.

Vulkan, R.; Zhao, F.-J.; Barbosa-Jefferson, V.; Preston, S.; Paton, G. I.; Tipping, E.; McGrath, S. P. 2002. Copper speciation and impacts on bacterial biosensors in the pore water of copper-contaminated soils. *Environmental Science and Technology*, *34,* 5115-5121.

Wang, D.; Shin, J. Y.; Cheney, M. A.; Sposito, G.; Spiro, T. G. 1999. Manganese dioxide as a catalyst for oxygen-independent atrazine dealkylation. *Environmental Science and Technology*, *33,* 3160-3165.

Wang, F.; Sayre, L. M. 1992. Kinetics and mechanism of aliphatic amine oxidation by aqueous $(batho)_2Cu^{II}$. *Journal of the American Chemical Society*, *114,* 248-255.

Wang, M. C.; Huang, P. M. 2000. Ring cleavage and oxidative transformation of pyrogallol catalyzed by Mn, Fe, Al, and Si oxides. *Soil Science*, *165,* 934-942.

Weber, E. J.; Colon, D.; Baughman, G. L. 2001. Sediment-associated reactions of aromatic amines. 1. Elucidation of sorption mechanisms. *Environmental Science and Technology*, *35,* 2470-2475.

Wersin, P.; Charlet, L.; Karthein, R.; Stumm, W. 1989. From adsorption to precipitation: sorption of manganese(2+) on solid iron(II) carbonate. *Geochimica et Cosmochimica Acta*, *53,* 2786-2796.

Wetzstein, H.-G.; Stadler, M.; Tichy, H.-V.; Dalhoff, A.; Karl, W. 1999. Degradation of ciprofloxacin by basidiomycetes and identification of metabolites generated by the brown rot fungus *Gloeophyllum striatum*. *Applied and Environmental Microbiology*, *65,* 1556-1563.

Wiater, I.; Born, J. G. P.; Louw, R. 2000. Products, rates, and mechanism of the gas-phase condensation of phenoxy radicals between 500-840 K. *European Journal of Organic Chemistry*, 921-928

Wu, F.; Deng, N. 2000. Photochemistry of hydrolytic iron (III) species and photoinduced degradation of organic compounds. A minireview. *Chemosphere*, *41,* 1137-1147.

Zachara, J. M.; Ainsworth, C. C.; Felice, L. J.; Resch, C. T. 1986. Quinoline sorption to subsurface materials: role of pH and retention of the organic cation. *Environmental Science and Technology*, *20,* 620-627.

Zachara, J. M.; Felice, L. J.; Sauer, J. K. 1984. Sorption of aniline on selected Alfisols from the eastern coal region. *Soil Science*, *138,* 209-219.

Zhang, H.; Huang, C. H. 2003. Oxidative transformation of triclosan and chlorophene by manganese oxides. *Environmental Science and Technology*, *37,* 2421-2430.

Zhang, H.; Huang, C. H. 2004. Oxidative transformation of fluoroquinolone antibacterial agents by manganese dioxides (δ-MnO_2). *Environmental Science & Technology*, Manuscript in preparation.

VITA

Huichun Zhang (Judy) was born in AnHui, China on February 9, 1974. She received her bachelor's degree from Department of Environmental Science and Engineering in Nanjing University in China in July 1994. She then enrolled at the same university to pursue a master's degree in Environmental Chemistry. During her graduate studies, she worked as a research assistant. After getting her master's degree in July 1997, she joined Green Water Treatment Company in Jiansu, China and worked there for three years as an environmental engineer. She has participated in many wastewater treatment designing projects during the three-year period. In July 2000, she started to pursue her Ph. D. degree in School of Civil and Environmental Engineering at Georgia Institute of Technology. Her research was focused on metal oxide-facilitated oxidation of three groups of widely used antibacterial agents. After completing her Ph. D. in July 2004, she will join the Graduate Studies of Environmental Toxicology at Cornell University as a Postdoctoral Research Associate.